Mesoporous Carbon Supported NiMo Catalyst for the Hydrotreating of Coker Gas Oil

A thesis submitted to the College of Graduate Studies & Research in partial fulfillment of the requirements for the Master of Science Degree in the Department of Chemical Engineering,

University of Saskatchewan

Saskatoon, SK, Canada

By

PRABHU NARAYANASARMA

May, 2011

© Copyright Prabhu Narayanasarma, May 2011. All rights reserved.

COPYRIGHT

The author has consented that the libraries of the University of Saskatchewan may make this thesis freely available for inspection. Furthermore, the author agrees that permission for the copying of this thesis in any manner, either in whole or part, for scholarly purposes be granted primarily by the professor(s) who supervised this thesis or in their absence by the Department Head of Chemical Engineering or the Dean of the College of Graduate Studies. Duplication, publication, or any use of this thesis, in part or in whole, for financial gain without prior written approval by the University of Saskatchewan is prohibited. It is also understood that due recognition shall be given to the author of this thesis and to the University of Saskatchewan for any use of the material in this thesis.

Request for the permission to copy or make use of the material in this thesis in whole or in part should be addressed to:

The Department Head of Chemical Engineering

College of Engineering

University of Saskatchewan

57 Campus Drive

Saskatoon SK Canada

S7N 5A9

ABSTRACT

New catalyst development for the hydrotreating process, employing functionalized mesoporous carbon (mC) support is studied. mC support was prepared by the volume templating of alkali modified SBA-15 using sucrose as the carbon source and then functionalized using nitric acid of various concentrations (upto 8M HNO_3). A series of NiMo catalysts (12% Mo and 2.4% Ni) were prepared using these functionalized mC supports. The supports and catalysts were characterized by N_2 physisorption, SAXS, XRD, FTIR, TGA, SEM, TEM, H_2-TPR and HRTEM. SAXS results indicated mild reduction in ordered structure of mesoporous carbons after functionalization. N_2 physisorption analysis indicated progressive reduction in surface area and pore volume with the increase in nitric acid concentration. Enhancement of surface functional groups and acidity after functionalization were observed through FTIR spectroscopy and Boehm titration. SEM images showed the retention of needle like morphology in all functionalized carbon supports. TEM images showed that the increase in nitric acid concentration causes excessive etching, resulting in the reduction of ordered structure of functionalized mesoporous carbons. Hydrotreating study of these NiMo/mC catalysts were carried out under industrial operating conditions in a laboratory scale trickle bed reactor using coker light gas oil derived from Athabasca bitumen as feedstock. NiMo catalyst supported on 6M acid treated mC (i.e. NiMo/mC-6M) showed the highest activity due to higher surface functional groups, higher acidity and better textural properties. The HDS and HDN activities of NiMo/mC-6M catalyst were higher than that of NiMo/γ-Al_2O_3 catalyst owing to lower support metal interaction (SMI), higher surface area and effective functionalization. Using the mC-6M support, NiMo catalysts with

different metal loading (12 – 27% Mo, 2.4 to 5.4% Ni) were prepared and characterized. Hydrotreating activity study of these catalysts indicated that the catalyst with 22% Mo and 2.9% Ni loading was the optimum catalyst on 6M functionalized mC support. Higher metal loading (>22%Mo) led to excessive pore blockage and improper metal dispersion resulting in decreased activity. Kinetic study of the optimum catalyst was carried out by varying temperature (330°C to 370°C), gas-to-oil ratio (400 – 1000 Nm^3/m^3), LHSV (1.0 to 2.5 hr^{-1}) and pressure (7.8 to 9.8 MPa) and the data was fitted by non-linear regression method using power law model. The calculated reaction orders and activation energies were 2.8, 1.5 and 189 KJ/mol, 98.9 KJ/mol for HDS and HDN, respectively. The results of HRTEM and H_2-TPR indicated lower SMI in mC supported catalyst resulting in the generation of qualitatively Type-II like NiMoS phase on functionalized mC supports, which is considered to be very active for hydrotreating. The hydrotreating activity of the optimum catalyst was higher than that of commercial catalyst (supported on γ-Al_2O_3). Long term deactivation experiment carried out over a total period of 10 weeks confirmed the durability of NiMo/mC catalyst for the duration of operation. This study reveals the immense capability of functionalized mC supports to become the potential alternative catalyst support to conventional γ-Al_2O_3 for the hydrotreating of gas oil feedstocks.

Keywords: hydrodesulphurization, mesoporous carbon, NiMo, functionalization, gas oil, hydrotreating kinetics, HDS, HDN, metal support interaction, CMK, multiparameter model.

ACKNOWLEDGEMENT

I would first like to thank my supervisors, Dr. Ajay Dalai and Dr. John Adjaye, for their valuable guidance and supervision throughout my research work. I greatly appreciate the time and effort they have invested to review and provide recommendations to my written materials. I would also like to thank Dr. H.Wang and Dr. D.K.Hwang, for their suggestions, comments and guidance in carrying out my research work. Also, I would like to thank Dr. D.Y.Peng and Dr. G.A.Hill for their guidance in the coursework.

Secondly, I would like to thank Mr. Richard Blondin, Mr. Dragan Cekic, Mr. Rlee and Ms. Heli Eunike for their assistance in carrying out the laboratory work that contributed to my project. My thanks also go to the Natural Science and Engineering Research Council of Canada and Syncrude Canada Limited for their much-appreciated financial assistance. I also greatly appreciate the assistance from Structural Science Centre and Geology Department of University of Saskatchewan, University of New Brunswick and University of British Columbia in catalyst characterizations.

Lastly, I would like to express my gratitude to my fellow students and members of catalysis and chemical reaction engineering laboratories, who were supportive to me during my graduate study in the University of Saskatchewan. Above all, I express my heartfelt thanks to my mother, father and sisters for their unconditional love and constant encouragement. Also, I would like to extend my thanks to my wife Piyali for her continuous support all along. Finally, I thank God Almighty for his blessings.

TABLE OF CONTENTS

COPY RIGHT i

ABSTRACT ii

ACKNOWLEDGMENT iv

TABLE OF CONTENTS v

LIST OF TABLES xii

LIST OF FIGURES xiv

NOMENCLATURE xviii

CHAPTER 1. INTRODUCTION 1

1.1 Knowledge gap: 6

1.2 Hypothesis: 7

1.2.1 Research Objective 7

1.2.2 Phase I: Effect of functionalization 7

1.2.3 Phase II: Optimization of metal loading 8

1.2.4 Phase II: Kinetic studies 8

CHAPTER 2. LITERATURE REVIEW 9

2.1 Hydrotreating process 9

2.2 Necessity of hydrotreating process 10

2.2.1 Environmental Concerns 10

2.2.2 Efficient operation of downstream units 11

2.2.3 Corrosion concerns 11

2.2.4 Improvement of product quality 11

2.3 Hydrotreating in tar sands processing 12

2.3.1 Tar sands upgrading process 12

2.3.2 Hydrotreating process 14

2.3.2.1 Feed filtration unit 14

2.3.2.2 Feed preheat section 14

2.3.2.3 Hydrotreating reactor 15

2.3.2.4 Vapor liquid separation section 15
2.3.2.5 Water wash system 16
2.3.2.6 Fractionation section 16
2.4 Factors affecting hydrotreating process 16
2.4.1 Feed quality 18
2.4.2 Process conditions 19
2.4.2.1 Liquid hourly space velocity (LHSV) 19
2.4.2.2 Hydrogen partial pressure 20
2.4.2.3 Gas-to-oil ratio 20
2.4.2.4 Reactor temperature 21
2.4.3 Catalyst 21
2.5 Hydrotreating reactions 21
2.5.1 Hydrodesulphurization reactions 22
2.5.2 Recombination reactions 26
2.5.3 Hydrodenitrogenation reaction 27
2.5.4 Reaction mechanism 30
2.6 Hydrotreating catalysts 31
2.7 Catalyst development 33
2.7.1.1 New Catalyst metals 34
2.7.1.2 Active phase variation 34
2.7.1.3 Different catalyst preparation methods 35
2.7.1.4 Use of additives 36
2.7.1.5 New supports 36
2.8 Structural models of hydrotreating catalysts 38
2.8.1 Monolayer Model 38
2.8.2 Intercalation model 38
2.8.3 Contact synergy model 38
2.8.4 Modified Contact Synergy Model 39
2.8.5 Co-Mo-S model 39
2.8.6 Rim-edge model 40
2.9 Improvement in catalysts support 41
2.9.1 Silica supports 41

2.9.2 Metal doped Silica supports 41
2.9.3 Carbon supports 41
2.10 Preparation of mesoporous carbon support 42
2.10.1 Volume Template Process 44
2.10.2 Surface Template Process 47
2.10.3 Direct synthesis 53
2.11 Functionalization of carbon supports 54
2.11.1 Overview of functionalization of carbon supports 54
2.11.2 Chemistry of nitric acid functionalization 56
2.11.3 Effect of functionalization of carbon supports on catalyst characteristics and activity 57
2.11.4 Interaction of Catalyst metal with surface functional groups of carbon 59
2.11.5 Summary of literature review on functionalization 61
2.12 Hydrotreating applications of carbon supported catalysts 61
2.12.1 Hydrotreating using activated carbon and CNT supported catalysts 62
2.12.2 Hydrotreating applications of mesoporous carbon supported catalysts 65
2.13 Catalyst deactivation 69
2.13.1 Deactivation by Coke 69
2.13.1.1 Coking propensity: Carbon vs Alumina 71
2.13.2 Metal deposition 72
2.13.3 Poisoning 74
2.13.4 Change in catalyst structure / Sintering 75
2.14 Kinetic study 76
2.14.1 Hydrodynamics parameters 76
2.14.2 Mass transfer effects 78
2.14.3 Kinetic models 81
2.14.4 Power law model 82
2.14.5 Langmuir-Hinshelwood models 83
2.14.6 Multi-Parameter model 85
CHAPTER 3. EXPERIMENTAL 87
3.1 Preparation of mesoporous carbon support 87

3.1.1 Preparation of Primary template 87
3.1.2 Preparation of mesoporous carbon 88
3.2 Functionalization of carbon supports 93
3.3 Preparation of NiMo Catalysts 93
3.4 Support and Catalyst Characterization 95
3.4.1 N_2 Physical Adsorption 95
3.4.2 Thermogravimetric Analysis 95
3.4.3 Boehm Titration 95
3.4.4 Fourier Transform Infrared Spectroscopy (FTIR) 96
3.4.5 Transmission Electron Microscopy 96
3.4.6 Scanning Electron Microscopy 96
3.4.7 X-Ray Diffraction (XRD) 97
3.4.8 Small Angle X-Ray Scattering (SAXS) 97
3.4.9 Elemental analysis 98
3.4.10 Raman Spectroscopy 98
3.4.11 Temperature Programmed Reduction 99
3.5 Hydrotreating activity study 100
3.5.1 Analysis of sulphur and nitrogen: 106
3.5.1.1 Estimation of nitrogen: 106
3.5.1.2 Estimation of sulphur: 107
3.5.2 Simulated distillation: 107
3.6 Study of effectiveness on functionalization (Phase-I) 108
3.7 Optimization of metal loading (Phase-II) 108
3.8 Plan for Kinetic and Long term deactivation study 112
CHAPTER 4. EFFECT OF FUNCTIONALIZATION OF MESOPOROUS CARBON SUPPORT ON THE HYDROTREATING ACTIVITY OF SUPPORTED NiMo CATALYSTS 114
4.1 Characterization of supports 114
4.1.1 N_2 Physical adsorption 114
4.1.2 Thermo Gravimetric Analysis (TGA) 117
4.1.3 Raman Spectroscopy 118

4.1.4 Small angle X-Ray scattering (SAXS) 118
4.1.5 Scanning Electron Microscopy (SEM) 122
4.1.6 Transmission Electron Microscopy (TEM) 122
4.1.7 Fourier Transform Infrared Spectroscopy (FTIR) 126
4.1.8 Boehm Titration 127
4.2 Characterization of catalysts 128
4.2.1 N_2 Physical Adsorption 128
4.2.2 X-Ray Diffraction (XRD) 128
4.2.3 Elemental analysis 129
4.2.4 Scanning Electron and Transmission Electron Microscopy 131
4.2.5 High Resolution Transmission Electron Microscopy (HRTEM) 134
4.3 Hydrotreating activity study 136
4.4 Conclusions: 140
CHAPTER 5. OPTIMIZATION OF METAL LOADING OVER FUNCTIONALIZED MESOPOROUS CARBON SUPPORT 141
5.1 Characterization of catalysts 141
5.1.1 N_2 Physical Adsorption 141
5.1.2 Scanning Electron Microscopy (SEM) 142
5.1.3 Transmission Electron Microscopy (TEM) 144
5.1.4 X-Ray Diffraction 144
5.1.5 Elemental Analysis 148
5.1.6 Temperature Programmed Reduction (H_2-TPR) 149
5.1.7 High Resolution Transmission Electron Microscopy (HRTEM) 149
5.2 Hydrotreating activity study 154
5.3 Conclusions: 160
CHAPTER 6. KINETIC AND LONG TERM DEACTIVATION STUDY 162
6.1 Hydrodynamics in trickle bed reactor 162
6.2 Mass transfer effects 163
6.2.1 External mass transfer evaluation 163
6.2.2 Internal mass transfer evaluation 165
6.3 Effect of variation in process parameters 167

6.3.1 Effect of LHSV 167
6.3.2 Effect of Pressure 168
6.3.3 Effect of Gas-to-Oil ratio 170
6.3.4 Effect of Temperature 170
6.4 Kinetic modeling 173
6.4.1 Power Law model 173
6.4.2 Langmuir-Hinshelwood model 174
6.4.3 Multiparameter model 177
6.5 Long time deactivation study 178
CHAPTER 7. CONCLUSIONS AND RECOMMENDATIONS 180
7.1 Conclusions 180
7.1.1 Phase-I: Effect of functionalization 180
7.1.2 Phase-II: Optimization of metal loading 181
7.1.3 Phase-III: Kinetic and Long term Deactivation Study 181
7.2 Recommendations 182
CHAPTER 8. REFERENCES 183

APPENDIX-A Calculation of molar product concentrations of nitrogen / sulphur and reaction rates of HDN/HDS 204
APPENDIX-B Calculated product concentration for HDS and HDN reactions from Kinetic Study 205
APPENDIX -C Evaluation of external mass transfer resistance for HDS and HDN reactions 207
APPENDIX- D Summary of the external mass transfer resistances study 215
APPENDIX- E Evaluation of internal mass transfer resistances for HDS and HDN reactions 218
APPENDIX-F Summary of isothermality evaluation for NiMo/mC catalyst pellets 225
APPENDIX-G Summary of the dimensionless modulus and effectiveness factors for the internal mass transfer 224

	resistance study - HDS	
APPENDIX- H	Summary of the dimensionless modulus and effectiveness factors for the internal mass transfer resistance study – HDN	226
APPENDIX- I	Effect of operating parameters on HDS and HDN reaction rates	228
APPENDIX- J	Arrhenius plot, Van't hoff plot and Regression plot for kinetic models	
	J-1A: Arrhenius plot for power law model	231
	J-1B: Regression plot for power law model	232
	J-2A: Arrhenius plot for multiparameter model	233
	J-2B: Regression plot for multiparameter model	234
	J-3A: Arrhenius plot for L-H model - I	235
	J-3B: Van't hoff plot for L-H model - I	236
	J-3C: Regression plot for L-H model - I	237
	J-4A: Arrhenius plot for L-H model - III	238
	J-4B: Van't hoff plot for L-H model - III	239
	J-4C: Regression plot for L-H model - III	241
APPENDIX-K	Permissions to use figures	242

LIST OF TABLES

Table 1.1	Canadian Regulation on diesel sulphur content	3
Table 2.1	Relative degree of difficulty in desulphurization	23
Table 2.2	Comparison of relative HDS activity within group	23
Table 2.3	Relation between catalytic activity and required temperature raise	33
Table 2.4	Examples of textural properties of few improved supports and derived catalysts used for hydrotreating	43
Table 2.5	Mesoporous carbon support by volume template synthesis process	50
Table 2.6	Mesoporous carbon support by surface template synthesis process	51
Table 2.7	Summary on the hydrotreating application of mesoporous carbon supported catalysts	67
Table 2.8	Criteria for hydrodynamic parameter evaluation in a trickle bed reactor	78
Table 2.9	Comparison of power law model and L-H model	85
Table 3.1	Characteristics of KLGO feed	109
Table 3.2	Hydrotreating reactor operating conditions	109
Table 4.1	BET surface area, pore diameter and pore volume results of SBA-15 template and mesoporous carbons	115
Table 4.2	BET surface area, pore diameter and pore volume results of mesoporous carbon supported NiMo catalysts	128
Table 4.3	Elemental composition analysis of NiMo/mC catalysts	131
Table 4.4	Summary of characterization results: Phase -I	135
Table 5.1	BET surface area, pore diameter and pore volume results of mesoporous carbon supported NiMo catalysts	142

Table 5.2	Elemental composition analysis of NiMo/mC catalysts	148
Table 5.3	Comparison of MoS_2 stacking distribution in Cat-A and Cat - E	152
Table 5.4	Summary of characterization results: Phase-II	153
Table 6.1	Results of hydrodynamic parameter evaluation	163
Table 6.2	Effect of temperature on conversion	170
Table 6.3	L-H Models for HDS and HDN reactions	171
Table 6.4	Results of L-H Models for HDS and HDN reactions	176

LIST OF FIGURES

Figure 1.1	Sulphur content in various feedstocks	2
Figure 1.2	Trend of product sulphur content in Canadian diesel	2
Figure 2.1	Block diagram of synthetic crude production Units	13
Figure 2.2	Typical process flow diagram of a hydrotreating unit	17
Figure 2.3	Factors affecting effectiveness of hydrotreating process	18
Figure 2.4	Sulphur compounds in petroleum feedstocks	23
Figure 2.5	Typical hydrodesulphurization reactions	25
Figure 2.6	Hydrodesulphurization reaction pathway	26
Figure 2.7	Nitrogen compounds in petroleum feedstock	27
Figure 2.8	Hydrodenitrogenation reaction pathway a. Pyridine conversion b. Quinoline conversion	29
Figure 2.9	Hydrotreating reaction mechanism	30
Figure 2.10	Good characteristics of a support	37
Figure 2.11	Co-Mo-S and Ni-Mo-S model; Monolayer: Co-Mo-S Type-I for γ-Al_2O_3 support or Type-II for carbon support, Multilayer : Type-II for γ-Al_2O_3 support	40
Figure 2.12	Rim-Edge Model	40
Figure 2.13	Volume template synthesis process for the preparation of mesoporous carbon	48
Figure 2.14	Effect of interconnected pores in the preparation of mesoporous carbon	49
Figure 2.15	Mesoporous carbon support by surface template synthesis process	52
Figure 2.16	Mesoporous carbon support by direct synthesis method	53

Figure 2.17	Interaction of Mo on carbon surface a. with carboxylic group; b. with ether like group	60
Figure 2.18	Coke forming reactions	69
Figure 2.19	Diffusion in a chemical reaction	80
Figure 3.1	Flow diagram depicting SBA-15 synthesis	90
Figure 3.2	Experimental set up for carbonization	91
Figure 3.3	Process sequence in the synthesis of mesoporous carbon support	92
Figure 3.4	Experimental set up used for the functionalization of mesoporous carbon	94
Figure 3.5	Experimental set up for hydrotreating activity study	103
Figure 3.6	Reactor catalyst loading diagram	104
Figure 3.7	Work flow diagram for Phase-I	110
Figure 3.8	Hydrotreating study plan	111
Figure 3.9	Work flow diagram for Phase-II	113
Figure 4.1	N_2 Physical Adsorption isotherm of SBA-15 and mesoporous carbon supports	116
Figure 4.2	Thermogravimetric analysis data of mesoporous carbon support	117
Figure 4.3	Raman spectroscopy results of virgin and functionalized mesoporous carbon supports	119
Figure 4.4	SAXS data of SBA-15 and mesoporous carbon support	120
Figure 4.5	SAXS data of functionalized carbon supports	121
Figure 4.6	SEM images of functionalized mC supports a. mC-6M, b. mC 8M	123

Figure 4.7	Transmission Electron Microscopy images of virgin and functionalized mesoporous carbon supports. a. SBA-15, b. mC-0M, c. mC-6M, d. mC-8M.	124
Figure 4.8	FTIR spectra of virgin and functionalized mesoporous carbons	127
Figure 4.9	Broad angle XRD results of mesoporous carbon supported catalysts. a. mC-0M, b. Cat- 2M, c. Cat- 4M, d. Cat -6M, e. Cat - 8M	130
Figure 4.10	Scanning Electron Microscopy images of Cat - 6M	132
Figure 4.11	Transmission Electron Microscopy images of Cat - 6M	133
Figure 4.12	HRTEM images of Cat-6M	134
Figure 4.13	HDS activity comparison of NiMo catalysts supported on functionalized mesoporous carbons	138
Figure 4.14	HDN activity comparison of NiMo catalysts supported on functionalized mesoporous carbons	139
Figure 5.1	N_2 physical adsorption isotherm of NiMo/mC catalysts	143
Figure 5.2	SEM images of mC supported NiMo Catalysts a. Cat-A; b. Cat-E; c. Cat-C; d. Cat-D	145
Figure 5.3	TEM images of mC supported NiMo Catalysts a. Cat-A; b. Cat-E; c. Cat-C; d. Cat-D	146
Figure 5.4	XRD data of mC supported NiMo catalysts	147
Figure 5.5	Temperature programmed reduction results of mC supported NiMo catalyst (Cat-E)	150
Figure 5.6	HRTEM images of mC supported NiMo catalysts (Cat-A and Cat-E)	151

Figure 5.7	HDS activity comparison of NiMo/ mC catalysts with varying Mo loading	156
Figure 5.8	HDN activity comparison of NiMo/ mC catalysts with varying Mo loading	157
Figure 5.9	HDS activity comparison of NiMo/ mC catalysts with varying Ni loading	158
Figure 5.10	HDN activity comparison of NiMo/ mC catalysts with varying Ni loading	159
Figure 6.1	Effect of variation in LHSV	169
Figure 6.2	Effect of variation in Pressure	171
Figure 6.3	Effect of variation in Gas-to-oil ratio	172
Figure 6.4	Long term deactivation study results of optimum NiMo/mC catalyst	179

NOMENCLATURE

β_{HDS}	Isothermality ratio for the catalyst pellet in a hydrodenitrogenation reaction, dimensionless
β_{HDN}	Isothermality ratio for the catalyst pellet in a hydrodesulphurization reaction, dimensionless
γ_P	Tortuosity of the catalyst pellets, dimensionless
$\Delta\rho_T$	Temperature density correlation, lbs/ft3
$\Delta\rho_P$	Pressure density correlation, lbs/ft3
$\Delta H_{R,HDN}$	Heat of the hydrodenitrogenation reaction, kJ/mol
$\Delta H_{R,HDS}$	Heat of the hydrodesulphurization reaction, kJ/mol
ε	Catalyst bed porosity, dimensionless
ε_P	Porosity of the catalyst pellets, dimensionless
$[\eta_O]_N$	Effectiveness factor at the inlet of the hydrodenitrogenation reaction, dimensionless
$[\eta_P]_S$	Effectiveness factor at the inlet of the hydrodesulphurization reaction, dimensionless
$[\eta_O]_N$	Effectiveness factor at the outlet of the hydrodenitrogenation reaction, dimensionless
$[\eta_P]_S$	Effectiveness factor at the outlet of the hydrodesulphurization reaction, dimensionless
$[\Phi_O]_N$	Dimensionless Thiele modulus at the inlet of the hydrodenitrogenation reaction
$[\Phi_O]_S$	Dimensionless Thiele modulus at the inlet of the hydrodesulphurization reaction
$[\Phi_P]_N$	Dimensionless Thiele modulus at the outlet of the hydrodenitrogenation reaction
$[\Phi_P]_S$	Dimensionless Thiele modulus at the inlet of the hydrodesulphurization reaction

λ_{H_2}	Hydrogen solubility in KLGO, mL/(kg·MPa)
λ_N	Adsorption energy for all nitrogen heteroatoms within coker light gas oil, J/mol
λ_S	Adsorption energy for all sulfur heteroatoms within coker light gas oil, J/mol
μ_L	Viscosity of KLGO at the operating temperature, g/(s·cm)
$\rho_{15.6}$	Density of KLGO at 15.6°C, g/mL
ρ_T	Density of KLGO at the operating conditions, g/mL
a_L	Interfacial surface area over unit volume of a catalyst, cm^{-1}
a_S	Liquid/solid interfacial surface area, cm^{-1}
°API	American Petroleum Institute gravity of petroleum liquids, dimensionless
A	Arrhenius constant, $(mol/L)^{(1-n)}$ s^{-1}
'A'	Reacting species – sulphur or nitrogen
AC	Activated carbon
BET	Brunauer-Emmett-Teller method
BP	Biphenyl
BPCV	Back pressure control valve
c	Empirical constant for LHSV in multiparameter model
C_A	Concentration of reacting species 'A' (sulphur or nitrogen), mol/L
C_{H_2}	Hydrogen concentration in the liquid phase at equilibrium, mol/L
CCVD	Catalytic chemical vapour deposition
CHB	Cyclohexyl benzene
CNT	Carbon nanotubes
CRU	Catalytic reforming unit
d_P	Average diameter of the catalyst particles, cm
$[D_N]_E$	Effective diffusivity of organonitrogen compounds, cm^2/g

$[D_S]_E$	Effective diffusivity of organosulfur compounds, cm^2/g
D_L	Diffusivity of hydrogen in KLGO, cm^2/s
D_N	Bulk diffusivity of organonitrogen compounds, cm^2/g
D_S	Bulk diffusivity of organosulfur compounds, cm^2/g
DBT	Dibenzothiophene
DCH	Dicyclohexyl
DMDBT	Dimethyl dibenzothiophene
E_A	Activation energy for the hydrotreating reaction of species 'A', J/mol
EOR	End of run
FBP	Final boiling point
FCC	Fluidized catalytic cracker
FID	Flame ionization detector
FTIR	Fourier transform infrared
G/O	Gas-to-oil ratio
h	Empirical constant for hydrogen partial pressure in multiparameter model
HCR	Hydrocracking
HDM	Hydrodemetallization
HDN	Hydrodenitrogenation
HDS	Hydrodesulphurization
H_{H_2}	Henry's constant for hydrogen in KLGO, $MPa \cdot m^3/mol$
HRTEM	High resolution transmission electron microscopy
IBP	Initial boiling point
I_D	D-band intensity Raman spectroscopy, dimensionless
I_G	G-band intensity Raman spectroscopy, dimensionless
k_A	Rate constant for species 'A' , $(mol/L)^{(1-n)}\ s^{-1}$

K_A	Adsorption rate constant for species 'A', L/mol
$K_{H_2S\ (or\ H_2)}$	Adsorption rate constant for H_2S (or H_2), 1/MPa
k_L	H_2/KLGO mass transfer coefficient – gas/liquid side, cm/s
k_{OVR}	Overall mass transfer coefficient for hydrogen, cm/s
k_S	H_2/KLGO mass transfer coefficient – liquid/solid side, cm/s
k_t	Thermal conductivity of the NiMo/MWCNT catalyst pellet, J/(cm·K)
KLGO	Coker light gas oil
L_A	Liquid mass flow over cross-sectional area, g/(s·cm^2)
LHSV	Liquid hourly space velocity, hr^{-1}
m	Empirical constant for inhibition parameter
mC	Mesoporous carbon
M_{AVE}	Average molecular weight of KLGO, g/mol
n	Reaction order constant, dimensionless
NC	Nanoporous carbon
NOx	Nitrogen oxides
mC	Mesoporous carbon
OPA	Ortho-propylaniline
$P_{H_2\ (H_2S)}$	Partial pressure of hydrogen (or hydrogen sulphide), MPa
PB	Propylbenzene
PCHA-2	Propylcyclohexylamine
PCHE	Propylcyclohexene
PCH	Propylcyclohexane
PV	Pore volume, cm^3/g
q	Empirical constant for G/O ratio in multiparameter model
Q	Quinoline

r_A	Reaction rate of species 'A', mol/(L·s)
R	Universal gas constant, J/(mol-K)
R^2	Coefficient of regression for the reaction models, dimensionless
SA	Surface area, m^2/g
$SAXS$	Small-angle X-ray scattering
$SBA\text{-}15$	Santa Barbara amorphous-15
S_{BET}	Surface area found from BET analysis, m^2/g
SDA	Structure directing agent
SEM	Scanning electron microscopy
SG	Specific gravity, dimensionless
SMI	Support metal interaction
SOR	Start of run
SOx	Sulphur oxides
T_b	Average boiling point of KLGO, K
T_S	Pellet surface temperature, K
TCD	Thermal conductivity detector
TEM	Transmission electron microscopy
$TEOS$	Tetra ethyl ortho silicate
TGA	Thermo gravimetric analysis
$TH\text{-}DBT$	Tetrahydro Dibenzothiophene
$THQ\text{-}1$	1, 2, 3, 4-tetrahydroquinoline
$THQ\text{-}5$	5, 6, 7, 8-tetrahydroquinoline
TPR	Temperature programmed reduction
v_C	Critical specific molar volume of KLGO, mL/mol
v_{Cm}	Critical specific mass volume, mL/g

v_i	Molar volume of sulphur/nitrogen under standard conditions, mL/mol
v_L	Molar volume of KLGO under standard conditions, mL/mol
v_N	Hydrogen molar volume at standard conditions, L/mol
V_b	Hydrogen molar volume at the normal boiling point, mL/mol
V_C	Volume of loaded catalyst, mL
V_P	Total pore volume, cm^3/g
$WHSV$	Weight hourly space velocity, h^{-1}
x_{HDN}	Stoichiometric ratio of H_2 consumption for nitrogen removal, dimensionless
x_{HDS}	Stoichiometric ratio of H_2 consumption for sulphur removal, dimensionless
XRD	X-ray diffraction

CHAPTER 1

INTRODUCTION

Industrial development has revolutionized the living standards of human, but has introduced additional problem in terms of increased pollution. Automobile emissions using hydrocarbon fuels are one of the significant contributors of pollution and hence Governments around the world have introduced very stringent environmental regulations.

The conventional source of crude oil with low / medium sulphur was the main contributor for the overall crude oil basket in past years. However, the rapid increase in oil consumption and the shortage of low / medium sulphur crude oils have forced the world to turn from the conventional oil source towards heavier non-conventional oil sources. Canada, with its vast oil-sand reserves tops the list of non-conventional oil sources (Ancheyta and Speight, 2007). Heavy oil derived from tar sands / bitumen has large impurities in terms of sulphur, nitrogen and metals, among others. Figure 1.1 provides the comparison on sulphur content of various crude oil sources. From the figure, one can understand the extent of deterioration of quality of feedstock available for processing.

While the feedstock quality is deteriorating, the product sulphur specification has become more stringent as seen from Figure 1.2, which shows average sulphur content in diesel fuel. Table 1.1 provides the Canadian Government specification on sulphur in diesel fuel. Purification of these fuels becomes essential to reduce SOx, NOx emissions, particulate emissions, corrosion in downstream processing equipment and also to increase product stability on storage (Grange and Vanhaeren, 1997)

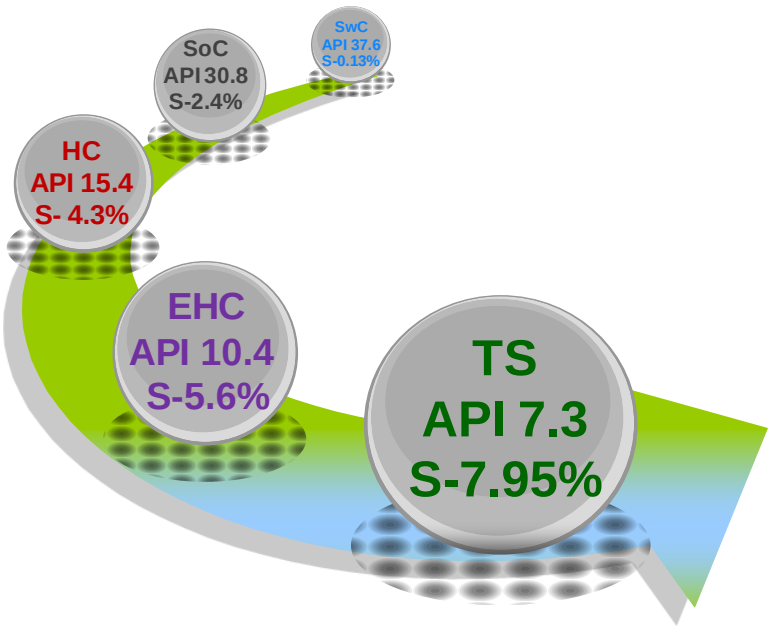

Figure 1.1: Sulphur content in various feedstocks (Jones and Pujado, 2006; Leyva et al., 2007)

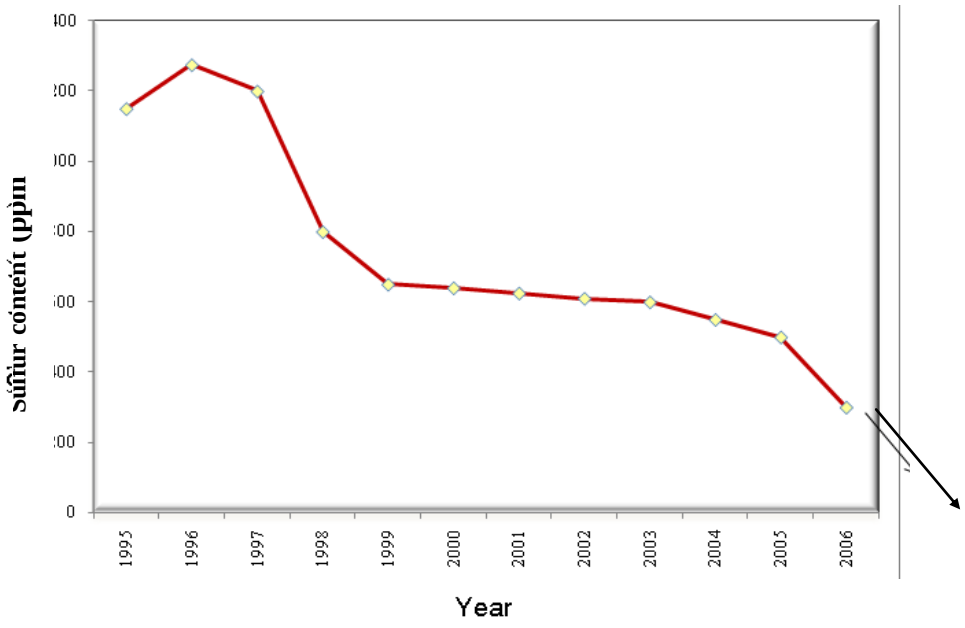

Figure 1.2: Trend of average sulphur content in Canadian diesel fuel (Environment Canada)

Hydrotreating is the widely used process for the removal of sulphur and nitrogen from gas oil. Development of more active hydrotreating catalysts can provide effective solution for tackling the challenges involved in sulphur and nitrogen removal. For the removal of sulphur from 500 ppm to 50 ppm, the catalyst activity should be 4.2 times higher (Knudsen, 1999), thus stressing the importance of extensive research in the field of hydrotreating catalysts. Improvement on hydrotreating catalyst can be done by using new catalyst metals, additives, change of active phase or by using new support materials (Grange and Vanhaeren, 1997). Utilization of new supports has been understood to be an important strategy to develop new catalyst materials (Breysse et al., 2003).

Table 1.1: Canadian Regulation on Diesel sulphur content (Dieselnet)

Fuel	**Sulphur, ppm**	**At production point (year)**	**At Sale point (year)**
On road diesel	500	1997	1998
	15	2006	2006
Off-Road diesel	500	2007	2007
	15	2010	2010
Locomotive and marine	500	2007	2007
	15	2012	2012

Sulphides of transition metals (Mo, W) promoted by other transition metals (Ni, Co) supported on γ- Al_2O_3 are widely used as hydrotreating catalysts for many years (Hussain and Ihm, 2009). γ- Al_2O_3 has good textural as well as mechanical properties. However, its ability to become the best support is retarded by the presence of very high support metal interaction (SMI) which does not help in effective transition of oxide phase of the catalyst into sulphide phase (Sigurdson et al., 2009). Carbon based supports with

good textural properties, mechanical properties and lower SMI can provide effective solution to the problem (Breysse et al., 2003). The order of specific activity of supported CoMo catalysts for the hydrodesulphurization (HDS) of model compounds such as thiophene was found to increase with change in support as Alumina < Carbon (Topsøe and Clausen, 1986). The main reasons for the increased activity of carbon supports were attributed to the lower SMI coupled with higher surface area. Many researchers have studied the utilization of carbon as catalyst support for hydrotreating. Few of the carbon supports found suitable for hydrotreating include activated carbon (Farag et al., 1998; Farag et al., 1999; Kouzu et al., 2003), carbon nanotubes (Sigurdson et al., 2009) and mesoporous carbon (Hussain and Ihm, 2007; Hussain and Ihm, 2009; Lee et al., 2003). Though activated carbons possess very good surface area (Kouzu et al., 2003), their application to gas oil feedstocks is limited by the significant presence of micropores (Lee et al., 2003). Though carbon nanotubes are successfully applied for the hydrotreating of gas oil feedstocks (Eswaramoorthi et al., 2008; Sigurdson et al., 2009), their potential could be restrained by the limited surface area. Mesoporous carbon material has better surface area than carbon nanotube, higher pore volume and pore diameter than activated carbon and it can be a reasonable choice as catalyst support for the hydrotreating of gas oil feedstocks.

Mesoporous carbon supported CoMo catalysts were found to exhibit higher activity than the conventional CoMo/γ-Al_2O_3 catalysts for the HDS of thiophene (Hussain and Ihm, 2009). The increased activity was attributed to the presence of oxygen functional groups, larger pore size and enhanced metal dispersion over the support. The HDS activity of mesoporous carbon supported catalysts was further enhanced by the

incorporation of additional oxygen functional groups by functionalization using nitric acid (Hussain and Ihm, 2009).

The main objective of functionalization is to create large number of hydrophilic groups on the surface (such as -OH and -COOH groups) which can act as the anchors for attaching the catalyst metals (Sigurdson, 2009). Surface functional groups present on carbon surface produce good interaction of oxygen-nickel when present in appropriate quantities and also enhance the promotional effect of nickel to result in better hydrotreating activity (Calafat et al., 1996b). The functional groups are also helpful in creating certain degree of acidity on the support (Bazuła et al., 2008) that can increase catalytic activity.

Bazuła et al. (2008) used nitric acid for functionalizing CMK-3 & CMK-5 and found that the increase in acid concentration helped to increase the amount of surface functional groups, however, with reduction in certain textural properties. Functionalization process decreases certain textural properties such as surface area and pore volume which can affect their effectiveness for their catalytic applications. For gas oil feedstocks, it is necessary to have a balance between such textural properties and other properties such as surface functional groups and acidity.

Because of its higher surface area and pore volume, it might be possible to load more active metals on the surface of the mesoporous of carbon support. Typically, certain commercial catalysts contain 13% Mo, 2.5% Ni with some amount of phosphorous added to it (Sigurdson et al., 2009). Effective higher metal loading can reduce the physical

quantity of the catalyst needed to be filled in the reactor (or possible high throughput for the same volume of catalyst) and can offer some economic advantages.

Studies using mesoporous carbon supported catalysts for the hydrotreating of gas oil is seldom available in the open literature. This research work is focussed on studying the effect of functionalization of mesoporous carbon supports on the hydrotreating activity and analysing the changes in catalyst characteristics due to the variation of nickel and molybdenum loading and their implication on hydrotreating. Furthermore, the HDS and HDN activities of the optimum NiMo/mC catalyst are compared with that of commercial catalyst (active metals supported on γ-Al_2O_3). In addition, kinetic parameter estimation and study on mass transfer effects are also carried out using the optimum NiMo/mC catalyst.

1.1 Knowledge gap:

From the open literature review on new generation hydrotreating catalysts and their applications for gas oil feedstocks, it was found that no study has been done using potentially active mesoporous carbons supports. The studies on hydrotreating using mesoporous carbon supports were only limited to model compounds. However, the results of these studies cannot be directly applied for feedstocks such as coker gas oil, due to the presence of various refractory sulphur compounds which can have different behaviour as well as interference with each other (Ancheyta and Speight, 2007). Moreover, detailed studies on the effects of functionalization of mesoporous carbon supports on the hydrotreating activity of supported NiMo catalysts, using gas oil feedstocks, are not available. In addition, effect of variation in Ni-Mo loading and resultant hydrotreating activity related to mesoporous carbon supports is seldom

available. Macro and micro kinetic studies on mesoporous carbon supported catalysts have not been done in the past. In addition, there is no study available on the durability of the NiMo catalyst supported on mesoporous carbon for long term operation using real feeds.

1.2 Hypothesis:

The hypotheses for the project are

- Nitric acid functionalization will help to improve surface functional groups in mesoporous carbon support
- Lower metal support interaction and higher surface area of functionalized mesoporous carbon supported NiMo catalysts will help to reduce the temperature of reduction and to increase the active metals leading to increased hydrotreating activity compared to that of γ-Al_2O_3 supported hydrotreating catalysts.

1.2.1 Research Objective

The research objective is to develop new mesoporous supported NiMo catalysts with suitable characteristics that can exhibit superior activity for the hydrotreating of coker gas oil (KLGO) derived from Athabasca bitumen. The research project is divided into three main phases to achieve the objective.

1.2.2 Phase I: Effect of functionalization

- Synthesizing mesoporous carbon (mC) support by volume templating process using alkali modified SBA-15 as the primary template; characterizing primary template and derived supports

- Functionalizing the mesoporous carbon support using nitric acid of various concentrations (upto 8M); characterization of all these supports and studying the changes in textural properties due to functionalization
- Preparation and characterization of NiMo catalyst (12%Mo and 2.4% Ni) supported on functionalized mC supports; hydrotreating activity study of these catalysts to identify optimum functionalization and also comparing the activity with that of NiMo/γ-Al_2O_3 catalyst using KLGO feed.

1.2.3 Phase II: Optimization of metal loading

- Preparation and characterization of NiMo/mC catalysts having various Ni and Mo loadings
- Hydrotreating activity study of NiMo/mC catalysts prepared as above, to identify the optimum catalyst, using KLGO feed
- Comparative hydrotreating activity study of optimum catalyst with that of commercial catalyst using KLGO feed.

1.2.4 Phase II: Kinetic studies

- Kinetic parameter study using the optimum NiMo/mC catalyst (identified from Phase-II) for both HDS and HDN reactions
- Long term deactivation study using the optimum NiMo/mC catalyst over KLGO feed.

CHAPTER 2

LITERATURE REVIEW

Information obtained from open literature survey on the hydrotreating process, reaction mechanisms, characteristics of hydrotreating catalysts, effect of supports on catalytic activity, application of carbon supports for hydrotreating and other relevant information are briefly discussed in this literature review section.

2.1 Hydrotreating process

Hydrotreating is the process of removing certain objectionable impurities from petroleum feedstocks by reacting them with hydrogen at high temperature and pressure (Jones and Pujado, 2006) to produce clean fuel. Key reactions that need to be considered in hydrotreating process include,

- Hydrodesulphurization (HDS) – Removal of sulphur from organic compounds in the form of H_2S
- Hydrodenitrogenation (HDN) – Removal of nitrogen from organic compounds in the form of NH_3
- Hydrodeoxygenation (HDO) – Removal of oxygen from organic compounds in the form of H_2O
- Hydrodearomatization (HDA) – Saturation of aromatic compounds
- Mild Hydrocracking (MHC) – Mild Cracking of gas oil molecules into smaller molecules, which in many cases is considered as undesired side reaction.

2.2 Necessity of hydrotreating process

Hydrotreating process plays an important role in upgrading the quality of products derived from petroleum feedstocks. Some of the key factors that necessitate the incorporation of hydrotreating process in a petroleum refinery are described below.

2.2.1 Environmental Concerns

The main factor that necessitates hydrotreating is the pollution associated with sulphur compounds that produces SOx emissions in the atmosphere. Short term exposure to SO_2 can result in asthma symptoms as well as other respiratory problems. Formation of particulate matter by the reaction of SOx with other compounds is a significant concern as these particles can worsen the respiratory problems and aggravate cardiovascular diseases (U.S.Environmental Protection Agency, 28-Jan-2011). The major precursors in the production of acid rain include sulphur and nitrogen oxides. These can result in the acidification of soils causing damage to vegetation, acceleration of corrosion in buildings, generation of smog resulting in decreased visibility, lack of biodiversity and damage to aquatic and terrestrial ecosystems (Clean air trust, 1999; Environment Canada, 01-Feb-2011). NOx can react with volatile organic compounds in the atmosphere in presence of sunlight to form ozone, which can have adverse effect on lung function. Moreover, NOx and ozone can combine with common organic chemicals to form toxic products that can cause biological mutations. As the gaseous pollutants can be transported easily by wind, the problem becomes global, needing serious attention (Wikipedia, 15-Feb-2011). The environmental legislation by the Canadian Government (Table 1.1) reflects the pollution concerns.

2.2.2 Efficient operation of downstream units

Sulphur compounds are serious poisons to many catalysts used in the downstream processing units. For example, a naphtha desulphurization unit is required to protect the noble metal catalyst used in the catalytic reforming unit (CRU) that produces high octane gasoline (Jones and Pujado, 2006) from sulphur poisoning. Nitrogen is a temporary poison to many catalysts. Notably, the presence of excessive nitrogen in fluidized catalytic cracker or hydrocracker unit may necessitate severe operating conditions, leading to accelerated catalyst deactivation (Reza, 2000). Removal of nitrogen to very low levels is sought to handle such processes making it necessary to have hydrotreating units in a fuel processing complex.

2.2.3 Corrosion concerns

Sulphur compounds can produce H_2S in the downstream process units, which can cause corrosion (Jones and Pujado, 2006). This will necessitate increased capital cost affecting the profitability of the process.

2.2.4 Improvement of product quality

Presence of oxygenated compounds in petroleum feedstocks can pose challenges to product stability due to the formation of derivatives that can solidify and create blockings in the downstream process equipment. Hydrotreating can effectively remove such compounds thereby increasing the product stability on storage. Hydrotreating process can help to improve the color, viscosity index and stability of lube oil (Jones and Pujado, 2006). Saturation of some olefins and aromatics can help to improve certain product properties such as cetane number of diesel fuel or smoke point of kerosene fuel

(Ancheyta and Speight, 2007). Hydrodesulphurization process can help to produce products with acceptable odour (Speight, 1999).

2.3 Hydrotreating in tar sands processing

2.3.1 Tar sands upgrading process

Production of synthetic crude oil from Canadian tar sands involves both carbon rejection and hydrogen addition processes. Carbon rejection process (such as delayed coking or fluid coking process) redistributes the carbon number by generating solid coke with lower H/C atomic ratio and fluid product with higher H/C ratio (ratios with reference to the feed). Incorporation of hydrogen into feed molecules by hydrogen addition process (such as hydrotreating) increases the overall H/C atomic ratio of resultant products (Speight, 1999).

Block flow diagram of a typical synthetic crude production process from Canadian tar sands is shown in Figure 2.1 (Yui, 2008). The products from various units (atmospheric distillation, vacuum distillation, fluid coker and ebullated bed hydrocracker) are combined suitably and sent to various hydrotreating units. The final products from hydrotreating units are combined to form synthetic crude oil which is transported to refinery sites as and when required. Hydrogen required for the process is provided by natural gas reforming unit. Offgas containing H_2S from various process units is cleaned in amine treating unit and sent to utilities for power generation. From the processing methods, one can see that hydrotreating process plays an important role in the value addition of Canadian tar sands.

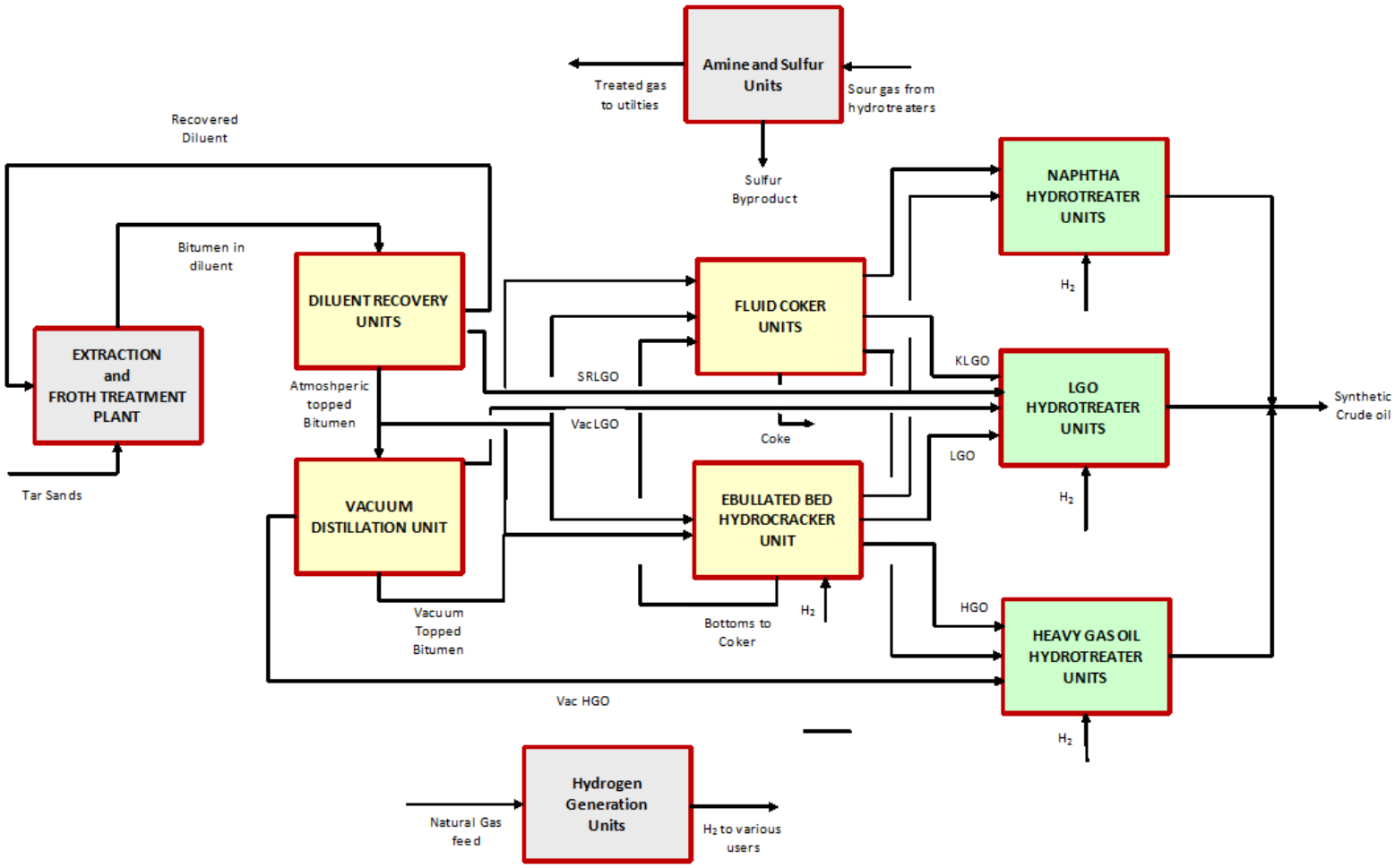

Figure 2.1: Block diagram of synthetic crude production Units (Yui, 2008) (Reproduced with permission)

2.3.2 Hydrotreating process

The process configuration of hydrotreating unit is fundamentally similar for the processing of different gas oil feedstocks. Figure 2.2 shows the typical process flow diagram of a gas oil hydrotreating unit and a brief process description is given below (Jones and Pujado, 2006; Meyers, 2003; Speight, 1999).

2.3.2.1 Feed filtration unit

The gas oil feed can be received as hot feed from the upstream process unit or from an intermediate storage facility. The possibility of contaminants due to corrosion or due to oxygen ingress during storage makes it necessary to have feed filtration system. Automatic backwash filtration systems, which operate based on filter pressure drop or timer (whichever is earlier) are widely used due to safety and ease of operation, though it is possible to use manual filter (disposable cartridge type). The filtered feed is stored in nitrogen blanketed surge drums.

2.3.2.2 Feed preheat section

Gas oil feed from the surge tank is pumped by high pressure pumps (often employed with power recovery turbines using reactor effluent stream) to feed-reactor effluent heat exchangers for preheating the feed. Additional heat exchangers are employed in some cases to recover heat from product streams of fractionation section. Heat integration schemes are necessary for the efficient recovery of heat of reaction. Feed from preheat exchangers is mixed with recycle gas stream and the temperature of the mixture is raised to final temperature (i.e. the reactor inlet temperature) in a fired heater.

In some configurations, preheating of recycle gas is also done using the heat from reactor effluent stream before mixing with feed stream.

2.3.2.3 Hydrotreating reactor

The feed-recycle gas mixture is introduced into the reactor containing hydrotreating catalyst. To achieve efficient wetting of catalyst, vapor-liquid distributors are used in the reactor. The size of the reactor widely depends on mass velocity, pressure drop and other design conditions. The length of the catalyst bed is often limited by the overall temperature raise created by the exothermic reaction. If the maximum allowable overall temperature raise of 42°C is not breached, single catalyst bed is sufficient. In other cases, multiple beds are employed with intermediate cold recycle gas quench streams to control temperature raise.

2.3.2.4 Vapor liquid separation section

The reactor product stream containing the hydrotreated liquid product and gaseous components (NH_3, H_2S, H_2 and off gas if any), called as reactor effluent is heat exchanged with feed and/or recycle gas stream. Depending on heat integration schemes, multiple separator vessels are employed for vapor liquid separation. In a typical scheme, hot high pressure separator (HHPS) is used to flash the lower boiling materials for achieving heat recovery followed by cold high pressure separator (CHPS) and cold low pressure separator (CLPS) to achieve further separation. Power recovery turbines are often employed to recover the pressure energy from reactor effluent (between CHPS and CLPS). Gaseous stream from the separators is sent to the reactor directly if H_2S content is very low (<3 % v/v) or through a recycle gas scrubber system for reducing H_2S content.

Make up hydrogen gas is added to the recycle gas stream to maintain the hydrogen concentration in recycle gas.

The liquid streams from CHPS and CLPS are combined and sent to the stripper column to remove dissolved gases and residual H_2S. Liquid product from stripper is sent to the fractionation section.

2.3.2.5 Water wash system

Reactor effluent stream from CHPS contains NH_3 and H_2S which can form ammonium salts that can cause corrosion and fouling in pipelines and in exchangers. Continuous stream of wash water is injected in the reactor effluent stream to keep ammonium salts dissolved in water so that they are not precipitated.

2.3.2.6 Fractionation section

Liquid product after removal of dissolved gases is sent to the fractionation section. The configuration of fractionation section depends on the quality of feedstock and desired end product. In this section, various product streams such as naphtha, diesel and heavy oil are separated according to their final product specification. If the final product is a component of synthetic crude oil, extensive fractionation process may not be required.

2.4 Factors affecting hydrotreating process

The factors affecting the effectiveness of hydrotreating process can be divided into three categories as shown in Figure 2.3 (Mapiour, 2009).

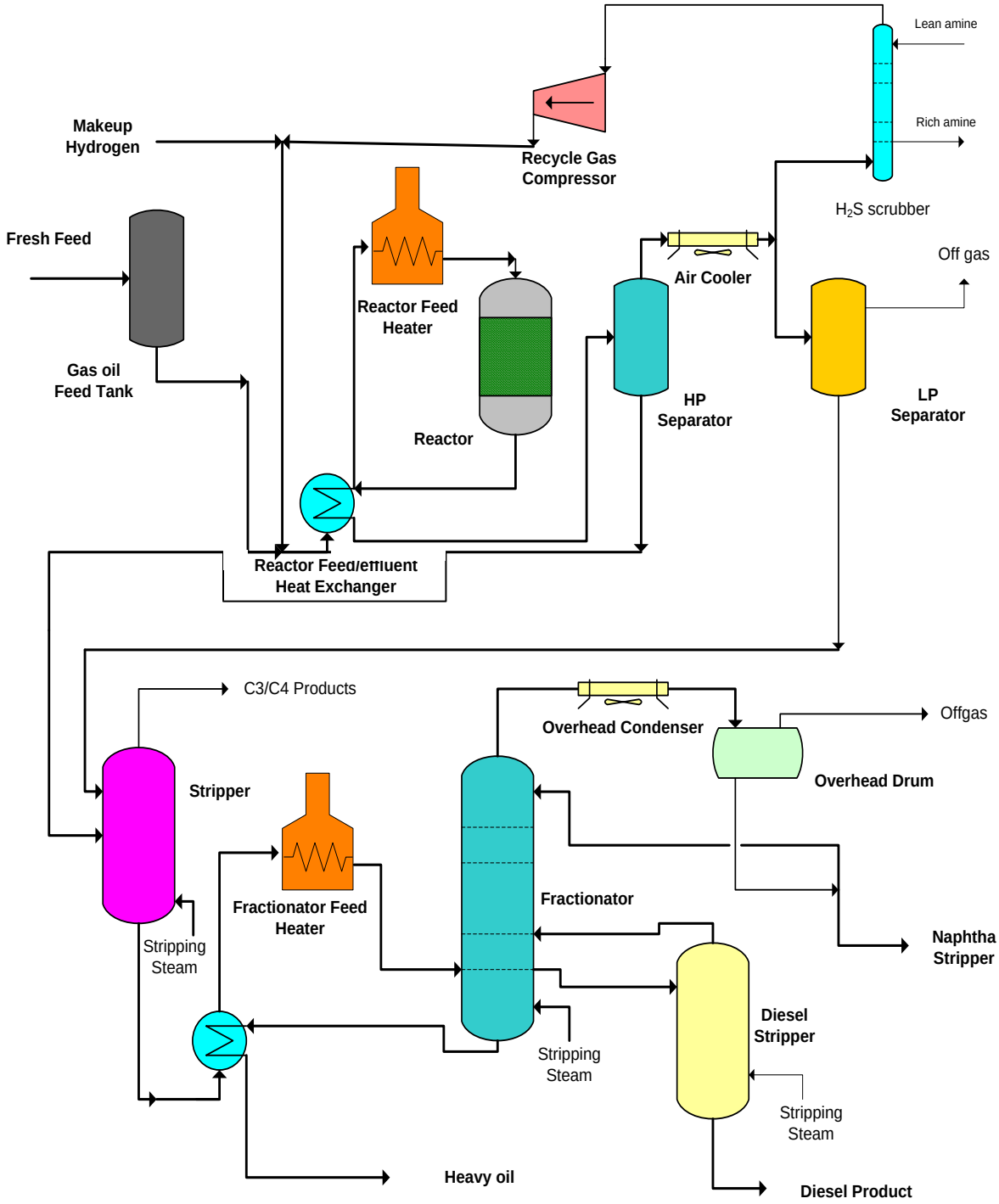

Figure 2.2: Typical process flow diagram of a hydrotreating unit (Jones and Pujado, 2006)

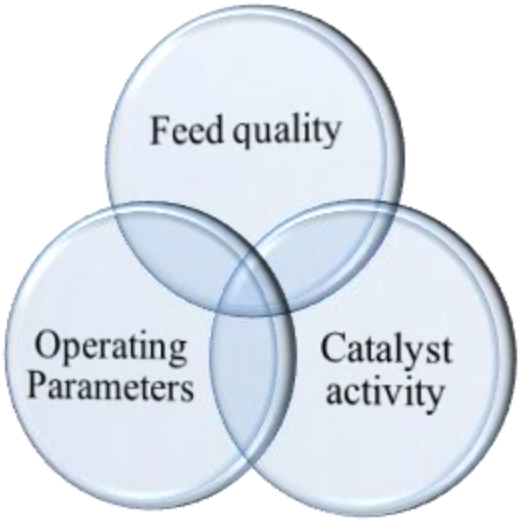

Figure 2.3: Factors affecting effectiveness of hydrotreating process (Mapiour, 2009)

2.4.1 Feed quality

The design parameters of the hydrotreating reactor and the quantity of catalyst loaded are based on the quality of feedstock to be processed in the reactor (Jones and Pujado, 2006). Extensive variation in feed quality will force the plant operators to raise the reactor temperature in order to maintain constant conversion, leading to accelerated deactivation of the catalyst. Some of the parameters that are used to define feed quality in a commercial reactor include,

- Density (or specific gravity) / API gravity
- Boiling range (Distillation)
- Carbon residue content
- n-heptane (or n-pentane) insolubles
- Sulphur and nitrogen content

A reduction in API gravity for the same boiling range indicates the increased presence of unsaturate content. Hydrogen consumption can be much higher for processing such feeds and can limit the plant operation if not designed suitably. This is also an indication of coke forming materials in feed. Carbon residue is indicative of residue forming material that is present in the feed (this excludes metal content). In general, higher the carbon residue content, heavier the feed. Asphaltene content was measured by n-heptane insoluble analysis. Higher asphaltene content indicates the increased presence of coke forming components. Nitrogen compounds can cause inhibition to HDS reactions and the product sulphur content can be affected by the excessive presence of nitrogenous compounds. Higher final boiling point of feedstock indicates the presence of tough-to-remove refractory sulphur and nitrogen compounds.

2.4.2 Process conditions

Various process conditions that are needed to be maintained for efficient operation a hydrotreating reactor are given below (Jones and Pujado, 2006; Meyers, 2003).

2.4.2.1 Liquid hourly space velocity (LHSV)

LHSV is defined as,

$$LHSV = \frac{Feed\ rate\ m^3/hr}{Catalyst\ loaded\ in\ reactor,\ m^3}$$

The design of the reactor is specified by LHSV. Changing the feed rate extensively (i.e. LHSV change) can affect the product quality and /or catalyst life.

2.4.2.2 Hydrogen partial pressure

In industrial reactor, hydrogen partial pressure is the product of % hydrogen in recycle gas and system pressure. Lower H_2 partial pressures than design values are not desired due to lower aromatic conversion and increased coking propensity. Higher than desired H_2 partial pressure can lead to increased need in capacity of equipments thereby increasing the capital costs. An optimum balance has to be maintained between H_2 partial pressure and capital cost.

2.4.2.3 Gas-to-oil ratio

Gas-to-oil ratio is defined as

$$Gas - to - oil\ ratio = \frac{Total\ gas\ flow\ to\ the\ reactor\ , Nm^3/hr}{Feed\ flow\ rate, m^3/hr}$$

Hydrogen rich recycle gas act as heat sink for removing the exothermic heat of reaction from the catalyst and also helps in distribution of feed over the catalyst bed. A generally accepted minimum gas flow rate is at least four times the amount of hydrogen consumption. Hydrogen consumption in the hydrotreating process is determined by summation of following parameters,

- Chemical hydrogen consumption
- Solution losses
- Mechanical losses
- Venting losses.

In addition, recycle gas purity needs to be maintained above certain minimum level in order to maintain H_2 partial pressure and also to limit the impurities concentration. This is done by – venting the offgas from high pressure separator, H_2S

removal by amine absorption and also by increasing the purity of makeup hydrogen from supplier units.

2.4.2.4 Reactor temperature

The most important parameter in hydrotreating process is the reactor temperature. The activity loss due to deactivation of catalyst is compensated by increasing the reactor inlet temperature. Catalyst replacement in the reactor is done when it is no longer possible to increase the reaction temperature in order to maintain the desired conversion levels due to catalyst deactivation. The reactor outlet temperature is controlled by removing the exothermic heat of reaction through quench recycle gas.

2.4.3 Catalyst

Catalytic activity has a pronounced effect on hydrotreating reaction. Utilization of highly active catalysts can have impact on process configuration and economics of the process.

2.5 Hydrotreating reactions

Hydrotreating reactions are exothermic and generate considerable amount of heat that needs to be taken into account while designing a reactor (Jones and Pujado, 2006). The reaction of heteroatoms are not generally limited by thermodynamics, however, the hydrotreating of aromatics are limited by thermodynamic considerations (Ancheyta and Speight, 2007). Important hydrotreating reactions, reaction mechanisms and thermodynamics associated with those reactions are discussed in this section.

2.5.1 Hydrodesulphurization reactions

Sulphur is generally found in all boiling range of petroleum fractions in a variety of compounds. Most of these sulphur compounds can be classified into six categories, namely, mercaptans, sulphides, disulfides, thiophenes, benzothiophenes and dibenzothiophenes (Jones and Pujado, 2006). Figure 2.4 shows the chemical structure of some of these sulphur compounds present in gas oil feedstocks. Among the various sulphur compounds, mercaptans and sulphides are easy to convert. Table 2.1 provides a comparison of relative degree of difficulty in converting the sulphur compounds.

Table 2.1: Relative degree of difficulty in desulphurization (Jones and Pujado, 2006)

Sl	Sulphur Compound	Relative degree of difficulty in desulphurization
1	Disulfide	1
2	Thiophene	5
3	Benzothiophene	16
4	Dibenzothiophene	20

In lighter feedstocks such as naphtha, the sulphur compounds are generally present in the form of mercaptans and sulphides, hence easier to remove. However, the presence of benzothiophene and dibenzothiophenes in gas oil feeds makes the desulphurization process difficult and challenging (Jones and Pujado, 2006). Even within the group of compounds the relative activity towards desulphurization can be quite different (Table 2.2) and the presence of various types of such sulphur compounds in real feeds reinforces the challenges in hydrotreating. Figure 2.5 shows the chemical reactions involving these sulphur compounds (Ancheyta and Speight, 2007; Jones and Pujado, 2006).

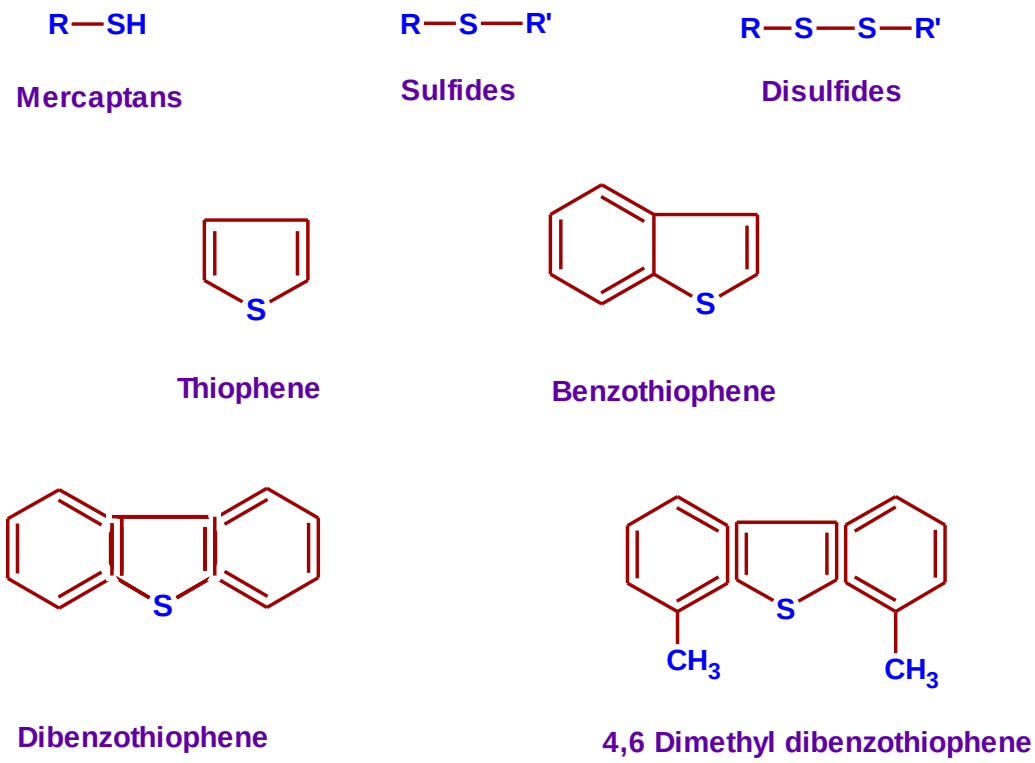

Figure 2.4: Sulphur compounds in petroleum feedstocks (Jones and Pujado, 2006)

Table 2.2: Comparison of relative HDS activity within group

Type of sulphur compound	**Relative Activity within group**
Thiophene	2,5-dimethyl < 2-methyl < no added group < 3-methyl
Benzothiophene	3-methyl < 2-methyl = no added group 3,7 – dimethyl < 3-methyl = 2-methyl = 7-methyl < no added group
Dibenzothiophene	4,6-dimethyl < 4-methyl < no added group < 3,7-dimethyl < 2,8 – dimethyl

Hydrotreating reactions are generally considered to follow two pathways and the preferred pathway depends on the structure of sulphur compound (Girgis and Gates, 1991; Speight, 1999)

- The first pathway can be direct removal of sulphur (direct hydrogenolysis) without any saturation of aromatic ring. (DDS route)
- The second pathway can be through hydrogenation of aromatic ring followed by C-S cleavage (HYD route). This process consumes more hydrogen and can produce products with high cetane number.

Typical reaction pathways for the HDS of dibenzothiophene are provided Figure 2.6. When DDS route is the reaction pathway, the product of HDS reaction is biphenyl compounds (BP). However, the products of HYD pathway can be cyclohexylbenzene (CHB), which is due to partial hydrogenation and dicyclohexyl (DCH), which is the product of complete hydrogenation. The intermediate product in the HYD pathway can be tetrahydro dibenzothiophene (TH-DBT)

Hydrotreating reactions of gas oil are industrially carried out at high pressures (9 – 14 MPa) and moderate temperatures (317 – 425^{o}C) and the reactions are exothermic (Speight, 1999). Equilibrium constants for hydrodesulphurization reactions (estimated by group contribution methods) were found to be positive in most cases for the temperatures below 350° C (at 10 MPa) indicating that desulphurization reactions can be irreversible for these conditions (Ancheyta and Speight, 2007). However at higher temperatures (around 400°C) the equilibrium constant values for dibenzothiophene hydrogenation indicate reverse reaction (Ancheyta and Speight, 2007) which can affect the HDS conversions of gas oil when hydrogenation pathway is the primary route for HDS reaction.

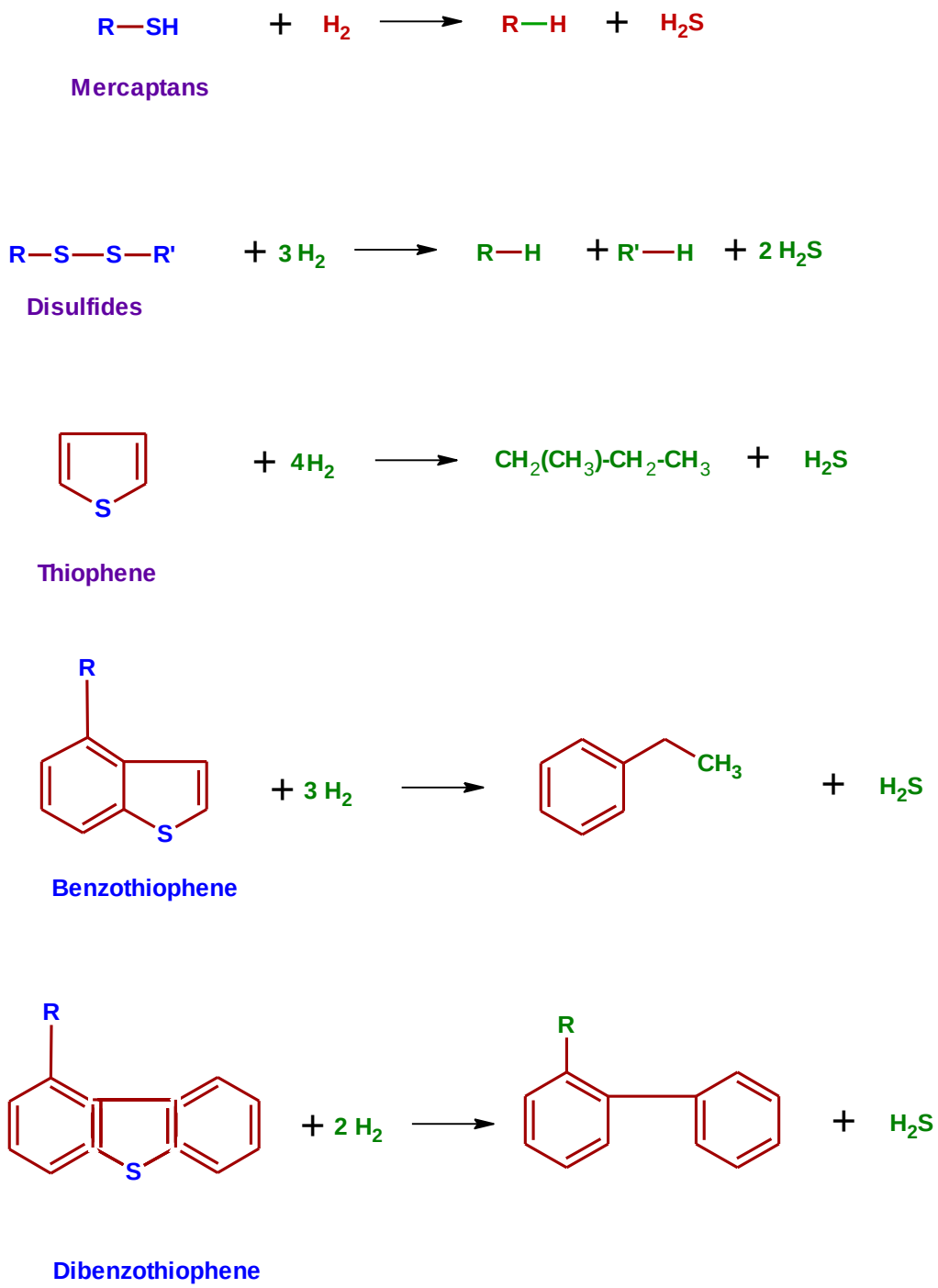

Figure 2.5: Typical hydrodesulphurization reactions (Ancheyta and Speight, 2007; Jones and Pujado, 2006)

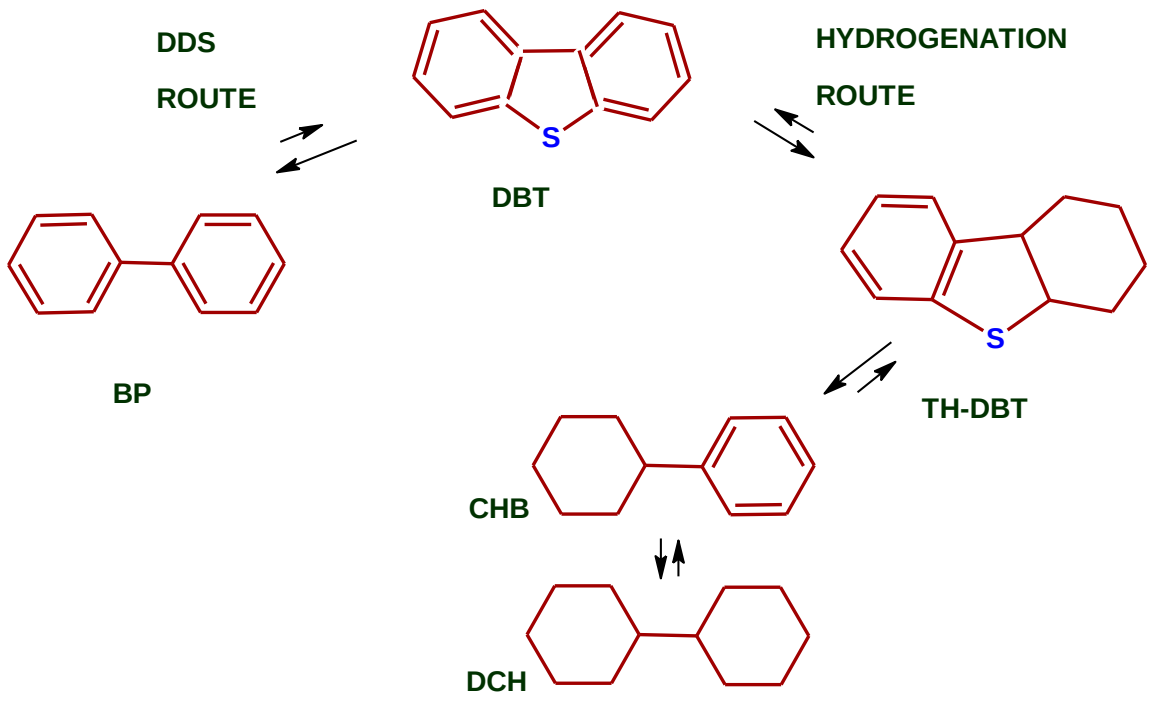

Figure 2.6: Hydrodesulphurization reaction pathway (Girgis and Gates, 1991; Speight, 1999) (Reproduced with permission)
(DBT- Dibenzothiophene; BP- Biphenyl; TH-DBT- Tetrahydro Dibenzothiophene; CHB – Cyclohexyl benzene; DCH- dicyclohexyl)

2.5.2 Recombination reactions

During the desulphurization of naphtha, it was observed that some of the alkenes recombine with H_2S to form mercaptans resulting in increased sulphur content in product (Ancheyta and Speight, 2007). Equilibrium constants for the reactions are higher at lower temperatures indicating that these reactions can occur when the reactor effluent passes through the heat exchanger train. This needs to be taken into account for light gas oil if it contains significant naphtha precursors.

2.5.3 Hydrodenitrogenation reaction

Nitrogen in petroleum fractions is generally present as unsaturated heterocyclic compounds. Some amount of non-heterocyclic nitrogen compounds such as anilines, aliphatic amine and nitriles are also found in the fractions. Non-heterocyclic compounds are relatively more reactive than heterocyclic compound and hence easier to denitrogenate (Cocchetto and Satterfield, 1976). Nitrogen compounds can be basic (such as quinoline, acridine) or non-basic (such as indole, carbazole) (Ancheyta and Speight, 2007). Figure 2.7 shows some of the nitrogen compounds present in petroleum feedstocks.

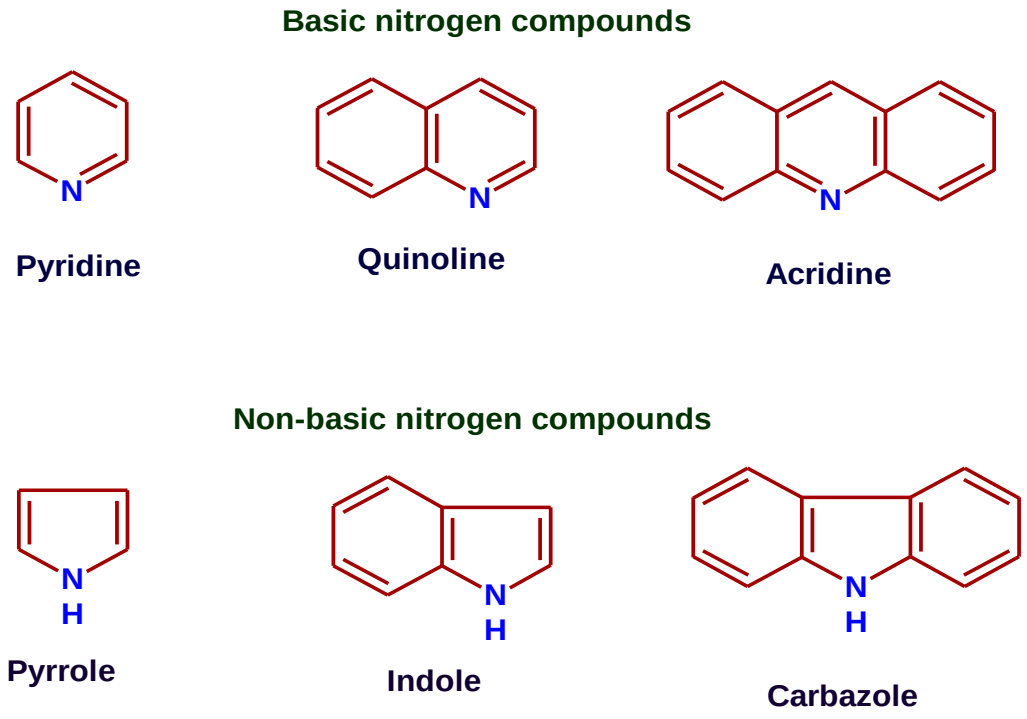

Figure 2.7: Nitrogen compounds in petroleum feedstock

The reactivity of nitrogen compounds are generally found as (Schulz et al., 1986)

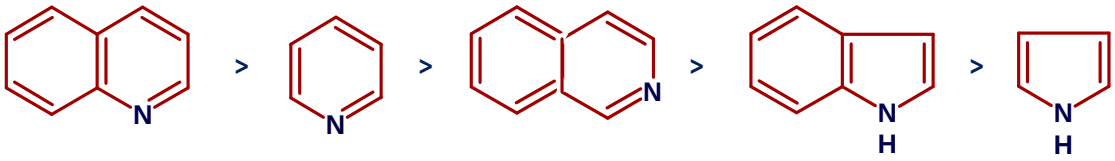

From the above comparison it can be seen that non-basic nitrogen compounds have lower reactivity than basic nitrogen compounds.

HDN reactions of heterocyclic compounds are generally preceded by aromatic saturation in contrast to HDS reaction wherein direct desulphurization is a possible pathway. This is because the cleavage of C(aromatic)-N requires much higher energy (615 kJ/mol) compared to C(aliphatic)-N bond cleavage (305 kJ/mol) favouring ring saturation (Ancheyta and Speight, 2007) whereas the C=S or C-S bond energies are equal at 536 KJ/mol (Mapiour, 2009). Thus hydrogenation pathway is not thermodynamically advantageous for HDS whereas the same pathway is advantageous for HDN. The HDN reaction involves three major steps,

- Saturation of aromatic ring containing N
- Cleavage of C-N bond , forming an amine intermediate
- Hydrogenolysis of amines to hydrocarbons and ammonia

A typical HDN reaction pathway of pyridine that produces piperidine, n-pentylamine and n-pentane is given in Figure 2.8a (Sonnemans et al., 1976). The HDN reaction pathway of quinoline is not as simple as pyridine and is shown in Figure 2.8b (Cocchetto and Satterfield, 1981).

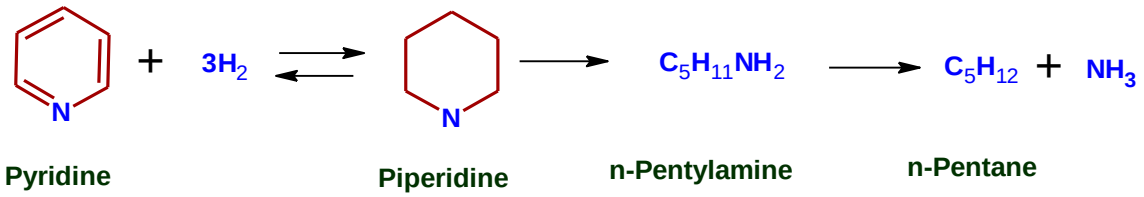

a. Pyridine conversion

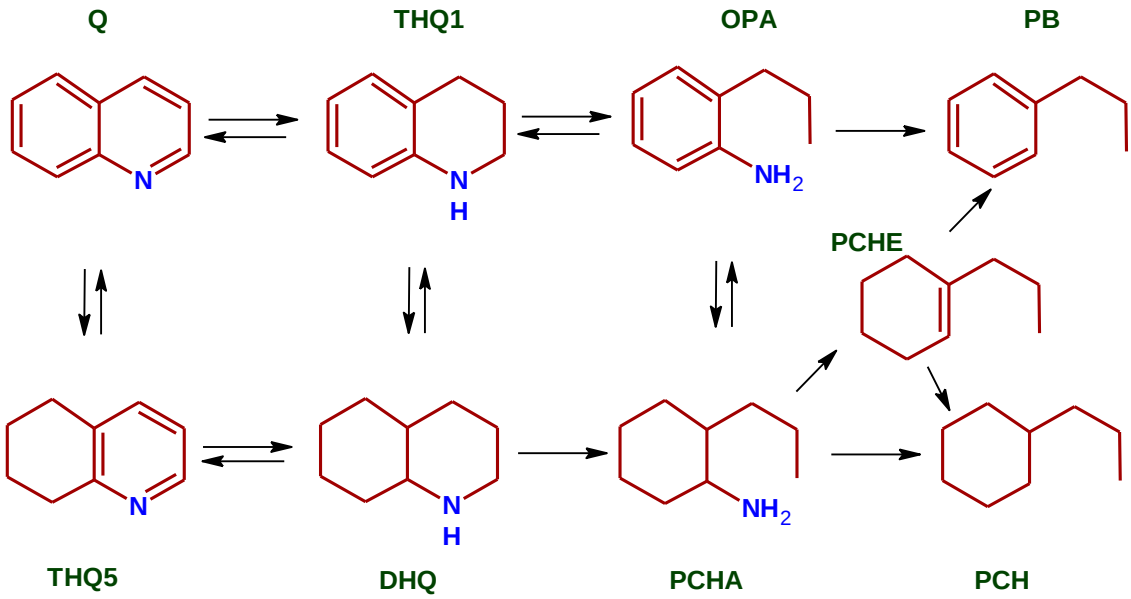

b. Quinoline conversion

Figure 2.8: Hydrodenitrogenation reaction pathway (Reproduced with permission)

a. Pyridine conversion (Sonnemans et al., 1976)

b. Quinoline conversion (Cocchetto and Satterfield, 1981)

(Q - quinoline; THQ - 5,5,6,7,8-tetrahydroquinoline; DHQ - decahydroquinoline; THQ - 1,1,2,3,4-tetrahydroquinoline; OPA - *ortho*-propylaniline; PB – propylbenzene; PCHA - 2-propylcyclohexylamine; PCHE - propylcyclohexene; PCH - propylcyclohexane)

2.5.4 Reaction mechanism

The reaction mechanism for HDS is explained by the concept of vacancies (Mochida and Choi, 2004) as shown in Figure 2.9. Upon sulfidation, the oxide catalysts are converted into metal sulphide species. Reaction of hydrogen with the sulphide group results in the generation of H_2S product as well as sulphur vacancy on the catalysts. The vacant site is thermodynamically unstable compared to the stable non-vacant site and hence there will be a propensity to recreate the original (non-vacant) sites. This propensity acts as the driving force for sulphur compounds to occupy the sites and relieve the 'S' atom on the site. The desulphurized product desorbs from the active site making vacancy for further reaction.

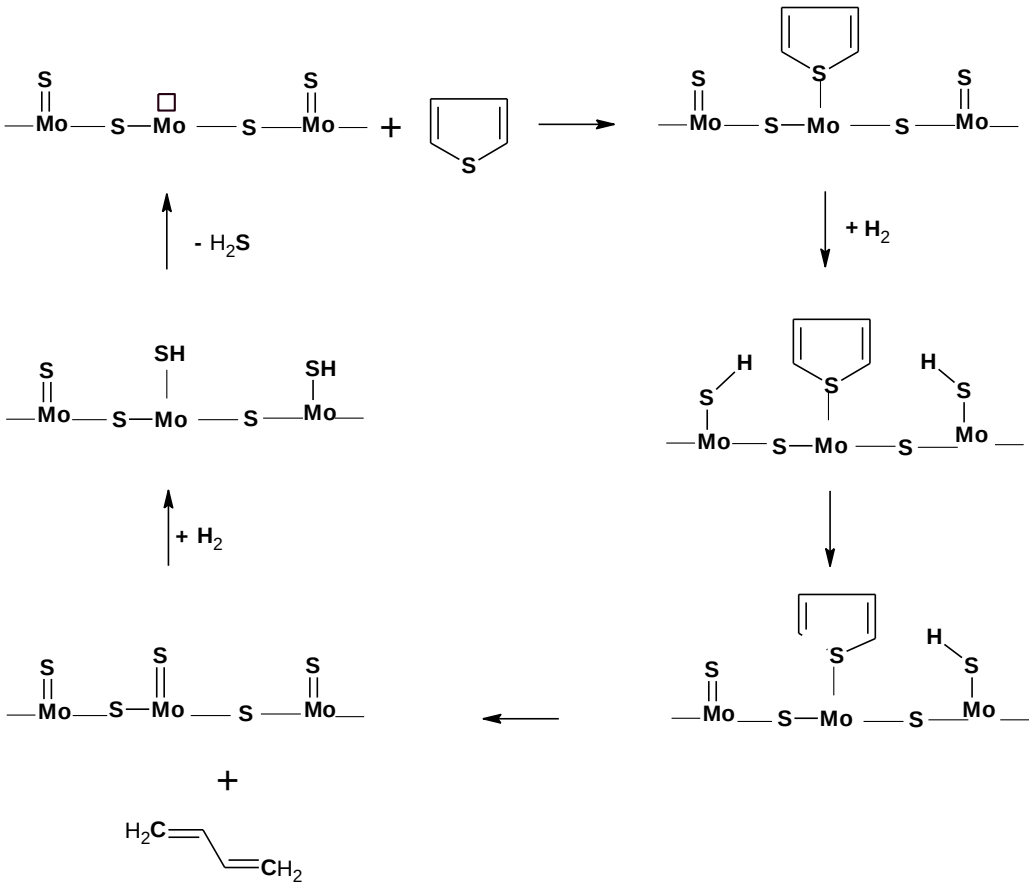

Figure 2.9 Hydrotreating reaction mechanism (Mochida and Choi, 2004)

2.6 Hydrotreating catalysts

Hydrotreating catalysts essentially consist of active metals and promoters dispersed over a support. Special additives are added in some occasions. In addition, materials such as binders are added during the preparation step (Satterfield, 1991). The components of hydrotreating catalysts are discussed briefly in this section.

Transition metal sulphides such as Mo and/or W promoted by Co or Ni are widely used as hydrotreating catalyst metals for many years (Grange and Vanhaeren, 1997; Hussain and Ihm, 2009). Notable are the combinations of CoMo, NiMo and NiW. The role of promoter in enhancing the hydrotreating activity of the active metal include,

- Increase in active phase dispersion (De Beer et al., 1974)
- Modification in sulfur-sulfur interaction (Burdett and Chung, 1990)
- creating sulfur vacancies in Co-Mo-S structure (Moses et al., 2009)
- decrease in metal-sulfur bond energy (Nørskov et al., 1992)

CoMo catalysts are found to be very active for HDS reactions but possess less hydrogenation capability (Jones and Pujado, 2006). Due to the lower hydrogenation performance, the hydrogen consumption for a given sulphur content is lower when using CoMo catalysts compared to other combinations.

Ni as a promoter generates increased number of MoS_2 layers (upto 5 layers) compared to that of Co, which primarily generates monolayered stacks (Ryan et al., 1989). In other words, more rim sites are formed in Ni promoted catalyst, compared to that in Co promoted catalyst. These rim sites are considered to be active for hydrogenation activity, whereas the edge atoms are considered to be active for both hydrogenation and direct hydrogenolysis (Daage and Chianelli, 1994). Since HDN

reaction follows hydrogenation pathway (unlike HDS which can have both pathways), Ni promoted catalysts are found to be exhibit superior hydrogenation and HDN activity than CoMo catalysts; this makes NiMo catalyst as the preferred one, when both HDN and HDS are important (Jones and Pujado, 2006). Because hydrogenation is dependent on H_2 partial pressures, the activity of NiMo catalyst for HDS and HDN is found to be more sensitive to hydrogen partial pressures than CoMo catalysts. The preference of NiMo catalyst can be very high when producing feedstocks for other process units (such as FCC, HCR) due to higher HDN as nitrogen creates temporary poisoning effects on the catalysts (such as zeolites). Moreover, the presence of higher amount of unsaturated components in feedstocks (especially in cracked feeds such as coker gas oil used in this project) can result in gum formation while in storage necessitating the use of a catalyst such as NiMo that possess HDS, HDN and hydrogenation potential. As expected, the hydrogen consumption is higher for NiMo catalysts compared to CoMo for the same level of HDS (Jones and Pujado, 2006).

NiW catalysts exhibit highest activity for aromatic saturation (Stanislaus and Cooper, 1994). These catalysts exhibit higher HCR activity compared to NiMo and CoMo, however show very poor HDS activity at the pressures used in hydrotreating process (Jones and Pujado, 2006). Application of NiW is found in selective saturation of one of the double bonds in diolefins in feed that are needed in certain hydrotreating processes (Jones and Pujado, 2006).

In addition to the above set of catalysts, various other combination of these metals (Mo,Co,Ni,W) and utilization of precious metals have been tried for application in hydrotreating by many researchers (Absi-Halabi et al., 1998; Nava et al., 2005; Sigurdson et al., 2008).

γ-Al_2O_3 is widely used as the support in commercial hydrotreating catalysts (Farag et al., 2000). It possesses good mechanical properties, acidity and regenerability (Satterfield, 1991). However, the limitation with γ-Al_2O_3 is its higher metal support interaction that does not facilitate easy generation of active sulphide (MoS_2) species, retarding its ability to become excellent support (Sigurdson et al., 2009). Activity of hydrotreating catalysts supported on γ-Al_2O_3 is found to increase by the incorporation of additives (Sigurdson et al., 2008).

2.7 Catalyst development

Development of more active hydrotreating catalysts can provide effective solution for tackling the challenges involved in sulphur and nitrogen removal. Table 2.3 provides an outlook on relative activity needed to achieve deep desulphurization levels of gas oil (Knudsen, 1999) and from the table one can understand the necessity of developing highly active HDS catalysts.

Table 2.3: Relation between catalytic activity and required temperature raise (Knudsen, 1999)

Product sulphur	Required catalyst activity	Required temperature increase (°C)*
500	Base =1.0	0
350	1.3	+7
200	1.9	+17
100	3.0	+29
50	4.2	+38

* For Co-Mo/Alumina catalyst

Improvement on hydrotreating catalyst can be done by changing active metals, supports, preparation methods and/or incorporating additives (Eswaramoorthi et al., 2008; Eswaramoorthi et al., 2008; Grange and Vanhaeren, 1997).

2.7.1.1 New Catalyst metals

Transition metals Mo and/or W are used as the active metals for hydrotreating process. Utilization of other active metals such as Pt, Pd and Ru has been studied by various researchers in the past (Grange and Vanhaeren, 1997). A comparative study on the hydrotreating activity of ruthenium supported on Y-zeolite and γ-Al_2O_3 with conventional NiMo catalyst supported on γ-Al_2O_3 support showed that ruthenium sulphide catalyst was more active for the HDN of quinoline and not for HDS of dibenzothiophene (Harvey and Matheson, 1986). Research studies on the improvement of hydrotreating catalysts using Pt, Ru, Ir and Re metals have been widely reported in the literature (Ferdous, 2003). However, application of these metals in commercial catalysts was not seen widely, which might be due to the significantly higher costs of these noble metals compared to that of conventionally used transition metals (Furimsky and Massoth, 1999). Their commercial application in hydroprocessing is seen in certain aromatic reduction processes related to diesel fuel (Furimsky and Massoth, 1999)

2.7.1.2 Active phase variation

Hydrotreating catalysts are prepared in oxide state which is then converted into sulphide species in the reactor. Sulphide phase is the active phase for hydrotreating process (Mochida and Choi, 2004). Efforts have been done to create other active phases such as phosphide, carbide and nitride (Choi et al., 1992; Choi et al., 1994; Lee and

Boudart, 1985; Oyama, 1992; Schlatter et al., 1988). Choi et al. (Choi et al., 1992) studied unpromoted Mo-nitride catalyst for the HDN of pyridine and found that the catalytic properties were superior to that of sulfided commercial CoMo catalyst. Superiority of Mo-nitride was reported by Colling and Thompson (Colling and Thompson, 1994) for the HDN of pyridine in comparison with commercial NiMo/γ-Al_2O_3 catalyst. A study by Li et al. (Li et al., 1999) indicated mild increase in catalytic activity by Mo nitride and carbide catalysts for the HDN of indole. Mo carbide exhibited higher activity for the HDN of quinoline, whereas tungsten carbide catalysts showed comparable HDN activity in comparison with commercial sulfided NiMo/γ-Al_2O_3 catalyst. Higher activity of Mo_2C / γ-Al_2O_3 compared to MoS_2 / γ-Al_2O_3 for the HDS of thiophene has been reported by McCrea e al. (McCrea et al., 1997). Superior hydrogen efficiency of Mo_2C and Mo_2N catalysts compared to MoS_2 catalysts (supported on γ-Al_2O_3) have been reported in literature (Furimsky and Massoth, 1999). When carbide phases were used for HDS reactions, a surface sulphide was formed under the reaction conditions (Lee and Boudart, 1985) indicating the instability of carbide phase. Long time performance study of metal nitride or carbides under commercial conditions is necessary to ascertain their performance (Furimsky and Massoth, 1999).

2.7.1.3 Different catalyst preparation methods

Different catalyst preparation methods have been studied by researchers for improving the performance of hydrotreating catalysts. Some of these methods are - sonochemical synthesis (Vishwakarma et al., 2007), inter-sulfidation between metal impregnation (Farag et al., 1998) and application of different precursors (Sundaramurthy et al., 2005)

2.7.1.4 Use of additives

Incorporation of a third component as additive to the γ-Al_2O_3 supported catalysts has been studied by researchers extensively. Activity of hydrotreating catalysts supported on γ-Al_2O_3 is found to increase by the addition of phosphorus for model compounds and for industrial feedstocks (Ferdous, 2003). Phosphate anions interact with γ-Al_2O_3 resulting in lesser interaction of metal oxidic precursors and γ-Al_2O_3 leading to higher MoS_2 stacking (Ferdous, 2003; McMillan et al., 1986; Ramírez et al., 1992). Such stack formation is indicative of Type-II Co-Mo-S which is considered to be active for hydrotreating (Topsøe and Clausen, 1986). This helps in increasing the sulfidability of Mo (Lewis and Kydd, 1992) and enhanced hydrotreating activity (Ferdous, 2003). Addition of boron was found to increase the hydrotreating activity of γ-Al_2O_3 supported catalyst (Lulić et al., 1989). Variation in hydrotreating activity by the incorporation of other additives such as B, F and Cl were also reported by many researchers (Eswaramoorthi and Dalai, 2006; Eswaramoorthi et al., 2008; Ferdous, 2003; Grange and Vanhaeren, 1997).

2.7.1.5 New supports

The important characteristics associated with good hydrotreating catalyst support are given in Figure 2.10 (Breysse et al., 2003). γ-Al_2O_3 is used as the hydrotreating catalyst support for many years. The advantages of γ-Al_2O_3 support include – good mechanical strength, thermal stability and higher acidity. However, the disadvantages that retard γ-Al_2O_3 to become the best support include,

- Lower surface area (Limitation in metal dispersion due to lower surface area)

- Higher metal support interaction (Retardation in the creation of active sulphide phase and hence reduced activity)
- Higher acidity (Increased coking propensity)

To overcome the difficulties associated with γ-Al_2O_3, many other supports have been studied in the past. It is possible to tune the textural and structural properties of catalysts with new supports and hence development of catalysts with new supports can offer a better solution for meeting the new challenges relevant to sulphur and nitrogen removal (Breysse et al., 2003; Grange and Vanhaeren, 1997). Developments in catalyst support are discussed in section 2.9.

Figure 2.10: Good characteristics of a support (Breysse et al., 2003)

2.8 Structural models of hydrotreating catalysts

Development of new catalysts necessarily involves understanding the structure of catalysts that are being used. This will help to develop, new, tailor-made catalysts. Various models have been proposed by researchers regarding the structure of hydrotreating catalysts and the important ones are briefly discussed in this section.

2.8.1 Monolayer Model

Monolayer model was one of the initial models on hydrotreating catalysts (Lipsch and Schuit, 1969a; Lipsch and Schuit, 1969b; Lipsch and Schuit, 1969c). It was suggested that surface OH groups are responsible for the interaction of Mo with alumina surface. Introduction of sulphur resulted in the replacement of oxygen ions (O^{2-}) by sulphide ions (S^{2-}). Presence of hydrogen caused the removal of some sulphide ions resulting in Mo^{3+} ions, which were considered to be active for hydrotreating. This model explained the initial phases of sulfidation but the not the subsequent steps.

2.8.2 Intercalation model

Voorhoeve and Stuiver (Voorhoeve and Stuiver, 1971; Voorhoeve, 1971) developed intercalation model in which Mo slabs were assumed to be sandwiched between two planes of sulphur atoms. Promoters such as Co or Ni were believed to occupy intercalation positions between the slabs.

2.8.3 Contact synergy model

In contact synergy model, Mo was believed to be present as MoS_2 and promoter Co was believed to be present as Co_9S_8 (Grange, 1980). The contact between these two phases resulted in the spill-over of hydrogen from Co_9S_8 to MoS_2, enhancing the activity of Mo.

2.8.4 Modified Contact Synergy Model

In the modified version of contact synergy model, presence of Co-Mo-S phase instead of MoS_2 phase was recognized and it was proposed that contact was between Co-Mo-S phase and Co_8S_9 phase (Karroua et al., 1989a; Karroua et al., 1989b). It was suggested that the surface diffusion of hydrogen produced by Co_8S_9 was able to activate Co-Mo-S species by remote control. The remote control action as well as the activity of Co-Mo-S were together responsible for the hydrotreating activity. Lack of direct measurement of surface diffusion of hydrogen was a weakness in the acceptance of this model.

2.8.5 Co-Mo-S model

The formation of Co-Mo-S structure was studied in detail by Topsoe and coworkers (Topsøe and Clausen, 1986; Topsøe et al., 1989). Multiple as well as single slab Co-Mo-S structures were observed depending on the sulfidation conditions. The edge location of promoters in these structures helped to increase the stability of the slabs. For γ-Al_2O_3 supported catalysts, single layered structures, in which catalyst metals strongly interact with the support (Type-I sites) through Mo-O-Al linkages were observed at low temperature sulfidation. Multilayer formation was observed at higher temperature sulfidation which exhibited lower interaction (Type-II sites) compared to Type-I. In carbon supported catalysts, single slab structures were found to have weaker interactions like in Type-II structures. Figure 2.11 shows the Type-I and Type-II structures indicated by Co-Mo-S model. Presence of Ni-Mo-S similar to Co-Mo-S was also found in their studies (Topsøe and Clausen, 1986; Topsøe and Topsøe, 1983). Among the various available models, Co-Mo-S model is widely considered as a representative model for hydrotreating catalysts.

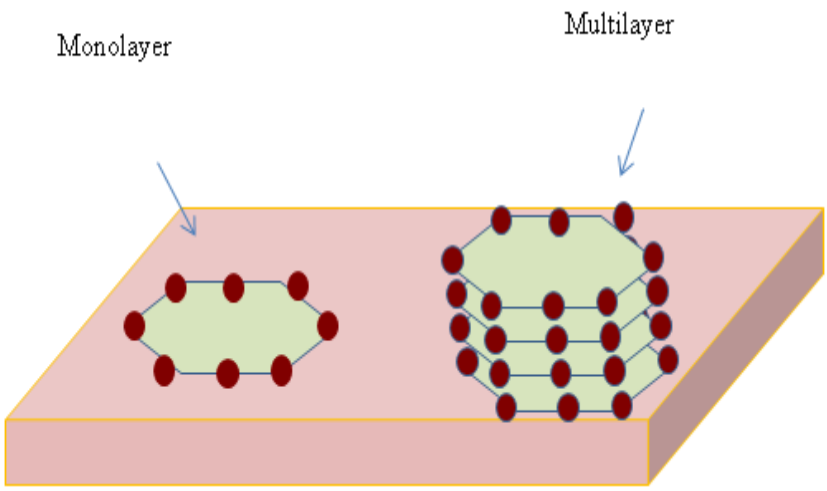

Figure 2.11 Co-Mo-S and Ni-Mo-S model (Topsøe and Clausen, 1986)
Monolayer: Co-Mo-S Type-I for γ-Al_2O_3 support or Type-II for carbon support
Multilayer : Type-II for γ-Al_2O_3 support

2.8.6 Rim-edge model

In the "Rim-edge" model, the catalyst particles are assumed as a stack of several discs as shown in Figure 2.12 (Daage and Chianelli, 1994). The top disc is described as "rim site" and the discs located in between the top and bottoms are described as "edge sites". According to this model, sulphur hydrogenolysis takes places both rim and edge sites, whereas hydrogenation takes place on the rim site only.

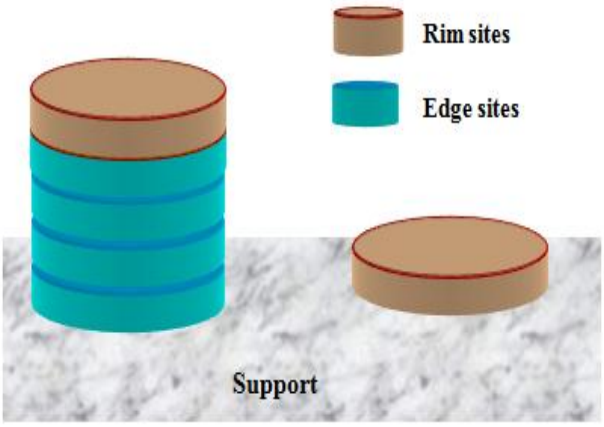

Figure 2.12 Rim-Edge Model
(Daage and Chianelli, 1994)
(Reproduced with permission)

2.9 Improvement in catalysts support

Considerable research has been done in the area of catalyst development by utilizing improved supports. Notable among them are the ones prepared using silica and carbon materials. Characteristics of some of the catalysts developed by improved supports are given in Table 2.4.

2.9.1 Silica supports

Silica supports have been utilized for developing hydrotreating catalyst for many years (Breysse et al., 2003). Hydrotreating activity of silica was found to be higher than that of γ-Al_2O_3 in many of the studies (Breysse et al., 2003). Following the development of ordered mesoporous support, MCM-41 (Kresge et al., 1992), many mesoporous siliceous supports have been developed by researchers and applied for hydrotreating. Notable among them is SBA-15 which has relatively higher surface area and good pore structure (Zhao et al., 1998).

2.9.2 Metal doped Silica supports

The metal support interaction in silica is very low compared to γ-Al_2O_3 that can result in inhomogeneous metal dispersion (Gutiérrez et al., 2006). Incorporation of heteroatoms such as Zr, Ti, Al were found to enhance the metal support interaction resulting in better dispersion of active metals leading to higher hydrotreating activity (Gutiérrez et al., 2006; Rayo et al., 2009).

2.9.3 Carbon supports

Carbon supports possess intermediate metal support interaction making it a good hydrotreating catalyst support (Breysse et al., 2003). Specific HDS activity of carbon supports were found to be higher than that of γ-Al_2O_3 (Topsøe and Clausen, 1986).

Recent progress in the development of mesoporous carbon, which possess ordered structure (Jun et al., 2000), mechanical stability (Vinu et al., 2007) and their successful catalytic application (Hussain and Ihm, 2007; Hussain and Ihm, 2009) has provided strong belief on the potential utilization of mesoporous carbon as the catalyst support for hydrotreating reactions. Detailed literature review on the hydrotreating activity of carbon supported catalysts is given in section 2-12.

2.10 Preparation of mesoporous carbon support

Various methods used for the synthesis of mesoporous carbon supports can be classified into three different categories, namely

a. Template Process -Volume filling: Synthesis by filling the pore volume of templates using carbon source
b. Template Process -Surface coating: Synthesis by coating the surface of template pores using carbon vapors or by partial filling of the pores using a liquid.
c. Direct synthesis – One step synthesis process involving the simultaneous addition of template and carbon source.

The textural characteristics of mC supports prepared by different synthesis process vary from one another significantly. Mesoporous carbon materials prepared from volume template synthesis and surface template synthesis process generally posses ordered structure. Materials synthesized by direct synthesis process are often does not possess ordered structure and exhibit foam like characteristics.

Table 2.4: Examples of textural properties of few improved supports and derived catalysts used for hydrotreating

Item/ Parameter	SA of support, BET m^2/g	SA of catalyst, BET, m^2/g	Pore dia-support (nm)	Pore dia-catalyst, (nm)	Pore vol-support, cm^3/g	Pore vol-catalyst, cm^3/g	Ref
CoMo/Ti-HMS	971	592	3.9	3.9	1.54	1.19	(Zepeda, 2008)
CoMo /Ti-SBA 15	911	397	5.5	4.5	1.17	0.83	(Zepeda, 2008)
CoMo/Ti-MCM 41	994	311	4.2	3.3	0.77	0.41	(Zepeda, 2008)
NiMo / SBA 15	840	550	5.6	5.5	1.12	0.78	(Gutiérrez et al., 2006)
NiMo / Ti-SBA 15	614	398	5.7	5.0	0.79	0.58	(Gutiérrez et al., 2006)
NiMo /Zr-SBA 15	543	450	5.7	5.5	0.71	0.65	(Gutiérrez et al., 2006)
CoMo /nC	782	561	10.7	10.8	2.09	1.51	(Lee et al., 2003)
CoMo /CMK-3	1244	751	3.7	3.7	1.28	0.79	(Hussain and Ihm, 2009)

2.10.1 Volume Template Process

The steps used in volume template synthesis procedure are

- Preparation of a primary template with suitable pore structure
- Using carbon precursors for the impregnation on primary template
- Carbonization of primary template-polymer complex
- Finally, removal of primary template by dissolution by suitable chemical agent.

By this procedure, the pores once occupied by the primary template become the carbon walls.

The breakthrough in template synthesis of mesoporous carbon was achieved with the preparation of mesoporous silica templates. Ryoo et al. synthesized mesoporous carbon material using a cubic mesoporous silica material (MCM-48) as the primary template and sucrose as the carbon source (Ryoo et al., 1999). In this procedure aqueous solution containing sucrose and sulphuric acid was impregnated on the pores of silica template. The resultant mixture was dried at 100°C and polymerized at 160°C. The impregnation process was repeated for effective incorporation of the carbon in the pores of silica template. Two-step impregnation was essential to have sufficient quantity of carbon to form a rigid structure. Sulphuric acid was used in the process which catalyzed the reaction of converting sucrose into carbon polymer. Later, this material was carbonized at 900 °C in a vacuum furnace. Primary template removal was carried out using the solution of NaOH in ethanol under reflux conditions. Typical steps involved in volume template synthesis process are shown in Figure 2.13. The replicated carbon material was not an exact replica of the primary template but assumed a new structure. It

was suggested in the study that various other carbon sources such as glucose, xylose, furfuryl alcohol or phenol resins can also be used for the synthesis but the use of sucrose was easier and superior. Kruk et al. (2000) found that CMK-1 synthesized using furfuryl alcohol rendered a less stable carbon framework and also reconfirmed the finding of by other researchers (Ryoo et al., 1999) on the lower structural ordering of furfuryl alcohol precursor. Following that, MCM-41 was used for the synthesis and characterization of ordered mesoporous carbon material in the similar manner as described above (Kruk, 2000). However the resultant carbon material lost its structural orderliness upon template removal (found by SAXS data) making them unsuitable for further use.

In further improvement to CMK-1, Jun et al. (2000) synthesized CMK-3 using another silica material, namely, SBA-15 as the primary template. Sucrose was used as the carbon precursor and sulphuric acid as the polymerization catalyst in the synthesis process. The resultant structure, termed as CMK-3, retained the hexagonal symmetry (p6mm) of SBA-15 and hence it was a real replica of SBA-15. It had higher surface area, pore diameter and pore volume than that of CMK-1 material (Hussain and Ihm, 2009).

MCM-41 as well as SBA-15 has 2D hexagonal symmetry (p6mm), however, the carbon replica of SBA-15 was stable whereas the carbon replica of MCM-41 collapsed. This is due to the presence of interconnecting micropore bridges in the SBA-15 walls (Figure 2.14). This was confirmed by many researchers (Joo et al., 2002; Lukens Jr. et al., 1999; Ryoo et al., 1999). Also, Liu et al. (Liu et al., 2000) observed separated nanowires when using MCM-41 as hard template confirming the absence of interconnecting bridges in MCM-41. The interwall bridges of SBA-15, when impregnated with carbon solution

during the template synthesis process, become the connecting rod in mesoporous carbon material. This explains the structural stability of CMK-3 material derived from SBA-15.

Synthesis conditions and processes adopted for SBA-15 can be modified to enhance the size of micropore bridges to convert them into mesotunnels (Fan et al., 2001). Such mesotunnels can become stronger rods compared to the ones derived from micropore bridges upon replication (Fan et al., 2001; Lu et al., 2003; Yu et al., 2002). The simple way was to increase the hydrothermal aging temperature (Galarneau et al., 2003; Lu et al., 2003). However the hydrothermal aging temperature of SBA-15 cannot be raised above 140°C, beyond which the decomposition of P123 occurs, which is the structure direction agent used in the SBA-15 synthesis process (Lu et al., 2005). Fan et al. (Fan et al., 2001) used 1,3,5-tri methyl benzene (TMB) as swelling agent alongwith high temperature hydrothermal aging to enlarge the opening of interconnecting bridges. It was suggested by them, that other solvents such as n-butanol, n-hexane can also be used for the process. Kruk et al. (Kruk and Cao, 2007) used hexane as the swelling agent in SBA-15 synthesis that yielded higher pore diameter for SBA-15, but reduced the pore wall thickness that is necessary to have good pore diameter for replicated carbon.

In a partial modification to the CMK-3 support preparation, an alternative synthesis process is developed for the preparation of SBA-15 by adding inorganic salt (such as KCl) to the regular SBA-15 reactant mixture (Yu et al., 2002). Hydrothermal treatment of this ‘tailor-made’ SBA-15 was done at 100°C or 130°C. The template thus obtained was used for the preparation of CMK-3. The resultant carbon support (CMK-3-100 or CMK-3-130) had higher pore size and larger BET surface area than the traditional CMK-3. In this material, the ordered structure of carbon supports was attributed to the

mesotunnels of this tailor-made SBA-15 unlike the micropore bridges of traditional SBA-15. Similar synthesis procedure was also reported by using NaCl as the inorganic salt (Sayari and Yang, 2005).

Over the years, various templates were used for the synthesis of mesoporous carbon supports by many researchers. A summary of few mesoporous carbon supports prepared by volume template process is given in Table 2.5.

2.10.2 Surface Template Process

The method of partial pore-filling of the template using a carbon source was employed by few researchers to synthesize mesoporous carbons. This method gave flexibility to tune the pore diameter by adjusting the amount of carbon filled in the pores. In one of the preparation methods, aluminium impregnated SBA-15 was used as a template for the preparation of mesoporous carbon by employing furfuryl alcohol as the carbon precursor along with TMB as the swelling agent (Lu et al., 2003; Lu et al., 2005). In this method, partial coating of carbon source over silica pore inner wall was accomplished by using the swelling agent. TMB helped to drive furfuryl alcohol towards silica walls thereby ensuring all the carbon source was used for making the walls. Heating the silica-carbon composite at 80°C in vacuum resulted in the removal of TMB and polymerization of furfuryl alcohol.

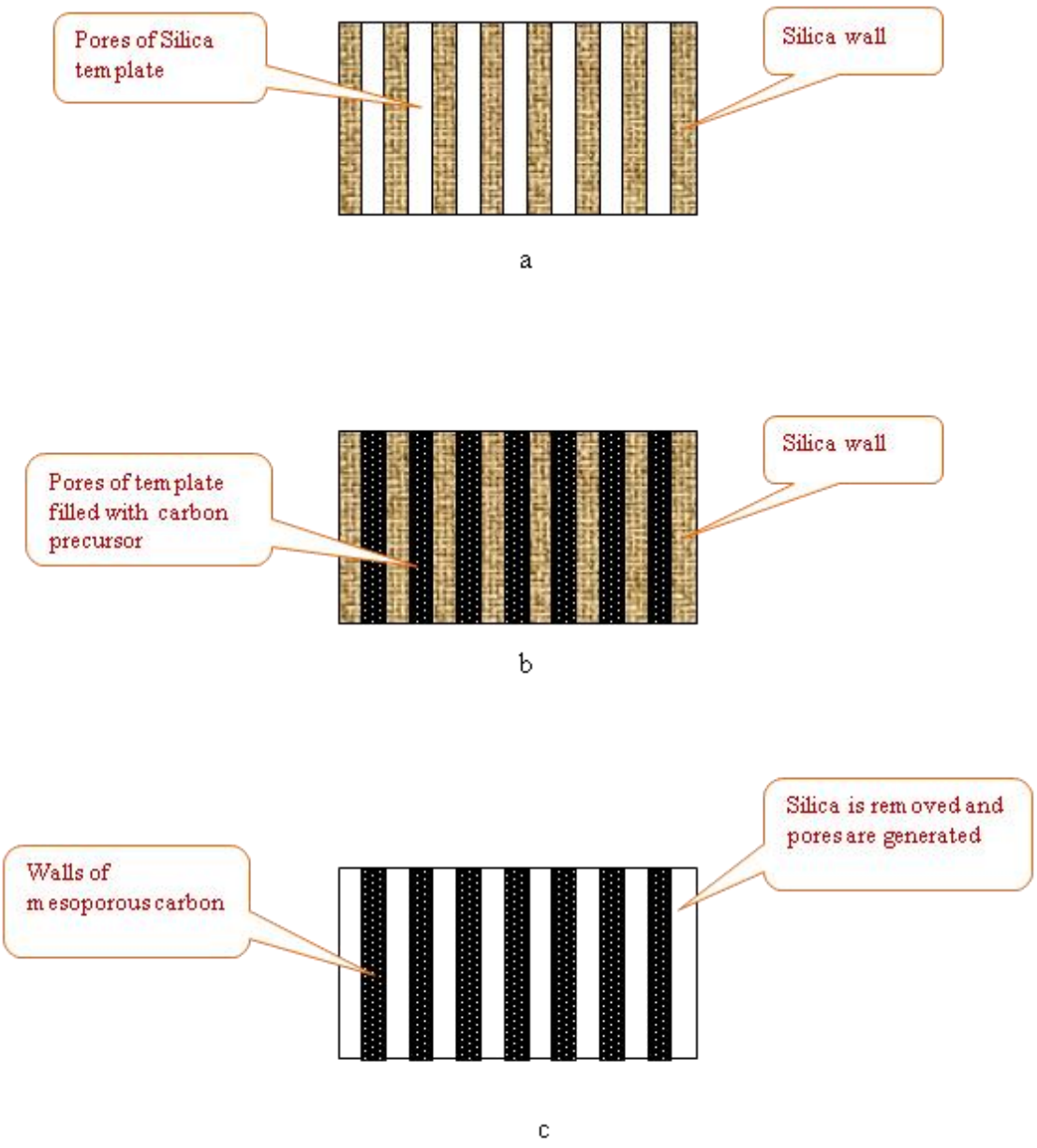

Figure 2.13: Volume template synthesis process for the preparation of mesoporous carbon (Jun et al., 2000; Ryoo et al., 1999) (Reproduced with permission)

a. Primary template (mesoporous silica such as MCM-48, SBA-15 etc.)
b. Primary template filled with carbon precursor
c. Mesoporous carbon obtained after removal of template

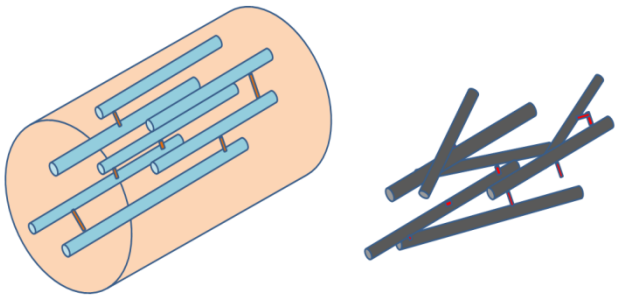

a. Carbon prepared using templates with disconnected pores

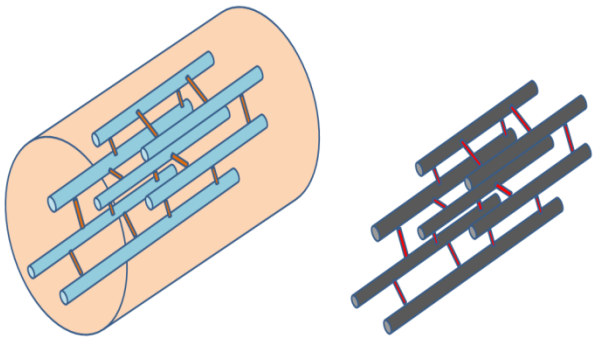

b. Ordered carbon support with support bridges (prepared from templates with interconnecting pore system)

Figure 2.14: Effect of interconnected pores in the preparation of mesoporous carbon supports (Ryoo et al., 2001) (Reproduced with permission)

Table 2.5: Mesoporous carbon support by volume template synthesis process

Support identifier	Template	Precursor	BET SA (m^2/g)	Pore dia (nm)	Pore Vol (m^3/g)	Remarks	Ref
CMK-1	MCM-48	Sucrose	1800	3.4	1.08		(Ryoo et al., 1999)
CMK-3	SBA-15	Sucrose	1520	4.5	1.3		(Jun et al., 2000)
CMK-3-130	SBA-15	Sucrose	1800	5.8	2.23	CMK-3 Modified with KCl	(Yu et al., 2002)
CMK-8	KIT-6	Sucrose	960	3	0.7	Similar to CMK-3	(Kleitz et al., 2003)
CMK-9	KIT-6	FA	2200	3, 6	2.15	Similar to CMK-5	(Kleitz et al., 2003)
C-MSU-H	MSU-H	Sucrose	1190	3.9	1.26		(Kim and Pinnavaia, 2001)
INC- 3	S- 3	FA	1800	3.0,28	2.21		(Fuertes, 2003)
MCA-130	Al-SBA15	Sucrose	1600	4.9	1.65		(Vinu and Ariga, 2005)
MC	MS (silica)	Sucrose	1110	5.6	1.55		(Karandikar et al., 2007)

Carbonization followed by washing of silica template yielded bimodal pores – one from the silica wall (by the removal of silica material) and another from partially filled pore itself (Figure 2.15). Apart from the use of liquid solutions, chemical vapor deposition methods also have been tried for the synthesis of mesoporous carbon materials. Li et al. (2002) synthesized CMK-5 material using ethylene as a carbon precursor over SBA-15, by catalytic chemical vapor deposition (CCVD) method (using cobalt catalyst). It was found that the increase in CCVD time helped to increase the orderliness of the product but decreased the surface area and pore diameter. In general, the wall thickness of carbon material obtained by surface templating process is lower than that derived by volume templating process. Summary of textural properties of few of the carbon supports prepared by surface template process are given in Table 2.6.

Table 2.6: Mesoporous carbon support by surface template synthesis process

Support name	**Template**	**Precursor**	**BET SA (m^2/g)**	**Pore dia (nm)**	**Pore Vol (m^3/g)**	**Remarks**	**Ref**
CMK-5	SBA-15	Ethylene	1353	2.97/ 4.89	na	By CVD;	(Li et al., 2002)
NCC-1	Al-SBA-15	Furfuryl alcohol(FA)	1800	5.1/ 10.6	3.1		(Lu et al., 2003)

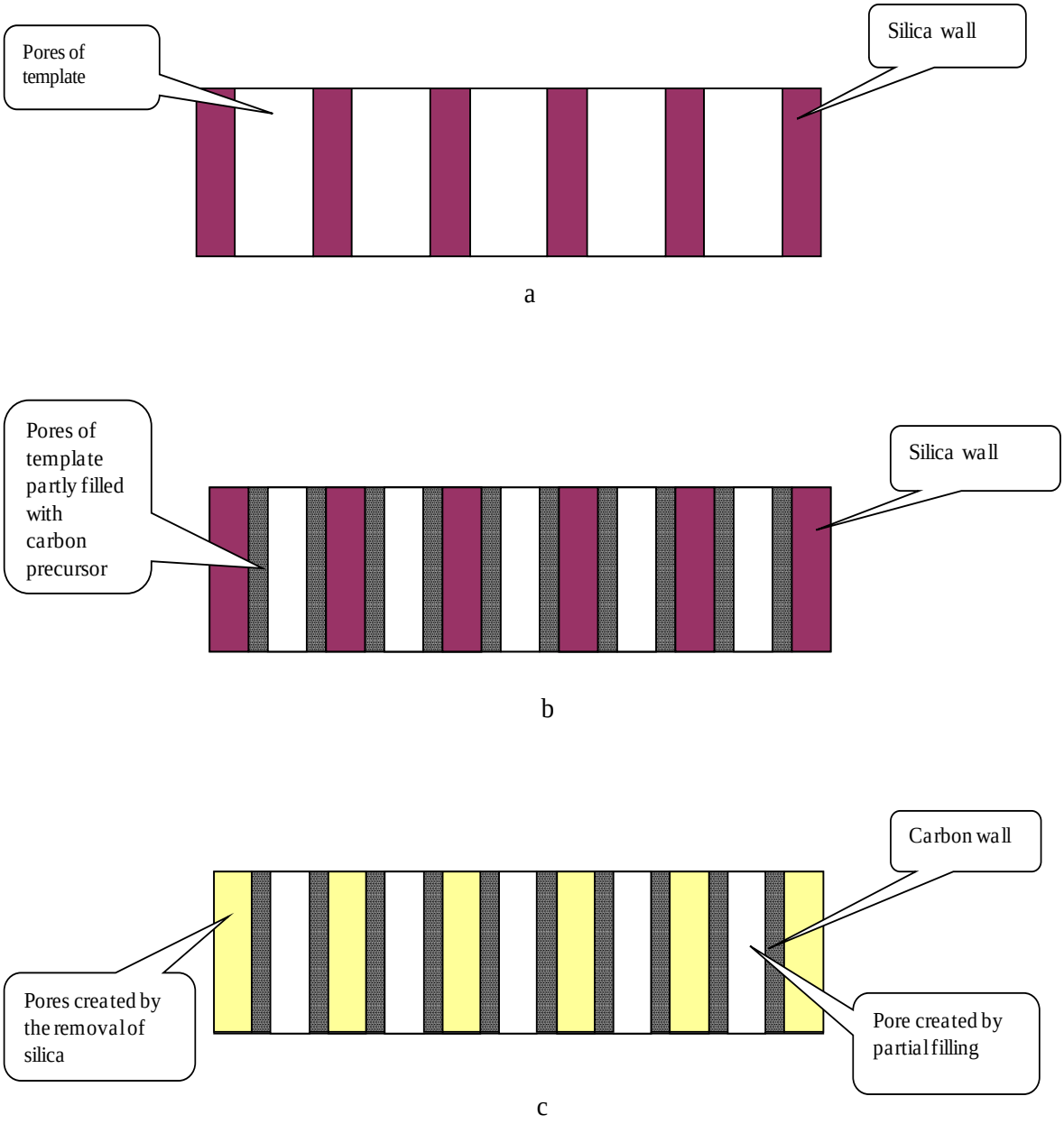

Figure 2.15: Mesoporous carbon support by surface template synthesis process

a. Primary Template
b. Primary template partially filled with carbon precursor
c. Mesoporous carbon obtained after removal of template

2.10.3 Direct synthesis

Instead of using a two step template process, a single preparatory step is used in the direct synthesis process. In a typical process (Han and Hyeon, 1999), mesoporous carbon material was synthesized using silica sol nanoparticles as template and resorcinol and formaldehyde (RF) as carbon precursor (Figure 2.16). The RF-silica gel composite was carbonized and then washed with HF acid (for template removal) to produce mesoporous carbon. Though textural properties (such as BET surface area and pore volume) of mesoporous carbon materials prepared by this direct synthesis process was better than the carbon materials produced by volume or surface template process, they do not possess ordered structure (Lee et al., 2006). Various direct synthesis processes have been reported in literature over the past decade.

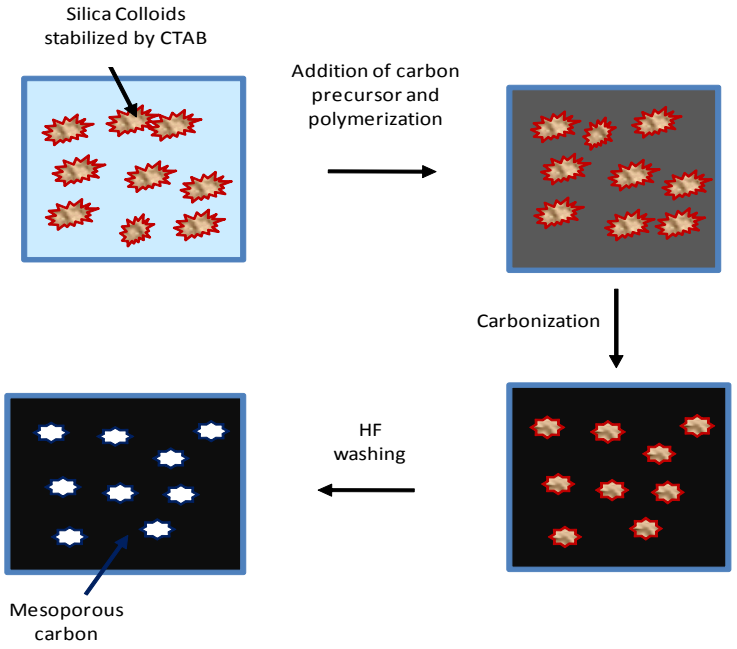

Figure 2.16: Mesoporous Carbon support by direct synthesis method (Han and Hyeon, 1999) (Reproduced with permission)

2.11 Functionalization of carbon supports

The process of creating surface functional groups on the surface of the carbon support is called as functionalization. The main objective is to create large number of hydrophilic groups on the surface (such as -OH and -COOH groups) which can act as anchors for attaching the catalyst metals (Sigurdson, 2009). These surface functional groups are considered to be responsible for many catalytic properties of carbon materials studied (Biniak et al., 1997; Szymański et al., 2002). Apart from catalysis, the oxygen surface functional groups are of important to the researchers due to their influence on adsorptions (Feron and Jansen, 1997; Mikhalev and Øye, 1996) energy storage and conversion (Rajalakshmi et al., 2000) and sensor technology (Lázaro et al., 2007) among others. The creation and the effect of surface functional groups in activated carbon supports is widely studied by researchers whereas limited studies have been done over ordered mesoporous carbons in this aspect. Nevertheless, the studies on functionalization of activated carbon are relevant due to the similarity in the process of generating surface functional groups and interaction of the functional groups with catalyst metals. However, the final conclusions on catalytic applications of these functionalized activated carbon supports needs to be evaluated with caution as the catalytic activity may depend on various other textural properties such as pore diameter and pore volume also.

2.11.1 Overview of functionalization of carbon supports

The process of creating surface functional groups can be done by various techniques such as oxidation, grafting, polymer coating, heat treatment and plasma treatment (Chen et al., 2003; Gómez-Serrano et al., 1999; Vinke et al., 1994) . Oxidative treatment may be carried out in gas phase (dry oxidation process) by passing through

gases such as oxygen, ozone over the carbon surface (Chen et al., 2003) or by wet oxidation treatment utilizing nitric acid, sulphuric acid, hydrogen peroxide and $SOCl_2$ among others (Barton et al., 1997; Chingombe et al., 2005; Lázaro et al., 2007; Pradhan and Sandle, 1999; Vasiliev et al., 2007). Heat treatment process under inert atmosphere generally creates hydrophobic carbon material (Lin and Teng, 2003; Menéndez et al., 1995) and might not be suitable for hydrotreating catalytic applications. Though Plasma treatment increases the surface oxygen functional groups, much of these groups are found to be present at the exterior surface rather than inside the pore structure (Boudou et al., 2000; García et al., 1998) limiting their choice towards catalytic applications.

Among various available functionalization treatments, oxidative treatment is widely adopted for carbon materials. It was generally found that dry oxidation process increased the concentration of hydroxyl and carbonyl groups whereas wet oxidation process increased the concentration of carboxylic groups also (Figueiredo et al., 1999). Nitric acid treatment was found to be very effective for imparting surface functional groups on the surface of activated carbon (Pradhan and Sandle, 1999; Vinke et al., 1994) and also it produced higher amount of such functional groups compared to the hypochlorite treatment (Gil et al., 1997; Vinke et al., 1994). Calvo et al. (2005) observed that the higher increase in oxygen surface functional groups was observed on activated carbon support by nitric acid treatment without significant change to the pore structure.

Jun et al. (2003) worked on the functionalization of mesoporous carbon CMK-1 and CMK-5 and found that the optimized treatment time was 15 minutes at 110°C, beyond which intactness of carbon framework could not be ensured. The necessity for a lower reaction time might be due to the absence of interconnecting micropores in CMK-1

(Jun et al., 2000) and reactive surfaces of CMK-5 (Lu et al., 2005). It has been found that the treatment of CMK-5 using hydrogen peroxide destroys the pore structure of the carbon material owing to very high reactivity of hydrogen peroxide over CMK-5 (Lu et al., 2005). Bazuła et al. (2008) used nitric acid for functionalizing CMK-3 and CMK-5 and found that the enhancement of functional groups starts to decrease between 80°C to 90°C when treated for 3 hours. The increase in acid concentration helped to increase the amount of surface functional groups, however, with reduction in textural properties. Li et al. (2006) carried out functionalization using nitric acid (upto 2M) and found that the ordered structure of mesoporous carbon gets collapsed when treatment time was more than 3 hours at 80° C, resulting in decreased electrochemical capacitance. Hussain and Ihm (2009) found that the maximum functional groups are obtained when the mesoporous carbon support was treated with 3M nitric acid at 60°C for 3 hours.

2.11.2 Chemistry of nitric acid functionalization

The process of creating surface functional groups by nitric acid on carbon surface is similar to that of the oxidation of aromatic compounds (Vinke et al., 1994). The oxidation process is considered to follow a radical mechanism. The sequence of reactions results in the incorporation of oxygen functional groups on the carbon basal planes. There could be many routes which can lead to different oxygen surface functional groups such as ketonic or carboxylic. The reaction of formation of dicarboxylic acid in carbon surface is similar to the nitric acid oxidation of 9,10 dihydrophinanthrene. Similarly when a single methylene group is present between two aromatic rings, formation of C=O group is expected by the reaction.

2.11.3 Effect of functionalization of carbon supports on catalyst characteristics and activity

Suh et al. (1993) studied the effect of surface oxygen functional groups on the dispersion of Pd metal over activated carbon. They found that the nitric acid treatment of activated carbon created hydrophilic functional groups on the carbon surface which help in the affinity of carbon surface towards aqueous metal solutions. This property helped in the deep penetration of aqueous metal solutions into the catalyst pores resulting in better dispersion of Pd metal over functionalized activated carbon support compared to that over untreated activated carbon. However the catalytic activity was not significantly affected primarily due to the blocking of micropores in activated carbons by dispersed metal (Suh et al., 1993). Similar results were observed by Calvo et al. (2005) and they concluded that the surface oxygen groups imparted by nitric acid acted as anchoring sites that enhanced the interaction between metals in aqueous solutions and functionalized carbon support leading to higher metallic dispersion as well as resistance to sintering. Li et al. (2005) found out that Pd dispersion on activated carbon was dependent on the concentration of nitric acid used for functionalization. It was concluded from the study that lower nitric acid concentration was desirable to have efficient dispersion of Pd.

Wang and Lu (1998) found that the dispersion of Ni catalyst was improved with acidic surface functional groups on activated carbon support. Martí'n-Gullón et al., (1993) functionalized activated carbon material by treatment with CO_2 (at various temperatures from 1223 K to 1773 K) followed by H_2O_2 and used it as catalyst support for Mo. Their conclusion was that the wettability of carbon surface was increased by the

incorporation of oxygen functional groups which facilitated the aqueous metal precursor solutions for easy access towards internal pore structure. However they stated that the presence of higher oxygen surface functional groups created higher SMI making it difficult for the creation of active phase during sulfidation resulting in lower HDS activity of Mo over functionalized activated carbon for the hydrotreating of thiophene. Similar result on the HDS activity was reported by other researchers for NiMo catalyst supported on activated carbon (Kouzu et al., 2004). These results on HDS activity were supporting the observations by some researchers (Derbyshire et al., 1986; Martí'n-Gullón et al., 1993) and contradictory to the observation by some other researchers (Solar et al., 1991; Vissers et al., 1987)

Muller et al. (1996) in a study found that the high density of active sites (i.e. surface oxygen functional groups) with a homogenous distribution helped in the filling of aqueous material in the pores. Water adsorption isotherm study of De La Puente and Menéndez (1998) indicated that the higher than required water quantity for monolayer filling of carbon surface was attributed to the movement of water molecules into the pores of carbon due to the presence of hydrophilic oxygen functional groups. Furthermore, De La Puente and Menéndez (1998) found that interaction of Mo with oxygen functional groups prevented the mobility of Mo on carbon surface during sulfidation (temperature of 400°C was used), thus avoiding sintering. Hussain and Ihm (2009) applied functionalized mesoporous carbon as a catalyst support for the HDS of thiophene and found that the CoMo metals supported on functionalized mesoporous carbon has higher HDS activity than that supported on virgin mesoporous carbon support.

Along with metal anchoring capability (Sigurdson, 2009), surface functional groups present on carbon surface produce good interaction between oxygen-nickel when present in appropriate quantities (Calafat et al., 1996b). The benefit of interaction was observed with the enhancement in promotional effect of nickel in creating oxidic precursor of Ni-Mo-S phase that is active for hydrodesulphurization (Calafat et al., 1996b). The functional groups are also helpful in creating certain degree of acidity on the surface (Bazuła et al., 2008).

2.11.4 Interaction of Catalyst metal with surface functional groups of carbon

The attachment of Mo over carbon surface can be through the interaction with surface functional groups or by weak electrostatic attraction with aromatic substrate (Vissers et al., 1987). Sintering of active phase will occur upon activation if the attachment between Mo and the carbon is simply through weak attraction. Study by De La Puente and Menéndez (1998) suggested that attachment of Mo on carbon surface was through the interaction with carboxylic groups as shown in Figure 2.17a. Similarly the interaction of Mo with ether like groups occurred by the opening of ether bridges (Figure 2.17b) (De La Puente et al., 1998; Vissers et al., 1987). The stability of Mo over functionalized carbon support without sintering at a temperature of 400° indicated that the interaction is predominantly through surface functional groups only (De La Puente and Menéndez, 1998).

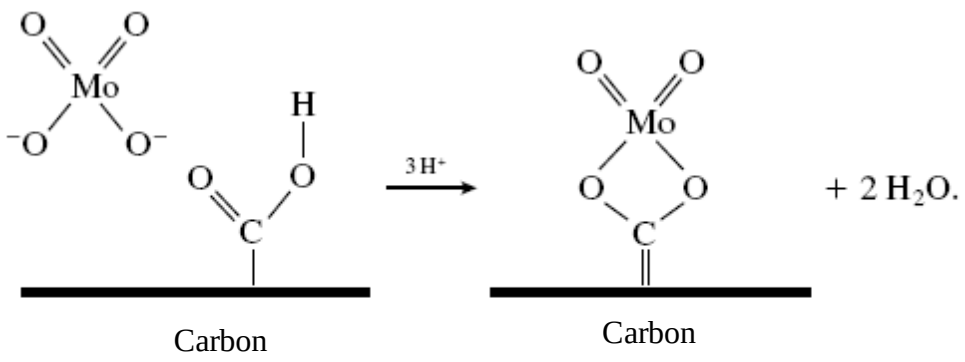

Figure 2.17a. Interaction of Mo on carbon surface with carboxylic group (De La Puente et al., 1998), (Reproduced with permission)

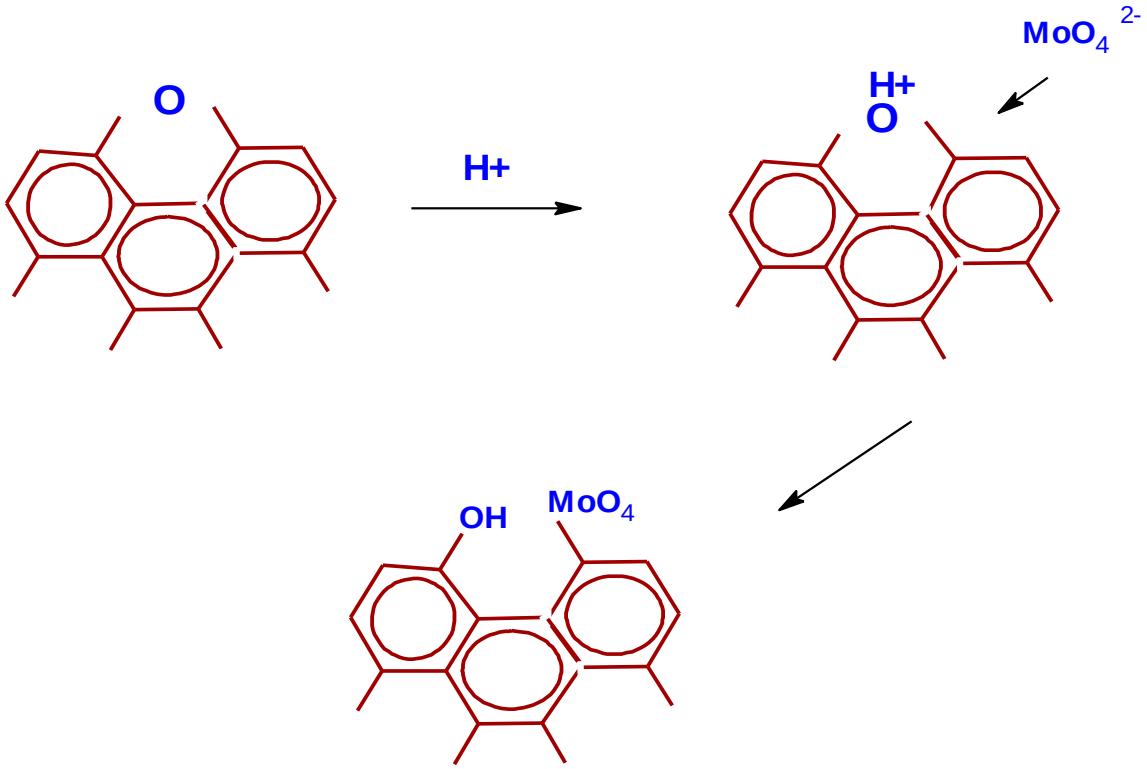

Figure 2.17b: Interaction of Mo on carbon surface with ether like group (Vissers et al., 1987), (Reproduced with permission)

2.11.5 Summary of literature review on functionalization

The literature review on functionalization of carbon supports indicates that,

- Nitric acid treatment of carbon support is superior to many other functionalization techniques for creating surface functional groups
- For mesoporous carbon supports, the structural orderliness can be affected if nitric acid concentration is very high
- The interaction of Mo with functionalized carbon surface is established through oxygen surface functional groups. Such anchoring process helps to avoid sintering of active phase at higher temperatures encountered in catalytic reactions.
- Increase in surface functional groups increases metal dispersion on catalyst support
- Very high oxygen surface functional groups do not necessarily lead to very high catalytic activity of the carbon supported catalyst due to the effect of changes in other textural and structural properties.

2.12 Hydrotreating applications of carbon supported catalysts

Hydrotreating of transition metals supported on carbon supports have been studied by researchers for many years. In most cases, the supports used in these studies were activated carbons. These studies can give fundamental understanding on some aspects of carbon supports relevant to hydrotreating. However, judicious assessment needs to be applied when extending the results from other carbon supports to mesoporous carbon supports due to significant difference in textural properties of various carbon supports. Hence this section is generally focused on hydrotreating catalysts supported on

activated carbon, CNT and various mesoporous carbons based on their relevance to this project.

2.12.1 Hydrotreating using activated carbon and CNT supported catalysts

The performance of CoMo/AC catalysts was studied and compared with γ-Al_2O_3 supported catalyst by Farag et al. (1999). AC supports derived from different sources were used to prepare CoMo catalysts and experiments were carried out in a batch reactor for short duration (< 1 hour). The HDS activity of CoMo/AC catalyst was found to be 3 times that of γ-Al_2O_3 supported catalyst irrespective of carbon sources for 4,6-DMDBT feed and also for DBT feed. They also studied the preferred reaction pathway by analyzing the reaction products. They observed that at lower temperatures, the reaction of 4,6-DMDBT was through both direct desulphurization (hydrogenolysis) and hydrogenation (aromatic saturation followed by 'S' removal), yet the latter being the preferred pathway. However at higher temperatures (>380 °C), direct desulphurization became the predominant pathway which might be due to equilibrium limitations associated with aromatic saturation. It was also reported that the activity of CoMo/AC catalysts were higher than that of commercial γ-Al_2O_3 supported catalysts.

Sakanishi et al. (2000) studied the activity of NiMo/AC catalysts derived from many sources for HDS of 4,6-DMDBT in a batch reactor. The observations from this study were similar to that of CoMo/AC catalysts done by Farag et al. (1999). In addition, they observed that the effect of reduction in hydrogenation pathway for HDS at higher temperatures (>380 °C) was less prominent for NiMo/AC than that for NiMo/ γ-Al_2O_3.

Farag et al. (Farag et al., 1998; Farag et al., 2000) studied the effect of catalyst preparation method on the activity of AC supported catalysts in a batch reactor for short reaction time (<1 hour). Three methods were used for preparing CoMo catalysts –

- Impregnation of Mo → impregnation of Co (Method –II)
- Impregnation of Mo → sulfidation → Impregnation of Co (Method –III)
- Impregnation of Co → sulfidation → Impregnation of Mo (Method – IIIb)
- Impregnation of Mo by equilibrium adsorption → sulfidation → Impregnation of Co by equilibrium adsorption (Method –IV)

They found that method IV produced catalyst with the highest HDS activity. It was further observed that catalyst activity of 4,6-DMDBT was higher when active metal (Mo) was impregnated first followed by promoter (Co). H_2S inhibition was observed to be higher in carbon supported catalyst compared to γ-Al_2O_3 supported catalysts, though the former showed comparatively higher HDS activity. This was attributed to higher surface area of carbon support and the propensity of H_2S to competitively adsorb on reaction sites. At lower temperatures the effect of H_2S inhibition was higher for direct desulphurization pathway than hydrogenation reactions, which resulted in hydrogenation being the preferred pathway. The study indicated that optimum Co/Mo atomic ratio was 0.326 for carbon supports.

Hensen et al. (2003) studied the effect of H_2S inhibition on various supports including AC supports in quartz microflow reactor at atmospheric pressure using thiophene as feed. They proposed a direct relation between support acidity and H_2S inhibition. They prepared CoMo and NiMo catalysts on γ-Al_2O_3 (Al) as well as on nitrilo-triacetic-acid (NTA) modified γ-Al_2O_3 (NTA-Al). Addition of NTA helped to

reduce metal support interaction of γ-Al_2O_3 supported catalysts resulting in increased MoS_2 stacks. Though reduction of SMI increased catalytic activity of CoMo (or NiMo) / NTA-Al, this had also resulted in increased H_2S inhibition. The HDS activity of NiMo (or CoMo) catalysts supported on carbon supports was higher than that supported on NTA-Al (or Al), in spite of higher H_2S inhibition in carbon supports. It was also observed that the intrinsic reaction rate for thiophene as well as H_2S inhibition in NiMo/AC catalysts was higher than that for CoMo/AC.

Brito et al. (1998) studied the promotion effect of Ni on carbon support on the HDS activity of thiophene using Mo as active metal (derived from thiomolybdate precursor). The results indicated that the catalyst prepared by successive impregnation method with a Ni:Mo atomic ratio of 1:3 was the most active among AC supported catalysts. However, the activity was lower than that of commercial NiMo/ γ-Al_2O_3 catalyst, which might be due to the variation in catalyst metal content. Mo content of 6.67% was used in this study whereas Mo content in commercial NiMo/ γ-Al_2O_3 can be around 13% (Sigurdson et al., 2009)

Relatively few studies exist on the hydrotreating performance of CNT supported catalysts. Sigurdson et al. (2009) and Eswaramoorthi et al. (2008) found that the activity of NiMo/CNT catalyst was higher than that of NiMo/ γ-Al_2O_3 catalyst for the HDS and HDN of gas oil feedstocks on catalyst mass basis. It was found that sequential impregnation method in which Mo was impregnated first followed by Ni gave higher HDS and HDN activities than that for the reverse order (i.e. Ni followed by Mo) for the hydrotreating of gas oil (Eswaramoorthi et al., 2008).

Shang et al. (2004b) found that CoMo/CNT catalysts were slightly less active than CoMo/ γ-Al_2O_3 catalyst for the HDS of model compounds.

2.12.2 Hydrotreating applications of mesoporous carbon supported catalysts

Hydrotreating study using new generation mesoporous carbons are sparingly available in the literature. All of the research has been done using model compounds only and not using real feeds. Detailed characterization of catalysts was also limited in these studies. This section provides an insight on hydrotreating activity studies done by various researchers using mesoporous carbon supported catalysts.

Hussain and Ihm (2009) studied the HDS activity of CoMo catalyst supported on mesoporous carbon (CMK-1 and CMK-3) in comparison with that supported on conventional γ-Al_2O_3 in a microflow reactor using thiophene feed. It was found that the performance of CMK-3 and CMK-1 supported catalysts, in terms of HDS activity was better than that of γ-Al_2O_3 supported catalyst. The better performance was attributed to higher amount of surface functional groups, higher metal dispersion and better structural connectivity. Hussain and Ihm (2007) conducted HDS activity test of unpromoted Mo catalyst using thiophene as model feed and concluded that CMK-3 supported catalyst is more active than catalysts supported on CMK-1, AC and γ- Al_2O_3. In these studies, it was reported that CoMo catalysts prepared after functionalization using nitric acid exhibited higher HDS activity than the virgin ones indicting the effectiveness of functionalization.

A comparative study on hydrotreating activity of CoMo catalyst supported on γ-Al_2O_3, activated carbon and nanoporous carbon (NC), was conducted by Lee et al.,

(2003). The activity test was conducted in a batch reactor using DBT and 4,6 DMDBT as feedstocks and it was found that nanoporous carbon was the most active among the three. Reason for the higher activity of CoMo/NC was attributed to better metal dispersion on the high surface area of nanoporous carbon support. The activity of CoMo/NC was higher than that of CoMo/AC (in spite of higher surface area of AC) and this could be due to the mesoporosity of CoMo/NC which facilitated the easy movement of bigger molecule.

Recently, Shi et al. (2010), studied the hydrotreating activity of CoMo catalysts supported on mesoporous carbon materials (CoMo/CMC) using thiophene as feed. CoMo/CMC catalyst (Co/Mo atomic ratio = 0.25) showed higher activity compared to CoMo catalysts supported on γ- Al_2O_3. The difference in activity was prominent at lower temperatures (around 220°C) than at higher operating temperatures (around 300°C) indicating the superiority of mesoporous carbon supported catalysts. In the same work, performance of NiMo/CMC (Ni/Mo atomic ratio = 0.25) towards HDS of model feed comprising of DBT (0.3%) and quinoline (0.02%) was studied. It was found that the HDS activity of NiMo/CMC catalyst was higher than that of certain commercial catalyst (FH-98) and NiMo/CMC catalyst gave an advantage of 40°C for the same level of conversion. A summary of literature review on the hydrotreating activity mesoporous carbon supported catalysts is given in Table 2.7.

Table 2.7: Summary on the hydrotreating application of mesoporous carbon supported catalysts

Support material	Catalyst used	Reaction conditions	Feed	Findings	Shortcomings	Ref
CMK-1, CMK-3	Unpromoted Mo (Various loading of Mo)	Pressure: 2.0 MPa; Temperature: 400°C; Reaction Time: 7 hours; Batch reactor.	Thiophene	Catalytic activity in the order of supports: γ-Al_2O_3 < AC < CMK-1 < CMK-3.	Reaction time was short; Only simple model compound was used; Though metal loading was optimized it was in a lower range (Mo < 15%); Effect of promoter was not studied; No information on long term operation.	(Hussain and Ihm, 2007)
CMK-1, CMK-3	Co-Mo on carbon supports (Various loading of Co and Mo); 3% Co and 7% Mo on γ-Al_2O_3	Pressure : 2.0 MPa; Temperature: 400°C; Reaction Time: 7 hours; Batch reactor.	Thiophene	Catalytic activity in the order of supports: γ-Al_2O_3 <AC< CMK-1 < CMK-3; Activity of functionalized CMK-3 supported catalyst was higher than virgin CMK-3 supported catalyst.	Reaction time was short; Only simple model compound was used; Though metal loading was optimized it was in a lower range (Co+Mo < 10 wt %); No information on long term operation.	(Hussain and Ihm, 2009)

Support material	Catalyst used	Reaction conditions	Feed	Findings	Shortcoming	Ref
SMC-1	2.1% Co and 11.2%	Pressure : 4.0 MPa; Temperature: 320°C; Reaction Time: 4 hours; Batch reactor.	DBT, 4,6-DMDBT.	Catalytic activity in the order of supports: γ-Al_2O_3 < AC < SMC-1.	Reaction time was very short; No information on functionalization and long term operation; No study on variation in metal loading.	(Lee et al., 2003)
CMC	17.8 % Mo with Co/Mo atomic ratio of 0.25	Pressure : 1.5 MPa; Temperature: 220 – 300 °C; Reaction LHSV: 2 hr^{-1}; Micro flow reactor.	0.05% sulphur as thiophene in mixture of n-hexane (20%) and n-heptane (balance).	Catalytic activity in the order of supports: γ-Al_2O_3 < AC < CMC Difference in activity was much higher at 220 °C compared with that at higher temperatures (300 °C).	No information on functionalization and long term operation; No study on variation in metal loading; Only simple model compound was used.	(Shi et al., 2010)
CMC	17.8 % Mo with Ni/Mo atomic ratio of 0.25	Pressure : 1.5 MPa; Temperature: 260 – 320 °C; Reaction LHSV: 2 hr^{-1}; Micro flow reactor.	0.3% sulphur from DBT, 0.02% nitrogen from Quinoline in a mixture of 5% tetralin, 0.5% n-octane and n-nonane (balance).	Catalytic activity in the order of supports: Commercial (γ-Al_2O_3) < CMC.	No information on functionalization and long term operation. Only model compounds were used.	(Shi et al., 2010)

2.13 Catalyst deactivation

Deactivation of hydrotreating catalysts occur due to the loss of active catalyst sites. Loss of activity can be temporary or permanent depending on the type of deactivation process. The causes for deactivation include coke formation, poisoning, metal deposition and sintering (Furimsky and Massoth, 1999).

In an industrial reactor, constant conversion levels are maintained by increasing the reaction temperature which can offset the effect of deactivation (Jones and Pujado, 2006). The phenomenon of raising the reactor temperature to compensate the deactivation over a period of operation follow a typical 'S' curve (Tamm et al., 1981). The initial rapid deactivation is mainly due to coke formation which is followed by slower deactivation, mainly due to deposition of metals. The final loss is attributed to increased coke generation and change in pore structure.

2.13.1 Deactivation by Coke

Coke formation in a hydrotreating reactor can occur through polymerization, dehydrogenation or thermal reactions as shown in Figure 2.18.

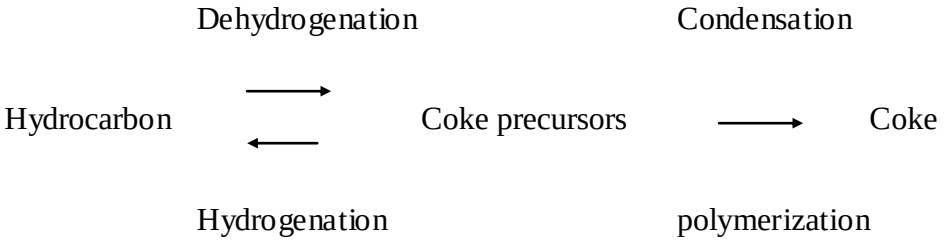

Figure 2.18: Coke forming reactions (Jones and Pujado, 2006)

Coke is carbon deficient material and stays on the surface of the catalysts, blocking the active sites. Coke built up is seen to increase with increase in molecular weight/boiling range of feedstock (Jones and Pujado, 2006). From the reaction scheme shown in Figure 2.18, one can see that dehydrogenation is a route for the formation of coke precursor. Hence thermally cracked feedstocks (such as coker gas oil feed), which are deficient in hydrogen, are prone to generate more coke over the catalyst which can lead to accelerated catalyst deactivation (Jones and Pujado, 2006).

Typical relation between coke laydown and surface area reduction pertaining to γ-Al_2O_3 supported catalysts was studied by Absi-Halabi et al. (1991) and two regions of coke were observed. In the first region, formation of coke was very rapid at the initial stages (SOR conditions) of the operation (fast coke) and attains a steady state. In the next region, a steady state increase of coke during the operation at lower rates was observed (slow coke). In was found from a study that the fast coke was formed within 50 hours of operation and takes up about one third of the porosity (Furimsky and Massoth, 1999). For remainder of the operation, slow coke and metals took up the pore volume. Near the EOR of the catalyst, coke build up rate increased due to higher operating temperatures. In addition, the catalyst surface acidity can also accelerate coke formation (Appleby et al., 1962).

Apart from temperature and acidity, hydrogen partial pressure can also affect the coke formation (Jones and Pujado, 2006). Hydrogen can help to convert the coke precursors into stable products before they are converted into coke precursors and hence increase in hydrogen partial pressure can help in retarding coke formation.

The quality of coke deposited remains soft for some duration of operation, after which structural transformations occur resulting in hard coke (Jones and Pujado, 2006). Removal of soft coke by in situ hot hydrogen stripping can help in achieving short term recovery of catalytic activity during the operation whereas regeneration is needed for the removal of hard coke (Jones and Pujado, 2006).

2.13.1.1 Coking propensity: Carbon vs. Alumina

One of the primary methods of catalyst deactivation is by the formation of coke, which is generally attributed to the presence of polynuclear aromatic compounds and olefins in gas oil feeds (Abotsi and Scaroni, 1989). The main aspect for coke formation is considered to be surface acidity of the catalyst. The direct relation between increase in coke formation and increase in acidity was explained by the formation and stability of carbenium ions. These are considered to be intermediates in coke formation and their formation is favoured by presence of strong acid sites (Scaroni et al., 1985). As the acidity of carbon support (and also supported Co-Mo catalysts) was lower than that of γ-Al_2O_3, the propensity of carbon support towards coke formation was lower (Scaroni et al., 1985). Coking propensity of Mo/C catalysts found to decrease with increase in hydrogen partial pressure due to minimization of dehydrogenation (and hence minimum polymerization) reactions. At a pressure of 6.9 MPa the coking tendency of Mo/C supports was three times lower than that of their γ-Al_2O_3 counterparts (Scaroni et al., 1985).

Similar observation on coking propensity of carbon in comparison with γ-Al_2O_3 was made by De Beer et al. (1984). They also found that the acidity of sulphide phase (MoS_2) was lower in carbon compared to γ-Al_2O_3. This study indicated that the coking

propensity of carbon supports was generally insensitive to the nature of active metal unlike γ-Al_2O_3. Increase in active metal (Mo) loading increased the coking propensity in both carbon and γ-Al_2O_3 supports, but the increase was more pronounced in γ-Al_2O_3 than in carbon.

The phenomenon of lower coking tendency in carbon supported catalysts compared to γ-Al_2O_3 supported ones was observed by Fukuyama et al. (2004), when processing vacuum residue feeds. In the reaction conditions adopted, they believed that the lower coking tendency in carbon supports was mainly due to the presence of active surface hydrogen in carbon supports. Micropore locations of carbon supports acted as hydrogen reservoirs and helped to store hydrogen, which was helpful in reducing coke formation.

The concept of acidity on coke formation can be applicable to variety of carbon supports. However, the benefit due to active hydrogen may not be a factor in reducing coking propensity of mesoporous carbon materials where the presence of micropores is very less.

2.13.2 Metal deposition

Metal deposition is irreversible and cannot be removed by regeneration also (Jones and Pujado, 2006). The nature of metal deposited on catalyst depends on the origin of feedstock as well as additives used in upstream processing units. Ni and V are the predominant metals in petroleum derived feedstocks and shale derived oils whereas Fe and Ti can be additional contaminants in coal derived oils (Furimsky and Massoth, 1999). Handling of Na in the separation process of bitumen from tar sands or caustic usage in

crude desalter can result in carryover of Na into downstream processing units. Dai and Chung (1996) reported catalyst poisoning in coker naphtha treating unit by silica gel, which got deposited on the catalyst surface. The origin of silica gel was found to be silicon oil that was added to coker drum as additive, which got transformed into silica gel in catalytic environment.

Poisoning of hydrotreating catalysts by Ni and V was widely studied by researchers (Furimsky and Massoth, 1999). Deposition of Ni and V was generally found to occur on the surface of the catalyst near the pore entrances, resulting in diffusion limitations and restricting the access to interior sections (Jones and Pujado, 2006). The deposition of vanadium was found to be in the surface of the catalyst particle supported on γ-Al_2O_3, whereas the deposition of vanadium was more uniform on AC supported catalysts indicating the advantage of carbon supports (Fukuyama et al., 2004). Deposited metals can also extensively modify the active phase of the catalyst thereby reducing the catalytic activity (Furimsky and Massoth, 1999). Other metals that deactivate the catalyst include arsenic and lead (Rase, 1977).

Unlike coke deposition, metal deposition is steadily increased during the operation of the catalyst (Oelderik et al., 1989). Many of the hydrotreating reactors are provided with HDM catalysts which take care of the metals in feed, thus preventing metal slippage. Because metal deposition is irreversible, it is a serious concern in commercial operations employing γ-Al_2O_3 supported catalyst.

2.13.3 Poisoning

Catalyst poisons can be defined as those substances that adsorb on active sites resulting in competition with reactant molecule for adsorption on active sites or incapacitate the active site by adsorption (Furimsky and Massoth, 1999). The final result of this process is reduction /loss of catalytic activity. Poisoning can be caused by reactant molecules, reaction intermediates, products or inert molecules present in the reacting mixture. It can be divided into three categories- irreversible, reversible or quasi-reversible. Deposition by coke or metals is treated as irreversible poisoning (Furimsky and Massoth, 1999).

The poisoning is termed as reversible if the catalyst regains its activity upon removal of such poisons (called as inhibition). In some cases, the activity is only partially restored upon removal of the poison and then it is called as quasi-reversible poisoning.

Nitrogen containing compounds, which adsorbs on active acidic sites can be poisons for hydroprocessing reactions (Furimsky and Massoth, 1999). In particular, 6-membered heteroatom nitrogen compounds or anilines are more basic in nature and strongly adsorb in the active acidic sites. When indole was adsorbed on the hydrotreating catalyst used for the HDS of DBT, the activity was only partially restored upon its removal. This is a quasi-reversible inhibition which is associated with slow desorption of poison from the reaction site (Furimsky and Massoth, 1999).

Ammonia, which is produced in the hydrotreating reactor has relatively weaker adsorption characteristics and hence not a very strong inhibitor compared with many

other nitrogen compounds (La Vopa and Satterfield, 1988). Inhibition by H_2S for hydrotreating catalyst supported on carbon has been widely reported by many researchers (Calafat et al., 1996a; Farag et al., 2000; Hensen et al., 2003).

2.13.4 Change in catalyst structure / Sintering

The stability of hydrotreating catalyst is affected by the prolonged exposure to higher temperatures (Furimsky and Massoth, 1999). Matsubayashi et al. (1995) observed the decomposition of Ni-Mo-S phase by preasphaltenes during the processing of coal derived liquids. This was observed at the entry of the catalyst bed but not at the exit where the deactivation was found to be due to the agglomeration of MoS_2. This might be due to the higher temperature experienced at the exit of the reactor compared to the inlet due to the exothermic heat of reaction. In an experiment by stohl et al. (Stohl et al., 1987), a temperature excursion of 470°C resulted in the sintering of Ni which ultimately resulted in the loss of active phase. Sintering is the loss of surface area of the catalyst due to crystallite growth (Moulijn et al., 2001).

Furthermore, generation of Type-I monolayered structure from Type-II multilayered was found to be the main cause of deactivation in CoMo/ γ-Al_2O_3, and NiMo/ γ-Al_2O_3 catalysts (Van Doorn et al., 1992). The loss of multilayer structure resulted in higher metal support interaction as well as reduced the number of active edges sites.

Apart from the various types of catalyst deactivation, mechanical deformation is another way of deactivation of catalyst (Moulijn et al., 2001) in trickle bed hydrotreating reactor. Smaller catalyst particles can reduce diffusion limitations, but will increase

reactor pressure drop thereby limiting the plant capacity. In addition, pressure drop can cause maldistribution and channelling which can lead to localized heating (hot spots) and sintering of catalyst. Leaching of active metals from the support during operation (by detachment of metal or by vaporization at higher temperatures) can also cause catalyst deactivation (Moulijn et al., 2001).

2.14 Kinetic study

Kinetic parameter estimation for new and improved catalysts is necessary for designing industrial reactor at a large scale from laboratory data. It serves as a tool to compare the performance of different catalysts and also to investigate the reaction pathways (Landau, 1997). Furthermore, kinetic study is useful for the improvement of process parameters, process configuration and optimization of operating condition.

Kinetic analysis for a trickle bed reactor can be divided into microkinetics and macrokinetics (Baldi, 1981). Microkinetics deals with the chemical and physical kinetics that include studying the mass transfer effects as well as estimating the reaction rates, activation energy and reaction order. Macrokinetics refers to the study of hydrodynamics such as back mixing and wetting. Design equation development for the industrial reactor necessarily involves the combination of these two results.

2.14.1 Hydrodynamics parameters

Laboratory microscale reactors are widely used to carry out catalyst development studies due to their economic advantage (Bej et al., 2000). However, it is a challenge to manage the hydrodynamic parameters for scaling up industrial reactors from laboratory data due to variation in process conditions that persist between the two. For example, the

liquid superficial velocities in pilot plant reactors are very low compared to industrial reactors due to much lower catalytic bed height (Baldi, 1981).

Some of the hydrodynamic problems that are to be dealt with when carrying out kinetic analysis for small scale reactors include (Ramírez et al., 2004)

- Wall effects
- Channelling and poor catalyst wetting
- Backmixing

It is very difficult to maintain both LHSV and hydrodynamic conditions in micro and commercial reactors at the same values (Baldi, 1981). For meeting hydrodynamic criterion in both reactors, the conversion level that needed to be kept in micro reactors must be very low. This is not a desired situation as heat effects can have profound impact on the catalytic performance (Baldi, 1981).

Utilization of inert diluents of appropriate size alongwith catalyst pellets was found to minimize the hydrodynamic problems (Bej et al., 2002). Ramirez et al. (Ramírez et al., 2004) reported elimination of certain hydrodynamic limitations by utilizing SiC diluent alongwith commercial catalyst. Table 2.8 summarizes the criteria used for finding out limitations on wetting, wall effects and backmixing in trickle bed reactors.

Table 2.8: Criteria for hydrodynamic parameter evaluation in a trickle bed reactor

Parameters	Correlation	Remarks	References
Wall effect	$\frac{D_b}{d_p} > 25$	Wall effect can be discarded if this criteria is satisfied	(Chu and Ng, 1989)
Wetting	$W = \frac{\eta_L u_L}{\rho_L d_p^{\,2} g} > 5 * 10^{-6}$	Wetting effect can be considered negligible if this criteria is satisfied	(Gierman, 1988)
Backmixing	$\frac{L}{d_p} > 100$	Backmixing can be neglected when this criteria is met	(Mapiour, 2009; Perego and Peratello, 1999)

The definitions for terms in Table 2.8 are,

D_b – Diameter of reactor, cm

d_p – Average diameter of catalyst particle (including diluent if any), cm

η_L - Liquid viscosity at operating conditions

u_L – Superficial velocity, cm/s

ρ_L – Liquid density at operating conditions, gm/cc

L- Length of the reactor, cm

g – Gravitational constant, cm/s^2

2.14.2 Mass transfer effects

Microkinetics analysis involves studying the mass transfer effects and reaction rates. To achieve better activity from the catalyst, it is essential for the reactant molecules to effectively reach to and quit from the active sites, which are widely dispersed in the catalyst (Fogler, 2006). Figure 2.19 provides the schematic of reactant concentration

profile across various locations in reaction medium, for a heterogeneous catalysis reaction. Typical steps for a three phase heterogeneous catalytic reaction in a trickle bed reactor are given below (Ramachandran and Chaudhari, 1983).

$$A+B \rightarrow C + D$$

A- Gaseous reactant,
B- Liquid reactant
C- Gaseous Product
D- Liquid product

1. Transportation of molecule A from bulk gas phase to gas-liquid interface and then to bulk liquid
2. Transportation of reactant molecules A and B from bulk liquid to catalyst surface
3. Intraparticle diffusion of reactant molecules into the pores of the catalyst
4. Adsorption on the catalyst sites
5. Surface reaction to yield products
6. Desorption of the products from the catalyst surface
7. Intraparticle diffusion to catalyst surface
8. Transportation of product molecules C and D to the bulk liquid
9. Exit of molecule C to the gas phase.

Steps 1-2 and 8-9 are characterized by external diffusion whereas step 3 and 7 are characterized by internal diffusion (Fogler, 2006).

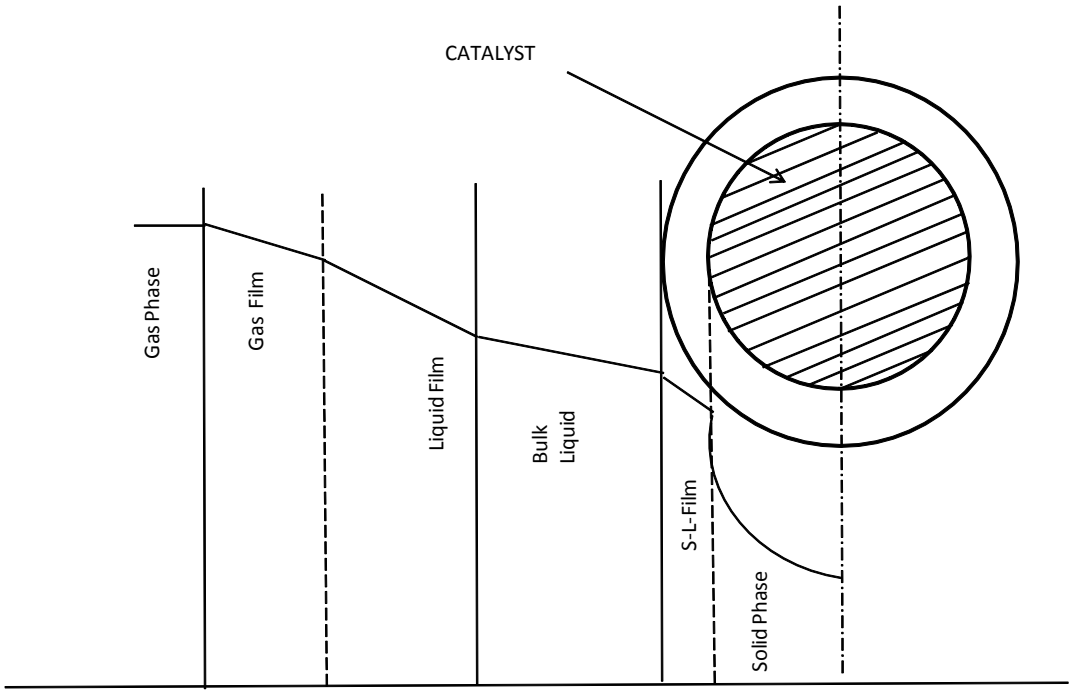

Figure 2.19: Diffusion in chemical reaction (Ramachandran and Chaudhari, 1983)

External mass transfer effects in hydroprocessing reactions are mainly associated with the diffusion of H_2 through the bulk liquid phase. This is calculated using Satterfield criterion (Satterfield et al., 1969) which is defined as,

$$\frac{10 d_p}{3 C_{H_2}} \left(\frac{-1}{V_C} \frac{dn}{dt} \right) > K_{OVR} \qquad \text{----------} \quad (2.1)$$

Left hand side (LHS) of Equation 2.1 is a measure of reaction rate whereas right hand side (RHS) of the equation gives diffusion coefficient for the diffusion of hydrogen in bulk gas and liquid phases. Details of individual terms of Equation 2.1 are given in Appendix-C.

Internal mass transfer limitations can be calculated using a dimensionless modulus analogous to Thiele modulus (Satterfield, 1970) as limited information is available on the intrinsic reaction rates for the hydroprocessing of real feedstocks using catalyst particle size comparable with commercial ones. For this purpose, it is necessary to assess the isothermality of the catalyst pellet as the equations are based on isothermal conditions. It is done by estimating β value (Equation 2.2) or by evaluating Anderson criteria (Equation 2.3) (Satterfield, 1991). Mass transfer effects become prominent at higher temperatures when surface reaction is very fast compared to diffusion rate (Fogler, 2006).

$$\beta = \frac{\triangle T_{MAX}}{T_S} = \frac{\triangle H_{R,i} \cdot D_i \cdot [C_i]_S}{k_t \cdot T_S} \qquad \text{----------} \quad (2.2)$$

$$\frac{|\triangle H_{R,i}| \cdot \{R_i\} \cdot d_P{}^2}{k_t \cdot T_S} < \frac{3 \cdot T_S \cdot R}{E_i} \qquad \text{----------} \quad (2.3)$$

In Equation 2.3, LHS value is the measure of heat generation and RHS value is the measure of heat dissipation. Details of individual terms of equations 2.2 and 2.3 are given in Appendix-E.

2.14.3 Kinetic models

Kinetic modeling of HDS and HDN reactions using model compounds and real feedstocks are widely available in the literature. It has been observed that the HDS and HDN reactions of model compounds follow first order kinetics (Ancheyta et al., 2002). But for real feeds that contain various kind of molecules (olefins, paraffins, aromatics and

naphthenes), it is not practical to consider different compounds to develop kinetic models. The variation in reactivity and structural differences of various molecules in petroleum feedstocks makes it impossible to develop single rate expression that can represent all the reactions (Ancheyta and Speight, 2007). Though the kinetic data using model compounds can give some direction, application of the models for real feedstocks can be erratic due to interference of secondary and tertiary products formed in the course of reaction and their potential to generate first compound (Ancheyta and Speight, 2007). Moreover, for different feedstocks, the composition of sulphur compound may be different based on their source and upstream processing. The reaction products such as ammonia and H_2S are found to affect the rate of reactions in many occasions (Korsten and Hoffmann, 1996). Most of the kinetic studies reported in the literature were conducted using catalysts supported on γ-Al_2O_3 and hence there can be differences in the kinetic model when a different support is used.

2.14.4 Power law model

Using a power law model, the rate of reaction for species A (sulphur or nitrogen) can be expressed as

$$r_A = -\frac{dC_A}{dt} = k_A * C_A{}^n \qquad \text{----------} \quad (2.4)$$

Power law model is widely used due to its simplicity in expressing the rate of reaction and also due to its mathematical simplicity (Ramachandran and Chaudhari, 1983). The activation energy is calculated from Equation 2.5.

$$k_A = A * e^{(-E_A/RT)} \qquad \text{----------} \quad (2.5)$$

Where,

n	-	Order of reaction
k_A	-	Reaction rate constant for species, $(mol/L)^{(1-n)}$ s^{-1}
C_A	-	Concentration of species A in the reaction mixture, mol/L
A	-	Arrhenius constant
E_A	-	Activation energy for the reacting species A, J/mol
R	-	Universal gas constant, J/mol-K
T	-	Temperature, K

It is generally found that the reaction order for HDS is between 1.0 to 3.0, whereas the same for HDN lies in the range of 0.5 to 1.5 (Ancheyta.J. et al., 2002; Aoyagi et al., 2003; Bej et al., 2001; Sigurdson, 2009). Though power law model is simple, it does not include aspects of adsorption or desorption of reactant / product molecules in calculating the reaction rate that may reduce their accuracy (Ramachandran and Chaudhari, 1983).

2.14.5 Langmuir-Hinshelwood models

Langmuir-Hinshelwood (L-H) model is also used to study the kinetics of HDS and HDN reactions. These following steps of reaction are considered in L-H model (Ramachandran and Chaudhari, 1983),

- Adsorption of A on catalyst surface
- Adsorption of B on catalyst surface
- Reaction between adsorbed A and B
- Desorption of reaction products thus making the active sites available for further reaction

The underlying assumptions in the construction of L-H models include (Satterfield, 1991),

- One active site is used for the adsorption of one species only
- Reaction takes place between adsorbed species on the catalyst active sites
- Surface energy is constant for each site

L-H models are considered to be superior and realistic to that of power law models because of the consideration of competitive adsorption of reactant, intermediate or product molecules (Ramachandran and Chaudhari, 1983). A brief comparison of Power law model and L-H model is given in Table 2.9.

For carbon supported catalysts, the inhibition effect of H_2S was found to be higher than that for γ-Al_2O_3 supported ones (Calafat et al., 1996a; Farag et al., 2000; Hensen et al., 2003). Equation 2.6 shows a form of L-H model, which can account for inhibition effects that can alter the reaction rate (r_A) is given by (Sigurdson, 2009),

$$r_A = -\frac{dC_A}{dt} = \frac{k_A * C_A{}^n}{(1 + K_A * C_A)^m} \qquad \text{----------} \qquad (2.6)$$

The terms k_A, C_A and n in equation 2.6 are similar to that defined for equations 2.4 and 2.5. Other terms are,

m - Empirical constant for inhibition term

K_A - Adsorption rate constant for species A, L/mol

In equation 2.6, n and m are experimentally determined constants considered to be independent of temperature. All the four terms – k, K, n and m are specific to a reaction system and are calculated by applying non-linear regression analysis on experimental kinetic data.

Table 2.9: Comparison of Power law model and L-H model (Ramachandran and Chaudhari, 1983)

	Power law model	L-H model
1	Does not consider adsorption/ desorption, inhibition effects and can give poor results at times.	More realistic due to the incorporation of adsorption/ desorption, inhibition behaviours.
2	Mathematically simple; hence sufficient for many occasions.	Calculations need rigorous procedure.
3	Applicable to limited range of concentration.	Applicable to wide range of concentration.
4	Intermediate product concentrations are not considered in the model.	Intermediate product concentration and their effects can be incorporated.

2.14.6 Multi-Parameter model

Multi parameter model includes variation in pressure and gas-to-oil ratio alongwith variations in LHSV and temperature in the estimation of reaction rate constant. It can be considered as an extended version of power law model. The rate of reaction by multi-parameter model is expressed by (Duan et al., 2005),

$$r_A = -\frac{dC_A}{dt} = k_A * C_A{}^n * P_{H_2}{}^h * (G/O)^q \qquad \text{----------} \quad (2.7)$$

The terms k_A, C_A and n in equation 2.7 are similar to that defined for equations 2.4 and 2.5.

Other terms are in equation 2.7 are,

P_{H_2} - Hydrogen partial pressure, MPa

G/O - Gas-to-oil ratio, Nm^3/m^3

h, q - Empirically determined constants for pressure and gas-to-oil ratio terms

From the kinetic parameter study and mass transfer evaluation, one can find out whether the calculated reaction rates are intrinsic or apparent.

CHAPTER 3

EXPERIMENTAL

The experimental procedures followed in this project can be split into six divisions as listed below.

- Synthesis of mesoporous carbon support
- Functionalization of mesoporous carbon support
- Synthesis of NiMo/mC catalysts
- Characterization of supports and catalysts
- Hydrotreating activity study
- Kinetic model development

The details of synthesis methods, characterization techniques and related scientific principles and research methodology used in this project are presented in this section.

3.1 Preparation of mesoporous carbon support

3.1.1 Preparation of Primary template

The first part in the preparation of mesoporous carbon was the synthesis of primary template that can be used to replicate carbon support. SBA-15 was used as the primary template in the project and it was prepared by sol-gel method (Yu et al., 2002; Zhao et al., 1998) using Tetra Ethyl Ortho Silicate (TEOS) as the silica source and triblock copolymer P-123 as the structure directing agent (SDA). P-123 is the polymer containing Polyethylene oxide – Polypropylene oxide- Polyethylene oxide chain with approximate molecular weight of about 5750 gm/mol.

In the first step, P-123 was added to 2M HCl acid solution along with KCl. The mixture was stirred using a magnetic stirrer for 4 hours at 40°C to ensure complete dissolution of P-123 in HCl-KCl solution. Then the silica source (TEOS) was added to the mixture with vigorous stirring. The molar ratio of P123: KCl: HCl: H_2O used is 0.016:0.8:6:166. Upon dissolution in HCl solution, the micelle of P-123 forms hydrophilic and hydrophobic parts. Addition of silica source into the solution leads to hydrolysis of silica and results in the formation of silica oligomers. This is followed by cooperative assembly, aggregation and condensation and continuous condensation of silica oligomers. The material was transferred into a closed vessel for hydrothermal treatment which was carried out in two stages to complete the condensation process. The first stage treatment was done at 40°C and the second stage at 130°C. Figure 3.1 shows the process flow of SBA-15 synthesis.

The material after hydrothermal treatment was filtered without washing in a vacuum system to remove the SDA template. It was air dried to remove the moisture and then calcined at 550°C for 4 hours to achieve complete removal of the SDA template, thus generating pores in SBA-15 structure.

3.1.2 Preparation of mesoporous carbon

Mesoporous carbon support was prepared as described by Jun et al. (Jun et al., 2000) using sucrose as carbon source and sulphuric acid as the polymerization catalyst. To avoid settling of sucrose on carbon surface, the impregnation was carried out in two stages. Approximately 60% of sucrose needed for filling the pores of SBA-15 was used in first stage. The aqueous solution containing carbon precursor was slowly added to the SBA-15 material with continuous manual stirring. The mixture was kept in an oven at

105°C for 6 hours for the removal of moisture and movement of sucrose into the pores. The temperature was raised to 160°C (@ 1^{o}C/min) and then held at that temperature for 6 hours for completing first stage polymerization. Second stage impregnation and polymerization of remaining sucrose was carried out in a similar way.

The carbon-silica polymer from the previous step was ground, transferred into quartz boats and placed in a glass reactor for carrying out carbonization. The material was heated under argon flow of 50 ml/min with a heating rate of 2°C/min till the temperature was reached to 900°C and then held at that temperature for 3 hours. Such slower heating rates can create homogeneous atmosphere during carbonization step which can help in enhanced structural ordering of carbon material during the replication process (Yang and Mokaya, 2008). The material was cooled under argon flow till the temperature was below 50 °C. The experimental setup used for the carbonization process is shown in Figure 3.2.

Finally, the removal of silica template from carbon was achieved by washing the silica-carbon composite in hydrofluoric acid. The silica-carbon carbonized matter was mixed with 8% HF acid solution and stirred at room temperature for 24 hours. The material was then filtered to remove the fluorosilicates. To ensure complete removal of silica, the washing was repeated with the same concentration of HF acid for another 24 hours. The template free mesoporous carbon material was filtered in a vacuum filter and washed multiple times to remove the residual HF acid followed by drying at 120°C for 12 hours to remove moisture. This material was termed as mC-V (virgin mesoporous carbon). A flow diagram for the synthesis of mesoporous carbon support is shown in Figure 3.3.

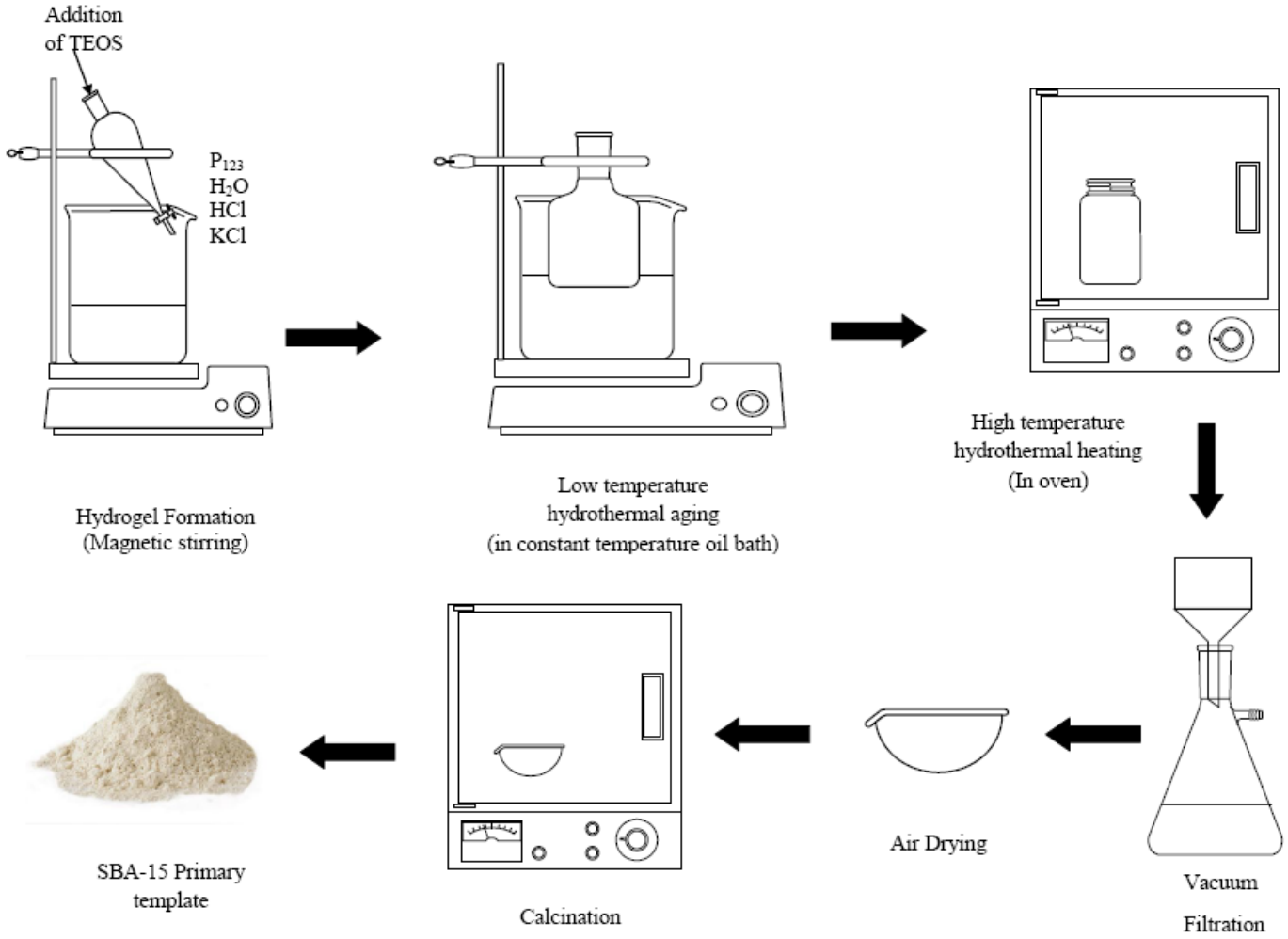

Figure 3.1: Flow diagram depicting SBA synthesis process

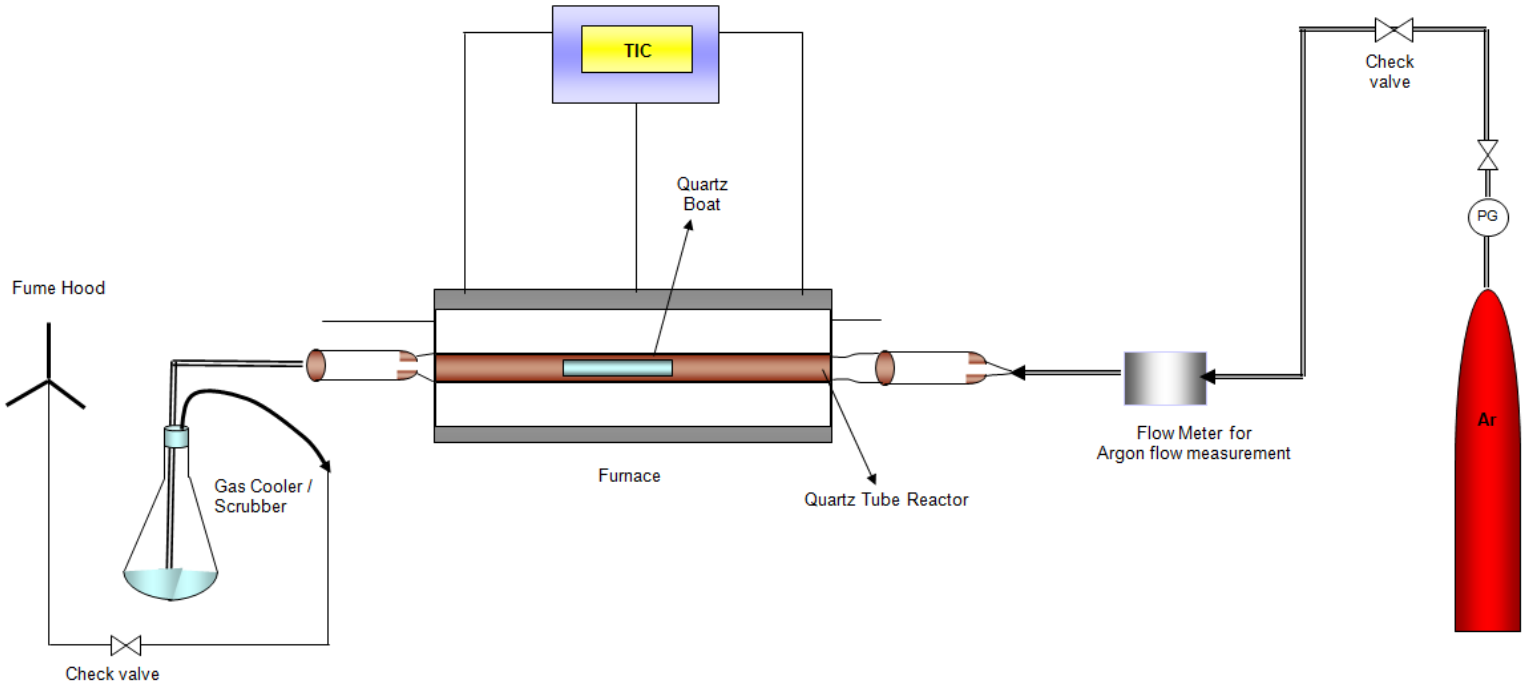

Figure 3.2: Experimental set up for carbonization

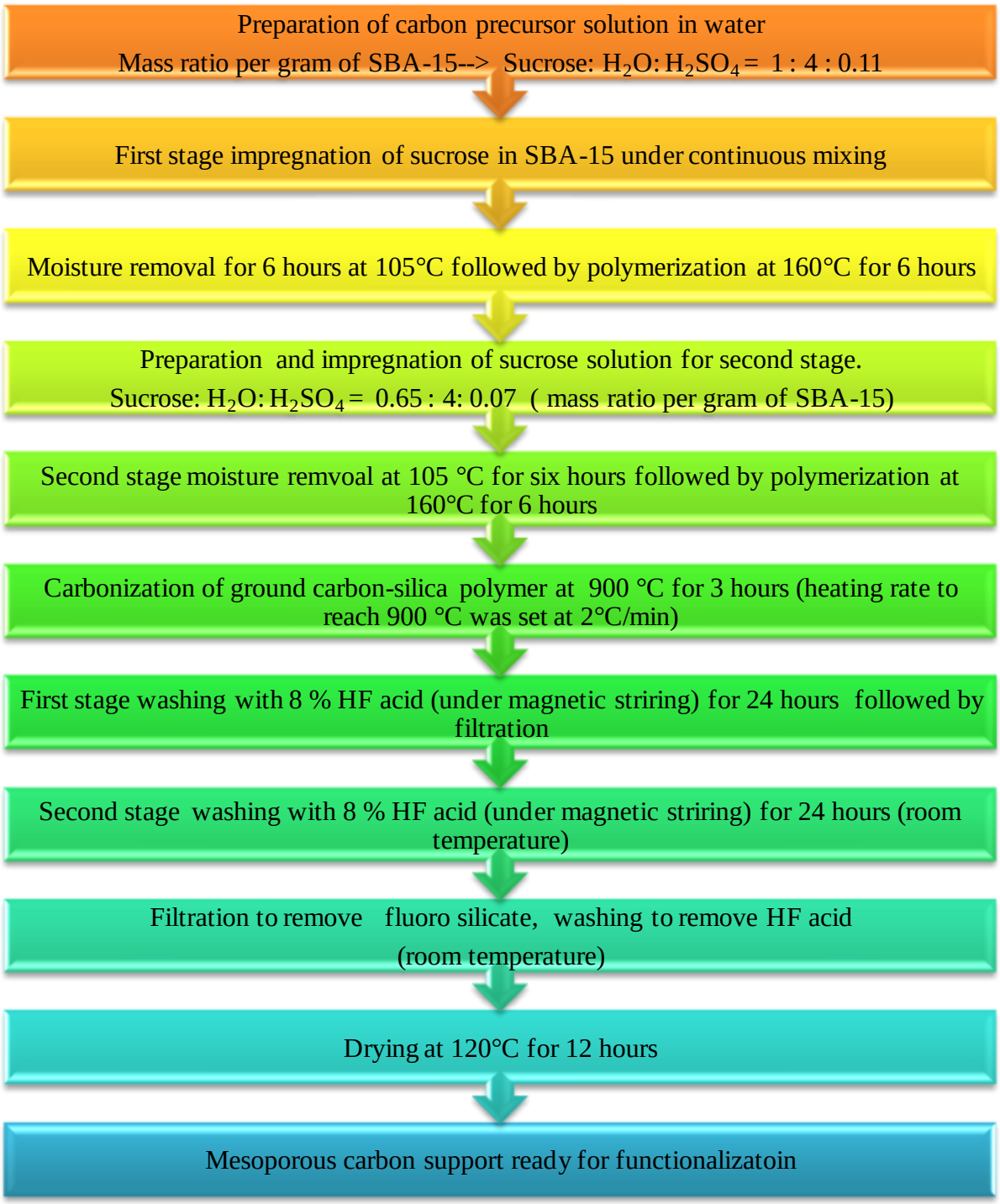

Figure 3.3: Process sequence in the synthesis of mesoporous carbon support

3.2 Functionalization of carbon supports

Functionalization of mesoporous carbon supports was carried out using nitric acid at a temperature of 85°C for duration of 3.5 hours under reflux condition and magnetic stirring fitted with a temperature monitor. Oil bath over a hot-plate was used to obtain uniform temperature in the carbon-nitric acid mixture (Figure 3.4). 5 mg/ml of supports were used in varying concentrations of nitric acid (2M to 8M) to produce mesoporous carbon material with different level of functional groups. The treated material was filtered and washed multiple times to remove residual nitric acid. The functionalized mC supports thus obtained were designated as mC-*x*M where *x* denotes the molarity of the nitric acid used.

3.3 Preparation of NiMo Catalysts

NiMo catalyst supported on functionalized mesoporous carbon was prepared by incipient wetness impregnation method. Ammonium heptamolybdate tetrahydrate was used as the precursor for molybdenum and nickel nitrate as the precursor for nickel. The impregnation was carried out in two stages to avoid the precipitation of catalyst metal from the saturated solution. The wet material was air dried at room temperature for 12 hours, dried at 120 °C for 12 hours, followed by calcination under argon flow of 50 ml/min at 450°C for 4 hours (heating @2°C/min).

Conventional γ-Al_2O_3 supported NiMo catalyst was prepared by the procedure given by Vishwakarma et al. (2007). Briefly, commercial γ-Al_2O_3 support was calcined at 450°C for 2 hours and then sequential metal impregnation was carried out using the aqueous solutions of ammonium heptamolybdate tetrahydrate and nickel nitrate. The wet material was air dried at room temperature for 12 hours, dried at 120 °C for 12 hours and then calcined at 500°C for 6 hours.

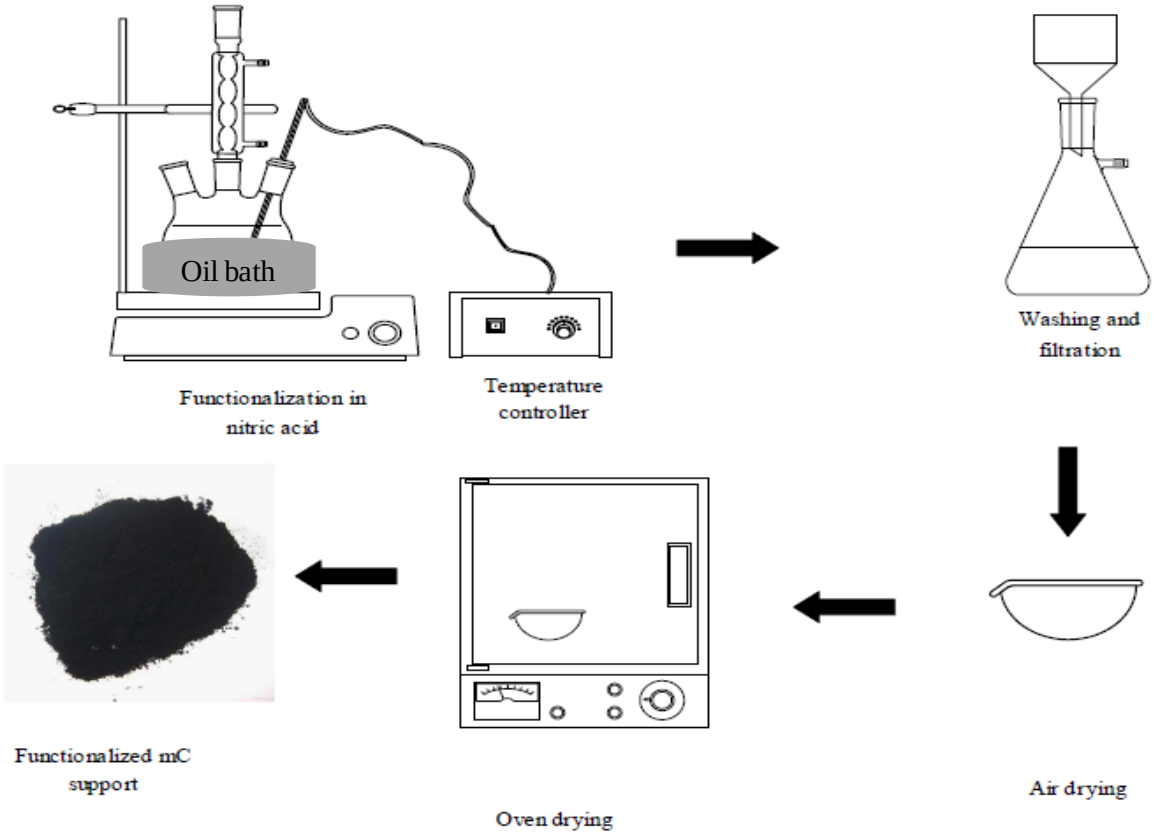

Figure 3.4: Experimental set up used for the functionalization of mesoporous carbon

3.4 Support and Catalyst Characterization

3.4.1 N_2 Physical Adsorption

The pore diameter, pore volume and surface area of the carbon supports and the catalysts were measured at 77K in a Micromeritics 2000 ASAP analyzer by N_2 adsorption-desorption method. Around 0.2 gram sample was degassed at 200°C for 1 hour in 0.55 mmHg vacuum to remove the moisture from the pores of the material. Pore diameter and mesopore volume were calculated from the adsorption isotherms using BJH method. Surface area was calculated using the adsorption data upto a relative pressure of 0.2 by BET method.

3.4.2 Thermogravimetric Analysis

Thermogravimetric analysis (TGA) was used to understand the phase purity of carbon. The weight changes in mC support upon heating under air flow of 50 ml/min were measured in a PerkinElmer TG/DTA thermo gravimetric differential thermal analyzer. A heating rate of 10°C was used to reach the maximum temperature of 600° from the initial temperature of 25°C.

3.4.3 Boehm Titration

The amount of surface acidic groups on virgin and functionalized mesoporous carbons were estimated by Boehm titration. 0.2 gram of the sample was mixed in 25 ml of 0.02N NaOH solution and stirred at room temperature for 24 hours. The mixture was filtered out and 5ml of this filtrate was titrated against 0.02N HCl. The amount of HCl consumed is used to calculate the quantity of total acidic groups (carboxylic, lactonic and phenolic groups) reacted with NaOH (Zhang et al., 2010).

3.4.4 Fourier Transform Infrared Spectroscopy (FTIR)

Almost all molecules absorb infrared radiation at certain specific frequencies and vibrate upon absorption of photons. This phenomenon can help to characterize the molecule in a unique way qualitatively as well as quantitatively as the absorption depends on the quantity. Surface functional groups over the functionalized and virgin mC supports were analyzed by FTIR spectroscopy in a JASCO FTIR 4100 instrument. A measured quantity of the sample was ground with KBr and placed in the measurement cell at room temperature. The average spectrum for each experimental run was found after 32 scans with a nominal 4 cm^{-1} resolution.

3.4.5 Transmission Electron Microscopy

The morphology of silica template, mC supports and catalysts was characterized using JEOL 2011 scanning Transmission Electron Microscope (TEM) at an accelerating voltage of 200 KeV. Sample specimens used for the analysis were prepared by ultrasonic dispersion of the catalysts in ethanol and the suspensions were dropped onto a carbon coated copper grid for recording the images.

3.4.6 Scanning Electron Microscopy

The morphology of silica template, mC supports and catalysts was further characterized using JEOL JSM6400 digital Scanning Electron Microscope (SEM) with Energy Dispersive X-ray Analyzer (EDAX - Genesis). Sample specimens used for the analysis were prepared by ultrasonic dispersion of the samples in ethanol. The sample was then coated with a thin layer of carbon to reduce charging and imaged in the SEM at an accelerating voltage of 15keV.

3.4.7 X-Ray Diffraction (XRD)

X-rays are emitted by the sudden stoppage of fast moving electrons. X-ray diffraction can be defined as the elastic scattering of x-ray photon by atoms in an ordered lattice. A constructive interference results in a peak from which the d-spacing could be calculated using the Bragg equation,

$$n\lambda = 2d\sin d\theta$$

Where,

λ - Wavelength of the X-rays (A°)

d - Distance between two lattice planes (nm)

θ – Angle of diffraction

n – Integer termed as order of reflection (taken as 1).

XRD studies were performed using a Rigaku X-ray diffractometer with a nickel filtered Cu Kα radiation (λ = 1.54 A°) filtered by a graphic monochromator at a voltage of 40kV and a current of 80 mA for identifying the presence of crystalline phases in mesoporous carbon supported catalysts. The powdered samples were spread with acetone over a glass slide and then dried at room temperature. The recording was carried out for 2θ angles from 10° to 60° at a scanning speed of 1°/min.

3.4.8 Small Angle X-Ray Scattering (SAXS)

Structural orderliness of the silica template and mC supports was analyzed by SAXS technique. A small amount of sample was placed in between two sheets of mylar

film supported by a flat, metal holder with a hole through it (for transmittance). Data was obtained using a still data collection for an exposure time of 300 seconds with a Bruker Smart6000 CCD detector on a 3-circle D8 goniometer. The source was a Rigaku RU200 Cu rotating anode generator fitted with parallel focusing cross-coupled mirrors and a 0.5mm pinhole collimator.

3.4.9 Elemental analysis

Elemental composition of catalyst metals (Mo and Ni) over the mC support were identified using inductively coupled plasma mass spectrometer (ICP-MS). Plasma containing equally charged positive and negative ions was created using the collision of electron with argon gas placed inside an induction coil chamber. A catalyst sample (about 0.05g) was dissolved in HF acid (48-51%) at a temperature of 100-150°C for three days. After cooling, samples were further dissolved in concentrated HNO_3 to ensure complete dissolution of the metals. Final solution was prepared using 0.2N HNO_3 and it was introduced into the plasma. In the inductively coupled plasma created by argon, metal gets ionized (M^+ and e^-). The M^+ ions were detected by a mass spectrometer and the detector response is proportional to the concentration of Mo and Ni present in the catalyst.

3.4.10 Raman Spectroscopy

When a molecule is impinged by monochromatic light, interaction of the light with the electron cloud and bonds of the molecule occur, which results in the excitation of the molecule. Upon emitting a photon, the molecule returns to a new energy level

leading to a shift in the frequency of emitted photon (inelastic scattering). This is called Raman Effect. The shift is characteristic of the bond of the molecule.

The vibration modes of mesoporous carbon supports were measured by Raman spectroscopy for wavelengths ranging from 1000 to 2000 cm^{-1}. A Renishaw Micro-Raman system 2000 spectrometer equipped with a laser source having a wavelength of 514 nm was used for this purpose. The laser spot size was approximately 50µm with a power of 5MW. For mesoporous carbon supports, the intensities of D-band (located in 1330 to 1350 cm^{-1}) and the G-band (located in 1580 to 1600 cm^{-1}) were used to understand the extent of change in their morphology due to functionalization.

3.4.11 Temperature Programmed Reduction

Sulphide phase is the active phase for hydrotreating process (Mochida and Choi, 2004). The oxide catalyst was reduced into its sulphide (MoO_3 (i.e. Mo^{6+}) → MoS_2 (i.e. Mo^{4+})) form upon loading into the reactor. Lower metal support interaction can help to achieve the sulfidation at relatively lower temperature (i.e. easy reducibility). Reducibility of the carbon supported NiMo oxide catalyst was studied using Temperature Programmed Reduction (TPR) using H_2 as the reducing agent before loading into the hydrotreating reactor.

Approximately, 0.1 gram sample was placed in the TPR reactor and was heated to a temperature of 130°C at a rate of 10°C/min and then held at this temperature for 30 minutes under a helium flow of 50 cm^3/min for removing moisture. After that, it was cooled to 40°C and hydrogen flow was started at a rate 50 cm^3/min (Gas composition: H_2 9.5% v/v, rest argon). The temperature was raised at a rate of 10°C/min from 40°C to

600°C and held at this temperature for 60 minutes. Consumption of H_2 was monitored by a thermal conductivity detector (TCD) attached to a Micromeritics AutoChem II chemisorption analyzer. The effluent gas was passed through a cold trap placed before the TCD, in order to remove the water. This ensures that, the observed signal in TCD is only due to H_2 consumption and not due to moisture.

3.5 Hydrotreating activity study

The hydrotreating activity in terms of hydrodesulphurization (HDS) and hydrodenitrogenation (HDN) of the NiMo catalyst supported on mesoporous carbon supports was studied in a laboratory scale trickle bed reactor using coker light gas oil (KLGO) derived from Athabasca bitumen as feedstock. The characteristics of the KLGO feed are shown in Table 3.1.

The reactor set up used for the activity study is shown in Figure 3.5. The system consisted of following equipment items.

- Gas supply – Hydrogen required for the reaction was supplied from a cylinder through a mass flow meter. Helium used as the inert carrier during start-up and shutdown was also supplied from a cylinder.
- Coker light gas oil feed was supplied from a feed tank through a metering pump. The feed tank (capacity 1 litre) was kept blanketed with inert gas (Helium at 50 psi) and was topped-up intermittently during the run. Feed was mixed up with hydrogen by online mixing before entering the reactor.
- Reactor was heated up using an enclosed furnace, in which automatic temperature control was used to maintain the reaction temperature.

- Wash water vessel –The reactor exit stream that contain ammonia and hydrogen sulphide alongwith liquid products was passed through wash water vessel. The vessel was filled up with water (upto 50 ml) that helps to quench the reactor effluent stream as well as to dissolve NH_3HS (formed by reaction of NH_3 and H_2S).
- High pressure (HP) separator– Quenched reactor effluent stream that contain vapor-liquid mixture was separated in the high pressure separator. The liquid product from HP separator was collected periodically.
- Back pressure control valve (BPCV) – The function of BPCV is to maintain the system pressure by venting the excess gases to the Scrubber.
- Scrubber – Gaseous products from HP separator was directed into the scrubber which was filled with caustic solution where most of the H_2S was removed. Rest of the effluent gas was vented to safe disposal.
- The reactor system was provided pressure safety valves and non-return valves to ensure safety during operation of the reactor.

The catalyst was made into pellets (average pellet diameter ≈ 1.7 mm) and loaded into the reactor alongwith silicon carbide diluents. The diluent materials help to overcome certain hydrodynamic limitations associated with laboratory reactors. The length of the reactor used in the study was 25 cm and diameter was 1 cm. The reactor was fitted with suitable filter to retain the catalyst and diluents before loading the catalyst.

At first, bottom of the reactor was loaded with glass beads of 3 mm diameter for a depth of 22 mm. This was followed by a silicon carbide layer (size 16 mesh) for 25 mm. After that, further addition of silicon carbide layers of 40 mesh and 60 mesh material for

depths of 10 mm each was carried out. Then two grams of the catalyst pellets was diluted with 12 ml of 90 mesh silicon carbide and loaded into the reactor in alternate layers (about 10 layers each). This was followed by the filling of higher sized diluents (60 mesh, 40 mesh and 16 mesh) for a depth of 8 mm each. Finally, glass beads (3 mm diameter) were filled for a length of 20 mm to complete the catalyst filling. The remaining top section of the reactor was kept empty and the reactor was installed in the set up. The reactor was pressurized with helium gas to 10.0 MPa to check for any leak. The pressure was reduced to the operating pressure of 8.8 MPa before introduction of any liquid stream. The reactor catalyst loading diagram is shown in Figure 3.6.

Sulphide is considered to be the active phase for hydrotreating (Mochida and Choi, 2004). Hence it is necessary to convert the oxide catalyst (MoO_3) into sulphide before the reaction. Many researchers carry out presulphidation separately before the reaction. However due to the difficulty in handling sulfided catalyst externally, in situ sulfidation is generally preferred in industrial reactors and the same method was followed for the project.

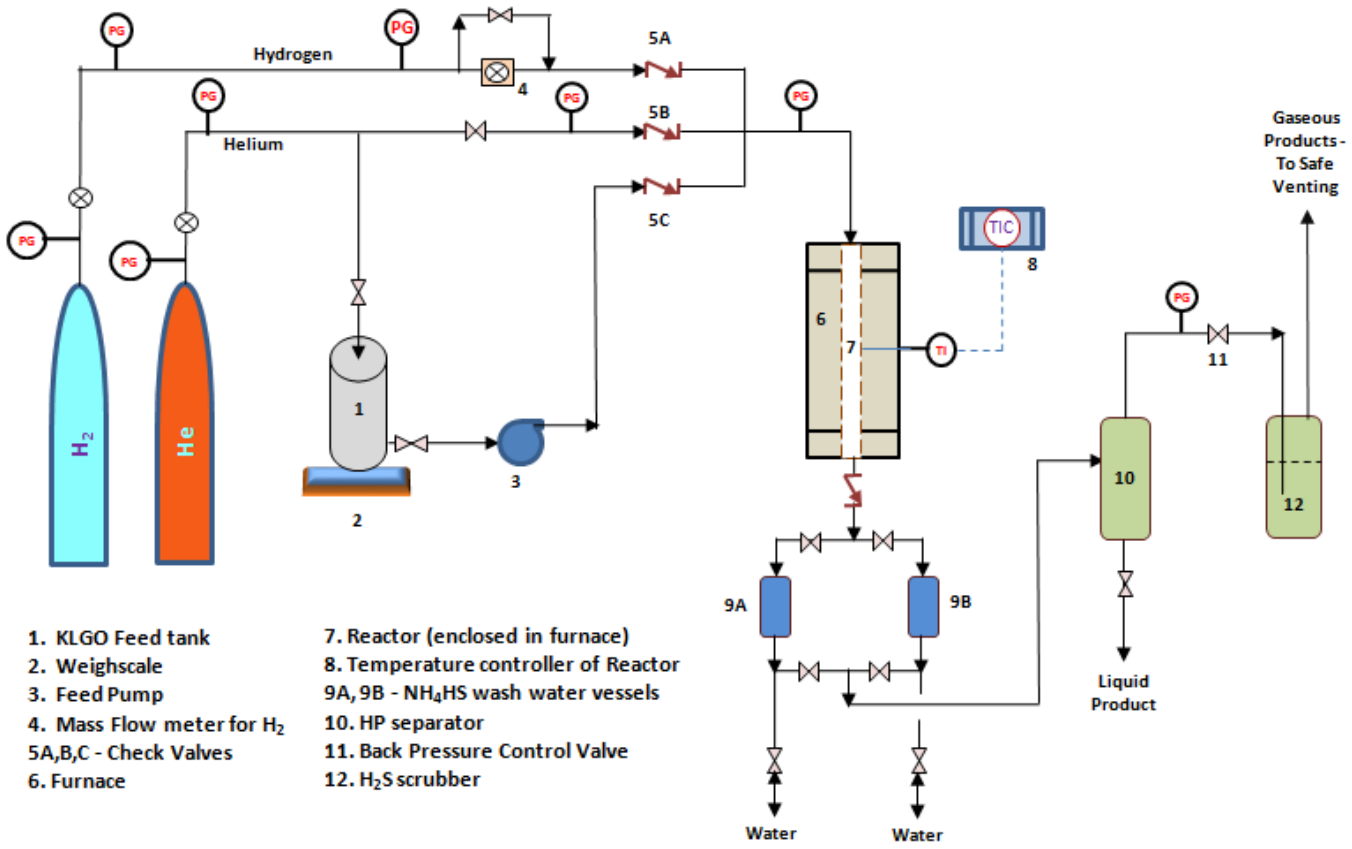

Figure 3.5: Experimental set up for hydrotreating activity study

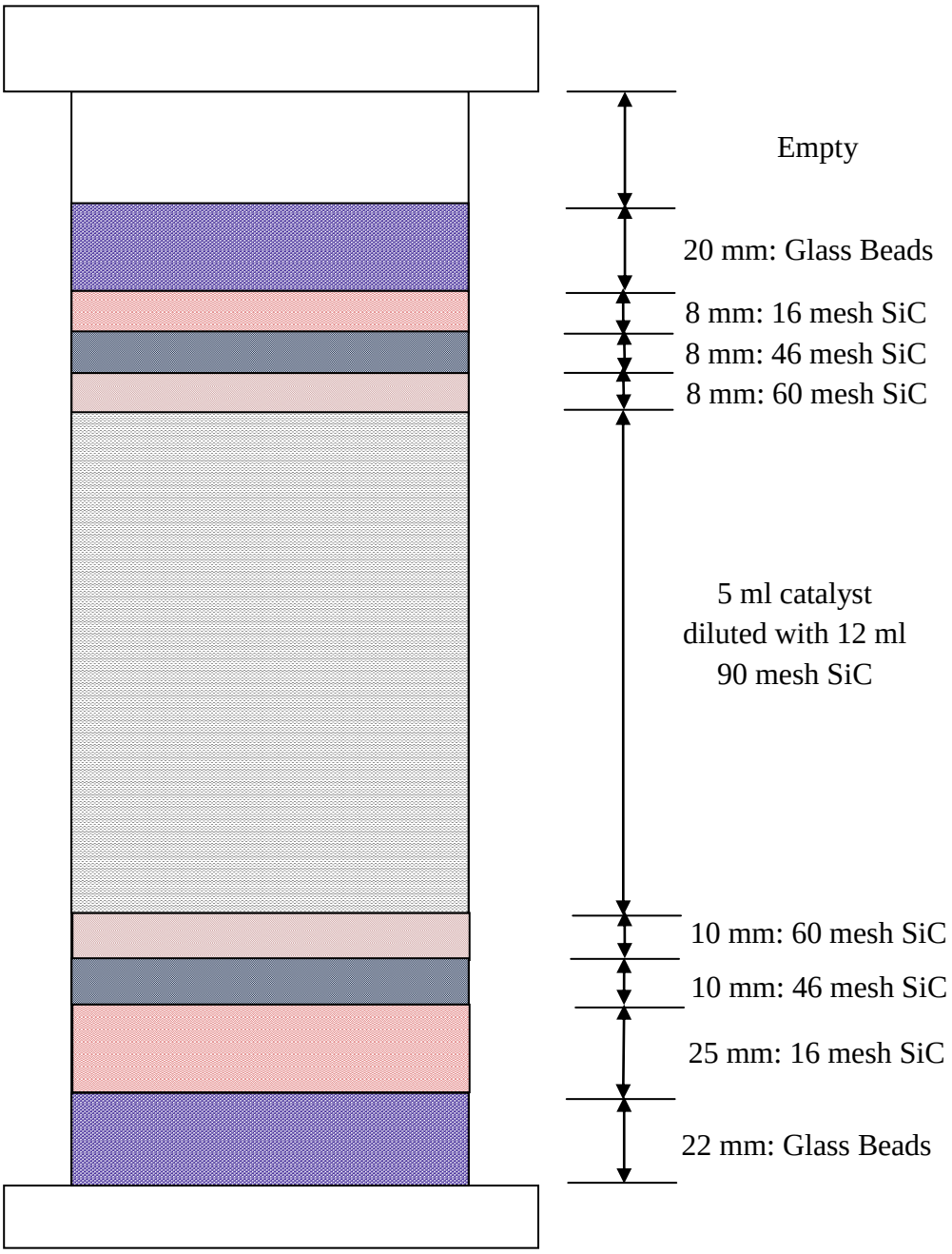

Figure 3.6 Reactor catalyst loading diagram

Measured quantities of clean gas oil and butanethiol were mixed to produce a gas oil blend with 1.0 wt% sulphur and it was filled in the feed tank. At this point, reactor temperature was raised to 100 °C and helium flow was resumed at 50 ml/min. Then gas oil blend was pumped to the reactor at a rate of 30 ml/hr for a period of 3.5 hours to ensure wetting of the catalyst material (pre-wetting process). After pre-wetting the catalyst, flow of gas oil blend was reduced to 5 ml/hr and the reactor temperature was raised to 193°C (@ 2°C/min). Helium flow was stopped and hydrogen was introduced at 50 ml/min rate to commence first stage sulfidation. After 24 hours of sulphidation at 193°C, the reactor temperature was raised to 343 °C (@ 2°C/min) to start the second stage sulfidation, which was carried out for 24 hours at 343°C. Sulfidation was done in two stages to avoid sintering of active phase and to achieve complete sulfidation of MoO_3 (Ferdous, 2003). During sulfidation $Mo^{6+}O_3$ gets reduced to $Mo^{4+}S_2$ (Nielsen et al., 2001) as per the reactions shown in equation 3.1

$$C_4H_{10}S + H_2 \longrightarrow H_2S + C_4H_{10} \quad \text{----------} \quad (3.1a)$$

$$Mo^{+VI}O_3 + 3H_2S^{-II} \longrightarrow Mo^{+IV}S_2 + H_2O + S^0 \quad \text{----------} \quad (3.1b)$$

$$S^0 + H_2 \longrightarrow H_2S^{-II} \quad \text{----------} \quad (3.1c)$$

At the end of sulfidation process, gas oil blend was replaced with KLGO feed and reactor temperature was raised to 370°C. The feed flow rate was set at 10 ml/hr and hydrogen flow set at 100 ml/min. The initial catalyst activity is generally high and unstable, but gets stabilized after some deposition of coke on the catalyst surface. The catalyst activity stabilization (pre-coking) was carried out for four days after which process conditions were changed. The catalytic activity measurement was done at three different

temperatures (370°C, 350°C, and 330°C). The product samples were collected at an interval of 12 hours. The samples were stripped by purging with nitrogen for 2 hours to get rid of the residual NH_3 and H_2S and then taken for the measurement of nitrogen and sulphur content.

3.5.1 Analysis of sulphur and nitrogen:

The important part of the study is to understand the catalyst activity towards desulphurization and denitrogenation of coker light gas oil feed. The total sulphur and nitrogen content of HDS and HDN gas oil feed and reaction products were measured using an Antek 9000 NS analyzer. Measured quantity of gas oil product (or feed) was diluted with xylene and 5 µL of the prepared sample was injected into the quarts sample boat. The sample was swept by argon which was used as the carrier gas (flow rate -140 mL/min) and oxygen which was used as the combustion gas (flow rate - 450 mL/min) into the combustion chamber. The gaseous products from the combustion process were passed through a membrane dryer to remove the moisture before entering into the detector chamber.

3.5.1.1 Quantification of nitrogen:

Measurement of nitrogen was done using chemiluminescence (ASTM D4629 method). Nitrogen in the sample was converted into nitric oxide gas in the combustion process and this gas was contacted with ozone to produce excited NO_2. The decay of excited NO_2 resulted in the emission of photons of specific wavelength (chemiluminescence process) and was detected by the photomultiplier tube. The chemiluminescence was specific to nitrogen and also proportional to the quantity of

nitrogen present in the sample. The detector response for known nitrogen concentrations (standards prepared using carbazole diluted in xylene) was used to quantify the nitrogen content in the sample

3.5.1.2 Quantification of sulphur:

Measurement of sulphur was done using fluorescence (ASTM 5453-06). Sulphur in the sample was converted into sulphur-di-oxide (SO_2). When the SO_2 gas (after moisture removal) was exposed to the ultra violet (UV) radiation, it absorbed the energy and got converted into excited SO_2^*. Upon returning of SO_2 from the excited level to stable level ($SO_2^* \rightarrow SO_2$) the absorbed energy was emitted (fluorescence) which was detected by a photomultiplier tube. The fluorescence signal was specific to sulphur atom and proportion to the amount of sulphur present in the sample. The detector response for known sulphur concentrations (standards prepared using dibenzothiophene diluted in xylene) was used to quantify the sulphur content in the sample.

3.5.2 Simulated distillation:

The boiling point distribution of feed and products was determined by simulated distillation using Varian model CP3800 gas chromatograph coupled with Varian CP8400 autosampler. The boiling temperature of the sample fractions was measured as a function of retention time as different fractions elute at different time. The eluted sample was detected by a flame ionization detector (FID). The sample was distributed into various fractions with 2% interval (by weight) thereby providing sufficient data points to develop a boiling point distribution. This method is useful to understand the heavy gas oil

fractions (i.e. non-diesel) present in KLGO feed and also to estimate other properties such as average molecular weight.

3.6 Study of effectiveness on functionalization (Phase-I)

The first phase of the work was to study the level of nitric acid functionalization of mesoporous carbon supports that can provide a balance between reduction in textural properties and benefits of increased surface functional groups. Various functionalized supports were used to prepare NiMo catalysts. The steps involved in the implementation of the Phase-I work are shown in Figure 3.7. For all the catalysts in Phase-I work, (including NiMo/γ-Al_2O_3), Mo content was set at 12 wt% with Ni/Mo atomic ratio of 0.33. The catalysts were termed as Cat-*x*M where *x* stands for the nitric acid concentration used for functionalization. The catalyst which showed the best activity was considered to have optimum functionalization and the same nitric acid concentration was used to prepare supports for Phase-II work. The reactor operating conditions and hydrotreating study plan used for Phase-I and Phase-II work are given in Table 3.2 and Figure 3.8 respectively.

3.7 Optimization of metal loading (Phase-II)

In phase-II, catalysts with different Mo and Ni loadings were prepared to find the optimum catalyst. The work flow diagram for phase-II work is given in Figure 3.9. The catalysts prepared with varying metal loading are termed as Cat-A to Cat-E and the detail of Mo and Ni content is given in Chapter 5. The optimum catalyst obtained from this work was used in the kinetic study.

Table 3.1: Characteristics of KLGO feed

Parameter	Value
Density (Kg/m^3)	901
Sulphur, ppm	23260
Nitrogen, ppm	1410
Distillation °C	**Recovery (wt%)**
IBP-250	21.8
250-300	24.6
301-350	25.5
351-400	17.2
401-450	7.2
451-FBP	3.7

Table 3.2: Hydrotreating reactor operating conditions

Parameter	Unit	Set value for Phase-I and Phase-II work	Set value for kinetic study
Reactor Pressure	MPa	8.8	7.8 to 9.8 (increment by 1.0)
Temperature	°C	330 - 370 (increment by 20)	330 – 370 (increment by 20)
Sulfidation temperature	°C	190 / 343	190 / 343
Gas-to-Oil ratio	Nm^3/m^3	600	400 – 1000 (increment by 200)
Catalyst Loading	gm	2	2
LHSV[a]	hr^{-1}	2	1.0 – 2.5 (increment by 0.5)

[a]- For γ-Al_2O_3 supported catalyst, catalyst mass loading was taken as basis and not LHSV.

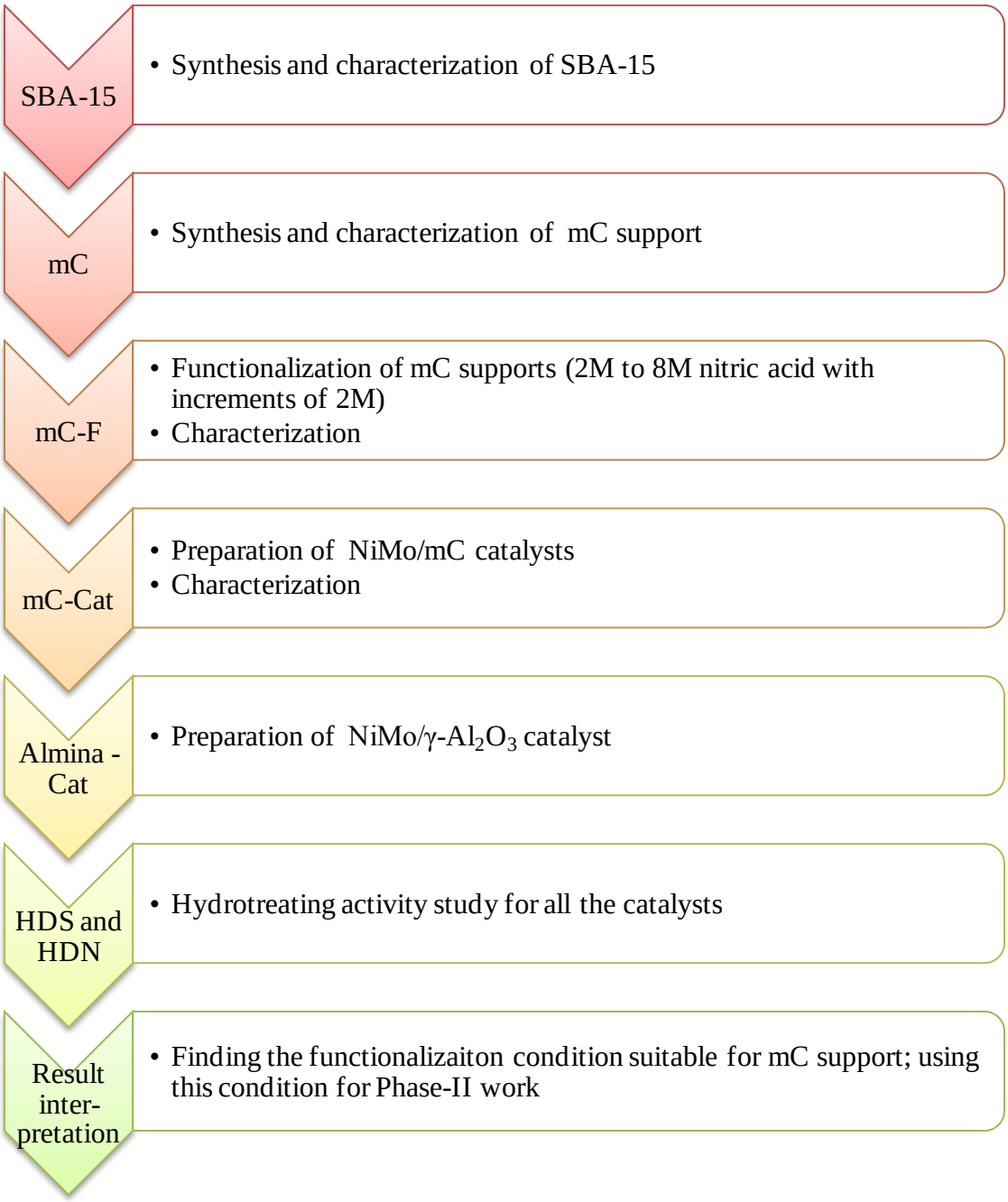

Figure 3.7: Work flow diagram for Phase-I

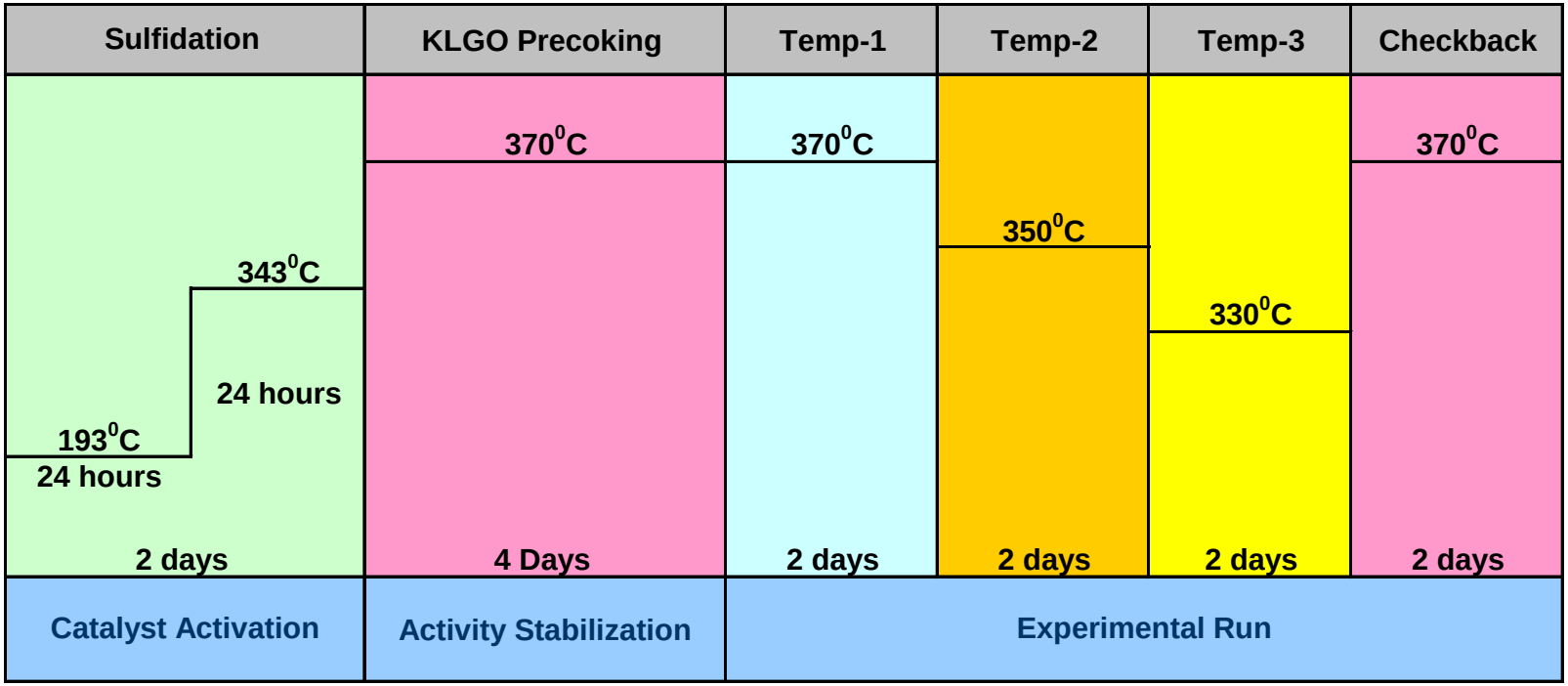

Figure 3.8: Hydrotreating study plan

3.8 Plan for Kinetic and Long term deactivation study

In the third phase of the project, kinetic study of the optimum catalyst was carried out. The study was divided into four parts-

- Studying the effect of various operating parameters (LHSV, Gas-to-oil ratio, pressure and temperature) on the hydrotreating activity of NiMo/mC catalyst. The conditions used in kinetic study are given in Table 3.2
- Studying the effect of mass transfer (external and internal) on HDS and HDN activities
- Kinetic modeling for HDS as well HDN using the generated data applying power law model, multi-parameter model and Langmuir-Hinshelwood model. Polymath software and Microsoft excel software were used to estimate kinetic parameters
- Most of the studies pertaining to mesoporous carbon supported catalysts reported in literature were carried out in batch reactors with few hours of operation (Table 2.7). However the catalyst performance can deteriorate upon prolonged operation and it is essential to study the effect on HDS and HDN activity on long term operation. The long term deactivation study was carried out in continuation of kinetic study. The temperature was kept at 370°C (this is the maximum temperature used in the study) with a LHSV of 2 hr^{-1}, pressure of 8.8 MPa and gas-to-oil ratio of 600 Nm^3/m^3.

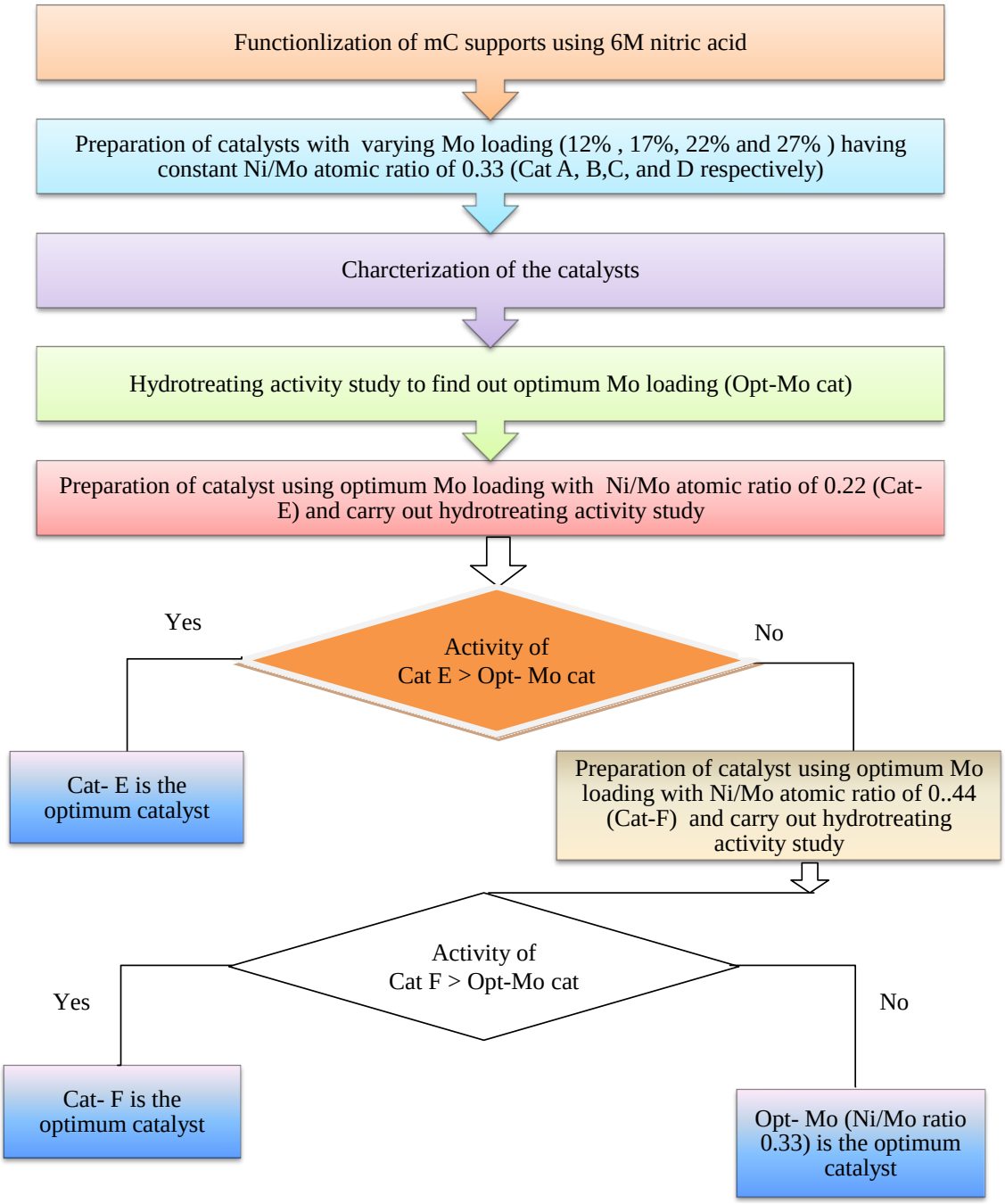

Figure 3.9: Workflow diagram – Phase II

CHAPTER 4

EFFECT OF FUNCTIONALIZATION OF MESOPOROUS CARBON SUPPORT ON THE HYDROTREATING ACTIVITY OF SUPPORTED NiMo CATALYSTS

The objective of the study on effect of functionalization was to understand the effectiveness of functionalization that can provide a balance between reduction in textural properties and benefits of increased surface functional groups. Mesoporous carbon support was synthesized using SBA-15 as the primary silica template and then functionalized using nitric acid of various concentrations (2M to 8M). The functionalized supports were termed as mC-*x*M where *x* stands for the acid concentration used in functionalization. The NiMo catalysts prepared using various functionalized supports were termed as Cat-*x*M where *x* stands for the nitric acid concentration used for functionalization (Mo content in all the catalysts was set at 12 wt% with Ni/Mo atomic ratio of 0.33). The catalyst that showed the highest hydrotreating activity was considered to have optimum functionalization of support.

4.1 Characterization of supports

4.1.1 N_2 Physical adsorption

The results of BET surface area, pore volume and pore diameter of silica template and mC supports measured by N_2 physical adsorption technique are given in Table 4.1. The mC support replicated from silica template has high BET surface area and mesopore volume (i.e. pore diameter between 2 nm and 50 nm (Sundaramurthy et al., 2008)) compared to the conventional γ-Al_2O_3 support. From Figure 4.1, it can be observed that

both silica template and carbon supports show type-IV isotherm, which is the characteristic of mesoporous materials (Gregg and Sing, 1991; Lázaro et al., 2007; Yu et al., 2002). The micropore volume in the alkali modified SBA-15 is lower compared to conventional ones as the micropores get converted into mesotunnels, which helps to obtain improved interconnectivity between nearby channels (Fan et al., 2001; Sayari and Yang, 2005; Yu et al., 2002). Carbonized silica-sucrose composite has almost zero pore volume (BET SA of 14.9 m^2/gm and PV of 0.02 cm^3/gm) compared to the pore volume of silica template indicating the complete impregnation of carbon precursor. As seen in Table 4.1, the surface area and pore volume of the functionalized carbons decrease with increase in acid concentration which can be mainly attributed to increase in surface functional groups. All of these functionalized supports exhibit a similar isotherm shape as exhibited by the virgin mesoporous carbon support.

Table 4.1: BET surface area, Pore diameter and Pore volume results of SBA-15 template and mesoporous carbons.

Material	**BET surface area (m^2/gm)**	**Total Pore Volume (cm^3/gm)**	**Pore dia[a] (nm)**	**Mesopore volume[b] (%)**
SBA-15	446	0.81	6.9	99.0
mC-V	1123	1.49	4.5	95.4
mC-2M	1052	1.31	4.2	93.9
mC-4M	1012	1.17	4.0	93.0
mC-6M	997	0.98	3.7	91.8
mC-8M	933	0.81	3.6	91.0
γ-Al_2O_3	198	0.65	na	97.7

[a] – BJH Pore diameter estimated from the adsorption branch of isotherm
[b] – Mesopore volume (%) = (Total pore volume - Micropore volume) x100/ Total pore volume

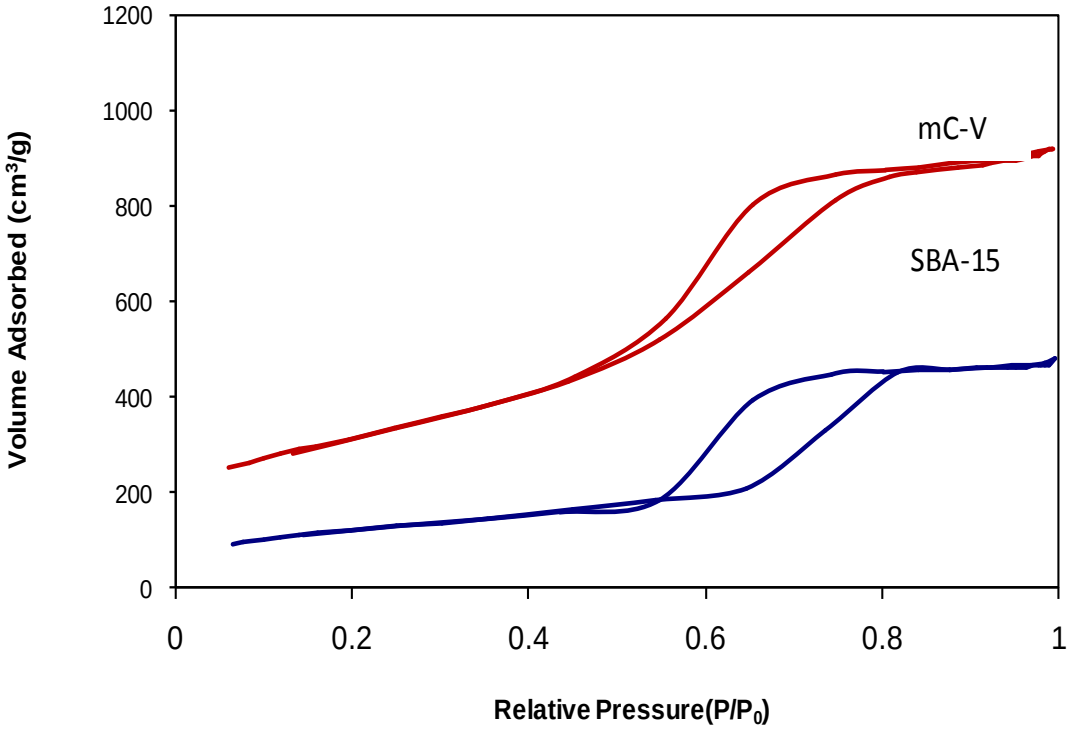

Figure 4.1: N_2 Physical Adsorption isotherm of SBA-15 and mesoporous carbon supports

4.1.2 Thermo Gravimetric Analysis (TGA)

The effective removal of silica template from the carbonized carbon-silica polymer was confirmed by TGA analysis done in flowing air (Figure 4.2). The weight loss at temperatures around 150°C is mainly due to vaporisation of residual moisture. Major weight loss occurs in the temperature range of 450 -575°C. The weight loss of carbon material is near complete at temperatures below 600°C indicating the absence of residual silica. Carbonized material after single wash using HF acid showed the presence of residual silica whereas the silica was completely removed after second HF acid treatment.

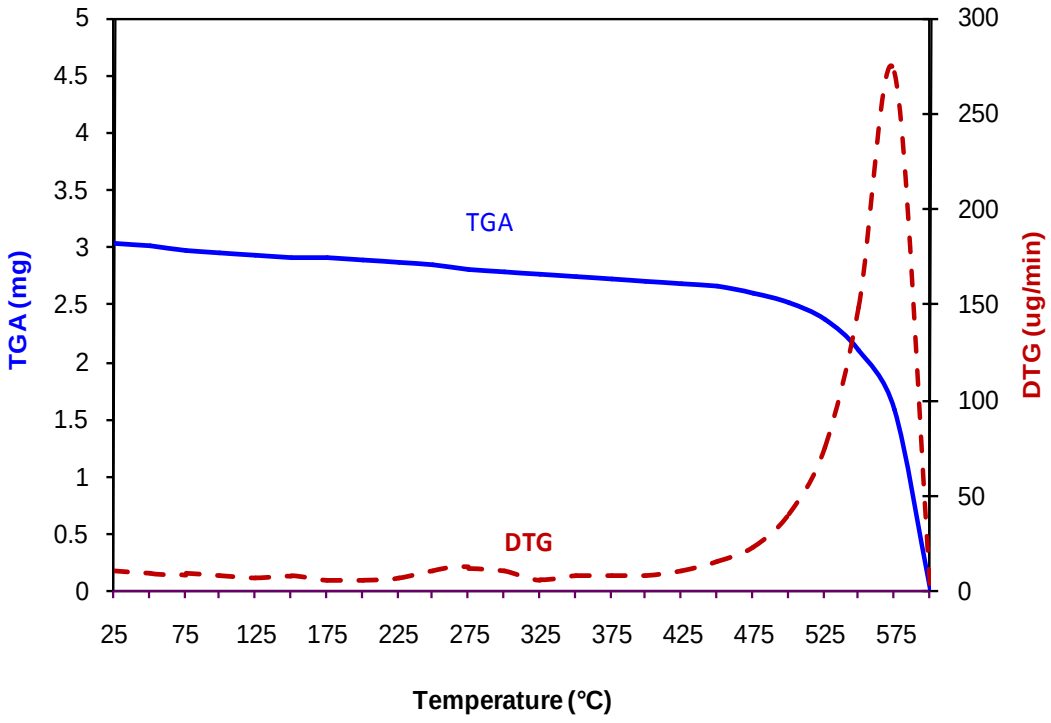

Figure 4.2: Thermogravimetric analysis data of mesoporous carbon support

4.1.3 Raman Spectroscopy

Figure 4.3 shows the vibrational characteristics of mesoporous carbon, studied by Raman spectroscopy. Two major bands, one in the range of 1330 to 1350 cm^{-1} (D band which is the characteristics of disorderliness) and another between 1580 to 1600 cm^{-1} (G band due to C-C stretching) are considered (Sigurdson, 2009). The G band is ascribed to the graphitic E_{2g} plane vibration and D band is ascribed to the A_{1g} plane that is due to the disorder parts such as grain edges (Shimodaira and Masui, 2002). The ratio of the intensity of D band to G band (I_D/I_G) is generally used to signify the disorderliness on the graphite layer of carbon material (Eswaramoorthi et al., 2008; Vinu et al., 2007). As nitric acid treatment results in etching of carbon walls, some amount of disorderliness is expected in the functionalized carbon materials. The I_D/I_G ratio in mC-V support is 0.9 and is in the range of 0.92 to 0.98 in mC-2M, mc-4M and mC-6M materials. However, there is a noticeable increase in the I_D/I_G ratio of mC-8M material ($I_D/I_G \approx 1.06$) which might be due excessive etching of the wall of the carbon material and increase in surface functional groups during functionalization with nitric acid of higher concentration. The I_D/I_G ratio of all the supports is much lower than commercial MWCNT supports (I_D/I_G=1.57) (Sigurdson, 2009) indicating that functionalized mesoporous carbons have lesser impurities compared to commercial MWCNTs.

4.1.4 Small angle X-Ray scattering (SAXS)

Small angle X-Ray scattering analysis shows that the SBA-15 material and its replicated carbon both show well resolved peaks (Figure 4.4), which can be assigned to (100), (110) and (200) reflections of a 2D hexagonal mesostructures (Yu et al., 2002). This confirms that the structure of mesoporous carbon material is preserved after washing with hydrofluoric acid at room temperature.

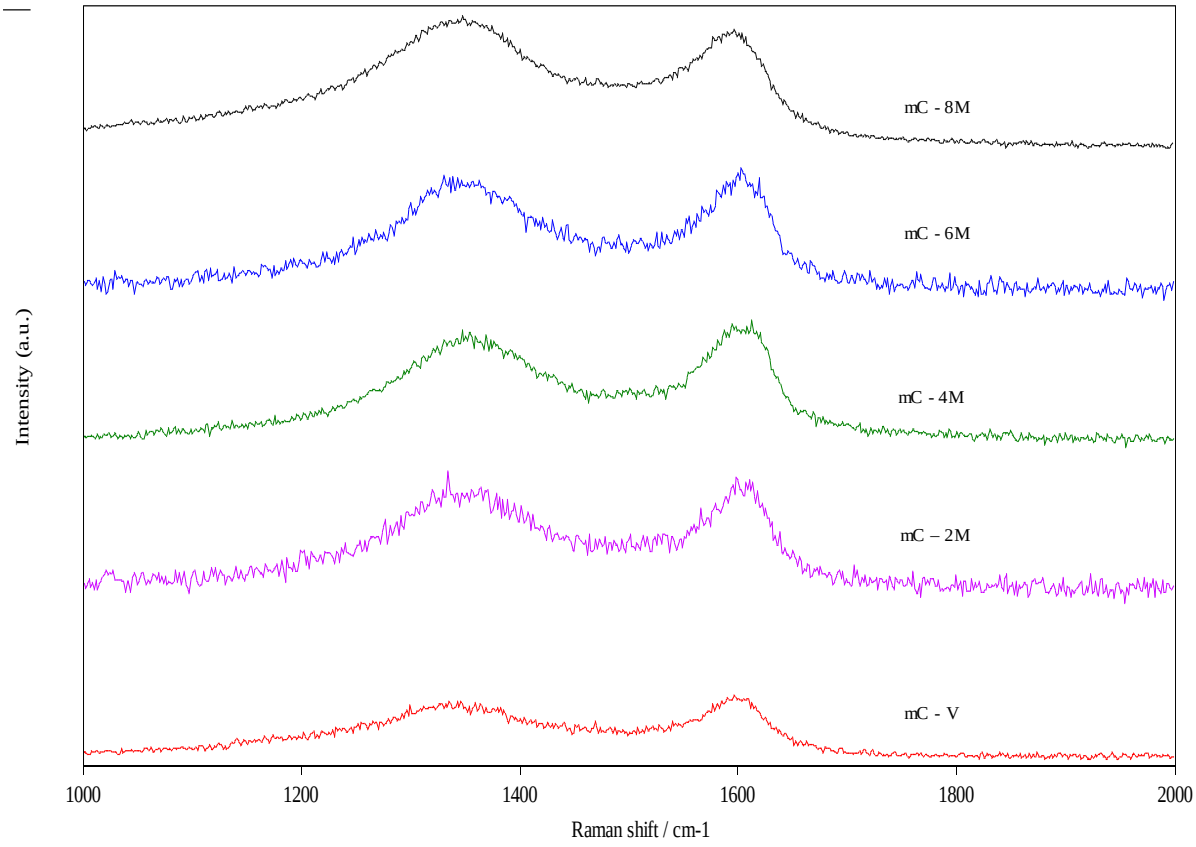

Figure 4.3: Raman spectroscopy results of virgin and functionalized mesoporous carbon supports

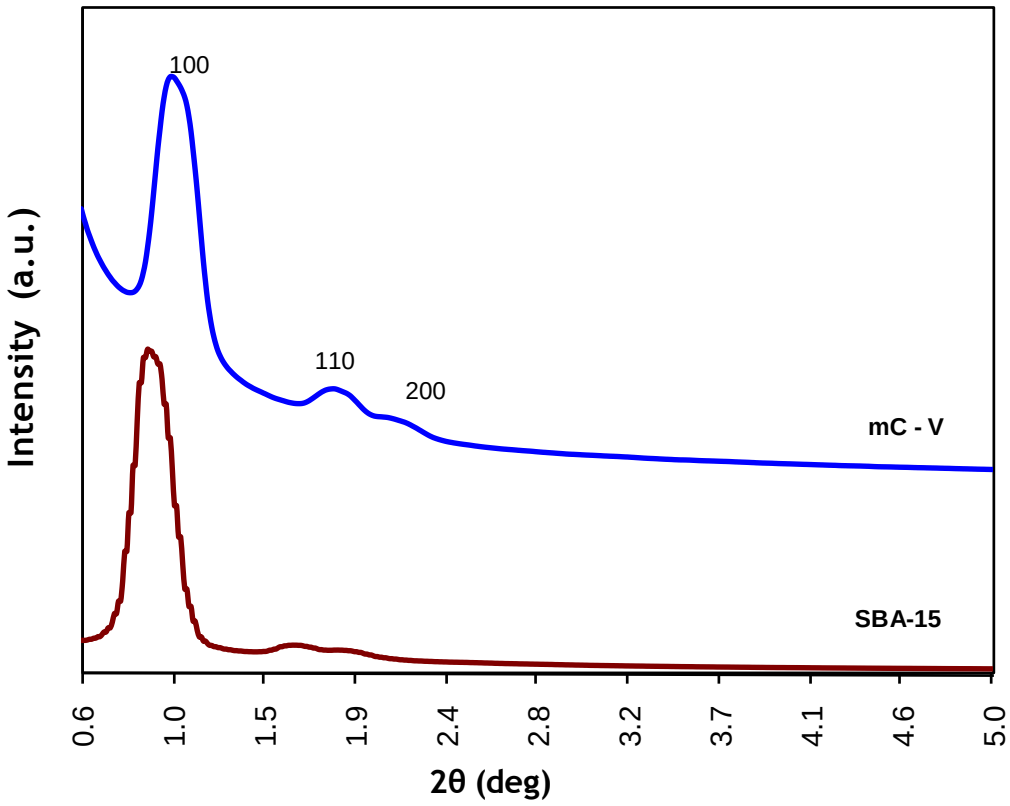

Figure 4.4: SAXS data of SBA-15 and mesoporous carbon support

The functionalized mesoporous carbon supports, mC-2M, mC-4M, mC-6M all show well resolved peaks as like virgin carbon support indicating the integrity of the structure after treatment with nitric acid at elevated temperatures (Figure 4.5). For mC-8M, the resolution is almost maintained but with slight reduction in peak intensity suggesting that some changes have occurred in its structure. This finding corroborates with the observation by Raman spectroscopy and N_2 physisorption analysis.

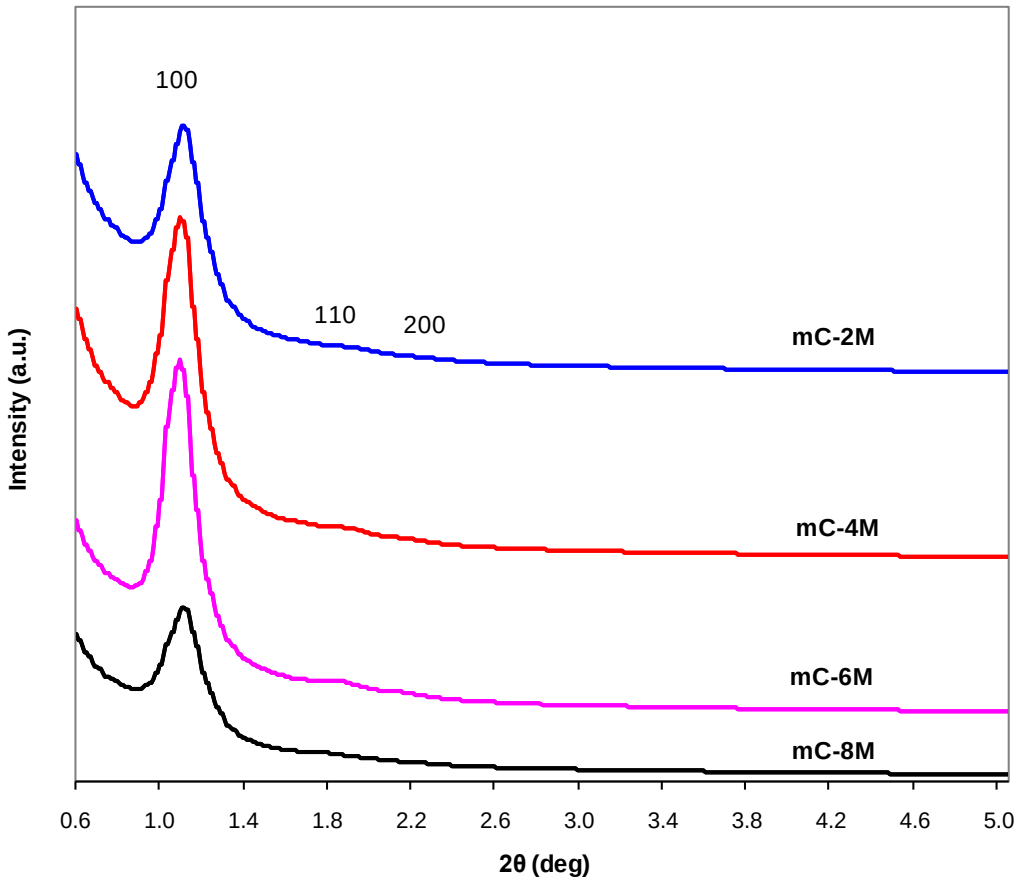

Figure 4.5: SAXS data of functionalized mesoporous carbon supports

4.1.5 Scanning Electron Microscopy (SEM)

Mesoporous carbon supports prepared from alkali modified SBA-15 template exhibit needle like morphology. This is slightly different from the observation by Yu et al., who reported rod like morphology of mesoporous carbon materials synthesized from alkali modified SBA-15 (Yu et al., 2002). The functionalized supports (mC-6M and mC-8M) retained the needle like structure as seen from SEM figures (Figure 4.6). Broad interconnection between the needles are also seen in the images and the needle length is estimated to be around 5-10μm. Within the resolution level of SEM, it is not possible to differentiate any significant changes between mC-6M and mC-8M materials.

4.1.6 Transmission Electron Microscopy (TEM)

Morphological characteristics of SBA-15 as analysed by TEM shows well ordered hexagonal structure of this silica template (Figure 4.7a). The replicated mesoporous carbon support mC-V also show a well ordered structure and supports the SAXS results on structural orderliness (Figure 4.7b). Similar result has been reported by other researchers (Yu et al., 2002). The TEM figure of functionalized carbon mC-6M also shows well ordered structure (Figure 4.7c). However the TEM image of mC-8M indicates a reduction in ordered structure compared to mC-V and mC-6M supports (Figure 4.7d). This finding suggests that high nitric acid concentration results in excessive etching of carbon surface resulting in decreased structural orderliness.

The EDX spectra of mC-6M and mC-8M supports show the presence of sulphur, fluorine, chlorine and silica in small quantities in the carbon supports. This indicates the trace retention of sulphur and chlorine (from H_2SO_4 and KCl, respectively) from the

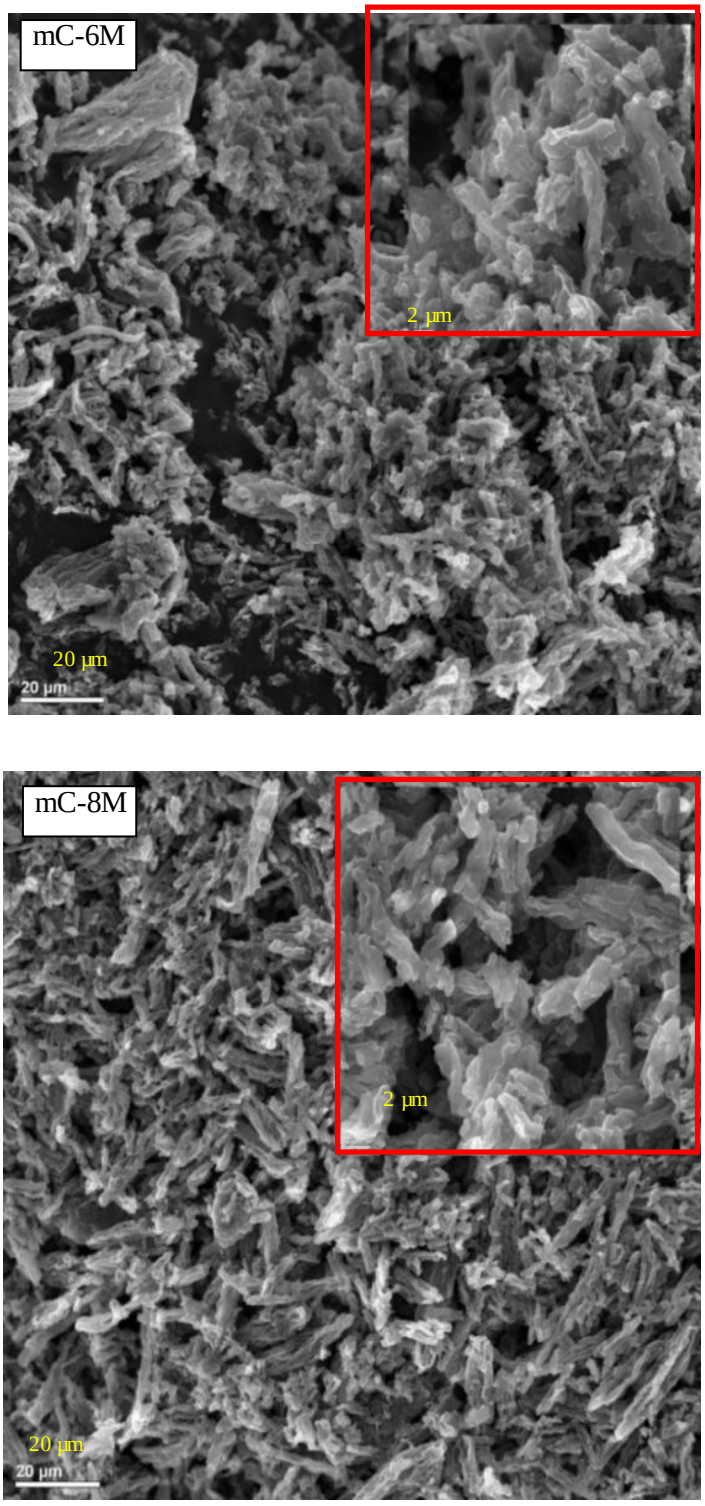

Figure 4.6: SEM images of functionalized mC supports a. mC-6M, b. mC-8M

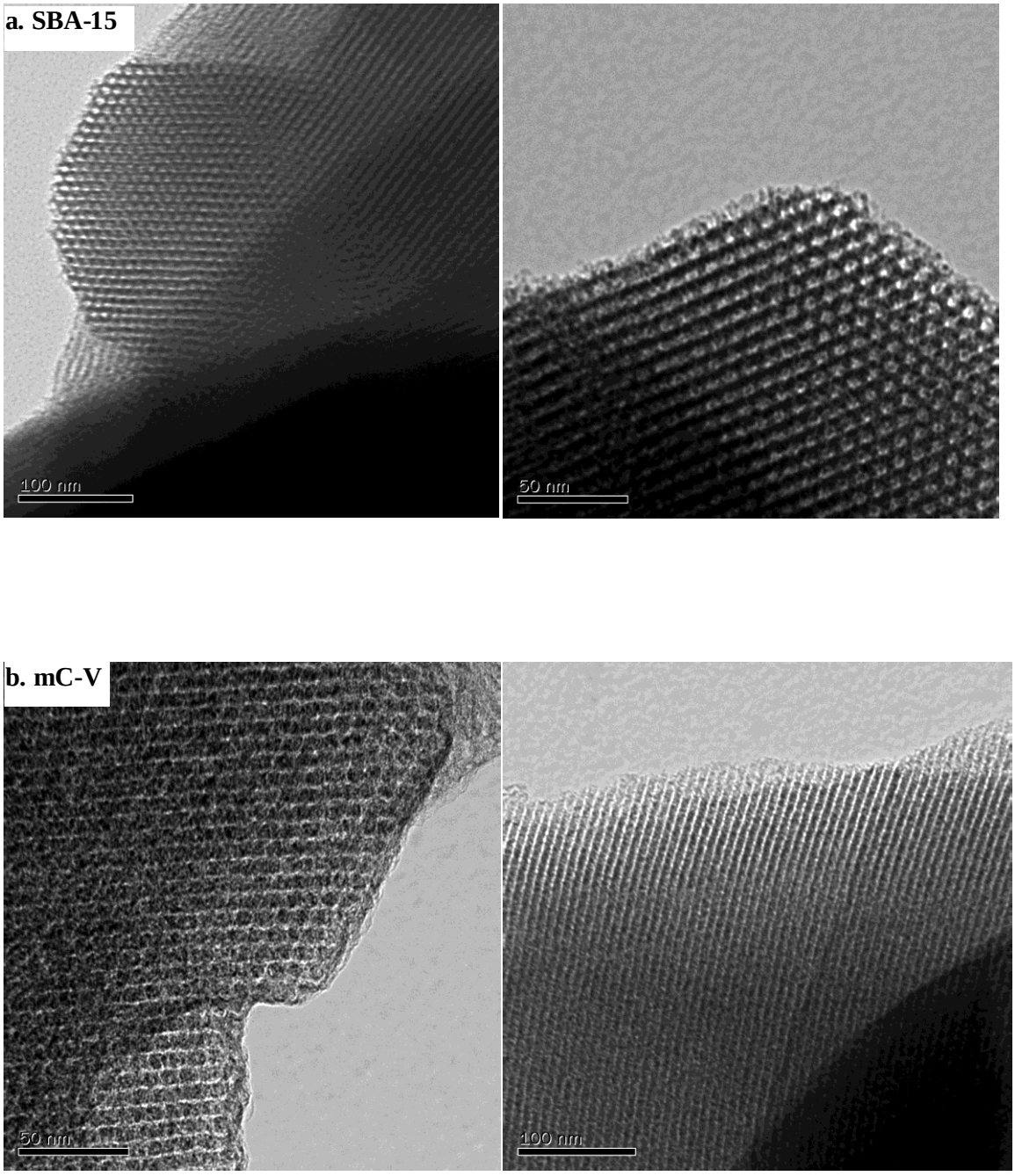

Figure 4.7: Transmission Electron Microscopy images of virgin and functionalized mesoporous carbon supports. a. SBA-15, b. mC-0M, (continued.)

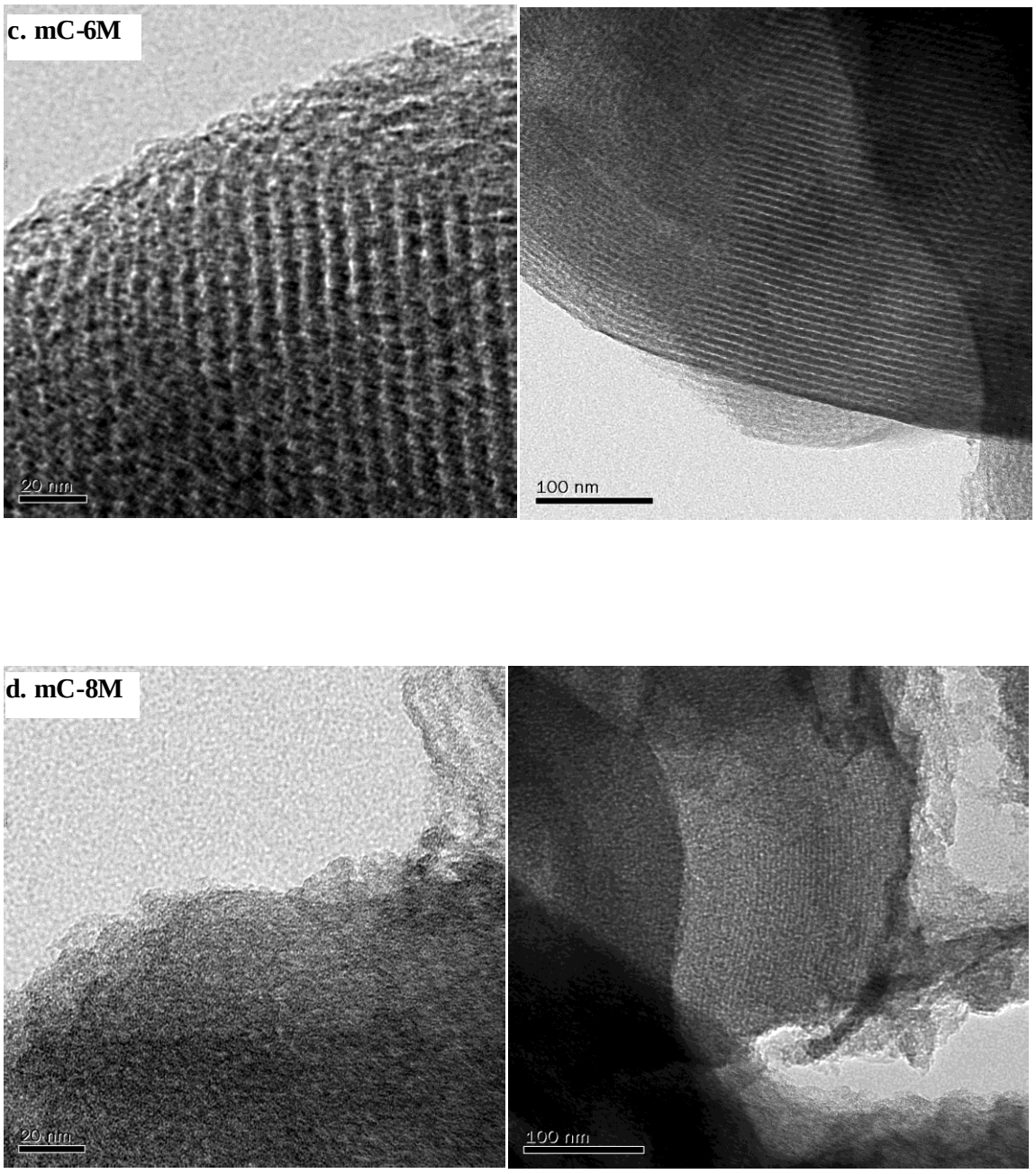

Figure 4.7: Transmission Electron Microscopy images of virgin and functionalized mesoporous carbon supports. c. mC-6M, d. mC-8M.

preparation step and some trace quantity of fluorine after HF washing. As confirmed from TGA, the removal of silica is near complete leaving only negligible traces of silica (<0.05%). The normalized atomic concentration of carbon and oxygen for mC-6M is 86.9% and 12.3% and for that of mc-8M is 81.4% and 17.5%, respectively. These results confirm the increase in oxygen functional groups with the increase in nitric acid concentration used for functionalization.

4.1.7 Fourier Transform Infrared Spectroscopy (FTIR)

FTIR spectra indicating the surface functional groups present in functionalized mesoporous carbons supports are shown in Figure 4.8. There is a clear indication on the strengthening of functional groups in the nitric acid treated carbon supports compared to virgin carbon. The bands in the range of 1665-1760 are assigned to carboxylic groups and the bands in 1675-1790 are assigned to lactonic group (Figueiredo et al., 1999). The peak around 1725 can be assigned to the C=O stretching of carboxyl groups (Bazuła et al., 2008), whereas the peak at 1587 can be attributed to the C=O aromatic stretching (Figueiredo et al., 1999). The shoulder present at 1250 can be assigned to C-O stretching of phenols, lactones and carboxylic anhydrides (Figueiredo et al., 1999). Marked increases in the intensity of these functional groups are observed between mC-V and mC-2M or between mC-2M and mC-4M supports. As seen from the comparison of four functionalized carbons with that of virgin carbon, the intensity of functional groups is increased with the increasing concentration of nitric acid, though, with a lower rate. It indicates that the increase in nitric acid concentration helps in the nonlinear increase of the intensity of surface functional groups on carbon surface.

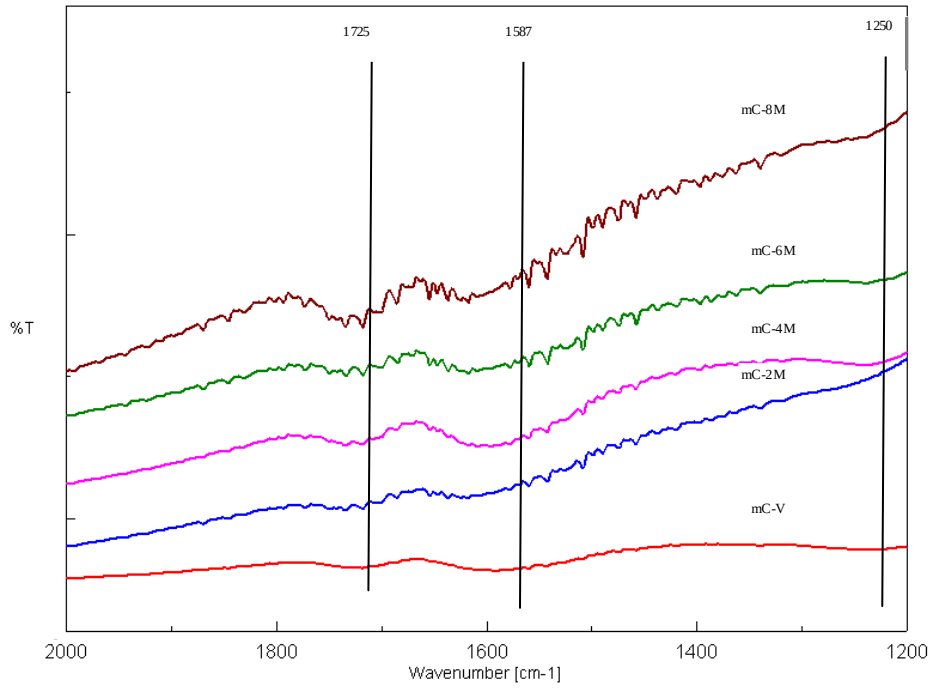

Figure 4.8: FTIR spectra of virgin and functionalized mesoporous carbons

4.1.8 Boehm Titration

Boehm titration results indicate increase in acidity caused by surface functional groups created during functionalization. The quantity of total acidic groups (in terms of carboxylic, lactonic, hydroxylic and phenolic) was found to increase with the concentration of nitric acid used. Taking mC-V as the reference (value taken as 1.00), the relative total acid groups in mC-2M, mC-4M, mC-6M and mC-8M was 1.18, 1.29, 1.35 and 1.41 respectively, reiterating the positive effect of increased acid concentration in enhancing the surface acidity of mesoporous carbon supports.

4.2 Characterization of catalysts

4.2.1 N_2 Physical Adsorption

NiMo catalysts supported on mesoporous carbon supports (12% Mo and 2.4% Ni) show type-IV isotherm, similar to the one exhibited by functionalized carbon supports. However, there is a reduction in the width between adsorption and desorption isotherms indicating reduction in pore mouth restriction. From Table 4.2, one can observe significant reduction in pore volume and BET surface area of the catalysts compared to the supports which may be due to the better dispersion of catalyst metals into the pores as well as blocking of some micropores. The contribution of mesopore volume in all samples is around 95% indicating the mesoporous nature of the catalysts.

Table 4.2: BET Surface area, Pore diameter and Pore volume results of mesoporous carbon supported NiMo catalysts.

Material	BET surface area (m^2/gm)	Total Pore Volume (cm^3/gm)	Pore dia[a] (nm)	Mesopore volume (%)
Cat-2M	634	0.69	3.9	94.8
Cat-4M	625	0.66	3.8	95.1
Cat-6M	609	0.62	3.7	94.2
Cat-8M	567	0.54	3.7	94.9

[a] – BJH Pore diameter estimated from the adsorption branch of isotherm
[b] – Mesopore volume (%) = (Total pore volume - Micropore volume) x100/ Total pore volume

4.2.2 X-Ray Diffraction (XRD)

XRD analysis was carried out to find the presence of crystalline phases of metal oxides in the prepared catalyst (Figure 4.9). A broad peak centering at 2θ=23°, which is

the peak of the 002 diffraction of graphite structure (Shanahan et al., 2008) and a peak around 2θ =43.5°, which is 101 reflection of graphite structure (Kim et al., 2003; Shanahan et al., 2008), are observed in virgin carbon support. This indicates that certain degree of graphitization occurs while carbonizing at 900°C. The broad peak at 2θ =23° has shifted to 2θ =26.5° after metal loading and the intensity of both the carbon peaks (23° & 43.5°) has decreased indicating a change in ordered structure (Tan et al., 2009) due to the introduction of metals. Catalysts Cat-4M, Cat-6M, Cat-8M do not show any significant presence of MoO_3 crystalline phase indicating better dispersion of this metal oxide over the surface. However, two low intensity peaks of MoO_3 crystalline phase (Eswaramoorthi et al., 2008) are observed in Cat-2M indicating slightly reduced dispersion of catalyst metals over the mC-2M carbon surface. This might be due to the lower acidity and lower amount of surface functional groups of mC-2M support compared to those of other functionalized carbons as observed from FTIR analysis and Boehm titration. Peaks associated with NiO (Eswaramoorthi et al., 2008) are not seen in any of the catalysts signifying the constructive promotion effect of Ni in enhancing the dispersion of Mo.

4.2.3 Elemental analysis

Table 4.3 shows the metal content in various catalysts as analyzed by inductively coupled plasma mass spectrometer (ICP-MS) method. There is no significant variation in Mo or Ni metal content in all of the catalysts suggesting that any variation in catalytic activity will not be due to the variation in metal content in catalysts. The Mo/Ni atomic ratio of NiMo/mC-6M obtained by EDX results is around 3.2, which is close to the ICP result of 3.1. Consistency in Mo/Ni atomic ratio by two different characterization

techniques coupled with broad angle XRD results, substantiates the inference of better and uniform dispersion of catalyst metals over the mC-6M support.

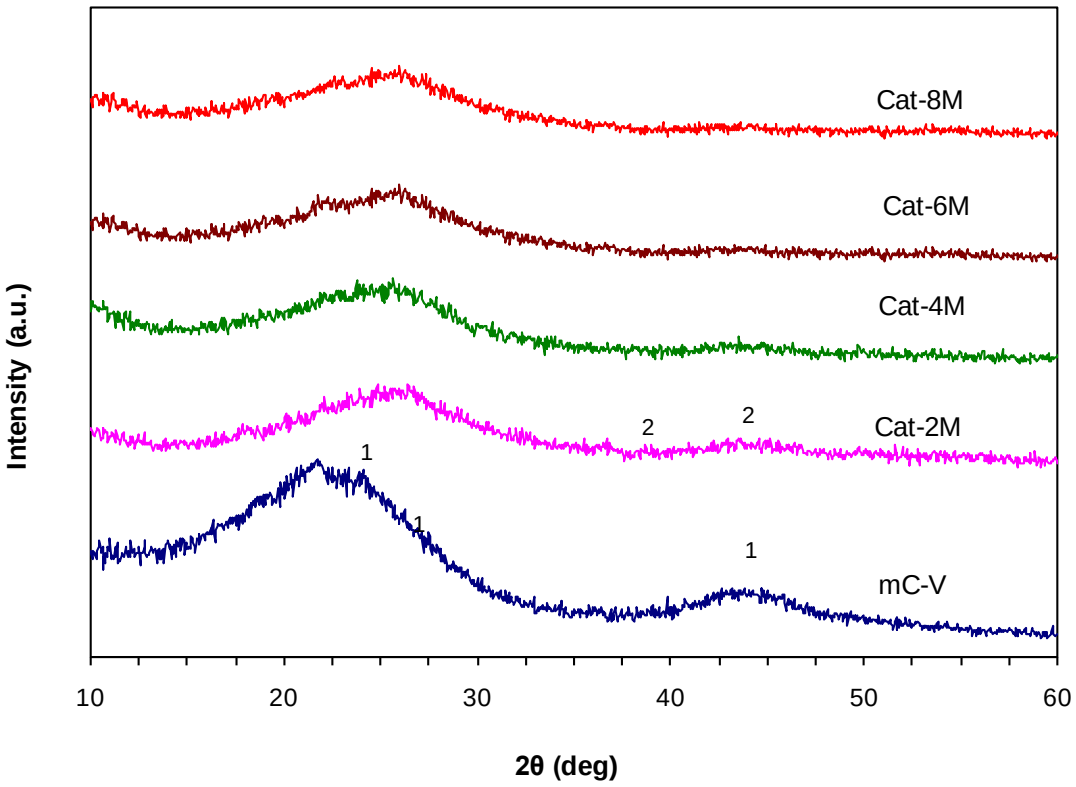

Figure 4.9: Broad angle XRD results of mesoporous carbon supported catalysts

Table 4.3: Elemental composition analysis of NiMo/mC catalysts

Catalyst	Ni (Wt%) Target / Achieved	Mo (Wt%) Target / Achieved	Atomic ratio Mo/Ni
Cat-2M	2.4 / 2.7	12.0 / 11.9	2.76
Cat-4M	2.4 / 2.6	12.0 / 11.7	2.78
Cat-6M	2.4 / 2.5	12.0 / 12.2	3.05
Cat-8M	2.4 / 2.6	12.0 / 12.4	2.89

4.2.4 Scanning Electron and Transmission Electron Microscopy

Surface morphology of Cat-6M was analysed by scanning electron microscopy (SEM) and transmission electron microscopy (TEM). The SEM image (Figure 4.10) confirms that the needle like ordered structure of the catalyst is maintained almost as in functionalized support. Such structure can better facilitate the orderly movement of reactant molecules (Yu et al., 2002) towards the active metal phase to achieve better catalytic activity. From the TEM image of Cat-6M, it can be deduced that the structural orderliness of the catalyst material (Figure 4.11) is not changed significantly. However, little change in pore structure is observed before and after metal loading due to the impregnation of metals in pores. This change in pore structure is substantiated by the XRD peak shift from $2\theta = 23°$ to $2\theta = 26.5°$. Similar result has been reported by other researchers (Tan et al., 2009). From the TEM images, one can see the uniform dispersion of catalyst metal over the support which is due to high surface area and effective functionalization.

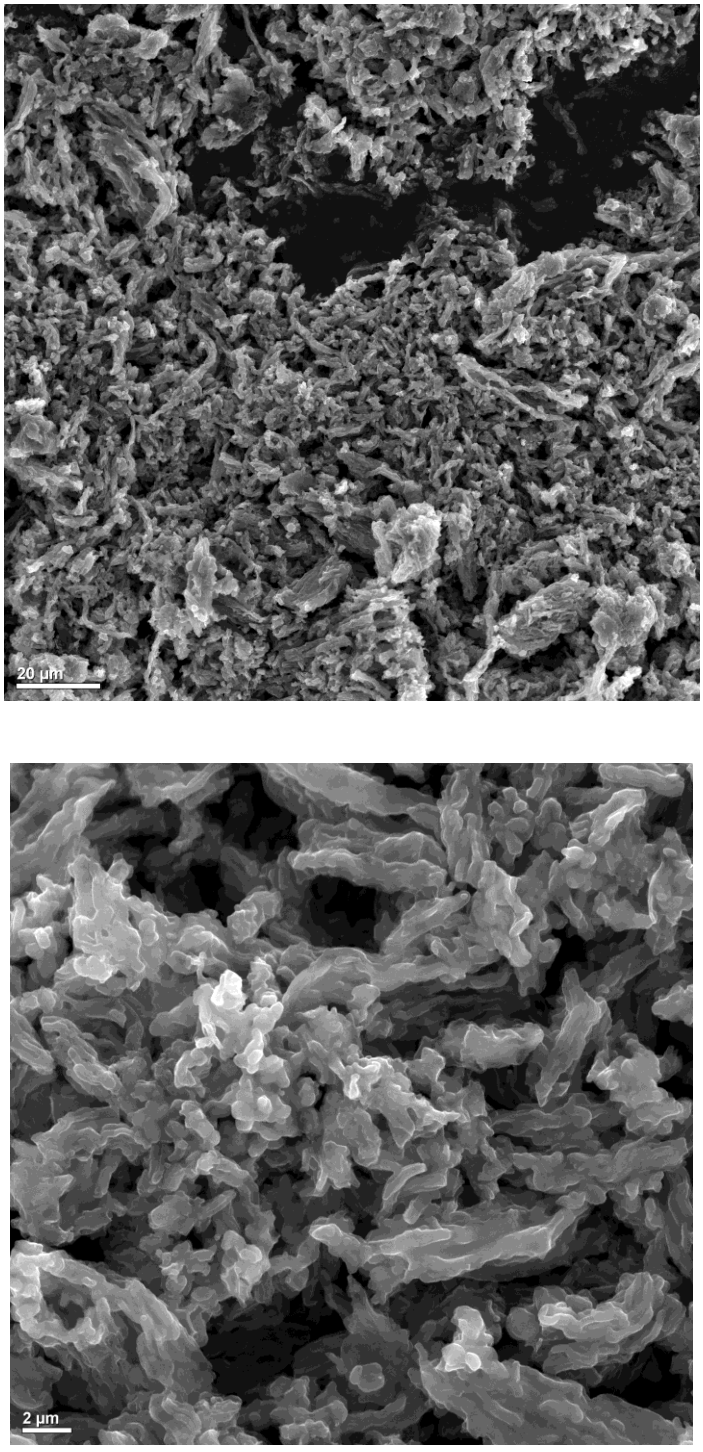

Figure 4.10: Scanning Electron Microscopy images of Cat-6M

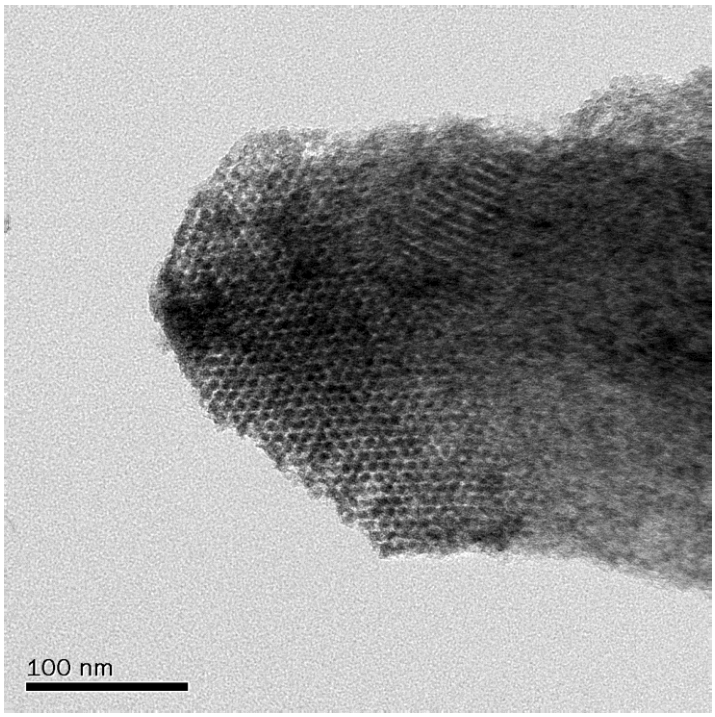

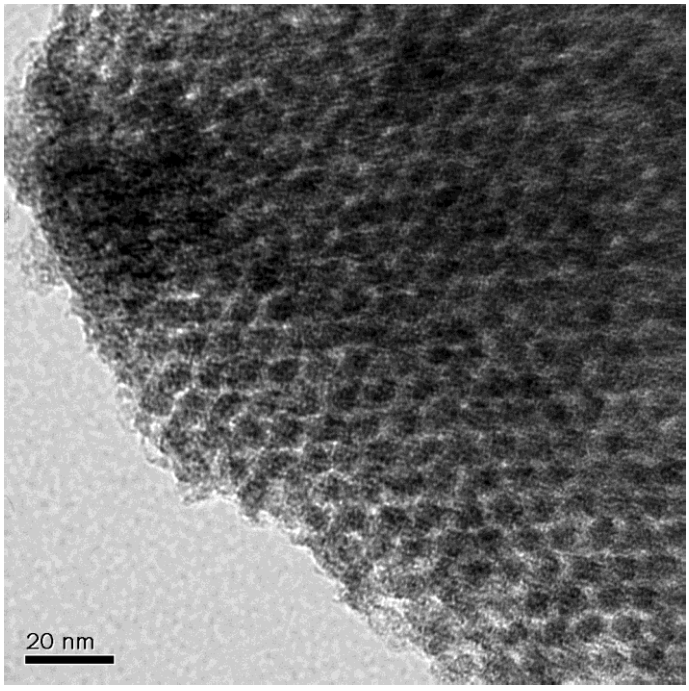

Figure 4.11: Transmission Electron Microscopy images of Cat-6M

4.2.5 High Resolution Transmission Electron Microscopy (HRTEM)

Cat-6M was sulfided as per the procedure described in Chapter 3 and was analyzed by HRTEM. The HRTEM micrograph of this sulfided catalyst is shown in Figure 4.12. Uniform dispersion of catalyst metals over mC-6M support is seen supporting the broad angle XRD data. Most of the active phase is single layered and it can be considered as qualitatively Type-II like NiMoS phase on carbon supports which possess lower support metal interaction. Type-II phase is considered active for hydrotreating (Topsøe and Clausen, 1986). The length of the layer is around 20-40A°. Absence of multilayer concentration in sulfided Cat-6M indicates that the SMI in mC-6M is lower (but not very weak) and hence there is homogeneous distribution and no noticeable agglomeration of active phase (Gutiérrez et al., 2006).

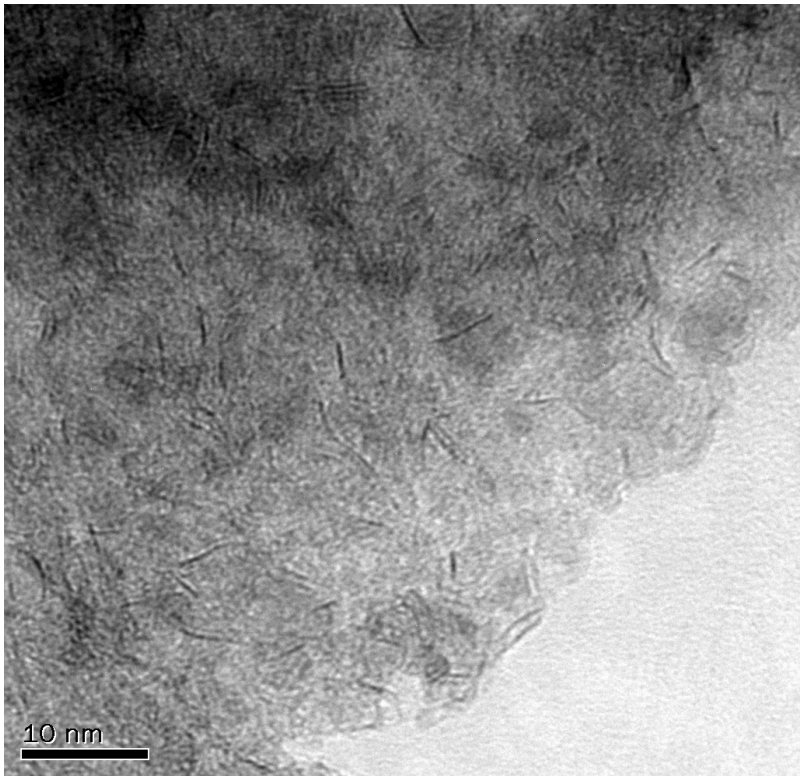

Figure 4.12: HRTEM images of Cat-6M

Table 4.3: Summary of characterization results – Phase I

Technique	Observations	Inference
N_2 Physical adsorption	- All supports and catalysts exhibit Type-IV isotherm - Progressive reduction in surface area and pore volume was observed with the increase in nitric acid concentration used.	- Mesoporous structure is retained - Surface functional groups are created resulting in decreased textural properties
TGA	- Almost all carbon material (mC-V) got oxidized below 600°C when heated with air	- Complete removal of silica is ensured by two stage HF washing
SAXS	- Reduction in SAXS peak intensity (for 100, 110, 200 reflections) in supports treated with higher nitric acid concentration was observed	- Increase in acid concentration accelerates the wall etching and reduces structural orderliness
SEM	- Needle like structure (as in mC-V) was retained in all functionalized supports and NiMo catalysts	- There is no extensive structural damage after acid treatment or catalyst loading within SEM resolution level
TEM	- Decrease in structural orderliness beyond 6M acid treatment - Mild decrease in structural orderliness after catalyst loading	- Acid concentration above 6M causes excessive etching - Catalyst metals are incorporated into the pores leading to mild structural change.
FTIR	- Increase in the intensity of –COOH, C=O and –OH peaks were observed with the increase in acid concentration; but the increase was not linear.	- Increase in nitric acid concentration helps in the nonlinear increase of the intensity of surface functional groups on carbon surface
Boehm Titration	- The total surface acid groups in carbon supports was found to increase with the increase in acid concentration	
XRD	- Mo oxide peaks were observed for catalysts prepared using mC-2M support. No significant peaks associated with Mo or Ni oxides were observed for other three carbon supported catalysts.	- Lower acid concentration does not provide sufficient acid surface functional groups to act as catalyst anchors.
HRTEM	- Lower concentration of multilayer MoS_2 phase was observed (predominantly monolayer) in the sulfided catalyst (Cat-6M)	- Lower support-metal interaction in carbon supports helps in the formation of qualitatively Type-II like NiMoS phase. These are considered to be active for hydrotreating (Topsøe and Clausen, 1986)

4.3 Hydrotreating activity study

Hydrotreating experiments were carried out in a trickle bed flow reactor under typical industrial operating conditions using Coker Light Gas Oil (KLGO) derived from Athabasca bitumen as feedstock. Initial activity stabilization was attained within two days for all the catalysts during precoking at 370°C. The precoking was continued for another two days before taking representative samples. The hydrotreating activity test was performed at three temperatures - 370°C, 350°C, 330°C and two representative samples for each temperature condition were collected. The results of HDS activity of all the four mesoporous carbon supported catalysts in comparison with NiMo/γ-Al_2O_3 catalyst of similar metal loading is shown in Figure 4.13. The HDS activity for the four mesoporous carbon supported catalysts is in the following order: Cat-6M > Cat-4M > Cat-2M > Cat-8M. The activities of Cat-4M and Cat-6M are very close to each other at all temperatures. The benefit of additional functionalization in terms of surface functional groups and acidity in Cat-6M is somewhat overshadowed by the changes in textural properties such as surface area and pore volume when compared to Cat-4M resulting in closer HDS activity. Cat-8M has the lowest HDS activity which might be due to the reduction in textural properties (structural orderliness, surface area & pore volume) caused by excessive etching of nitric acid. The lower activity of Cat-2M in spite of good textural properties might be attributed to the deficiency in functionalization resulting in reduced dispersion (as seen from XRD results) and possible lower metal retention capability. The HDS activity of the best carbon supported catalyst i.e. Cat-6M is higher than the HDS activity of conventional NiMo/γ-Al_2O_3 catalyst, which is due to lower metal support interaction, higher surface area and pore volume of mesoporous carbon supports.

The results of HDN activity of all the catalysts is shown in Figure 4.14. Similar to HDS results, the HDN activity of Cat-6M is higher than those of all other catalysts (Cat-6M > Cat-4M > Cat-2M > Cat-8M). The maximum difference between the HDN activity of Cat-6M and Cat-4M is 3.5% at 370°C. This is due to the additional acidity created over mC-6M by functionalization using higher concentration nitric acid. As seen for HDS, the HDN activity of NiMo/ γ-Al_2O_3 catalyst is lower than that of Cat-6M. Similar results on higher HDS activity of functionalized mesoporous carbon supported hydrotreating catalysts compared to that of γ-Al_2O_3 has been reported by other researchers for the hydrotreating of model compounds (Hussain and Ihm, 2009)

From the activity study one can deduce that the increased hydrotreating activity of Cat-6M compared to other functionalized mesoporous carbon supported catalysts is due to higher acidity and enhanced surface functional groups on the carbon surface, generated during 6M HNO_3 acid treatment without significant deterioration of the textural properties. The higher HDS and HDN activity of Cat-6M compared to that of NiMo/ γ-Al_2O_3 indicates the potential of functionalized mesoporous carbon as an effective support for hydrotreating catalysts.

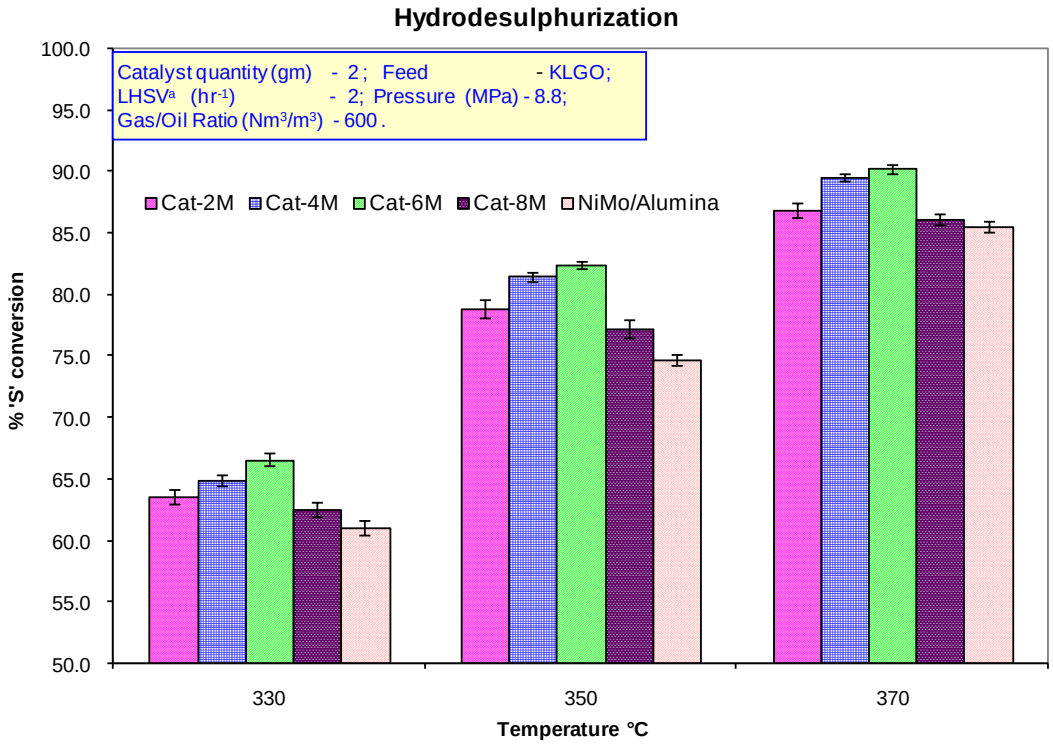

[a] For γ-Al_2O_3 supported catalyst, weight of the catalyst is taken as basis

Figure 4.13: HDS activity comparison of NiMo catalysts supported on functionalized mesoporous carbons

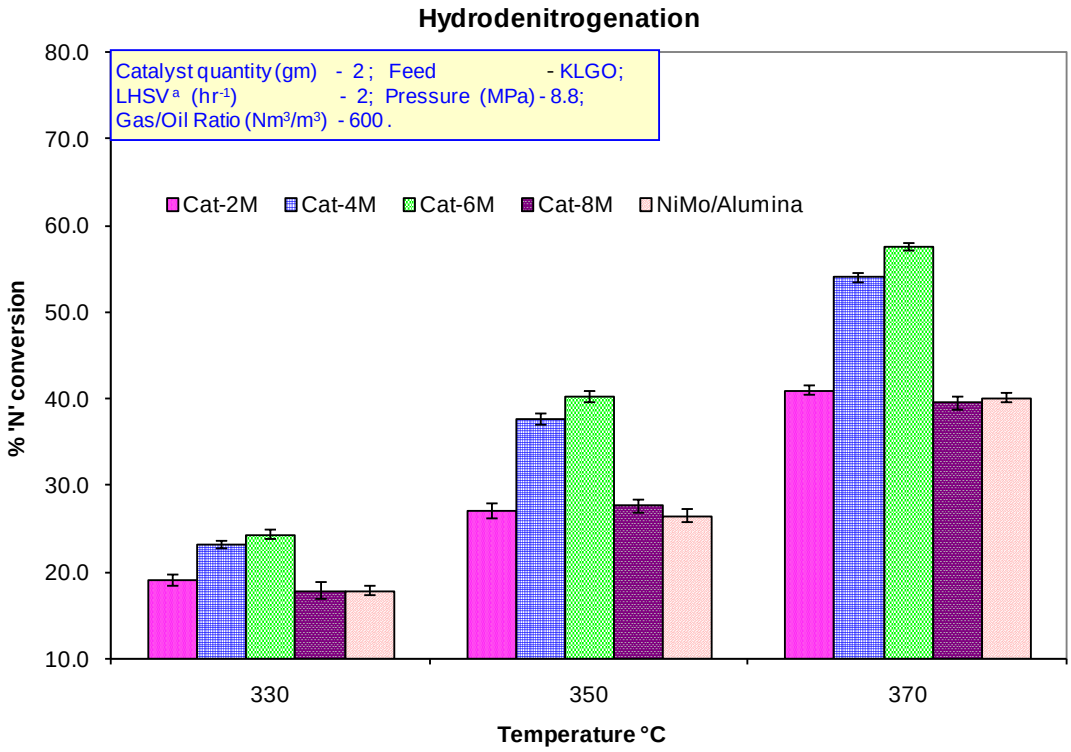

[a]For γ-Al2O3 supported catalyst, weight of the catalyst is taken as basis

Figure 4.14: HDN activity comparison of NiMo catalysts supported on functionalized mesoporous carbons

4.4 Conclusions:

Ordered mesoporous carbon supports were prepared from alkali modified SBA-15 template and then functionalized using nitric acid of various concentrations. All functionalized carbon supports show Type-IV isotherms similar to virgin carbon support. FTIR analysis showed that the intensities of surface functional groups (carboxyl, lactonic, phenolic) is increased with the increase in concentration of nitric acid used. SAXS analysis, TEM images and N_2 physisorption analysis confirmed the retention of ordered structure in mesoporous carbon material functionalized using 6M nitric acid or lower. Reduction in structural orderliness is observed when higher nitric acid concentration is used (>6M). TEM image of NiMo/mC catalyst indicated mild changes in ordered structure of the catalyst due to the introduction of metals inside the pores. Better dispersion of catalyst metals over the functionalized supports treated with higher nitric acid concentration (>2M) was observed through XRD analysis. SEM images confirmed the needle like morphology of functionalized carbons and supported NiMo catalyst, which can facilitate the orderly movement of reactant molecules. NiMo catalyst (12% Mo and 2.4% Ni) supported over mesoporous carbont treated with 6M nitric acid (Cat-6M) showed higher HDS and HDN activities for the hydrotreating of coker light gas oil derived from Athabasca bitumen due to higher acidity, higher surface functional groups and retention of ordered structure. Hydrotreating activity of Cat-6M was higher than that of conventional NiMo/γ-Al_2O_3 catalyst of similar metal loading due to the lower metal support interaction and higher surface area along with effective functionalization of carbon supports. It was demonstrated that functionalized mesoporous carbon supports with ordered structure show promising performance as a new generation catalyst support for the hydrotreating of gas oil feedstocks.

CHAPTER 5

OPTIMIZATION OF METAL LOADING OVER FUNCTIONALIZED MESOPOROUS CARBON SUPPORT

Mesoporous carbon supports possess higher surface area and pore volume than conventional γ-Al_2O_3 support. Hence, it might be possible to achieve higher metal loading over mesoporous carbon support without significant MoO_3 crystallite formation. The objective of this part of the project was to identify the optimum metal loading on functionalized mesoporous carbon support. At first, Mo variation was carried out with constant Ni loading to find optimum Mo loading. It was followed by Ni variation using optimum Mo catalyst. The catalysts with Mo content of 12%, 17%, 22% and 27% (by weight) with a constant Ni/Mo atomic ratio of 0.33 were termed as Cat-A, Cat-B, Cat-C and Cat-D respectively. Catalyst with Mo content of 22% and Ni content of 2.9% was termed as Cat-E. The metal loading values mentioned are based on weight percentages, unless otherwise stated differently. The optimum catalyst obtained from this work was used in the kinetic parameter study.

5.1 Characterization of catalysts

5.1.1 N_2 Physical Adsorption

The results of BET surface area, pore volume and pore diameter of mesoporous carbon supported catalysts are given in Table 5.1. All of the NiMo catalysts supported on mesoporous carbon supports (Cat A to Cat- E) show type-IV isotherm (Figure 5.1), similar to the one exhibited by the parent support. Reduction in pore volume and BET surface area are seen in the results (Table 5.1), which is due to the better dispersion of

catalyst metals into the pores as well as blocking of some micropores. The contribution of mesopore volume is increased from 94% (Cat-A) to 99.8% (Cat-D) with the simultaneous increase in average pore diameter from 3.7 to 4.4 nm as the loading of molybdenum is increased from 12% to 27 % (Mo/Ni ratio is constant). This is the result of blocking of some micropores by additional metals. Thus, the increase in metal loading has pronounced effect in decreasing textural characteristics of NiMo catalyst supported on functionalized mesoporous carbon material.

Table 5.1: BET surface area, Pore diameter and Pore volume results of mesoporous carbon supported NiMo catalysts.

	BET Surface area (m^2/gm)	**Total Pore volume (cm^3/gm)**	**Pore dia[a] (nm)**	**Mesopore volume[b] (%)**
Cat-A	609	0.63	3.7	94.1
Cat-B	467	0.51	3.7	98.4
Cat-E	360	0.38	3.8	98.7
Cat-C	339	0.36	3.8	99.1
Cat-D	228	0.27	4.4	99.8

[a] – BJH Pore diameter estimated from the adsorption branch of isotherm

[b] – Mesopore volume (%) = (Total pore volume - Micropore volume) x100/ Total pore volume

5.1.2 Scanning Electron Microscopy (SEM)

The surface morphology of mesoporous carbon support replicated from alkali modified SBA-15 was studied using SEM. The mC support exhibits a needle like structure (Figure 4.6). The needle structure is retained by all the catalysts (Figure 5.2 a, b, c and d). Such structures are said to be good for catalytic applications (Yu et al., 2002) as they can facilitate the easy movement of reactant molecules.

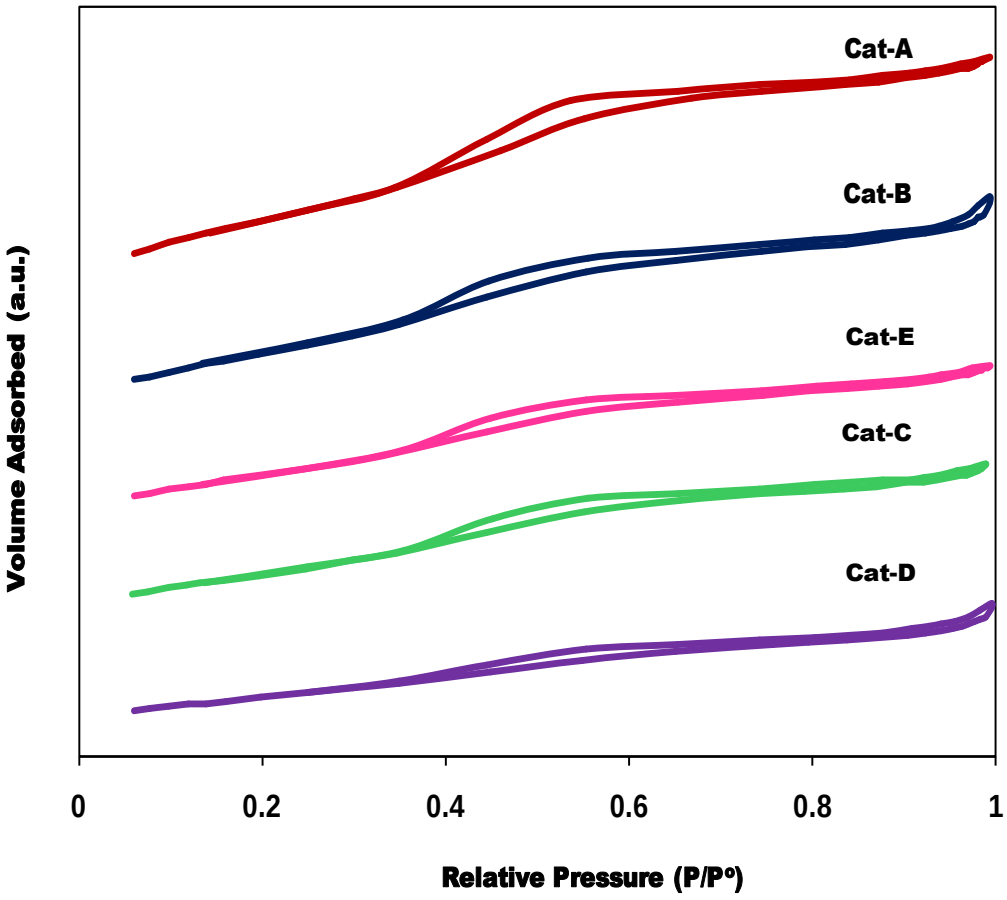

Figure 5.1: N_2 physical adsorption isotherm of NiMo/mC catalysts

5.1.3 Transmission Electron Microscopy (TEM)

Morphological characteristics of mesoporous carbon supported catalysts as analysed by TEM are shown in Figure 5.3. Compared to the functionalized supports (Figure 4.7), a mild change is observed in the structure of the catalyst after metal loading, which might be due to the blocking of some of the pores. TEM images show qualitative dispersion of catalyst metals over the mC supports. At lower metal loading (12% Mo), the dispersion is good (Figure 5.3a). There is a marginal reduction in dispersion with the increase in metal loading upto 22 wt% Mo (Figure 5.3b and c). High metal loading (27 wt% Mo and 5.4 wt% Ni) significantly affects the ordered structure as well as the metal dispersion (Figure 5.3d) which might be due the formation of metal crystallites that can create additional pore blockage.

5.1.4 X-Ray Diffraction

Broad angle XRD results of various NiMo/mC catalysts together with virgin carbon support (mC-V) are shown in Figure 5.4. For mC-V, the broad peak centering at $2\theta=23°$ is the peak of the 002 diffraction of graphite structure (Shanahan et al., 2008) and the peak around $2\theta = 43.5°$ is 101 reflection of graphite structure (Kim et al., 2003; Shanahan et al., 2008). A peak shift from $2\theta = 23°$ to 2θ around 26.5° is observed in all of the catalyst samples. This might be due to the change in ordered structure after metal loading (Tan et al., 2009). The intensity of major carbon peaks (23° & 43.5°) gets decreased after metal loading, which is also observed by other researchers (Tan et al., 2009). Cat-A to Cat-C do not show any significant peaks associated with MoO_3 crystalline peak, thus qualitatively indicating good dispersion of catalyst metals over carbon surface. For Cat-D, many strong MoO_3 peaks are observed (Eswaramoorthi et al., 2008).

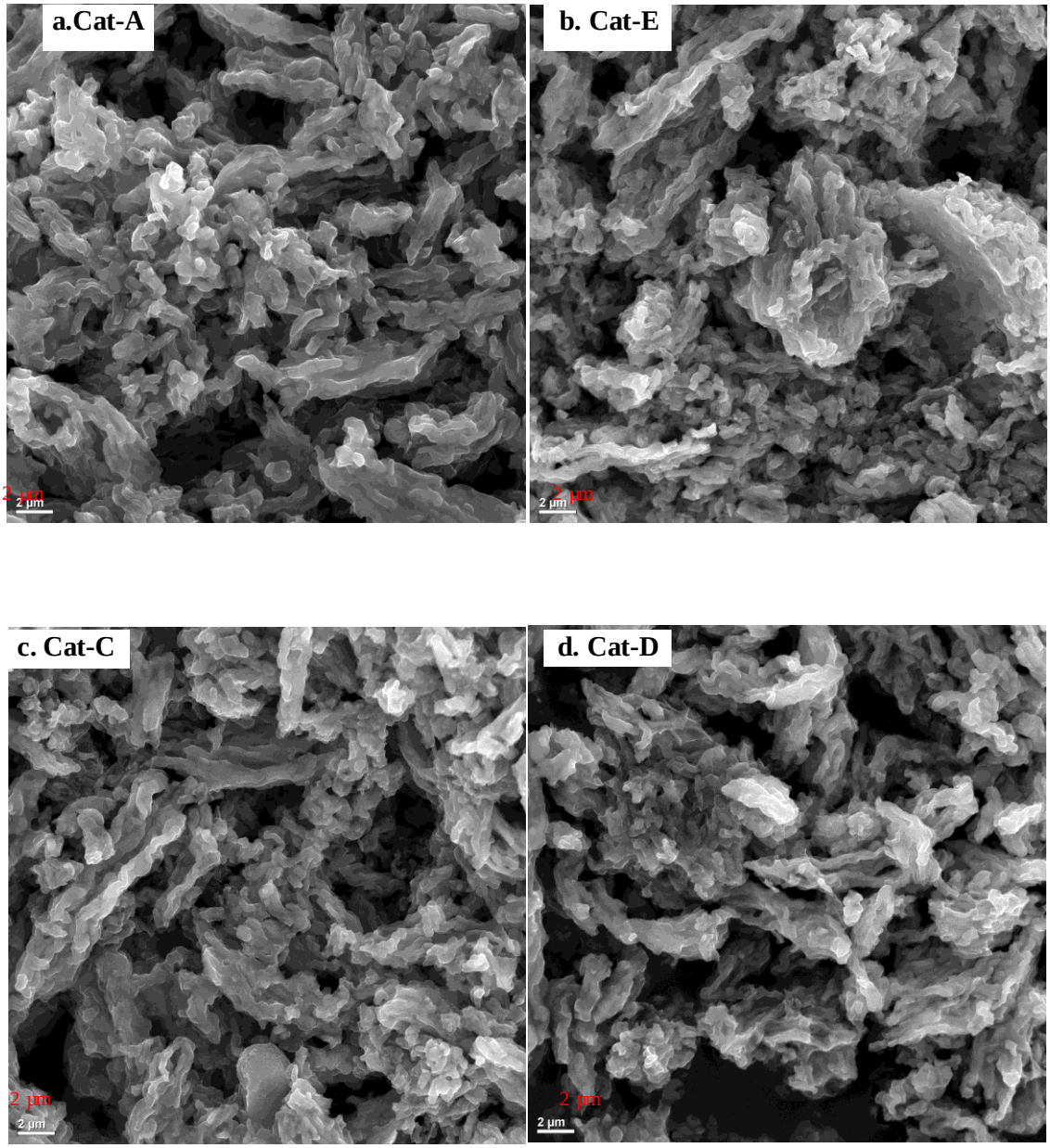

Figure 5.2: SEM images of mC supported NiMo Catalysts
a. Cat-A; b. Cat-E; c. Cat-C; d. Cat-D

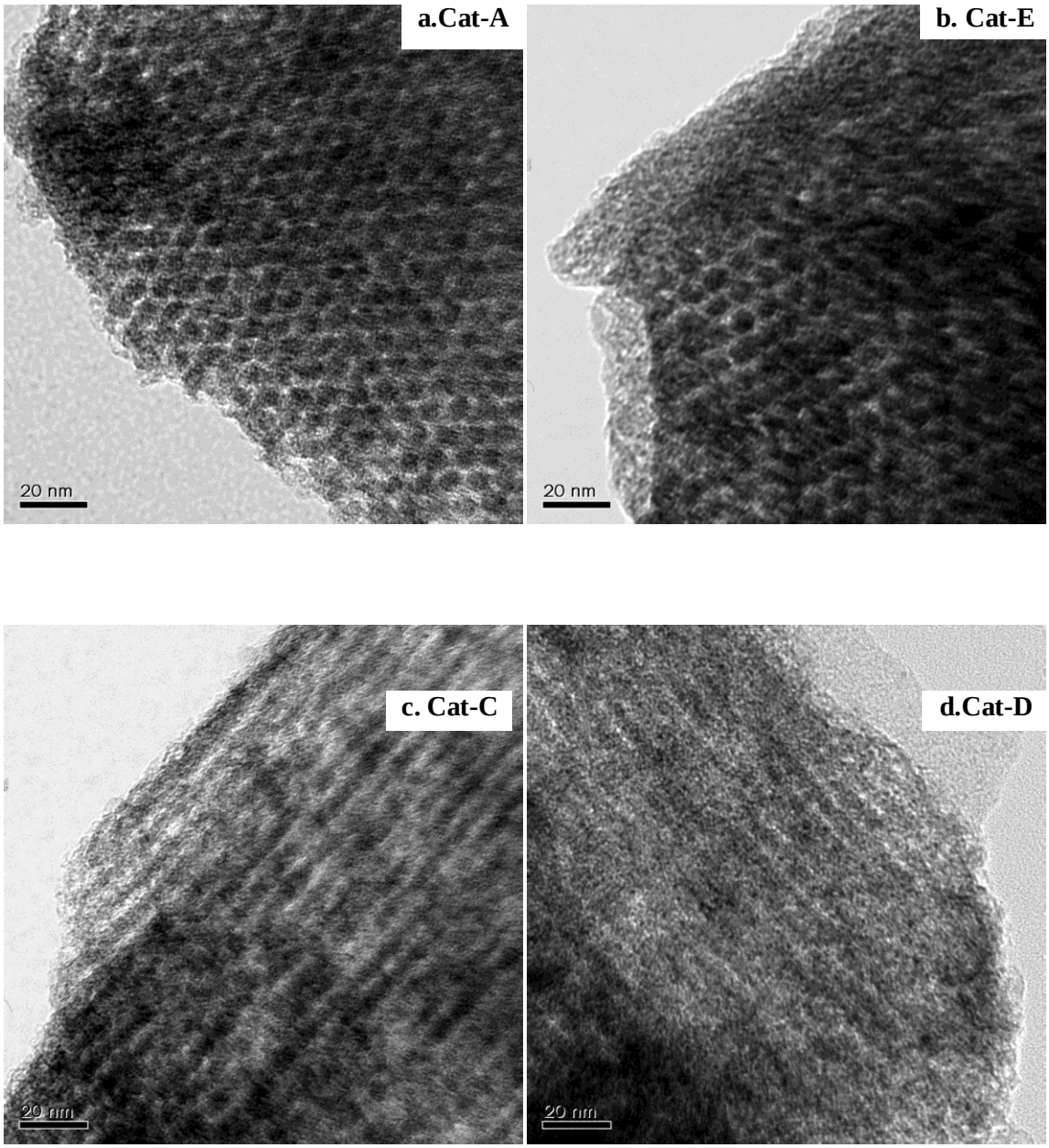

Figure 5.3: TEM images of mC supported NiMo Catalysts
a. Cat-A; b. Cat-E; c. Cat-C; d. Cat-D

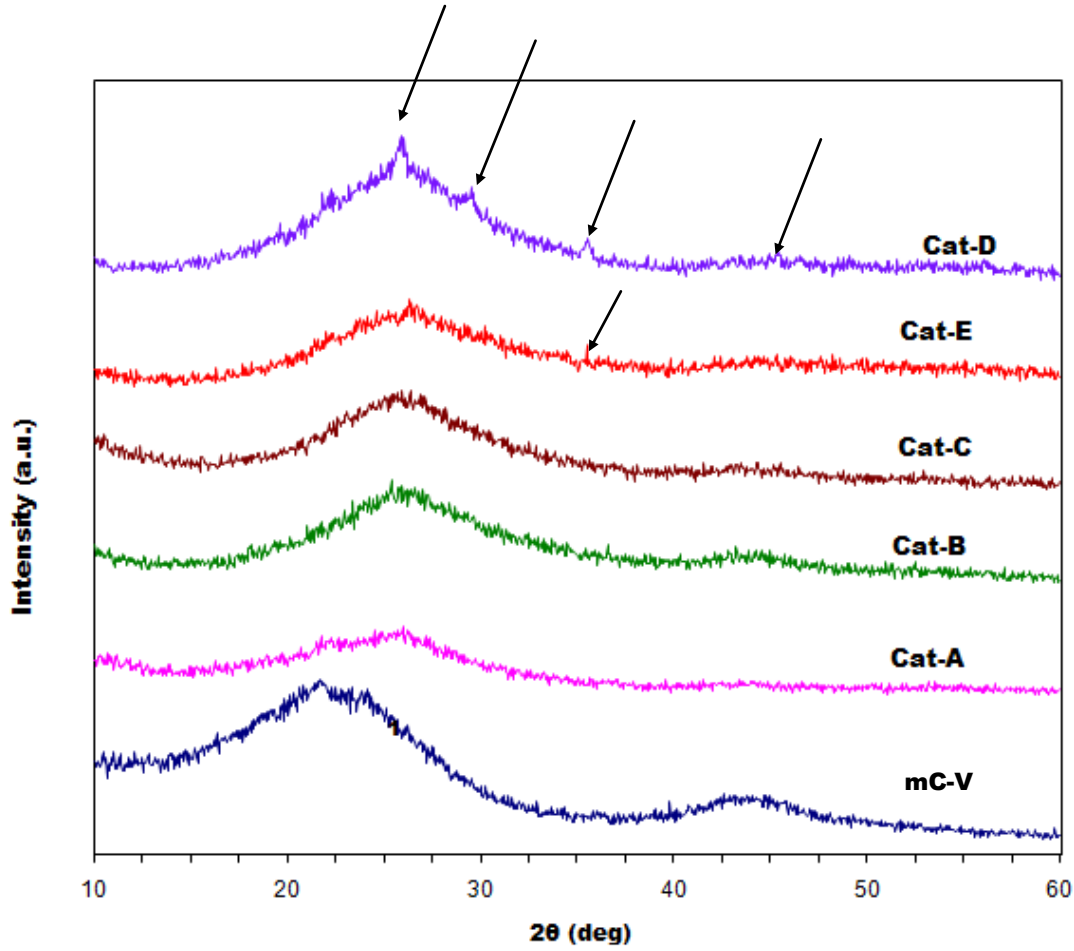

Figure 5.4: XRD data of mC supported NiMo catalysts

This indicates that addition of metals beyond 22% Mo significantly affects the metal dispersion over carbon surface which can have adverse effect on catalytic activity. XRD results qualitatively support the TEM images of Cat-D for poor metal dispersion. Upon decreasing nickel content from 4.4% in Cat-C to 2.9% in Cat-E (Mo constant at 22%), one mild peak at around 35° started to appear which corresponds to MoO_3 phase (Eswaramoorthi et al., 2008). Considering this as an incipient peak, we can infer that 2.9% Ni is sufficient for the dispersion of 22% Mo over functionalized mesoporous carbon surface.

5.1.5 Elemental Analysis

Table 5.2 shows the elemental Mo and Ni composition in the prepared catalysts analyzed by ICP-MS. The variation in target and actual metal loading is very low at 12% Mo loading. Mild variation, though not significant, is observed at higher metal loadings which might be due the combined effect of mild reduction in metal dispersion and handling losses during preparation. Nevertheless, the results indicate that the metal loading achieved is representative for the intended purpose of the study.

Table 5.2: Elemental composition analysis of NiMo/mC catalysts (by ICP-MS)

Catalyst	**Ni (wt%)**	**Mo (wt%)**
	Target / Achieved	**Target / Achieved**
Cat-A	2.4 / 2.5	12.0 / 12.2
Cat-B	3.4 / 2.8	17.0 / 16.2
Cat-E	2.9/2.6	22.0/ 23.8
Cat-C	4.4 /3.7	22.0 / 23.9
Cat-D	5.4 / 5.3	27.0 / 28.3

5.1.6 Temperature Programmed Reduction (H_2-TPR)

The reducibility of the catalyst can be related to its HDS and HDN activities (Eswaramoorthi et al., 2008; Shang et al., 2004a). Sulfidation of the catalyst is a combined process of reduction of oxides and sulfidation. Under the presence of excess sulphur source and hydrogen (which is typical during the sulfidation process), the catalyst that is reduced at lower temperature can form higher number of active sites leading to increased hydrotreating activity (Yu et al., 2008). The reducibility of Cat-E was analyzed by H_2-TPR and the result is shown in Figure 5.5. A major reduction peak at around 350°C and a minor shoulder at around 470°C were observed, which can be attributed to the reduction of easily reducible Mo species i.e. reduction of polymeric octahedral Mo species from Mo^{6+} to Mo^{4+} (Arnoldy et al., 1985; Feng et al., 2000; Sundaramurthy et al., 2008) or the reduction of nickel molybdate phase (Calafat et al., 1996b). The corresponding reduction temperature of commercial γ-Al_2O_3 supported hydrotreating catalyst was found to be 506°C (Sigurdson, 2009), which is higher than that of cat-E. The result of H_2-TPR analysis indicates that the support metal interaction is lower in mesoporous carbon supported NiMo catalyst compared to that of commercial γ-Al_2O_3 supported hydrotreating catalyst

5.1.7 High Resolution Transmission Electron Microscopy (HRTEM)

Cat-A and Cat-E were sulfided and analyzed by HRTEM. The HRTEM micrographs of these sulfided catalysts are shown in Figure 5.6. Uniform dispersion of catalyst metals in both Cat-A and Cat-E are seen supporting the broad angle XRD data. The length of the MoS_2 layer is around 20-40A° in both Cat-A and Cat-E.

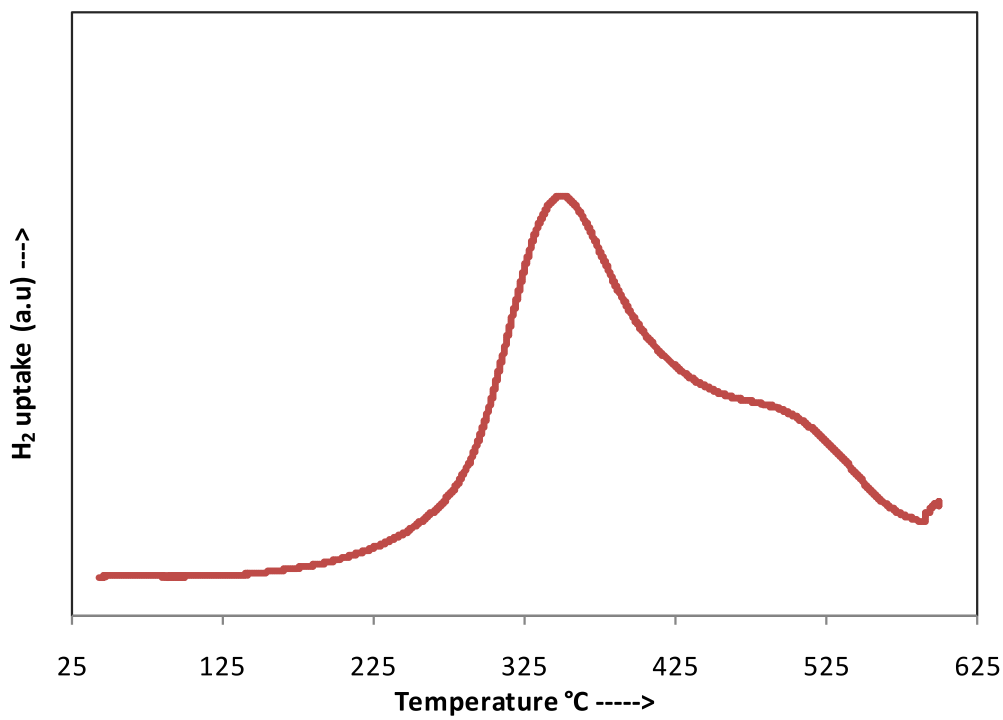

Figure 5.5: Temperature Programmed Reduction data of mC supported NiMo catalyst

(Cat-E)

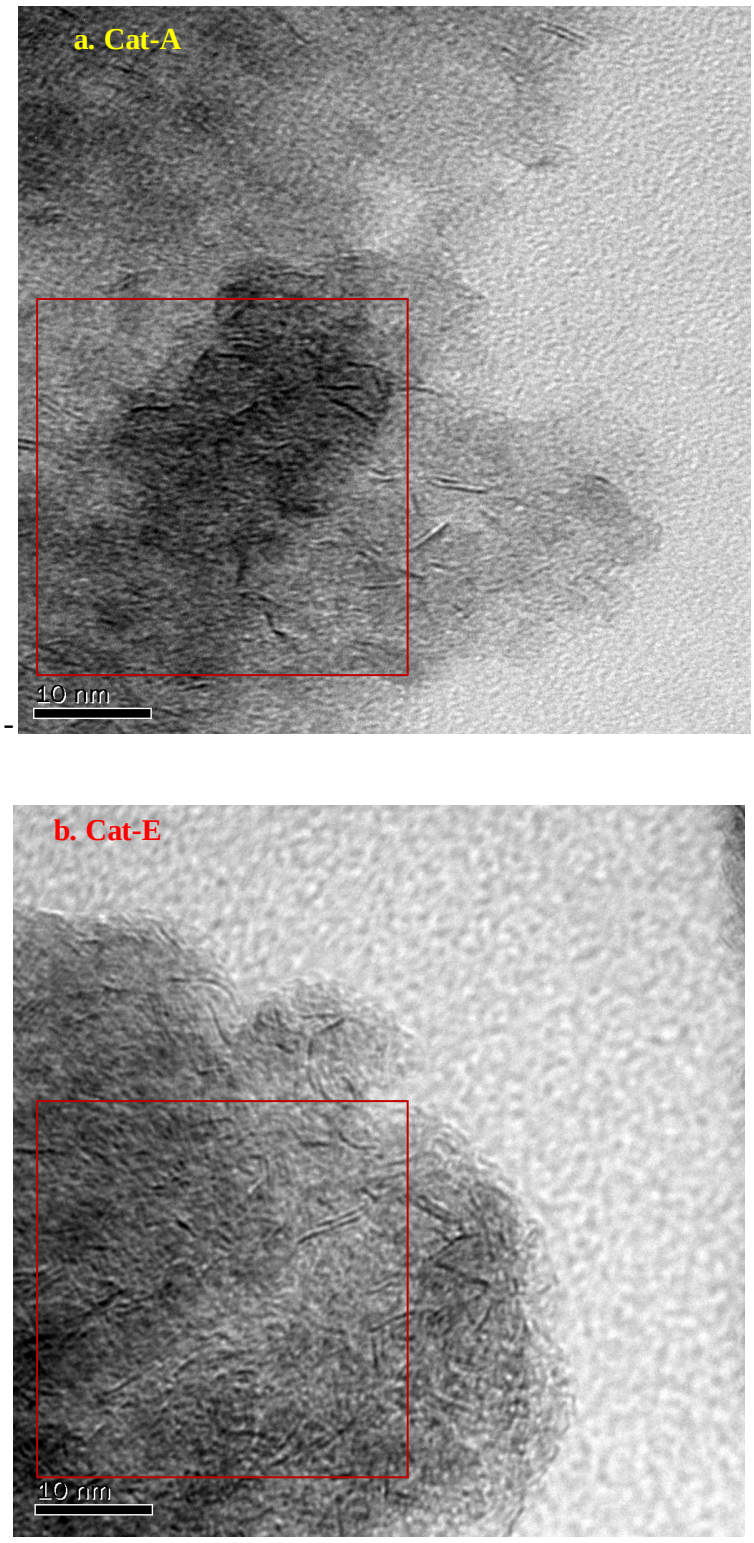

Figure 5.6: HRTEM images of mC supported NiMo catalysts (Cat-A and Cat-E)

From Figure 5.6, one can see that most of the active phase is single or two layered. A comparison of stack distribution (based on number of layers in a stack) in sulfided Cat-A and Cat-E is provided in Table 5.3. Though single layers are predominant in both catalysts, an increase in stacking is observed in Cat-E compared to Cat-A, which might be due to the increase in metal content. From the table, it can be seen that no excessive multilayer formation (>3 layers) is observed in Cat-E. H_2-TPR results indicate lower SMI in mC supported catalyst (Section 5.1.6). Combining H_2-TPR and HRTEM results, one can conclude that for a support like mesoporous carbon with lower SMI, even with predominantly single layered construction, a qualitatively Type-II like NiMoS phase (i.e. weaker SMI) is generated. Such Type-II NiMoS phase is considered to be active for hydrotreating (Topsøe and Clausen, 1986). Absence of excessive multilayer concentration in sulfided Cat-A and Cat-E indicates that there is homogeneous distribution and no noticeable agglomeration of active phase (Gutiérrez et al., 2006) for Mo loading upto 22%. Summary of results from all the characterization techniques is given in Table 5.4.

Table 5.3: Comparison of MoS_2 stack distribution in sulfied NiMo/mC catalysts (For equal area as marked in Fig 5.6)

Catalyst	**Stack layer distribution[a] (%)**			
	Single	Double	Triple	Multi (>3)
Cat-A	92.2	7.8	0	0
Cat -E	85.7	11.4	2.9	0

[a]distribution (%) in the selected equal area =

$$\frac{Number\ of\ stacks\ (single\ or\ double\ or\ triple\ of\ multi\ layered,\ as\ applicatble)}{Total\ stacks\ in\ the\ area\ (Single + double + triple + multi\ layered)}\ x\ 100$$

Table 5.4: Summary of characterization results from Phase-II study

Technique employed	**Observations**	**Inference**
N_2 Physical adsorption	- All catalysts exhibit Type-IV isotherm - Reduction in pore volume was steep at very high metal loading (Mo > 22%)	- Mesoporous structure is retained - Significant pore blockage is occurring at very high metal loading
SEM	- Needle like structure (as in mC-V) was retained in all the catalysts	- There is no extensive structural damage after catalyst loading within SEM resolution level
TEM	- Dispersion was poor at very high metal loading (Mo – 27%)	- Significant agglomeration is occurring at very high metal loading
XRD	- Significant Mo oxide peaks were observed for Cat-D (27% Mo) - No significant Mo oxide peaks were observed for Mo loading upto 22 % (Mo/Ni weight ratio= 5) - A mild incipient Mo oxide peak was observed when Mo/Ni ratio increased by 50% (for the same Mo loading of 22%)	- Metal loading beyond 22% Mo causes reduced dispersion resulting in MoO_3 Crystallites - 2.9% Ni is sufficient to disperse 22% Mo over mC-6M support
H_2 -TPR	- Reduction temperature of mC supported catalyst (Cat-E) under H_2 flow is lower than commercial γ-Al_2O_3 supported catalyst	- Proof for the presence of lower SMI in mC supported catalyst when compared to γ-Al_2O_3 supported catalyst. Lower SMI helps in transition from oxide phase into active sulphide phase at lower temperatures (Sigurdson, 2009).
HRTEM	- Lower concentration of multilayer MoS_2 phase were observed (predominantly monolayer) in sulfided Cat-A - The concentration of multilayer was found to increase in sulfided Cat-E (but not more than 3)	- Lower support-metal interaction in carbon supports helps in the formation of qualitatively Type-II like NiMoS phase which are active for hydrotreating (Topsøe and Clausen, 1986).

5.1 Hydrotreating activity study

Hydrotreating experiments were carried out in a trickle bed flow reactor under typical industrial operating conditions using coker light gas oil (KLGO) derived from Athabasca bitumen as feedstock. All the catalysts were subjected to precoking for 4 days at 370°C for stabilizing their activity. Typically, the stability was attained after two days for all the catalysts. The experimental temperatures at which representative sample collection was carried out were 370°C, 350°C and 330°C. Two representative samples were taken for each temperature and analyzed for residual nitrogen and sulphur content. The results of HDS activity of all the four mC supported catalysts with varying Mo loading (constant Ni/Mo ratio) are given in Figure 5.7.

The HDS activity increases progressively as the Mo loading is increased from 12% (Cat-A) to 22% (Cat-C) and then starts declining at higher Mo loading (Cat-D). Higher metal loading in Cat-D (27%) causes the agglomeration of Mo (as seen by XRD) resulting in lower HDS activity. As in HDS, the HDN activity of Cat-C is the highest among the four catalysts studied (Figure 5.8).

In the next step of hydrotreating activity study, Ni loading was reduced from 4.4% (Cat-C) to 2.9% (Cat-E) keeping the Mo level constant at 22%. The resulting catalyst, (Cat-E) showed higher hydrotreating activity than Cat-C (Figures 5.9 and 5.10). From this result, one can say that 2.9% Ni is sufficient to have promotion effect for 22% Mo on functionalized mesoporous carbon support. The XRD results for Cat-E showed a small MoO_3 crystallite peak. However, the hydrotreating activity of Cat-E is higher than Cat-C suggesting that 2.9% Ni is the incipient level and the hence the metal loading of 22%Mo

and 2.9% Ni is optimum on functionalized mesoporous carbon support for the hydrotreating of KLGO.

From Figures 5.7 to 5.10, it can be seen that the extent of variation in HDS activity among the five catalysts (Cat-A to Cat-E) is lower than that for HDN activity. HDN reactions follow hydrogenation pathway whereas HDS reactions can follow both hydrogenation and direct hydrogenolysis pathway (Section 2.5). According to rim-edge model (Daage and Chianelli, 1994), the top and bottom rim sites are the active sites for hydrogenation whereas edge sites are active for hydrogenation and direct hydrogenolysis. Based on the HRTEM results (Fig 5.6 and Table 5.3), one can see increase in stacking degree in Cat-E compared to that of Cat-A, which indicates the presence of additional rim sites in Cat-E. These sites help in HDN reactions through hydrogenation pathway, resulting in significant increase in HDN activity compared to that of HDS.

Finally, the HDS and HDN performance of the optimum catalyst was compared with that of commercial catalyst (typically, NiMo with Phosphorous, supported on γ-Al_2O_3 (Sigurdson, 2009)) and results are shown in (Figures 5.9 and 5.10). It can be seen that NiMo/mC catalyst (Cat-E) outperforms commercial catalyst for both HDS and HDN. Similar result on higher HDS activity of NiMo catalysts supported on mesoporous carbon compared to that of commercial catalysts has been reported by other researchers for the hydrotreating of model compounds (Shi et al., 2010). The higher HDN and HDS activities of mesoporous carbon supported catalyst compared to that of commercial catalyst can be attributed to lower support metal interaction (as observed by TPR and HRTEM), higher surface area (as found by N_2 physisorption), effective nitric acid functionalization (as evidenced from FTIR) alongwith effective higher metal bearing capacity (as found by ICP-MS, XRD, TEM).

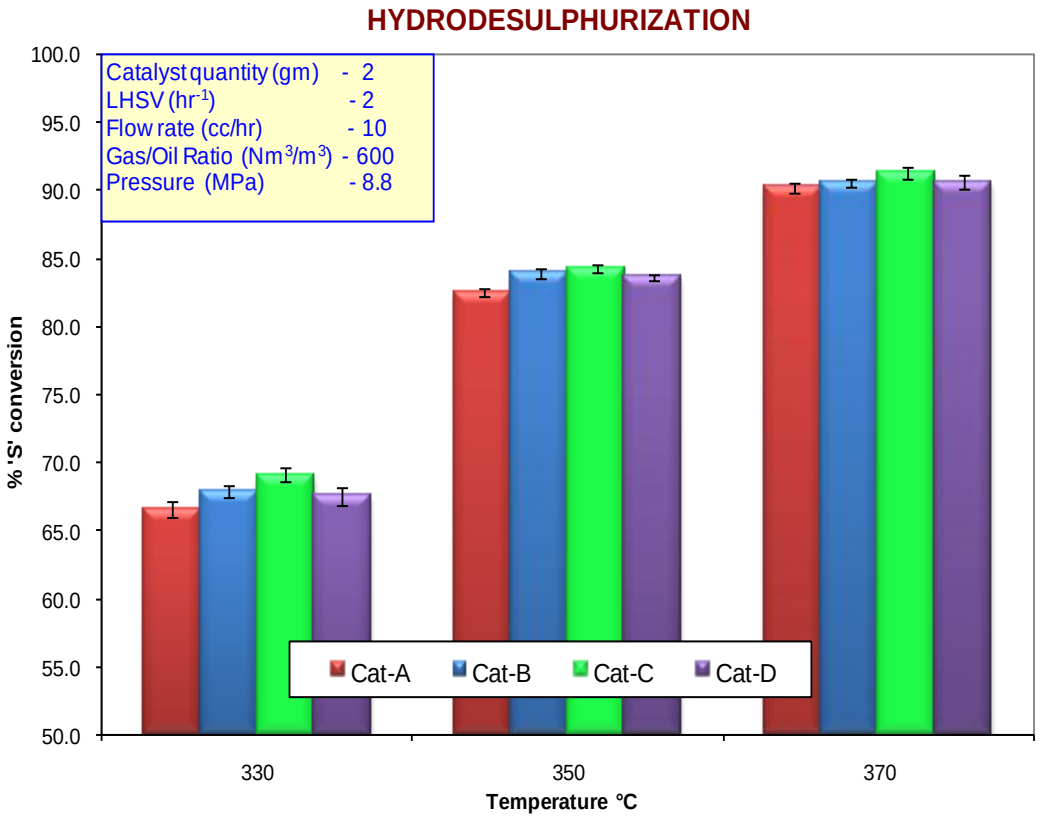

Figure 5.7: HDS activity comparison of NiMo/ mC catalysts with varying Mo loading

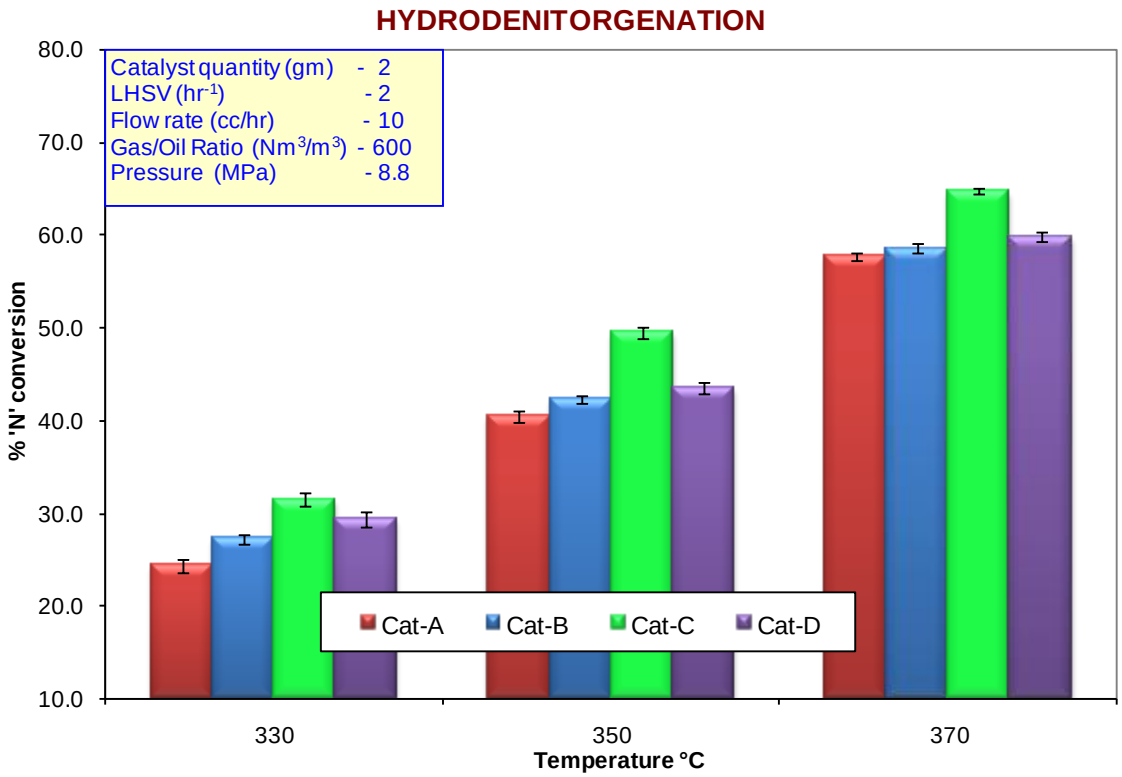

Figure 5.8: HDN activity comparison of NiMo/ mC catalysts with varying Mo loading

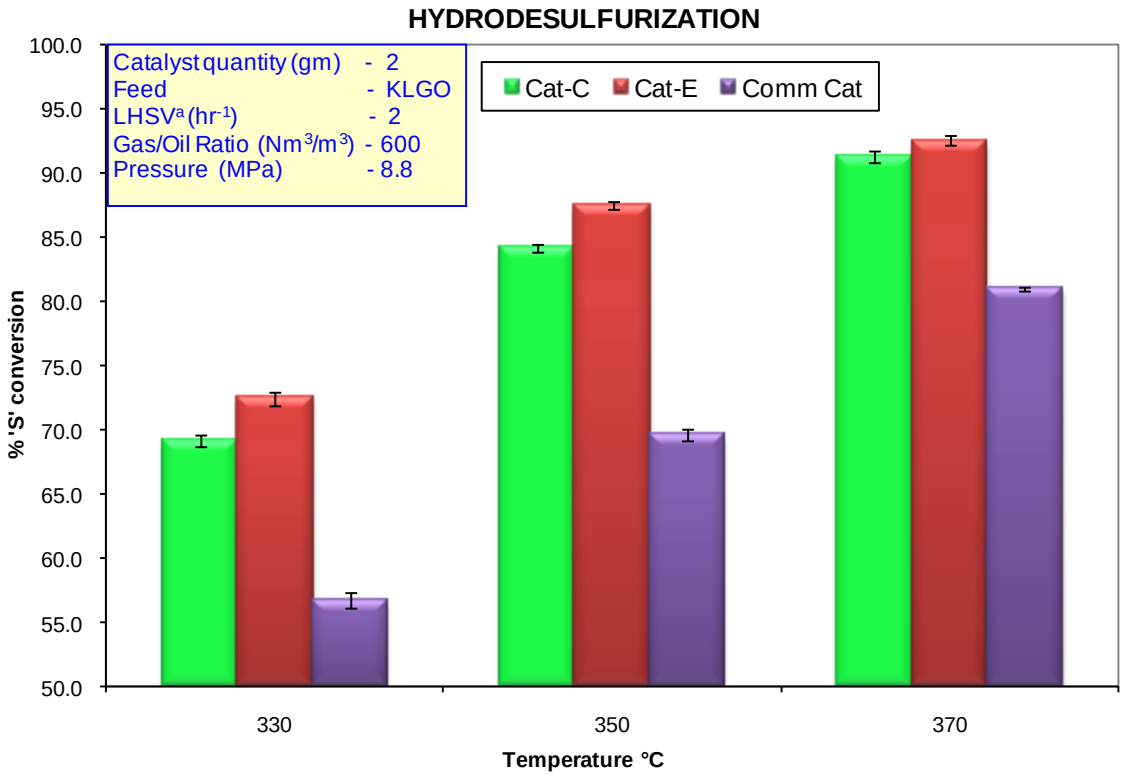

a- For γ-Al_2O_3 supported catalyst, weight of the catalyst is taken as basis

Figure 5.9: HDS activity comparison of NiMo/ mC catalysts with varying Ni loading

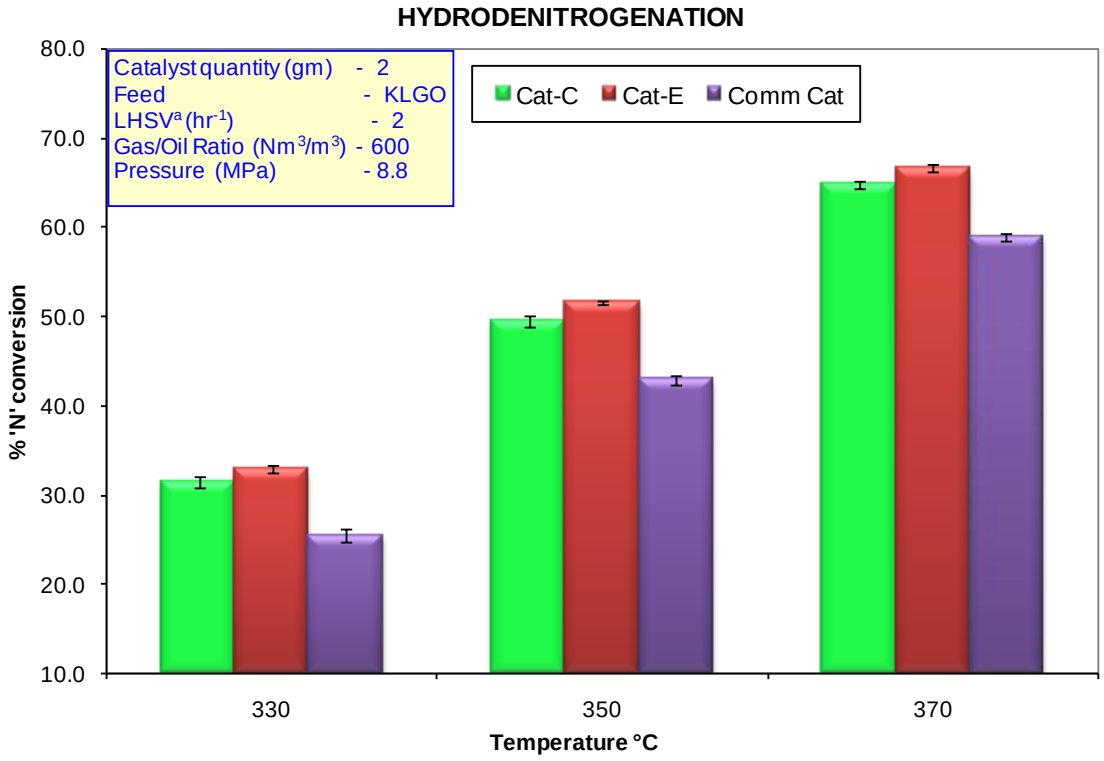

a- For γ-Al_2O_3 supported catalyst, weight of the catalyst is taken as basis

Figure 5.10: HDN activity comparison of NiMo/ mC catalysts with varying Ni loading

5.2 Conclusions:

Mesoporous carbon supports with higher surface area and pore volume were prepared using alkali modified SBA-15 template and functionalized using 6M nitric acid. A series of catalysts were prepared with varying Mo and Ni loading (Mo 12 – 27%; Ni 2.4 – 5.4%) supported on functionalized mesoporous carbon. Progressive reduction in pore volume and surface area of the catalysts was observed with the increase in metal loading indicating the effective dispersion of catalyst metals as well as blocking of some micropores (as found by N_2 physisorption). Beyond 22% Mo loading, significant presence of MoO_3 crystallites were observed indicating agglomeration at higher metal loading (as seen by XRD). Reduction of Ni/Mo ratio by more than 50% did not produce any significant MoO_3 crystalline phase indicating the sufficiency of lower Ni/Mo ratio in functionalized mesoporous carbon support. All of the catalysts retain needle like morphology even at very high metal loading (as seen by SEM), though with reduced orderliness (as seen by TEM) at very high metal loading. Mesoporous carbon supported catalysts possess lower support metal interaction (SMI) compared to commercial catalysts supported on γ-Al_2O_3 (as seen by TPR). Such lower SMI facilitated the generation of qualitatively Type-II like NiMoS phase (i.e. lower SMI) on the sulfided catalysts (as seen by HRTEM) which are active for hydrotreating. Hydrotreating study carried out using these NiMo catalysts supported on mesoporous carbon support using coker light gas oil feed derived from Athabasca bitumen indicated that the catalyst with 22%Mo and 2.9% Ni has the highest HDS and HDN activities. This is the optimum level of metal loading over mesoporous carbon support with respect to better dispersion, structural orderliness and generation of more of MoS_2 layers per stack. This optimum catalyst has higher HDS and HDN activities compared to commercial catalyst (Typically,

NiMo catalyst with Phosphorous additive, supported on γ-Al_2O_3). The higher activity of mesoporous carbon supported catalyst is attributed to lower support metal interaction, higher surface area, effective functionalization alongwith higher metal bearing capacity.

CHAPTER 6

KINETIC AND LONG TERM DEACTIVATION STUDY

Kinetic parameter estimation study, analysis on the effects of mass transfer and hydrodynamic parameters were carried out using the optimum catalyst (22% Mo and 2.9% Ni) found from the metal optimization study discussed in Chapter 5. The operating conditions used in the kinetic study were: LHSV -- 1.0 to 2.5 hr^{-1}; Pressure -- 7.8 to 9.8 MPa; Gas-to-Oil ratio -- 400 to1000 Nm^3/m^3 and Temperature -- 330 to 370°C. The calculation procedure used to estimate sulphur and nitrogen conversion and also the conversion data (obtained in kinetic study) are given in Appendix-A and Appendix-B respectively; the results are discussed below.

6.1 Hydrodynamics in trickle bed reactor

The results of hydrodynamic parameter evaluation in terms of wetting, wall effects and backmixing are presented in Table 6.1. The criteria used for estimating the hydrodynamic parameters are given in section 2.14.1.Complete wetting was not ensured under undiluted conditions in the laboratory scale reactor used for the experiment. However, the problem was overcome by adding SiC diluent in the reactor as shown in Table 6.1. Furthermore, one can see from the results that diluents addition helps in removing problems associated with wall effect which otherwise can affect the conversion. The changes in viscosity and density offset each other to some extent for maintaining wetting parameter. However, wetting parameter is relatively lower (though stays above the minimum required level) at reduced LHSV values. Backmixing effects were also overcome by the utilization of diluents.

Table 6.1: Results of hydrodynamic parameter evaluation

Parameter	Criteria value	Calculated value without dilution	Calculated value with dilution	Result interpretation
Wetting	$>5 \times 10^{-6}$	1.3×10^{-6} to 4.4×10^{-6}	37×10^{-6} to 110×10^{-6}	Dilution helps to remove wetting limitation
Wall effects	>25	5.9	54.1	Dilution helps to eliminate wall effects
Backmixing	>100	37.1	1168.9	Backmixing problem has been overcome by dilution

6.2 Mass transfer effects

Mass transfer calculations were carried out to understand the effects of mass transfer resistance in NiMo/mC catalyst for the hydrotreating of KLGO and their implication on kinetic parameter evaluation. The analysis was divided into two sections - external mass transfer evaluation and internal mass transfer evaluation as detailed in this section.

6.2.1 External mass transfer evaluation

The diffusion of hydrogen gas to the surface of catalyst particle through bulk H_2 rich gas phase and KLGO rich liquid phase is considered under external mass transfer evaluation. Satterfield criterion (Satterfield et al., 1969) was used to carry out the calculations. This criterion evaluates the rate of hydrogen mass transfer through the bulk liquid phase in comparison with the rate of hydrogen conversion for HDS and HDN to determine which one is controlling. Detailed calculation procedure used in the evaluation

of external mass transfer is given in Appendix C. The range of values of relevant parameters estimated while calculating external mass transfer for different operating conditions are given in Appendix D. The right hand side– RHS (i.e. mass transfer parameter) value is considered to be same for both HDS and HDS reaction as there is no segregation in hydrogen flow for these two reactions. However the left hand side - LHS (i.e. reaction rate parameter) is different for HDS and HDN reactions.

For HDS reactions, LHS value of the Satterfield criterion was higher than RHS value for all the operating conditions (i.e. the criterion is satisfied). It indicates that diffusion resistance for hydrogen flow through bulk gas phase and bulk liquid phase cannot be neglected for HDS reactions. The LHS value of the criterion was much higher at lower LHSV values (i.e. higher conversion). Contrary to HDS reactions, LHS value of the Satterfield criterion was lower than RHS value for HDN reactions under all the operating conditions (i.e. the criterion is not satisfied). It indicates that external mass transfer resistance is not a significant concern for HDN reactions.

The difference in external mass transfer resistance for HDS and HDN reactions are due to the difference in requirement of hydrogen for these reactions. The sulphur concentration in KLGO feed is much higher than nitrogen and the HDS conversion is also much higher than HDN conversion, thus indicating the significant amount of hydrogen consumed in HDS reactions. For example, the hydrogen consumption for HDS reaction can be more than nine times than that for HDN reaction making the sufficient availability of hydrogen much more difficult for HDS reactions. The findings of external mass transfer calculations suggest that HDS reaction rates from kinetic studies cannot be treated as intrinsic.

6.2.2 Internal mass transfer evaluation

The diffusion limitation for the movement of reactant molecule towards the reaction sites inside the catalyst particle is characterized by internal mass transfer limitation. This is studied by calculating the effectiveness factor (η), which is defined as (Fogler, 2006)

$$\eta = \frac{Actual\ overall\ reaction\ rate}{Overall\ reaction\ rate\ without\ internal\ diffusion\ limitation}$$

Many correlations used for estimating internal mass transfer limitations assume isothermal conditions throughout the catalyst pellet. Hence it is necessary to check whether isothermal conditions are maintained across the catalyst pellet. This is done by estimating the maximum potential temperature difference between the core and surface of the catalyst pellet (β) (Satterfield, 1991). The details of the calculation are provided in Appendix-E and a summary of range of β values for various operating conditions is provided in Appendix-F. The maximum value of ΔT (for HDS and HDN together) was less than 0.06 K and it was mainly dictated by the ΔT_{max} for HDS reaction as the concentration and conversion level of sulphur was much higher than that of nitrogen. With such lower temperature gradient, we can assume that isothermal condition is maintained in catalyst pellet.

Isothermal condition of the NiMo/mC catalyst pellet was also checked by using Anderson criterion (Mears, 1971). This criterion compares the generation of heat (LHS of equation 2.3) with that of dissipation (RHS of equation 2.3). For all the process conditions, the RHS values are significantly higher than LHS values for both HDS and HDN reactions, confirming the isothermal condition in catalyst pellet. The detailed

calculation and summary of calculated values for different operating conditions are given in Appendix-E and F respectively.

Estimation of effectiveness factor is generally done using Thiele modulus values (Fogler, 2006). However, utilization of Thiele modulus requires intrinsic reaction rates and cannot be used for overall reaction rates (Sigurdson, 2009; Vishwakarma et al., 2007). Hence, another dimensionless modulus (Φ), which employ global reaction rate was used to evaluate effectiveness factors (Satterfield, 1970). Bulk diffusivities for the calculations were assumed to be same for all the compounds in KLGO feedstock including sulphur and nitrogen. Since hydrogen diffusivity through KLGO bulk phase was approximately 10 times higher than the diffusivities of KLGO, only the diffusivities of sulphur and nitrogen compounds were considered for internal mass transfer calculations. The results of Φ and η values for different operating conditions are given in Appendix-G (for HDS) and Appendix-H (for HDN).

The results of Φ for HDS reactions were in the range of 0.56 to 0.93 at the reactor inlet and 1.26 – 3.97 at the reactor outlet. The results show that Φ increases over the length of the reactor from inlet to outlet. The effectiveness factor values estimated from Φ were in the range of 0.947 to 0.979 at the reactor inlet and 0.566 – 0.908 at the reactor outlet. Furthermore, lower η values were observed at reactor outlet especially at higher conversions (at higher Temperature and lower LHSV) indicating the increase in internal mass transfer limitation with the decrease in concentration gradient of sulphur in KLGO.

The results of Φ for HDN reactions were in the range of 0.43 to 0.74 at the reactor inlet and 0.56 – 1.27 at the reactor outlet. The results show that Φ increases over the

length of the reactor from inlet to outlet. The effectiveness factor values estimated from Φ were in the range of 0.966 to 0.988 at the reactor inlet and 0.907 – 0.979 at the reactor outlet. For η values of 0.95 or higher, one can consider that internal mass transfer limitations are not present. For HDN reactions, η values for most of the operating conditions and also the average η value, were more than 0.95 and hence one can conclude that HDN reactions for KLGO in NiMo/mC catalyst is not significantly affected by internal mass transfer limitations.

The reasons for lower η values for HDS reactions include higher conversions and relatively higher concentration for sulphur compounds. Thus, both external and internal diffusion effects cannot be eliminated during sulphur removal from KLGO using NiMo/mC catalyst. From the mass transfer studies, one can conclude that HDS reaction rate calculated from kinetic models is apparent rate whereas the same for HDN is intrinsic rate.

6.3 Effect of variation in process parameters

The behaviour of the catalyst for changes in operating conditions was studied in terms of HDS and HDN conversions. The parameters used in the study are given in Table 3.2 and the results are discussed in this section. In addition, the effects of operating parameters on the HDN and HDS reaction rates are included in Appendix- I.

6.3.1 Effect of LHSV

Effect of LHSV on HDS and HDN activities at various reaction temperatures are shown in Figure 6.1. As expected, at lower residence time (i.e. higher LHSV), the conversion reduced at all temperatures for both HDS and HDN reactions.

At a given temperature for HDS, the change in conversion due to variation in LHSV was very low at higher temperatures compared to the change observed at lower temperatures. It might be due to lower rate of reaction through hydrogenation pathway at higher temperatures for sulphur conversion (Farag et al., 1999) and also possibly due to the diffusional resistances. At a given temperature for HDN, the change in conversion due to variation in LHSV was appreciable and more-or-less linear, unlike the results for HDS.

The difference between the response in conversion of sulphur and nitrogen for the changes in LHSV might be due to relatively higher conversion of sulphur (87.3% @ 350^{o}C and 2.0 hr^{-1}) compared to that of nitrogen conversion (51.1% @ 350^{o}C and 2.0 hr^{-1}), which indicates the lower concentration gradient for HDS reaction than that for HDN reaction.

6.3.2 Effect of Pressure

The changes in HDS and HDN activities with the change in system pressure are shown in Figure 6.2. Increase in system pressure raised the hydrogen partial pressure resulting in increased conversion of both HDS and HDN. The change in HDN conversion between 7.8 and 9.8 MPa is much higher (≈ 7.5%) compared to the corresponding change in HDS (≈ 4.2%). It is due to the fact the HDN reactions of aromatic compounds take the route of hydrogenation which is a strong function of H_2 partial pressure (Sigurdson, 2009) compared to HDS which takes the routes of hydrogenation as well as direct desulphurization.

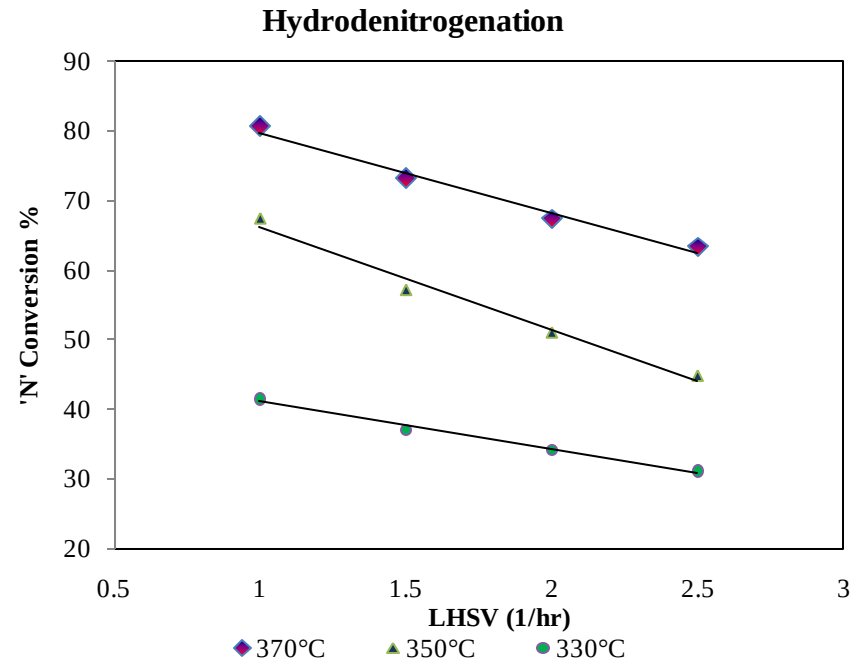

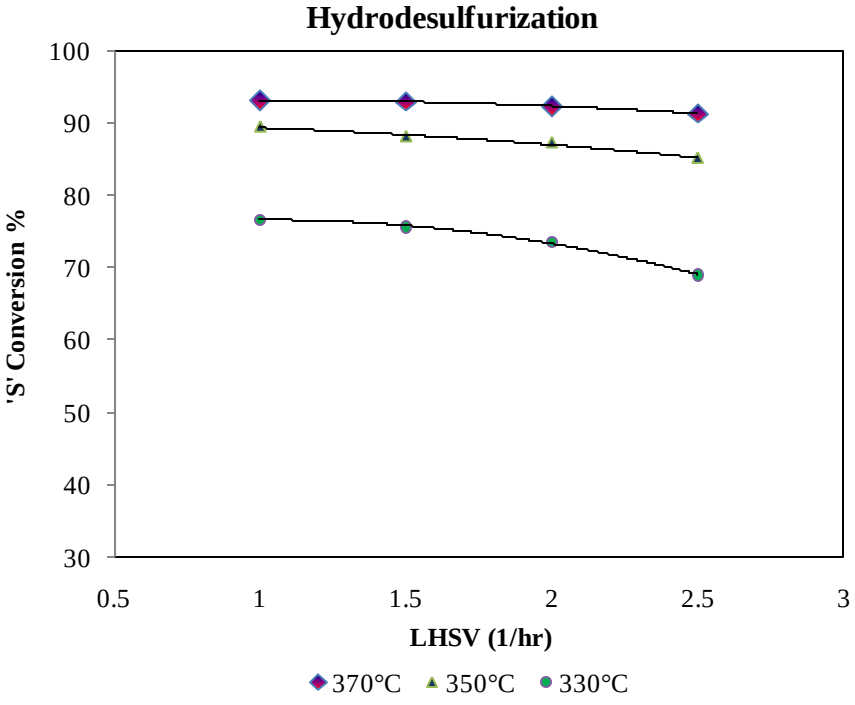

Figure 6.1: Effect of variation in LHSV

(Feed: KLGO; Pressure: 8.8 MPa; Gas/Oil ratio: 600 Nm^3/m^3)

6.3.3 Effect of Gas-to-Oil ratio

The changes in HDS and HDN activities with the variation in gas-to-oil ratio are shown as Figure 6.3. Reduction in gas flow for the same oil rate might decrease effective distribution of the feed stream as well can increase the H_2S partial pressure resulting in decreased activity (H_2S inhibits HDS reaction (Botchwey et al., 2004)). The change in HDS activity is significant for the reduction in gas–to-oil ratio than an increase of it from the reference value of 600 Nm^3/m^3. The rate of increase in HDS activity is relatively lower beyond 800 Nm^3/m^3. Increase in hydrogen flow can help to reduce the external mass transfer limitations and can help to increase HDS conversions.

For HDN, however, the change in activity is marginal for a change of gas-to-oil ratio from 400 to 1000 Nm^3/m^3. This might be due to the absence of external mass transfer limitation in HDN reactions and any change observed might be primarily due to the inhibition effects of components like H_2S.

6.3.4 Effect of Temperature

The temperature effect on HDS and HDN was studied at three different temperatures (Table 6.2). The change in temperature was prominent for HDN in increasing the conversion than that for HDS. This can be attributed to the external and internal diffusion effects, which are significant for HDS reactions compared to HDN reactions.

Table 6.2: Effect of temperature on conversion
(Feed: KLGO; LHSV: 2.0 hr^{-1}; Pressure: 8.8 MPa; Temperature: 350^oC)

Temperature °C	HDN wt %	HDS wt %
330	34.1	73.5
350	51.1	87.3
370	67.4	92.4

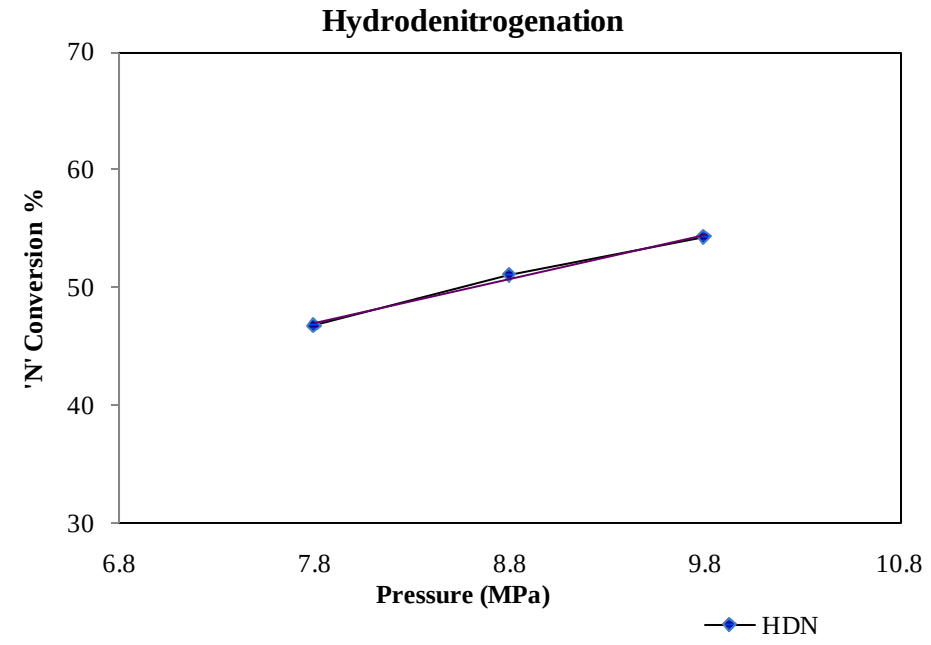

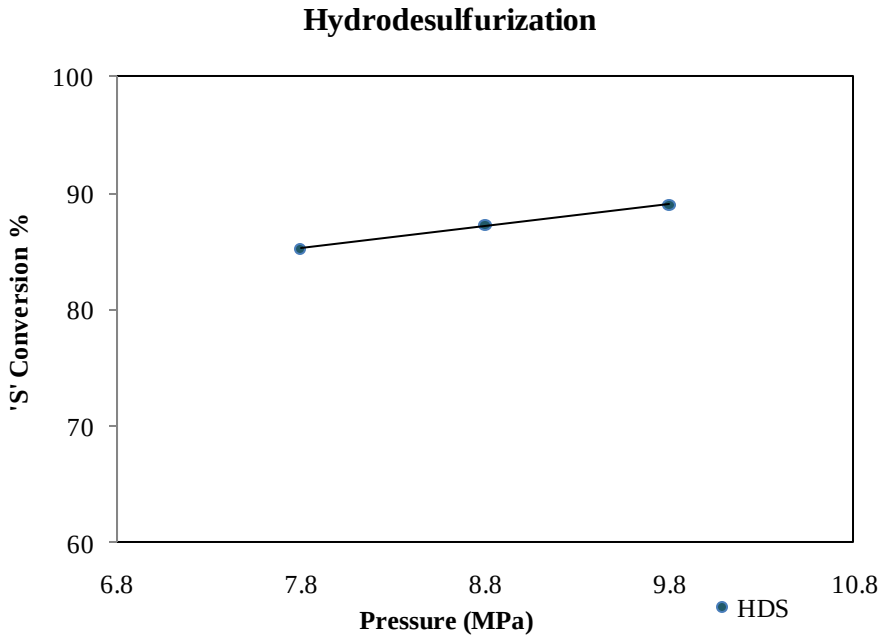

Figure 6.2: Effect of variation in Pressure

(Feed: KLGO; LHSV: 2.0 hr^{-1}; Gas/Oil ratio: 600 Nm^3/m^3; Temperature: 350^oC)

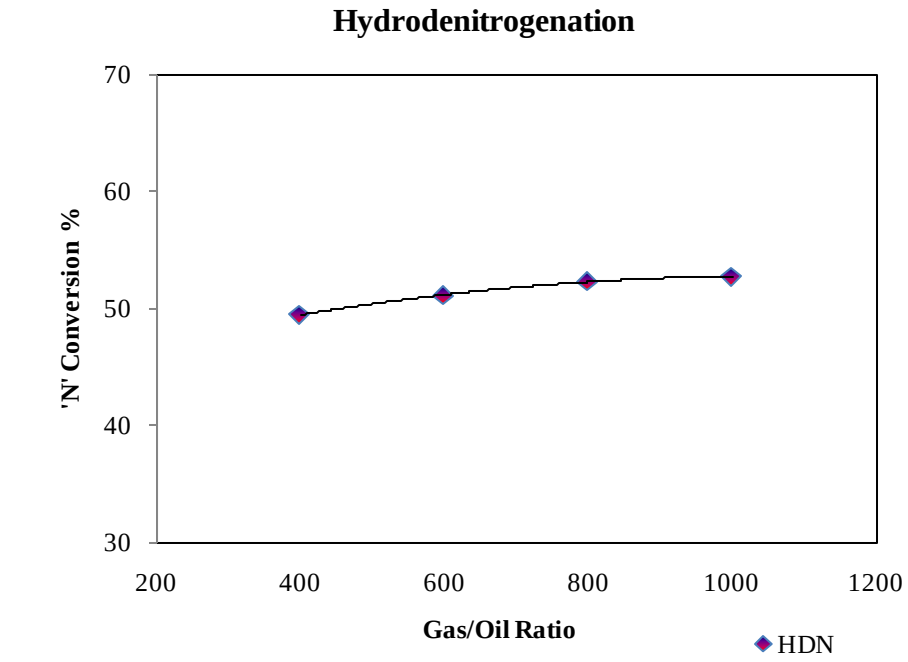

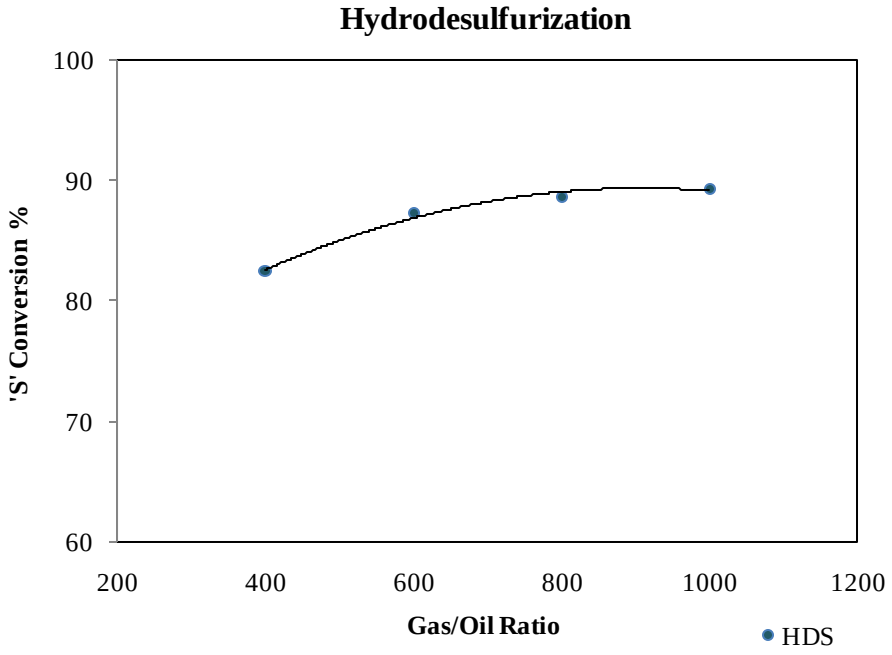

Figure 6.3: Effect of variation in gas-to-oil ratio

(Feed: KLGO; LHSV: 2.0 hr^{-1}; Pressure: 8.8 MPa; Temperature: 350^{o}C)

6.4 Kinetic modeling

Kinetic parameter estimation for kinetic models is useful for the scale up of laboratory reactors to pilot level or to industrial scale. Among the various available models, power law model is simple to develop; however, it does not consider inhibition by various molecules that can affect the reaction rate. Langmuir-Hinshelwood model, which includes the inhibition effects, can be more realistic; however, the mathematical solutions are often complicated.

6.4.1 Power Law model

Using power law model the reaction rate, r_A can be expressed as (Fogler, 2006)

$$r_A = -\frac{dC_A}{dt} = k_A * C_A{}^n \qquad \text{----------} \quad (2.4)$$

The solution for rate constant 'k_A' is given by (Bej et al., 2001)

For $n \neq 1$

$$k_A = (\frac{1}{n-1}) * (\frac{1}{C_{Ap}{}^{n-1}} - \frac{1}{C_{Af}{}^{n-1}}) * LHSV \qquad \text{----------} \quad (6.1)$$

And for n = 1

$$k_A = \ln(\frac{C_{Af}}{C_{Ap}}) * LHSV \qquad \text{----------} \quad (6.2)$$

The activation energy was estimated from k_A at different temperatures by equation 2.5,

$$k_A = A * e^{(-E_A/RT)} \qquad \text{----------} \quad (2.5)$$

In equations 6.1 and 6.2, C_{A_f} and C_{A_p} are the concentration of reacting species 'A' in feed and product respectively. Based on the power law model, the activation energies for HDS and HDN were found to be 189 and 98.9 KJ/mol respectively with good fitting of data (R^2 value 0.96). The estimated reaction orders for HDS and HDN were 2.8 and 1.5 respectively. The calculated activation energy values are in the similar magnitude as identified by some other researchers (Ferdous et al., 2006; Sigurdson, 2009; Vishwakarma et al., 2007) for gas oil hydrotreating.

6.4.2 Langmuir-Hinshelwood model

Langmuir-Hinshelwood (L-H) models are useful in incorporating inhibition effects that can occur during hydrotreating reactions either by inhibition of various reactants (S, N, H_2) or by some product molecules (H_2S). Three models were considered based on different assumptions using L-H concept for this project as shown in Table 6.3

Table 6.3 L-H Models for HDS and HDN reactions

Model ID	Assumption	Model Equation
L-H Model I	Competitive adsorption of individual reacting species (S or N) only	$-r_A = \frac{k_A * K_A * C_A^{\ n}}{(1 + K_A * C_A)}$
L-H Model II	Adsorption of reacting species (S or N, H_2) in different sites	$-r_A = \frac{k_A * K_A * C_A^{\ n} * K_{H_2} * P_{H_2}}{(1 + K_A * C_A) * (1 + K_{H_2} * P_{H_2})}$
L-H Model III	Competitive adsorption of reacting species(S or N) and reaction product (H_2S)	$-r_A = \frac{k_A * K_A * C_A^{\ n}}{(1 + K_A * C_A + K_{H_2S} * P_{H_2S})}$

Terms in the above equations are,

A	-	Reacting species (N or S)
C_A	-	Concentration of reacting species, mol/L
k_A	-	Arrhenius constant
K_A	-	Absorption rate constant, L/mol
n	-	Reaction order
$K_{H_2 (\text{or } H_2S)}$	-	Absorption rate constant for H_2 (or H_2S), 1/MPa
$P_{H_2 (\text{or } H_2S)}$		Partial Pressure of H_2 (or H_2S), MPa

Activation energies are estimated from k and K values obtained for different temperatures using Arrhenius plot and Van't hoff plot respectively (Appendix-I).

Out of the three models, model-II gave lower regression (R^2<0.7) compared to other two models for both HDS and HDN and hence not evaluated further. The results for Model I and Model-III are presented in Table 6.4. Regression plots for both the models are provided in Appendix-I. The incorporation of NH_3 inhibition in Model-III did not give significant variation compared to that of H_2S. This might be due to significantly lower nitrogen content of the feed and also lower nitrogen conversion compared to that of sulphur i.e. significantly higher concentration of H_2S in product compared to that of NH_3 masks the inhibition effect NH_3.

Between the two L-H models evaluated, Model III has better fitting based on R^2 values indicating the presence of H_2S inhibition alongwith inhibition from sulphur and nitrogen species for hydrotreating reactions in NiMo/mC catalysts. However, the R^2 value for HDS in Model III is lower than that for HDN indicating the limited suitability of the model for HDS reactions. The reason for this could be that the conversion of sulphur compounds is already very high under experimental conditions studied and the variation in model prediction of conversion in HDS reactions (for different LHSVs) is higher than that for HDN reactions leading to lower R^2 values in L-H models for HDS.

Table 6.4 Results of L-H Models for HDS and HDN reactions

Model ID	**Model Equation**	**Activation Energy (KJ/mol)**
L-H Model I	$-r_i = \frac{k_i * K_i * C_i^n}{(1 + K_i * C_i)}$	E_S = 47.2 E_N = 69.1 λ_N = 3.6 λ_S = 5.7 n = 1 (pseudo first order) R^2_{HDS}= 0.80 R^2_{HDN}= 0.86
L-H Model III	$-r_i = \frac{k_i * K_i * C_i^n}{(1 + K_i * C_i + K_{H_2S} * P_{H_2S})}$	E_S = 63.0 E_N =79.1 λ_N = 3.6 λ_S = 5.7 λ_{H_2S} = 34.6 n = 1 (pseudo first order) R^2_{HDS}= 0.82 R^2_{HDN}= 0.98

6.4.3 Multiparameter model

The equation that represents multi-parameter model (Duan et al., 2005) is given by

$$r_A = -\frac{dC_A}{dt} = k_A * C_A{}^n * P_{H_2}{}^h * (G/O)^q \qquad \text{----------} \quad (2.7)$$

The solution for the equation 2.7 is given by

For n≠ 1

$$\ln \frac{C_{Af}}{C_{Ap}} = \frac{k_A * e^{(-E_A/RT)} * P_{H_2}{}^h * (G/O)^q}{LHSV^c} \qquad \text{----------} \quad (6.6)$$

For n =1

$$\frac{1}{n-1} * \left(\frac{1}{C_{Ap}{}^{n-1}} - \frac{1}{C_{Af}{}^{n-1}}\right) = \frac{k_A * e^{(-E_A/RT)} * P_{H_2}{}^h * (G/O)^q}{LHSV^c} \qquad \text{----------} \quad (6.5)$$

The terms k_A, C_A, and n in equation 2.7 are similar to that defined for equations 2.4 and 2.5. C_{A_f} and C_{A_p} are the concentration of reacting species 'A' in feed and product respectively. The terms h, q and c are the empirical constants for pressure, gas-to-oil ratio and LHSV terms respectively.

Based on the multi-parameter law model, the activation energies for HDS and HDN were found to be 203.3 and 91.2 KJ/mol respectively with good fitting of data (R^2 > 0.98). The estimated reaction orders for HDS and HDN were 2.9 and 1.2 respectively. The values of h, q and c were 3.18, 0.07, 0.64 for HDS and 1.72, 0.0.03, 0.62 for HDN respectively.

Among the various models studied in the project, best fitting was obtained from multi-parameter model. However, realistic results are provided by L-H models that indicate inhibition by H_2S. Arrhenius plot and Regression plots for power law model and multiparameter model are given in Appendix-I.

6.5 Long time deactivation study

In order to understand the effectiveness of catalyst for industrial environment, it is necessary to study its stability under long time operation. The optimum catalyst obtained from phase-II was subjected to long time operation study. This was a continuation of kinetic study in order to ensure the catalyst durability under strained operating condition (because significant variations in parameters were done during kinetic study) and it was carried out at maximum operating temperature used in the project (370 ^{o}C). The total period for the long term deactivation study (after sulfidation) was 10 weeks. The HDS and HDN activities of the catalyst during long term operation (Figure 6.4) were compared with that of initial activity (Post precoking at 370 ^{o}C) to ascertain its longevity. From the figure, one can see that the activity was almost steady for the period of study. The comparative average reduction in HDS and HDN activities were not more than two percent indicating the reasonable durability of NiMo/mC catalyst.

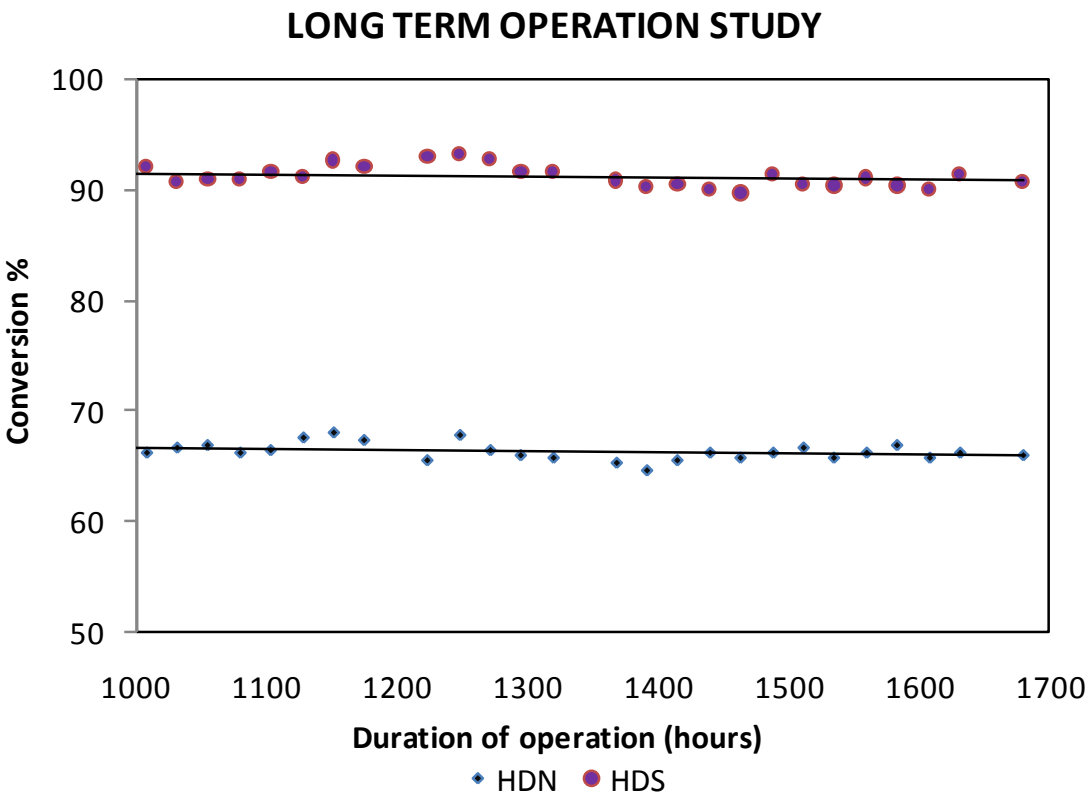

Figure 6.4: Long term deactivation study results of optimum NiMo/mC catalyst (Feed: KLGO; LHSV: 2.0 hr^{-1}; Gas/Oil ratio: 600 Nm^3/m^3; Temperature: 370^oC; Pressure: 8.8 MPa)

CHAPTER 7

CONCLUSIONS AND RECOMMENDATIONS

7.1 Conclusions

The objective of this work was to develop a new catalyst for the hydrotreating of gas oil feedstocks by means of utilizing new generation functionalized mesoporous carbon supports. Key conclusions obtained from this work are summarized below.

7.1.1 Phase-I: Effect of functionalization

- Mesoporous carbon supports synthesized from alkali modified SBA-15 possess ordered structure and needle like morphology.
- Increase in nitric acid concentration (2M to 8M) during functionalization, helps to increase surface functional groups (such as carboxylic, carbonyl and phenolic) on mesoporous carbon surface, but also results in reduction in textural properties (such as BET surface area and pore volume).
- NiMo catalyst supported on 6M HNO_3 treated mesoporous carbon (Cat-6M) exhibits the highest hydrotreating activity compared to other functionalized mC supported catalysts. This is due to the optimum functionalization resulting in enhanced surface functional groups without causing significant reduction in textural properties of mC-6M support.
- The hydrotreating activity of Cat-6M is higher than that of conventional NiMo/γ-Al_2O_3.

7.1.2 Phase-II: Optimization of metal loading

- Metal dispersion over mesoporous carbon support gets reduced beyond 22% Mo loading (for a constant Ni/Mo atomic ratio of 0.33). Ni loading of 2.9% is found to be sufficient to disperse 22% Mo over mC-6M surface (Ni/Mo atomic ratio = 0.22).
- Predominantly single layered construction, but qualitatively Type-II like NiMoS phase (i.e. weaker SMI) is observed in mesoporous carbon supported catalysts.
- Hydrotreating activity study using KLGO indicated that catalyst with 22% Mo and 2.9% Ni (Cat-E) possess the highest hydrotreating activity among the five catalysts studied. This is considered as the optimum catalyst.
- HDN and HDS activities of mesoporous carbon supported catalyst (Cat-E) are higher than that of commercial catalyst supported on γ-Al_2O_3, due to lower support metal interaction, higher surface area, nitric acid functionalization alongwith effective higher metal bearing capacity.

7.1.3 Phase-III: Kinetic and Long term Deactivation Study

- The activation energies for HDS and HDN based on Power law model are 189 KJ/mol and 98.9 KJ/mol, respectively.
- The activation energies for HDS and HDN based on multi-parameter model was 203.3 KJ/mol and 91.2 KJ/mol, respectively. Among the various model studied for the project, multi-parameter model gave very good fitting for the experimental data.

- External and internal mass transfer studies indicated that the measured reaction rate for HDN is intrinsic and that for HDS is apparent.
- Long term deactivation study confirmed the durability of the catalyst for the period of study.

7.2 Recommendations

With the completion of the study of NiMo/mC catalysts for the hydrotreating of coker gas oil feedstock, following recommendations are put forth for future studies.

- Different feedstocks such as naphtha (lighter than KLGO), heavy gas oil (heavier than KLGO) and straight run light gas oil (lower 'N' content than in KLGO) should be used to study the relative performance of NiMo/mC catalysts as the characteristics of feedstocks can have tremendous effect on the hydrotreating activity.
- Performance of other bimetallic catalysts such as CoMo, NiW, CoW (supported on functionalized mesoporous carbons) should be studied to understand their effectiveness in comparison with NiMo/mC catalysts for hydrotreating process.
- Pilot plant study of the optimum catalyst should be carried out before application to industrial reactors for ensuring effective scale up.

CHAPTER 8

REFERENCES

Abotsi, G.M.K. and A.W. Scaroni, "A review of carbon-supported hydrodesulfurization catalysts," Fuel Processing Technology. 22, 107-133 (1989).

Absi-Halabi, M., A. Stanislaus and K. Al-Dolama, "Performance comparison of alumina-supported Ni-Mo, Ni-W and Ni-Mo-W catalysts in hydrotreating vacuum residue," Fuel. 77, 787-790 (1998).

Absi-Halabi, M., A. Stanislaus and D.L. Trimm, "Coke formation on catalysts during the hydroprocessing of heavy oils," Applied Catalysis. 72, 193-215 (1991).

Ahmed, T., "Hydrocarbon phase behavior," Gulf Publishing Company, Houston (1989).

Ancheyta, J. and J.G. Speight, Eds., "Hydroprocessing of heavy oil and residua ," CRC Press, Florida (2007).

Ancheyta, J., M.J. Angeles, M.J. Macías, G. Marroquín and R. Morales, "Changes in apparent reaction order and activation energy in the hydrodesulfurization of real feedstocks," Energy and Fuels. 16, 189-193 (2002).

Ancheyta.J., Angeles.M.J., Macias.M.J., Marroquin.J.G. and Morales.R, "Changes in apparent reaction order and activation energy in the hydrodesulfurization of real feedstocks," Energy Fuels, 2001, 15 (2), Pp 377–383. 1, 189-193 (2002).

Aoyagi, K., W.C. McCaffrey and M.R. Gray, "Kinetics of Hydrocracking and Hydrotreating of Coker and Oilsands Gas Oils," Petroleum Science and Technology, 21:5, 997 - 1015. 21, 997-1015 (2003).

Appleby, W.G., J.W. Gibson and G.M. Good, "Coke formation in catalytic cracking," Industrial & Engineering Chemistry Process Design and Development. 1, 102-110 (1962).

Arnoldy, P., J.C.M. De Jonge and J.A. Moulijn, "Temperature-programmed reduction of MoO_3 and MoO_2," Journal of Physical Chemistry. 89, 4517-4526 (1985).

Baldi, G., "
Design and scale-up of trickle bed reactors - Solid liquid contacting effectiveness," in " Multiphase chemical reactors volume II - Design methods," Rodrigues.A.E, Calo.J.M. and Sweed.N.H., Eds. Sijthoff & Noordhoff, Alphen aan den Rijn (1981), pp. 323.

Barton, S.S., M.J.B. Evans, E. Halliop and J.A.F. MacDonald, "Acidic and basic sites on the surface of porous carbon," Carbon. 35, 1361-1366 (1997).

Bazuła, P.A., A.H. Lu, J.J. Nitz and F. Schüth, "Surface and pore structure modification of ordered mesoporous carbons via a chemical oxidation approach," Microporous and Mesoporous Materials. 108, 266-275 (2008).

Bej, S.K., A.K. Dalai and J. Adjaye, "Kinetics of hydrodesulfurization of heavy gas oil derived from oil-sands bitumen," Petroleum Science and Technology. 20, 867-877 (2002).

Bej, S.K., A.K. Dalai and J. Adjaye, "Comparison of hydrodenitrogenation of basic and non basic compounds present in oil sands derived gas oil," Energy and Fuels. 15(2), 377-388 (2001).

Bej, S.K., R.P. Dabral, P.C. Gupta, K.K. Mittal, G.S. Sen, V.K. Kapoor and A.K. Dalai, "Studies on the performance of a microscale trickle bed reactor using different sizes of diluent," Energy and Fuels. 14, 701-705 (2000).

Biniak, S., G. Szymański, J. Siedlewski and A. Światkoski, "The characterization of activated carbons with oxygen and nitrogen surface groups," Carbon. 35, 1799-1810 (1997).

Botchwey, C., A.K. Dalai and J. Adjaye, "Two-stage hydrotreating of Athabasca heavy gas oil with interstage hydrogen sulfide removal: Effect of process conditions and kinetic analyses," Industrial and Engineering Chemistry Research. 43, 5854-5861 (2004).

Boudou, J.P., A. Martinez-Alonzo and J.M.D. Tascon, "Introduction of acidic groups at the surface of activated carbon by microwave-induced oxygen plasma at low pressure," Carbon. 38, 1021-1029 (2000).

Breysse, M., P. Afanasiev, C. Geantet and M. Vrinat, "Overview of support effects in hydrotreating catalysts," Catalysis Today. 86, 5-16 (2003).

Brito, J.L., F. Severino, N.N. Delago and J. Laine, "HDS activity of carbon-supported Ni-Mo catalysts derived from thiomolybdate complexes," Applied Catalysis. 173, 193 (1998).

Burdett, J.K. and J.T. Chung, "Volcano plots, hydrodesulfurization and surface atom pair potentials," Surface Science. 236, L353-L357 (1990).

Calafat, A., J. Laine and A. López-Agudo, "Hydrodenitrogenation of pyridine over activated carbon-supported sulfided Mo and NiMo catalysts. Effects of hydrogen sulfide and oxidation of the support," Catalysis Letters. 40, 229 (1996a).

Calafat, A., J. Laine, A. López-Agudo and J.M. Palacios, "Effect of surface oxidation of the support on the thiophene hydrodesulfurization activity of Mo, Ni, and NiMo catalysts supported on activated carbon," Journal of Catalysis. 162, 20-30 (1996b).

Calvo, L., M.A. Gilarranz, J.A. Casas, A.F. Mohedano and J.J. Rodríguez, "Effects of support surface composition on the activity and selectivity of Pd/C catalysts in aqueous-phase hydrodechlorination reactions," Industrial and Engineering Chemistry Research. 44, 6661-6667 (2005).

Chen, X., M. Farber, Y. Gao, I. Kulaots, E.M. Suuberg and R.H. Hurt, "Mechanisms of surfactant adsorption on non-polar, air-oxidized and ozone-treated carbon surfaces," Carbon. 41, 1489-1500 (2003).

Chingombe, P., B. Saha and R.J. Wakeman, "Surface modification and characterisation of a coal-based activated carbon," Carbon. 43, 3132-3143 (2005).

Choi, J.-., R.L. Curl and L.T. Thompson, "Molybdenum nitride catalysts. I. Influence of the synthesis factors on structural properties," Journal of Catalysis. 146, 218-227 (1994).

Choi, J.-., J.R. Brenner, C.W. Colling, B.G. Demczyk, J.L. Dunning and L.T. Thompson, "Synthesis and characterization of molybdenum nitride hydrodenitrogenation catalysts," Catalysis Today. 15, 201-222 (1992).

Chu, C.F. and K.M. Ng, "Flow in packed tubes with a small tube to particle diameter ratio," American Institute of Chemical Engineers Journal. 35, 148-158 (1989).

Clean air trust, "http://www.cleanairtrust.org/sulfurdioxide.html," 10-Mar-2011 (1999).

Cocchetto, J.F. and C.N. Satterfield, "Chemical equilibria among quinoline and its reaction products in hydrodenitrogenation," Industrial & Engineering Chemistry Process Design and Development. 20, 49-53 (1981).

Cocchetto, J.F. and C.N. Satterfield, "Thermodynamic equilibria of selected heterocyclic nitrogen compounds with their hydrogenated derivatives," Industrial & Engineering Chemistry Process Design and Development. 15, 272-277 (1976).

Colling, C.W. and L.T. Thompson, "The structure and function of supported molybdenum nitride hydrodenitrogenation catalysts," Journal of Catalysis. 146, 193-203 (1994).

Daage, M. and R.R. Chianelli, "Structure-Function Relations in Molybdenum Sulfide Catalysts: The "Rim-Edge" Model," Journal of Catalysis. 149, 414-427 (1994).

Dai, Q. and K.H. Chung, "Trona (mineral grade sodium carbonate) as a process aid for the hot water process," Journal of Canadian Petroleum Technology. 35, 57-59 (1996).

De Beer, V.H.J., T.H.M. Van Sint Fiet, G.H.A.M. Van Der Steen, A.C. Zwaga and G.C.A. Schuit, "The CoO-MoO3-γ-Al2O3 catalyst. V. Sulfide catalysts promoted by cobalt, nickel, and zinc," Journal of Catalysis. 35, 297-306 (1974).

De Beer, V.H.J., F.J. Derbyshire, C.K. Groot, R. Prins, A.W. Scaroni and J.M. Solar, "Hydrodesulphurization activity and coking propensity of carbon and alumina supported catalysts," Fuel. 63, 1095-1100 (1984).

De La Puente, G. and J.A. Menéndez, "On the distribution of oxygen-containing surface groups in carbons and their influence on the preparation of carbon-supported molydenum catalysts," Solid State Ionics. 112, 103-111 (1998).

De La Puente, G., A. Centeno, A. Gil and P. Grange, "Interactions between molybdenum and activated carbons on the preparation of activated carbon-supported molybdenum catalysts," Journal of Colloid and Interface Science. 202, 155-166 (1998).

Derbyshire, F.J., V.H.J. de Beer, G.M.K. Abotsi, A.W. Scaroni, J.M. Solar and D.J. Skrovanek, "The influence of surface functionality on the activity of carbon-supported catalysts," Applied Catalysis. 27, 117-131 (1986).

Dieselnet, "http://www.dieselnet.com/standards/ca/fuel.php " 10-Feb-2011.

Duan, A.J., C.M. Xu, S.X. Lin and K.H. Chung, "Hydrodesulfurization and hydrodenitrogenation kinetics of a heavy gas oil over NiMo/Al_2O_3 catalysts," Journal of Chemical Engineering of Chinese Universities. 19, 762-766 (2005).

Environment Canada, "http://www.ec.gc.ca/air," 10-Mar-2011 (01-Feb-2011).

Environment Canada, "http://www.ec.gc.ca/ceparegistry/documents/notices/COM623.pdf," 10-Feb-2010.

Eswaramoorthi, I. and A.K. Dalai, "Synthesis, characterisation and catalytic performance of boron substituted SBA-15 molecular sieves," Microporous and Mesoporous Materials. 93, 1-11 (2006).

Eswaramoorthi, I., V. Sundaramurthy, N. Das, A.K. Dalai and J. Adjaye, "Application of multi-walled carbon nanotubes as efficient support to NiMo hydrotreating catalyst," Applied Catalysis A: General. 339, 187-195 (2008).

Fan, J., C. Yu, L. Wang, B. Tu, D. Zhao, Y. Sakamoto and O. Teresaki, "Mesotunnels on the silica wall of ordered SBA-15 to generate three-dimensional large-pore mesoporous networks [15]," Journal of the American Chemical Society. 123, 12113 (2001).

Farag, H., I. Mochida and K. Sakanishi, "Fundamental comparison studies on hydrodesulfurization of dibenzothiophenes over CoMo-based carbon and alumina catalysts," Applied Catalysis A: General. 194, 147-157 (2000).

Farag, H., D.D. Whitehurst and I. Mochida, "Synthesis of active hydrodesulfurization carbon-supported Co-Mo catalysts. relationships between preparation methods and activity/selectivity," Industrial and Engineering Chemistry Research. 37, 3533-3539 (1998).

Farag, H., D.D. Whitehurst, K. Sakanishi and I. Mochida, "Carbon versus alumina as a support for Co-Mo catalysts reactivity towards HDS of dibenzothiophenes and diesel fuel," Catalysis Today. 50, 9-17 (1999).

Feng, L., X. Li, D.B. Dadyburjor and E.L. Kugler, "A temperature-programmed-reduction study on alkali-promoted, carbon-supported molybdenum catalysts," Journal of Catalysis. 190, 1-13 (2000).

Ferdous, D., "Surface morphology of Ni-Mo catalysts supported on Al_2O_3 : Impact on hydroprocessing of heavy gas oil derived from Athabasca bitumen," Thesis, University of Saskatchewan. (2003).

Ferdous, D., A.K. Dalai and J. Adjaye, "Hydrodenitrogenation and hydrodesulfurization of heavy gas oil using $NiMo/Al_2O_3$ catalyst containing boron: Experimental and kinetic studies," Industrial and Engineering Chemistry Research. 45, 544-552 (2006).

Feron, P.H.M. and A.E. Jansen, "The production of carbon dioxide from flue gas by membrane gas absorption," Energy Conversion and Management. 38, S93-S98 (1997).

Figueiredo, J.L., M.F.R. Pereira, M.M.A. Freitas and J.J.M. Órfão, "Modification of the surface chemistry of activated carbons," Carbon. 37, 1379-1389 (1999).

Fogler, S.H., "Elements of chemical reaction engineering, Volume 1," Prentice Hall PTR, Upper Saddle River - NJ (2006).

Froment, G.F. and K.B. Bischoff, " Chemical Reactor Analysis and Design," John Wiley & Sons, New York (1990).

Fuertes, A.B., "Template synthesis of mesoporous carbons with a controlled particle size," Journal of Materials Chemistry. 13, 3085-3088 (2003).

Fukuyama, H., S. Terai, M. Uchida, J.L. Cano and J. Ancheyta, "Active carbon catalyst for heavy oil upgrading," Catalysis Today. 98, 207-215 (2004).

Furimsky, E. and F.E. Massoth, "Deactivation of hydroprocessing catalysts," Catalysis Today. 52, 381-495 (1999).

Galarneau, A., H. Cambon, F. Di Renzo, R. Ryoo, M. Choi and F. Fajula, "Microporosity and connections between pores in SBA-15 mesostructured silicas as a function of the temperature of synthesis," New Journal of Chemistry. 27, 73-79 (2003).

García, A.B., A. Martínez-Alonso, C.A. Leon Y Leon and J.M.D. Tascón, "Modification of the surface properties of an activated carbon by oxygen plasma treatment," Fuel. 77, 613-624 (1998).

Gierman, H., "Design of laboratory hydrotreating reactors. Scaling Down of Trickle-flow Reactors," Applied Catalysis. 43, 277-286 (1988).

Gil, A., G. De La Puente and P. Grange, "Evidence of textural modifications of an activated carbon on liquid-phase oxidation treatments," Microporous Materials. 12, 51-61 (1997).

Girgis, M.J. and B.C. Gates, "Reactivities, reaction networks, and kinetics in high-pressure catalytic hydroprocessing," Industrial & Engineering Chemistry Research. 30, 2021-2058 (1991).

Gómez-Serrano, V., F. Piriz-Almeida, C.J. Durán-Valle and J. Pastor-Villegas, "Formation of oxygen structures by air activation. A study by FT-IR spectroscopy," Carbon. 37, 1517-1528 (1999).

Goto, S. and J.M. Smith, "Trickle bed reactor performance -1: Holdup and mass transfer effects." Amercian Institute of Chemical Engineers Journal. 21, 706-720 (1975).

Grange, P. and X. Vanhaeren, "Hydrotreating catalysts, an old story with new challenges," Catalysis Today. 36, 375-391 (1997).

Grange, P., "Catalytic hydrodesulfurization." Catalysis Reviews - Science and Engineering. 21, 135-181 (1980).

Gregg, S.J. and K.S.W. Sing , "Adsorption, Surface Area & Porosity," (1991).

Gutiérrez, O.Y., G.A. Fuentes, C. Salcedo and T. Klimova, "SBA-15 supports modified by Ti and Zr grafting for NiMo hydrodesulfurization catalysts," Catalysis Today. 116, 485-497 (2006).

Han, S. and T. Hyeon, "Simple silica-particle template synthesis of mesoporous carbons ," Chemical Communications., 1955-1956 (1999).

Harvey, T.G. and T.W. Matheson, "Hydroprocessing catalysis by supported ruthenium sulphide," Journal of Catalysis. 101, 253-261 (1986).

Hensen, E.J.M., V.H.J. De Beer, J.A.R. Van Veen and R.A. Van Santen, "On the sulfur tolerance of supported Ni(Co)Mo sulfide hydrotreating catalysts," Journal of Catalysis. 215, 353 (2003).

Hussain, M. and S.K. Ihm, "Synthesis, characterization, and hydrodesulfurization activity of new mesoporous carbon supported transition metal sulfide catalysts," Industrial and Engineering Chemistry Research. 48, 698-707 (2009).

Hussain, M. and S.K. Ihm, "Characteristics of mesoporous carbons supported Mo catalysts in thiophene hydrodesulfurization," Studies in Surface Science and Catalysis. 170, 1368-1373 (2007).

Jiménez, F., V. Kafarov and M. Nuñez, "Modeling of industrial reactor for hydrotreating of vacuum gas oils. Simultaneous hydrodesulfurization, hydrodenitrogenation and hydrodearomatization reactions," Chemical Engineering Journal. 134, 200-208 (2007).

Jones, D.S.J. and P.R. Pujado, Eds., "Handbook of Petroleum Processing," Springer, Dordrecht (2006).

Joo, S.H., R. Ryoo, M. Kruk and M. Jaroniec, "Evidence for general nature of pore interconnectivity in 2-dimensional hexagonal mesoporous silicas prepared using block copolymer templates," Journal of Physical Chemistry B. 106, 4640-4646 (2002).

Jun, S., M. Choi, S. Ryu, H.Y. Lee and R. Ryoo, "Ordered mesoporous carbon molecular sieves with functionalized surfaces," in "Studies in Surface Science and Catalysis," Sang-Eon Park, Ryong Ryoo, Wha-Seung Ahn,Chul Wee Lee and Jong-San Chang, Ed. Elsevier (2003), pp. 37-40.

Jun, S., Sang Hoon Joo, R. Ryoo, M. Kruk, M. Jaroniec, Z. Liu, T. Ohsuna and O. Terasaki, "Synthesis of new, nanoporous carbon with hexagonally ordered mesostructure ," Journal of the American Chemical Society. 122, 10712-10713 (2000).

Karandikar, P., K.R. Patil, A. Mitra, B. Kakade and A.J. Chandwadkar, "Synthesis and characterization of mesoporous carbon through inexpensive mesoporous silica as template," Microporous and Mesoporous Materials. 98, 189-199 (2007).

Karroua, M., P. Grange and B. Delmon, "Existence of synergy between "CoMoS" and Co9S8. New proof of remote control in hydrodesulfurization," Applied Catalysis. 50, L5-L10 (1989a).

Karroua, M., A. Centeno, H.K. Matralis, P. Grange and B. Delmon, "Synergy in hydrodesulphurization and hydrogenation on mechanical mixtures of cobalt sulphide on carbon and MoS2 on alumina," Applied Catalysis. 51, L21-L26 (1989b).

Kim, S.S. and T.J. Pinnavaia, "A low cost route to hexagonal mesostructured carbon molecular sieves," Chemical Communications., 2418-2419 (2001).

Kim, T.W., I.S. Park and R. Ryoo, "A synthetic route to ordered mesoporous carbon materials with graphitic pore walls," Angewandte Chemie - International Edition. 42, 4375-4379 (2003).

Kleitz, F., S.H. Choi and R. Ryoo, "Cubic Ia3d large mesoporous silica: Synthesis and replication to platinum nanowires, carbon nanorods and carbon nanotubes," Chemical Communications. 9, 2136-2137 (2003).

Knudsen, , "Catalyst and process technologies for ultra low sulfur diesel," Applied Catalysis. 189, 205 (1999).

Korsten, H. and U. Hoffmann, "Three-Phase Reactor Model for Hydrotreating in Pilot Trickle-Bed Reactors," American Institute of Chemical Engineers Journal. 42 (5), 1350-1360 (1996).

Kouzu, M., Y. Kuriki, F. Hamdy, K. Sakanishi, Y. Sugimoto and I. Saito, "Catalytic potential of carbon-supported NiMo-sulfide for ultra-deep hydrodesulfurization of diesel fuel," Applied Catalysis A: General. 265, 61-67 (2004).

Kouzu, M., Y. Kuriki, H. Farag, K. Sakanishi, Y. Sugimoto and I. Saito, "Catalytic potential of carbon-supported NiMo-sulfide for ultra-deep hydrodesulfurization of diesel fuel," ACS Division of Fuel Chemistry, Preprints. 48, 498-499 (2003).

Kresge, C.T., M.E. Leonowicz, W.J. Roth, J.C. Vartuli and J.S. Beck, "Ordered mesoporous molecular sieves synthesized by a liquid-crystal template mechanism," Nature. 359, 710-712 (1992).

Kruk, , "Characterization of ordered mesoporous carbons synthesized using MCM-48 silicas as templates," The Journal of Physical Chemistry.B. 104, 7960 (2000).

Kruk, M. and L. Cao, "Pore size tailoring in large-pore SBA-15 silica synthesized in the presence of hexane," Langmuir. 23, 7247-7254 (2007).

La Vopa, V. and C.N. Satterfield, "Poisoning of thiophene hydrodesulfurization by nitrogen compounds," Journal of Catalysis. 110, 375-387 (1988).

Landau, M.V., "Deep hydrotreating of middle distillates from crude and shale oils," Catalysis Today. 36, 393-429 (1997).

Lázaro, M.J., L. Calvillo, E.G. Bordejé, R. Moliner, R. Juan and C.R. Ruiz, "Functionalization of ordered mesoporous carbons synthesized with SBA-15 silica as template," Microporous and Mesoporous Materials. 103, 158-165 (2007).

Lee, J., J. Kim and T. Hyeon, "Recent progress in the synthesis of porous carbon materials," Advanced Materials. 18, 2073-2094 (2006).

Lee, J.J., S. Han, H. Kim, J.H. Koh, T. Hyeon and S.H. Moon, "Performance of CoMoS catalysts supported on nanoporous carbon in the hydrodesulfurization of dibenzothiophene and 4,6-dimethyldibenzothiophene," Catalysis Today. 86, 141-149 (2003).

Lee, J.S. and M. Boudart, "Hydrodesulfurization of thiophene over unsupported molybdenum carbide," Applied Catalysis. 19, 207-210 (1985).

Lewis, J.M. and R.A. Kydd, "The MoO3-Al2O3 interaction: Influence of phosphorus on MoO3 impregnation and reactivity in thiophene HDS," Journal of Catalysis. 136, 478-486 (1992).

Leyva, C., M.S. Rana, F. Trejo and J. Ancheyta, "On the use of acid-base-supported catalysts for hydroprocessing of heavy petroleum," Industrial and Engineering Chemistry Research. 46, 7448-7466 (2007).

Li, C., W.H. Zhang, C. Liang, H. Sun, Z. Shen, Y. Guan and P. Ying, "Synthesis of ordered mesoporous carbons composed of nanotubes via catalytic chemical vapor deposition," Advanced Materials. 14, 1776-1778 (2002).

Li, H., H. Xi, S. Zhu, Z. Wen and R. Wang, "Preparation, structural characterization, and electrochemical properties of chemically modified mesoporous carbon," Microporous and Mesoporous Materials. 96, 357-362 (2006).

Li, J., L. Ma, X. Li, C. Lu and H. Liu, "Effect of nitric acid pretreatment on the properties of activated carbon and supported palladium catalysts," Industrial and Engineering Chemistry Research. 44, 5478-5482 (2005).

Li, S., J.S. Lee, T. Hyeon and K.S. Suslick, "Catalytic hydrodenitrogenation of indole over molybdenum nitride and carbides with different structures," Applied Catalysis A: General. 184, 1-9 (1999).

Lin, Y.R. and H. Teng, "A novel method for carbon modification with minute polyaniline deposition to enhance the capacitance of porous carbon electrodes," Carbon. 41, 2865-2871 (2003).

Lipsch, J.M.J.G. and G.C.A. Schuit, "The CoOMoO3Al2O3 catalyst. II. The structure of the catalyst," Journal of Catalysis. 15, 174-178 (1969a).

Lipsch, J.M.J.G. and G.C.A. Schuit, "The CoOMoO3Al2O3 catalyst. III. Catalytic properties," Journal of Catalysis. 15, 179-189 (1969b).

Lipsch, J.M.J.G. and G.C.A. Schuit, "The CoOMoO3Al2O3 catalyst. I. Cobalt molybdate and the cobalt oxide molybdenum oxide system," Journal of Catalysis. 15, 163-173 (1969c).

Liu, Z., Y. Sakamoto, T. Ohsuna, K. Hiraga, O. Terasaki, C.H. Ko, H.J. Shin and R. Ryoo, "TEM studies of platinum nanowires fabricated in mesoporous silica MCM-41," Angewandte Chemie - International Edition. 39, 3107-3110 (2000).

Lu, A.H., W. Schmidt, B. Spliethoff and F. Schüth, "Synthesis of Ordered Mesoporous Carbon with Bimodal Pore System and High Pore Volume," Advanced Materials. 15, 1602-1606 (2003).

Lu, A.H., W.C. Li, N. Muratova, B. Spliethoff and F. Schüth, "Evidence for C-C bond cleavage by H2O2 in a mesoporous CMK-5 type carbon at room temperature," Chemical Communications., 5184-5186 (2005).

Lukens Jr., W.W., P. Schmidt-Winkel, D. Zhao, J. Feng and G.D. Stucky, "Evaluating pore sizes in mesoporous materials: a simplified standard adsorption method and a simplified Broekhoff-de Boer method," Langmuir. 15, 5403-5409 (1999).

Lulić, P., S. Zrnčević, H. Meider and D. Sevdicć, "The Relation Between the Quality of Catalyst and Feedstock in the Hydrotreating Process," Studies in Surface Science and Catalysis. 53, 451-461 (1989).

Mapiour, M.L., "Kinetics and effects of H2 partial pressure on hydrotreating of heavy gas oil " Thesis, University of Saskatchewan. (2009).

Martí'n-Gullón, A., C. Prado-Burguete and F. Rodríguez-Reinoso, "Effect of carbon properties on the preparation and activity of carbon-supported molybdenum sulfide catalysts," Carbon. 31, 1099-1105 (1993).

Matsubayashi, N., H. Shimada, T. Sato, Y. Yoshimura, M. Imamura and A. Nishijima, "Structural change of supported NiMo sulfide catalysts during the hydrogenation of coal-derived liquids," Fuel Processing Technology. 41, 261-271 (1995).

McCrea, K.R., J.W. Logan, T.L. Tarbuck, J.L. Heiser and M.E. Bussell, "Thiophene hydrodesulfurization over alumina-supported molybdenum carbide and nitride catalysts: Effect of Mo loading and phase," Journal of Catalysis. 171, 255-267 (1997).

McMillan, M., J.S. Brinen and G.L. Haller, "Solid-state magic-angle spinning 27Al NMR used to study alumina support and surface compound structure of catalysts," Journal of Catalysis. 97, 243-247 (1986).

Mears, D.E., "Tests for transport limitations in experimental catalytic reactors," Industrial and Engineering Chemistry: Process Design and Development. 10, 541-547 (1971).

Menéndez, J.A., M.J. Illán-Gómez, C.A.L. y León and L.R. Radovic, "On the difference between the isoelectric point and the point of zero charge of carbons," Carbon. 33, 1655-1657 (1995).

Meyers, R.A., Ed., "Handbook of Petroleum Refining Processes, Third edition ," McGraw-Hill, New York (2003).

Mikhalev, Y. and H.A. Øye, "Absorption of metallic sodium in carbon cathode materials," Carbon. 34, 37-41 (1996).

Mochida, I. and K.-. Choi, "An overview of hydrodesulfurization and hydrodenitrogenation," Journal of the Japan Petroleum Institute. 47, 145-163 (2004).

Moses, P.G., B. Hinnemann, H. Topsøe and J.K. Nørskov, "The effect of Co-promotion on MoS2 catalysts for hydrodesulfurization of thiophene: A density functional study," Journal of Catalysis. 268, 201-208 (2009).

Moulijn, J.A., A.E. Van Diepen and F. Kapteijn, "Catalyst deactivation: Is it predictable? What to do?" Applied Catalysis A: General. 212, 3-16 (2001).

Muller, E.A., L.F. Rull, L.F. Vega and K.E. Gubbins, "Adsorption of water on activated carbons: A molecular simulation study," Journal of Physical Chemistry. 100, 1189-1196 (1996).

Nava, H., F. Pedraza and G. Alonso, "Nickel-molybdenum-tungsten sulphide catalysts prepared by in situ activation of tri-metallic (Ni-Mo-W) alkylthiomolybdotungstates," Catalysis Letters. 99, 65-71 (2005).

Nielsen, L.P., M. Schønning, S.V. Christensen, S.V. Hoffmann, Z. Li, P. Hofmann, F. Besenbacher and B.S. Clausen, "Combined TPS, XPS, EXAFS, and NO-TPD study of the sulfiding of Mo/Al2O3," Catalysis Letters. 73, 85-90 (2001).

Nørskov, J.K., B.S. Clausen and H. Topsøe, "Understanding the trends in the hydrodesulfurization activity of the transition metal sulfides," Catalysis Letters. 13, 1-8 (1992).

Oelderik, J.M., S.T. Sie and D. Bode, "Progress in the catalysis of the upgrading of petroleum residue. A review of 25 years of R&D on Shell's residue hydroconversion technology," Applied Catalysis. 47, 1-24 (1989).

Oyama, S.T., "Preparation and catalytic properties of transition metal carbides and nitrides," Catalysis Today. 15, 179-200 (1992).

Perego, C. and S. Peratello, "Experimental methods in catalytic kinetics," Catalysis Today. 52, 133-145 (1999).

Pradhan, B.K. and N.K. Sandle, "Effect of different oxidizing agent treatments on the surface properties of activated carbons," Carbon. 37, 1323-1332 (1999).

Rajalakshmi, N., K.S. Dhathathreyan, A. Govindaraj and B.C. Satishkumar, "Electrochemical investigation of single-walled carbon nanotubes for hydrogen storage," Electrochimica Acta. 45, 4511-4515 (2000).

Ramachandran, P.A. and R.V. Chaudhari, "Three phase catalytic reactors," Gordon and Breach Science, Paris (1983).

Ramírez, J., V.M. Castaño, C. Leclercq and A.L. Agudo, "High-resolution electron microscopy study of phosphorus-containing MoS2/Al2O3 hydrotreating catalysts," Applied Catalysis A, General. 83, 251-261 (1992).

Ramírez, L.F., J. Escobar, E. Galván, H. Vaca, F.R. Murrieta and M.R.S. Luna, "Evaluation of diluted and undiluted trickle-bed hydrotreating reactor with different catalyst volume," Petroleum Science and Technology. 22, 157-175 (2004).

Rase, H.F., "Chemical Reactor Design for Process Plants," Wiley, New York (1977).

Rayo, P., J. Ramírez, M.S. Rana, J. Ancheyta and A. Aguilar-Elguézabal, "Effect of the incorporation of Al, Ti, and Zr on the cracking and hydrodesulfurization activity of NiMo/SBA-15 catalysts," Industrial and Engineering Chemistry Research. 48, 1242-1248 (2009).

Reid, R.C., J.M. Prausnitz and B.E. Poling, "The properties of gases and liquids, 4th ed.," McGraw-Hill, NewYork (1987), pp. 741.

Reza, S., Ed., "Fluid catalytic cracking handbook," Butterworth-Heinemann, Woburn (2000).

Ryan, R.C., R.A. Kemp, J.A. Smegal, D.R. Denley and G.E. Spinnler, "Stacking of molybdenum disulfide layers in hydrotreating catalysts," in "Studies in surface science and catalysis -Vol 50: Hydrotreating catalysts - Preparation, Characterization and Performance," M. L. Occelli and R. G. Anthony, Eds. Elsevier, Amsterdam (1989), pp. 21.

Ryoo, R., S.H. Joo and S. Jun, "Synthesis of highly ordered carbon molecular sieves via template-mediated structural transformation," Journal of Physical Chemistry B. 103, 7745-7746 (1999).

Ryoo, R., S.H. Joo, M. Kruk and M. Jaroniec, "Ordered mesoporous carbons," Advanced Materials. 13, 677-681 (2001).

Sakanishi, K., T. Nagamatsu, I. Mochida and D.D. Whitehurst, "Hydrodesulfurization kinetics and mechanism of 4,6- dimethyldibenzothiophene over NiMo catalyst supported on carbon," Journal of Molecular Catalysis A: Chemical. 155, 101-109 (2000).

Satterfield, C.N., "Heterogeneous catalysis in industrial practice," McGraw-Hill, New York (1991).

Satterfield, C.N., "Mass transfer in heterogeneous catalysis," M.I.T.Press, Cambridge (1970).

Satterfield, C.N., A.A. Pelossof and T.K. Sherwood, "Mass Transfer Limitations in a Tricle-bed reactor," American Institute of Chemical Engineers Journal. 15 (2), 226 (1969).

Sayari, A. and Y. Yang, "SBA-15 templated mesoporous carbon: New insights into the SBA-15 pore structure," Chemistry of Materials. 17, 6108-6113 (2005).

Scaroni, A.W., R.G. Jenkins and P.L. Walker Jr., "Coke deposition on Co-Mo/Al2O3 and Co-Mo/C catalysts," Applied Catalysis. 14, 173-183 (1985).

Schlatter, J.C., S.T. Oyama, J.E. Metcalfe III and J.M. Lambert Jr., "Catalytic behavior of selected transition-metal carbides, nitrides, and borides in the hydrodenitrogenation of quinoline," Industrial and Engineering Chemistry Research. 27, 1648-1653 (1988).

Schulz, H., M. Schon and N.M. Rahman, "Hydrogenative denitrogenation of model compounds as related to refining of liquid fuels
," in "Studies in surface science and catalysis, Vol-27, Catalytic hydrogenation
," Cerveny.L., Ed. Elsevier, New York (1986), pp. 201.

Shanahan, P.V., L. Xu, C. Liang, M. Waje, S. Dai and Y.S. Yan, "Graphitic mesoporous carbon as a durable fuel cell catalyst support," Journal of Power Sources. 185, 423-427 (2008).

Shang, H., C. Liu, Y. Xu and R. Zhao, "Activated carbon-supported Co-Mo catalyst for hydrodesulfurization I. Comparison of activated carbon and alumina supports," Chinese Journal of Catalysis. 25, 363-368 (2004a).

Shang, H., C. Liu, R. Zhao and F. Wei, "Effect of modification of carbon nanotube on the dispersion of CoMo/CNT catalysts," American Chemical Society, Division of Petroleum Chemistry, Preprints. 49, 84-87 (2004b).

Shi, G., Y. Zhao, Y. Huang and J. Shen, "Mesoporous carbon supported Co-Mo and Ni-Mo catalysts for hydrodesulfurization," Cuihua Xuebao/Chinese Journal of Catalysis. 31, 961-964 (2010).

Shimodaira, N. and A. Masui, "Raman spectroscopic investigations of activated carbon materials," Journal of Applied Physics. 92, 902 (2002).

Sigurdson, S., "Hydroreating of light gas oil using carbon nanotubes supported NiMoS catalsyts; Influence of Pore diameter," Thesis, University of Saskatchewan. (2009).

Sigurdson, S., V. Sundaramurthy, A.K. Dalai and J. Adjaye, "Effect of anodic alumina pore diameter variation on template-initiated synthesis of carbon nanotube catalyst supports," Journal of Molecular Catalysis A: Chemical. 306, 23-32 (2009).

Sigurdson, S., V. Sundaramurthy, A.K. Dalai and J. Adjaye, "Phosphorus promoted trimetallic NiMoW/γ-Al2O3 sulfide catalysts in gas oil hydrotreating," Journal of Molecular Catalysis A: Chemical. 291, 30-37 (2008).

Solar, J.M., F.J. Derbyshire, V.H.J. de Beer and L.R. Radovic, "Effects of surface and structural properties of carbons on the behavior of carbon-supported molybdenum catalysts," Journal of Catalysis. 129, 330-342 (1991).

Sonnemans, J., J.M. Janus and P. Mars, "Surface structure and catalytic activity of a reduced molybdenum oxide-alumina catalyst. 2. The mechanism of pyridine hydrogenation and piperidine dehydrogenation," Journal of Physical Chemistry. 80, 2107-2110 (1976).

Speight, J.G., Ed., "Desulfurization of heavy oil and residua ," Marcel Dekker, New york (1999).

Stanislaus, A. and B.H. Cooper, "Aromatic hydrogenation catalysis: A review," Catalysis Reviews - Science and Engineering. 36, 75-123 (1994).

Stohl, F.V., Q.A. Qader, F.E. Massoth and D.S. Thakur, "Studies of catalyst samples from a two-stage direct coal liquefaction run," Industrial and Engineering Chemistry Research. 26, 840-846 (1987).

Suh, D.J., P. TaeJin and K. Son I., "Effect of surface oxygen groups of carbon supports on the characteristics of Pd/C catalysts," Carbon. 31, 427-435 (1993).

Sundaramurthy, V., A.K. Dalai and J. Adjaye, "Effect of EDTA on hydrotreating activity of CoMo/γ-Al_2O_3 catalyst," Catalysis Letters. 102, 299-306 (2005).

Sundaramurthy, V., I. Eswaramoorthi, A.K. Dalai and J. Adjaye, "Hydrotreating of gas oil on SBA-15 supported NiMo catalysts," Microporous and Mesoporous Materials. 111, 560-568 (2008).

Szymański, G.S., Z. Karpiński, S. Biniak and A. Świątkowski, "The effect of the gradual thermal decomposition of surface oxygen species on the chemical and catalytic properties of oxidized activated carbon," Carbon. 40, 2627-2639 (2002).

Tamm, P.W., H.F. Harnsberger and A.G. Bridge, "Effects of feed metals on catalyst aging in hydroprocessing residuum," Industrial & Engineering Chemistry Process Design and Development. 20, 262-273 (1981).

Tan, Z.L., H.N. Xiao, R.D. Zhang, Z.S. Zhang and S. Kaliaguine, "Potential to use mesoporous carbon as catalyst support for hydrodesulfurization," Xinxing Tan Cailiao/ New Carbon Materials. 24, 333-343 (2009).

Topsøe, H. and B.S. Clausen, "Active sites and support effects in hydrodesulfurization catalysts," Applied Catalysis. 25, 273-293 (1986).

Topsøe, H., B.S. Clausen, N.Y. Topsøe and P. Zeuthen, "Progress in the Design of Hydrotreating Catalysts Based on Fundamental Molecular Insight," Studies in Surface Science and Catalysis. 53, 77-102 (1989).

Topsøe, N.Y. and H. Topsøe, "Characterization of the structures and active sites in sulfided CoMo Al_2O_3 and NiMo Al_2O_3 catalysts by NO chemisorption," Journal of Catalysis. 84, 386-401 (1983).

U.S.Environmental Protection Agency, "http://www.epa.gov/airquality/sulfurdioxide," 10-Mar-2011 (28-Jan-2011).

Van Doorn, J., H.A.A. Barbolina and J.A. Moulijn, "Temperature-programmed gasification of the coke on spent hydrotreating catalysts with oxygen and hydrogen," Industrial & Engineering Chemistry Research. 31, 101-107 (1992).

Vasiliev, A.N., L.V. Golovko, V.A. Povazhny, E. Zlotnikov, J. Chen and J.G. Khinast, "Functionalized nanoporous carbon as a catalyst for Suzuki coupling reactions," Microporous and Mesoporous Materials. 101, 342-347 (2007).

Vinke, P., M. van der Eijk, M. Verbree, A.F. Voskamp and H. van Bekkum, "Modification of the surfaces of a gasactivated carbon and a chemically activated carbon with nitric acid, hypochlorite, and ammonia," Carbon. 32, 675-686 (1994).

Vinu, A. and K. Ariga, "Preparation of novel mesoporous carbon materials with tunable pore diameters using directly synthesized AlSBA-15 materials," Chemistry Letters. 34, 674-675 (2005).

Vinu, A., P. Srinivasu, M. Takahashi, T. Mori, V.V. Balasubramanian and K. Ariga, "Controlling the textural parameters of mesoporous carbon materials," Microporous and Mesoporous Materials. 100, 20-26 (2007).

Vishwakarma, S.K., V. Sundaramurthy, A.K. Dalai and J. Adjaye, "Performances of Co-W/γ-Al_2O_3 catalysts on hydrotreatment of light gas oil derived from athabasca bitumen," Industrial and Engineering Chemistry Research. 46, 4778-4786 (2007).

Vissers, J.P.R., S.M.A.M. Bouwens, V.H.J. de Beer and R. Prins, "Carbon black-supported molybdenum sulfide catalysts," Carbon. 25, 485-493 (1987).

Voorhoeve, R.J.H., "Electron spin resonance study of active centers in nickel-tungsten sulfide hydrogenation catalysts," Journal of Catalysis. 23, 236-242 (1971).

Voorhoeve, R.J.H. and J.C.M. Stuiver, "Kinetics of hydrogenation on supported and bulk nickel-tungsten sulfide catalysts," Journal of Catalysis. 23, 228-235 (1971).

Voorhoeve, R.J.H. and J.C. Vlugter, "Mechanism and kinetics of the metal-catalyzed synthesis of methylchlorosilanes. IV. The mechanism of the synthesis of dimethyldichlorosilane from silicon and methyl chloride," Journal of Catalysis. 4, 220-228 (1965).

Wang, S. and G.Q. Lu, "Effects of acidic treatments on the pore and surface properties of ni catalyst supported on activated carbon," Carbon. 36, 283-292 (1998).

Wijngaarden, R.J., A. Kronberg and K.R. Westerterp, Eds., "<!--[if gte mso 10]> Industrial Catalysis: Optimizing Catalysts and Processes," Wiley-VCH, Weinheim (1998).

Wikipedia, "http://en.wikipedia.org/wiki/NOx " 10-Mar-2011 (15-Feb-2011).

Yang, Z. and R. Mokaya, "Probing the effect of the carbonisation process on the textural properties and morphology of mesoporous carbons," Microporous and Mesoporous Materials. 113, 378-384 (2008).

Yu, C., J. Fan, B. Tian, D. Zhao and G.D. Stucky, "High-yield synthesis of periodic mesoporous silica rods and their replication to mesoporous carbon rods," Advanced Materials. 14, 1742-1745 (2002).

Yu, Z., L.E. Fareid, K. Moljord, E.A. Blekkan, J.C. Walmsley and D. Chen, "Hydrodesulfurization of thiophene on carbon nanofiber supported Co/Ni/Mo catalysts," Applied Catalysis B: Environmental. 84, 482-489 (2008).

Yui, S., "Producing quality synthetic crude oil from Canadian oil sands bitumen," Journal of the Japan Petroleum Institute. 51, 1-13 (2008).

Zepeda, T.A., "Comparison and performance of different sulphided Ti-loaded mesostructured silica-supported CoMo catalysts in deep HDS," Applied Catalysis A: General. 347, 148-161 (2008).

Zhang, Z., M. Xu, H. Wang and Z. Li, "Enhancement of CO_2 adsorption on high surface area activated carbon modified by N_2 , H_2 and ammonia," Chemical Engineering Journal. 160, 571-577 (2010).

Zhao, D., J. Feng, Q. Huo, N. Melosh, G.H. Fredrickson, B.F. Chmelka and G.D. Stucky, "Triblock copolymer syntheses of mesoporous silica with periodic 50 to 300 angstrom pores," Science. 279, 548-552 (1998).

APPENDIX - A

Calculation of Molar Product Concentrations of N/S and Reaction Rates of HDN/HDS:

The sulphur and nitrogen concentrations in the feed and product gas oil liquids are found via the following equations:

$$C_S = \frac{(ppm_{wt}) \cdot \rho_L}{(10^6) \cdot M_S} = \frac{(ppm_{wt}) \cdot (0.9 \times 10^3)}{(10^6) \cdot (32.0640)} \qquad \text{----------} \quad (A.1)$$

$$C_N = \frac{(ppm_{wt}) \cdot \rho_L}{(10^6) \cdot M_N} = \frac{(ppm_{wt}) \cdot (0.9 \times 10^3)}{(10^6) \cdot (14.0067)} \qquad \text{----------} \quad (A.2)$$

ρ_L = Density of KLGO feedstock and product (assumed equal), gm/L

$C_{S/N}$ = Sulphur/nitrogen heteroatom concentration, mol/L

$M_{S/N}$ = Sulphur/nitrogen molecular weight, g/mol

The reaction rates of hydrodesulphurization and hydrodenitrogenation reactions are calculated based on the following equations:

$$\{R_{HDS}\} = \frac{([Co]_S - [C_P]_S) \cdot LHSV}{(3600) \cdot \rho_{CAT}} \qquad \text{----------} \quad (A.3)$$

$$\{R_{HDN}\} = \frac{([Co]_N - [C_P]_N) \cdot LHSV}{(3600) \cdot \rho_{CAT}} \qquad \text{----------} \quad (A.4)$$

$\{R_{HDS/HDN}\}$ = Global rate of the HDS/HDN reaction, mol/(s·kg-cat)

$[C_{O/P}]_{S/N}$ = Feedstock/product concentration of sulphur/nitrogen, mol/L

LHSV = Liquid hourly space velocity, hr^{-1}

ρ_{CAT} = Catalyst pellet density (NiMo/mC catalyst), gm/L.

APPENDIX - B:

Calculation of Product Concentration for HDS and HDN Conversion Obtained from Kinetic Study:

T	P	LHSV	Gas/oil ratio	Cs	C_N
°C	MPa	hr^{-1}	Nm^3/m^3	mol/L	mol/L
370	8.8	2	600	0.0561	0.0302
370	8.8	2	600	0.0549	0.0290
370	8.8	2	600	0.0537	0.0283
370	8.8	2	600	0.0482	0.0288
370	8.8	2	600	0.0524	0.0294
370	8.8	1.5	600	0.0486	0.0244
370	8.8	1.5	600	0.0450	0.0233
370	8.8	1	600	0.0444	0.0171
370	8.8	1	600	0.0477	0.0173
370	8.8	2.5	600	0.0560	0.0324
370	8.8	2.5	600	0.0571	0.0328
350	8.8	2.5	600	0.0976	0.0494
350	8.8	2.5	600	0.0965	0.0489
350	8.8	2	600	0.0827	0.0434
350	8.8	2	600	0.0835	0.0438
350	8.8	1.5	600	0.0797	0.0385
350	8.8	1.5	600	0.0768	0.0378
350	8.8	1	600	0.0703	0.0298

T	P	LHSV	Gas/oil ratio	Cs	C_N
°C	MPa	hr^{-1}	Nm^3/m^3	mol/L	mol/L
350	8.8	1	600	0.0675	0.0283
330	8.8	1	600	0.1527	0.0522
330	8.8	1	600	0.1520	0.0521
330	8.8	1.5	600	0.1575	0.0559
330	8.8	1.5	600	0.1601	0.0564
330	8.8	2	600	0.1720	0.0584
330	8.8	2	600	0.1735	0.0590
330	8.8	2.5	600	0.2076	0.0611
330	8.8	2.5	600	0.1968	0.0618
350	8.8	2	800	0.0811	0.0427
350	8.8	2	800	0.0810	0.0423
350	8.8	2	400	0.1283	0.0454
350	8.8	2	400	0.1265	0.0447
350	8.8	2	1000	0.0836	0.0419
350	8.8	2	1000	0.0850	0.0424
350	7.8	2	600	0.0979	0.0464
350	7.8	2	600	0.1142	0.0467
350	9.8	2	600	0.0914	0.0405
350	9.8	2	600	0.0915	0.0409

APPENDIX - C:

Evaluation of external mass transfer resistance for HDS and HDN reaction:

For determining whether the rate of hydrogen diffusion into heavy gas oil was the rate determining step or not, Satterfield criteria (Satterfield et al., 1969) was used. The criterion is defined as:

$$\frac{10 d_p}{3 C_{H_2}} \left(\frac{-1}{V_C} \frac{dn}{dt} \right) > K_{OVR} \qquad \text{----------} \quad (C.1)$$

K_{OVR} =Overall mass transfer coefficient for hydrogen, cm/s

C_{H_2} = Hydrogen concentration in the liquid phase at equilibrium, mol/mL

$\left(\frac{-1}{V_C} \frac{dn}{dt} \right)$ = Rate of hydrogen conversion in the reaction, mol/(s.mL)

V_C = Volume of loaded catalyst = 4.9 mL

D_p = Average diameter of the catalyst particles = 0.17 cm

The validation of the Satterfield criterion would determine that the mass transfer was dominant in the overall reaction.

Evaluation of the overall mass transfer coefficient (k_{OVR}):

The overall mass transfer coefficient was found by the following equation:

$$\frac{1}{k_{OVR}} = \frac{1}{k_L} + \frac{1}{k_S} \qquad \text{----------} \quad (C.2)$$

The variables are defined as:

k_L = Liquid film side hydrogen –gas oil mass transfer coefficient, cm/s

k_S = Solid side hydrogen –gas oil mass transfer coefficient, cm/s

Calculation of the gas/liquid mass transfer coefficient (k_L):

The gas/liquid mass transfer coefficient was estimated using a correlation by Goto et al., (Goto and Smith, 1975)

$$\frac{k_L \cdot a_L}{D_L} = \alpha_1 \cdot \left(\frac{L_A \cdot a_L}{\mu_L}\right)^{\alpha_2} \sqrt{\frac{\mu_L}{\rho_L D_L}} \qquad \text{----------} \qquad \text{(C.3)}$$

The variables are:

a_L = Interfacial surface area over unit volume $\left(\frac{6(1-\varepsilon)}{D_P}\right) \approx$ 24.7 cm^{-1}

(Assuming the interfacial surface area is equal to the catalyst pellet surface area)

ε = Bed porosity = 0.3 (Grange and Vanhaeren, 1997)

L_A = Liquid mass flow over cross-sectional area, g/(s·cm^2)

μ_L = Viscosity of KLGO at the operating temperature, g/(s·cm)

D_L = Diffusivity of hydrogen in KLGO, cm^2/s

ρ_L = Density of KLGO at the operating conditions, g/mL

α_1 = Constant based on the catalyst particle properties* = 7

α_2 = Constant based on the catalyst particle properties* = 0.4

* α_1 and α_2 values found by Korsten and Hoffman (1996) for d_P = 0.17 cm.

Calculation of KLGO viscosity (μ_L):

A correlation developed by Glasso (Ahmed, 1989) was used for determining the viscosity of KLGO at the operating temperatures:

$$\mu_L = 3.141 \times 10^{10} \cdot (T - 460)^{-3.444} (\log^0 API)^a \qquad \text{----------} \qquad \text{(C.4)}$$

$$a = 10.3133 \cdot \log(T - 460) - 36.447 \qquad \text{----------} \qquad \text{(C.5)}$$

The variables are defined as:

T = Operating temperature, °R

$°API = \dfrac{141.5}{SG} - 131.5$

SG = Specific gravity of KLGO at 15.6°C = 0.9

$°API \approx 25.72$

a = (-) 7.61 to (-) 7.12 (for temperatures ranging from 330°C to 370°C)

μ_L = 0.4369 cP to 0.5376 cP (for temperatures ranging from 330°C to 370°C)

Calculation of KLGO average molecular weight (M_{AVE}):

Average molecular weight of gas oil was evaluated from the Aspen software.

Calculation of diffusivity of hydrogen in gas oil (D_L):

A correlation by Wilke and Chang (1955) was used for calculating the effective diffusivity of hydrogen:

$$\frac{D_L \cdot \mu_L}{T} = (7.4 \times 10^{-8}) \sqrt{\frac{X \cdot M_{AVE}}{V_b^{0.6}}} \qquad \text{----------} \quad \text{(C.6)}$$

The variables are defined as:

X = Association parameter = 1 for hydrocarbon mixtures

V_b = Hydrogen molar volume at the normal boiling point

V_b = 14.3 mL/mol (Wijngaarden et al., 1998)

D_L = 2.48 × 10^{-4} cm^2/s to 3.36 ×10^{-4} cm^2/s

(for temperatures ranging from 330°C to 370°C)

Calculation of KLGO density at reaction temperatures and pressures:

A correlation by Standing and Katz (Jiménez et al., 2007)(Voorhoeve and Vlugter, 1965)(Voorhoeve and Vlugter, 1965) was used for determining the density of gas oils at reactor operating conditions:

$$\rho_L = \rho_{15.6} - \triangle\rho_T + \triangle\rho_P \qquad \text{----------} \qquad \text{(C.7)}$$

$\Delta\rho_T$ = Temperature density correlation, lbs/ft^3

$\Delta\rho_P$ = Pressure density correlation, lbs/ft^3

$$\triangle\rho_P = [0.167 + (16.181\times10^{-0.0425\rho_{15.6}})]\times[\frac{P}{1000}] - 0.01\times[0.299 + (263\times10^{-0.603\rho_{15.6}})]\times[\frac{P}{1000}]^2 \qquad \text{----------} \qquad \text{(C.8)}$$

$$\triangle\rho_T = [0.0133 + (152.4\times(\rho_{15.6} + \triangle\rho_P)^{-2.45})]\times[T - 520] - [8.10\times10^{-6} - (0.0622\times10^{-0.764(\rho_{15.6}+\triangle\rho_P)})]\times[T - 520]^2 \qquad \text{----------} \qquad \text{(C.9)}$$

The values applied to these equations were:

P = 7.8 MPa to 9.8 MPa

T = 1086 °R to 1158 °R (330°C to 370°C)

From these pressure and temperature values:

$\Delta\rho_P$ = 0.259 lbs/ft^3 to 0.3263 lbs/ft^3

$\Delta\rho_T$ = 9.332 lbs/ft^3 to 10.147 lbs/ft^3

ρ_L = 742 kg/m^3 to 755 kg/m^3

Finally, from the previously calculated values:

k_L = 2.31 ×10^{-4} cm/s to 3.78 1.13 × 10^{-4} cm/s

Calculation of the liquid/solid mass transfer coefficient (k_S):

The liquid/solid mass transfer coefficient was estimated using a correlation by Van Krevelen and Krekels (Froment and Bischoff, 1990).

$$\frac{k_S}{D_L \cdot a_S} = 1.8 \times \sqrt{\frac{L_A}{a_S \cdot \mu_L}} \times \left(\frac{\mu_L}{\rho_L \cdot D_L}\right)^{1/3} \qquad \text{----------} \quad \text{(C.10)}$$

The variables are defined as:

a_S = Liquid/solid interfacial surface area = a_L = 24.7 cm^{-1}

Using the previously determined terms:

k_S = 3.699 $\times 10^{-3}$ cm/s 7.299 $\times 10^{-3}$ cm/s

Calculation of the equilibrium concentration of hydrogen in gas oil (C_{H2}):

The equilibrium concentration of hydrogen in gas oil was calculated by applying Henry's constant with the assumption of limited solubility:

$$C_{H2} = \frac{P}{H_{H2}} \qquad \text{----------} \quad \text{(C.11)}$$

The variables are defined as:

H_{H2} = Henry's constant for hydrogen in KLGO, MPa·m^3/mol

P = Operating pressure = 7.8 MPa to 9.8 MPa

Henry's constant can be calculated using the equation below:

$$H_{H2} = \frac{\nu_N}{\lambda_{H2} \cdot \rho_L} \qquad \text{----------} \quad \text{(C.12)}$$

The variables are defined as:

v_N = Hydrogen molar volume at standard conditions = 22.4 L/mol

ρ_L = Density of KLGO at the operating conditions = 742 kg/m^3 to 755 kg/m^3

λ_{H_2} = Hydrogen solubility in KLGO, mL/(kg·MPa)

A correlation established by (Korsten and Hoffmann, 1996) was applied to estimate the solubility of hydrogen in gas oil fractions:

$$\lambda_{H2} = z_0 + z_1 \cdot T + z_2 \cdot \frac{T}{\rho_{20}} + z_3 \cdot T^2 + z_4 \cdot \frac{1}{(\rho_{20})^2} \quad \text{----------} \quad \text{(C.13)}$$

The parameters are defined as:

z_0 = -0.55973

z_1 = -0.42947×10^{-3}

z_2 = 3.07539×10^{-3}

z_3 = 1.94593×10^{-6}

z_4 = 0.83578

T = Operating temperature = 330°C to 370°C

ρ_{20} = Density of KLGO at 20°C = 0.899 g/mL

For the operating conditions, the following value ranges were found:

λ_{H_2} = 1.67 ×10^3 mL/(kg·MPa) 1.844 ×10^3 mL/(kg·MPa)

H_{H_2} = 1.637 MPa·m3/mol 1.776 MPa·m^3/mol

C_{H_2} = 4.54 ×10^{-4} mol/mL to 5.77 ×10^{-4} mol/mL

Calculating the hydrogen conversion rate for HDS and HDN:

The following simplified stoichiometric equations were used for finding the rate of hydrogen conversion for both hydrodesulphurization and hydrodenitrogenation:

$$|R-S|+x_{HDS}H_2 \longrightarrow |R-H|_{[2x_{HDS}-2]}+H_2S \qquad \text{(C.14)}$$

$$|R-S|+x_{HDN}H_2 \longrightarrow |R-H|_{[2x_{HDN}-2]}+NH_3 \qquad \text{(C.15)}$$

The rates of nitrogen and sulphur removal for varying operating conditions applied to the hydrotreating process were determined from section and Appendix B of the report. Equations C.14 and C.15 allow for the following substitutions:

$$\left(\frac{-1}{V_C}\cdot\frac{dn}{dt}\right)=\left(\frac{x_{HDS}\cdot r_{HDS}}{V_C}\right) \qquad \text{(C.16)}$$

$$\left(\frac{-1}{V_C}\cdot\frac{dn}{dt}\right)=\left(\frac{x_{HDN}\cdot r_{HDN}}{V_C}\right) \qquad \text{(C.17)}$$

Where r_{HDS} is the molar rate of sulphur removal and r_{HDN} is the molar rate of nitrogen removal achieved from the hydrotreating catalyst (mol/s). Assuming the hydrogenation of a 5-membered thiophenic ring for sulphur removal and a 6-membered basic pyridinic ring for nitrogen removal, the following stoichiometric values were assumed for the HDS and HDN reactions of heavy gas oil:

$$x_{HDS}=4.0 \qquad\qquad x_{HDN}=5.0$$

Given these assumed values for each reaction, the following value ranges were found for each side of the Satterfield inequality:

Hydrodesulphurization Reaction:

Left hand side of Satterfield's criterion = 6.34×10^{-4} cm/s to 17.46×10^{-4} cm/s

Right hand side of Satterfield's criterion = 2.18×10^{-4} cm/s to 3.59×10^{-4} cm/s

Hydrodenitrogenation Reaction:

Left hand side of Satterfield's criterion = 0.59×10^{-4} cm/s to 2.08×10^{-4} cm/s

Right hand side of Satterfield's criterion = 2.18×10^{-4} cm/s to 3.59×10^{-4} cm/s

A summary of all the operating conditions and estimated parameters contributing to these results can be found in Appendix-D.

APPENDIX - D

Summary of the external mass transfer resistances study performed for a trickle bed hydrotreating reactor loaded with NiMo/mC catalyst

Parameter	Symbol	Units	Value	Range
Pressure	P	Mpa	8.8	7.8-9.8
Temperature	T	^0C	350	330-370
Average boling point of KLGO	T_B	^0C	302	-
Liquid hourly space velosity	LHSV	hr^{-1}	2	1.0-2.5
Feed flow rate	L	g/hr	9	4.5-11.25
Catalyst particle size	d_P	cm	0.17	-
Bed porosity (Wijngaarden et al., 1998)	ε	-	0.3	-
Interfacial surface area per unit volume	α_L	cm^{-1}	24.7	-
Liquid mass flow per unit area	L_A	x 10^{-3} g/(cm^2.s)	3.18	1.59-3.98
KLGO density @ operating condition	ρ_L	kg/m^3	748.51	742-755
KLGO density @ 150C	ρ_{15}	kg/m^3	900	-
KLGO density @ 200C	ρ_{20}	kg/m^3	899	-
Pressure density correlation	$\Delta\rho_P$	lbs/ft^3	0.2925	0.259-0.3263
Temperature density correlation	$\Delta\rho_T$	lbs/ft^3	9.750	9.332-10.147
KLGO specific gravity @600F	SG	-	0.98	-
API density rating	^0API	-	25.72	-
Constant in viscosity correlation(Ahmed.T,1989)	α	-	-7.360	(-)7.61 - (-)7.12
KLGO average molecular weight	M_{AVE}	kg/mol	217.5	-
KLGO viscosity @ operating temp	μ_L	cP	0.483	0.4369-0.5376
Henry's constant	H_{H2}	x10^{-2} Mpa-m^3/gmol	1.704	1.637-1.776
H_2 molecular volume, std condition	v_N	cc/mol	22400	-
Concentration of H_2 in KLGO	C_{H2}	x 10^{-4} mol/cc	5.16	4.54-5.77
Solubility of H_2 in KLGO (Korsten & Hoffmann,1996)	λ_{H2}	x 10^3 cc/kg	1.76	1.67-1.844
Bulk diffusivity of H_2	D_L	x 10^{-4} cm^2/s	2.85	2.48-3.36
Particle properties constant (Korsten & Hoffmann,1996)	α_1	-	7	-
Particle properties constant (Korsten & Hoffmann, 1996)	α_2	-	0.4	-
Liquid side: H_2/KLGO mass transfer cofficient	k_L	x 10^{-4} cm/s	3.25	2.31-3.78
Solid side: H_2/KLGO mass transfer cofficient	k_S	x10^{-3} cm/s	5.86	3.699-7.299
Overall mass transfer cofficient	k_{OVR}	x 10^{-4} cm/s	3.08	2.179-3.594
Rate of H_2 consumption for HDS reaction	$(x_{HDS}.r_{HDS})/V_C$	x 10^{-7} mol.H_2/(s.cc)	12.63	5.54-16.55
Rate of H_2 consumption for HDN reaction	$(x_{HDN}.r_{HDN})/V_C$	x 10^{-7} mol.H_2/(s.cc)	1.26	0.513-1.97
Satterfield's criterian for HDS, LHS	S_{HDS}	x 10^{-4}	13.87	6.34-17.46
Satterfield's criterian for HDN, LHS	S_{HDN}	x 10^{-4}	1.38	0.588-2.078

APPENDIX – E

Evaluating the Internal Mass Transfer Resistances for the HDS and HDN Reactions

Before carrying out internal mass transfer calculation, it is necessary to find out whether the assumption on isothermal condition in the catalyst pellet is valid or not. To validate the assumption, determination of each pellet's degree of isothermality was performed in two ways: first method was to determine the maximum potential temperature rise between the core and the surface of the pellet (Fogler, 2006) as well as by confirming Anderson's criterion (Mears, 1971).

Maximum temperature rise (ΔT_{MAX}):

$$\beta = \frac{\triangle T_{MAX}}{T_S} = \frac{\triangle H_{R,i} \cdot D_i \cdot [C_i]_S}{k_t \cdot T_S} \qquad \text{----------} \qquad \text{(E.1)}$$

The variables are defined as:

$\Delta H_{R,i}$ = Heat of HDS/HDN reaction, kJ/mol

$[C_i]_S$ = Catalyst surface concentration of species 'i' (sulphur or nitrogen), mol/mL

k_t = Thermal conductivity of the NiMo/mC catalyst pellet.

T_S = Pellet surface temperature (assumed to be the reaction temperature)

Calculation of the HDS/HDN heats of reaction:

The hydrodesulphurization heat of reaction for heavy gas oil from Athabasca bitumen was approximated by using the heat of reaction range for most thiophene molecules; 63 to 66 kJ/mol of hydrogen consumed (Ancheyta and Speight, 2007). The

hydrodenitrogenation heat of reaction for KLGO from Athabasca bitumen was approximated by using the heat of reaction range for most quinoline molecules; 65 to 68 kJ/mol of hydrogen consumed (Cocchetto and Satterfield, 1981) These values were converted to units of kJ/mol of sulphur/nitrogen removed by using the stoichiometric coefficients ($\boldsymbol{x_{HDS}}$ and $\boldsymbol{x_{HDN}}$) discussed in Appendix C.

$\Delta H_{R,HDS}$ = 63 to 66 kJ/mol of H_2 consumed

$\Delta H_{R,HDS}$ = 260 kJ/mol of sulphur

$\Delta H_{R,HDN}$ = 65 to 68 kJ/mol of H_2 consumed

$\Delta H_{R,HDN}$ = 265 kJ/mol of nitrogen

Calculating the effective diffusivities of organosulphur and organonitrogen compounds in KLGO ($[D_S]_E/[D_N]_E$):

The effective diffusivity of sulphur compounds was estimated by the following equation:

$$[D_i]_E = \frac{\varepsilon_P \cdot D_i}{\gamma_P} \qquad \text{----------} \quad \text{(E.2)}$$

The variables are defined as:

ε_P = Porosity of the catalyst pellets

γ_P = Tortuosity of the catalyst pellets

D_i = Bulk diffusivity of organosulphur compounds, cm^2/g

A correlation by Probst and Wohlfahrt (1979) was used to find the ratio of porosity and tortuosity of pelletized catalysts:

$$\frac{\varepsilon_P}{\gamma_P} = [\frac{\varepsilon_P{}^m}{(2-\varepsilon_P)^{m+1}}] \qquad \text{----------} \quad \text{(E.3)}$$

Values of ***m*** were found to range from 0.70 to 1.65 for porous compressed catalysts (group D). It was recommended to use an ***m*** value of 1.05 when not otherwise determined (Wijngaarden et al., 1998). Porosity values were found to range from 0.05 to 0.65 (average value was used, 0.35). Based on these conditions, the porosity/tortuosity values were found:

$$\frac{\varepsilon_P}{\gamma_P} = 0.119$$

Calculating the bulk diffusivities of organosulphur and organonitrogen compounds in KLGO (D_S/D_N):

The assumption was made that the organosulphur and organonitrogen compounds held the same density, average boiling point, average molecular weight and average molar volume as the heavy gas oil feedstock. The bulk diffusivities of each species were found using the Tyn-Claus correlation (Reid et al., 1987)

$$D_i = (8.93\times10^{-8})\cdot\left(\frac{\nu_L^{\,0.267}}{\nu_i^{\,0.433}}\right)\cdot\left(\frac{T}{\mu_L}\right) = (8.93\times10^{-8})\cdot\left(\frac{T}{\mu_L\cdot\nu_i^{\,0.166}}\right) \qquad \text{----------} \qquad \text{(E.4)}$$

The variables are defined as:

T = Operating temperature

μ_L = KLGO viscosity at operating conditions = 0.437 cP to 0.538 cP

ν_i = Molar volume of sulphur/nitrogen molecules under standard conditions, mL/mol

ν_L = Molar volume of KLGO under standard conditions, mL/mol

The molar volume of the gas oil was found by the following:

$$\nu_i = (0.285)\cdot\nu_C^{\,1.048} \qquad \text{----------} \qquad \text{(E.5)}$$

ν_C = Critical specific molar volume of KLGO, mL/mol

The critical specific molar volume is given by:

$$\nu_C = \nu_C^{\,m} \cdot M_{AVE} \qquad \text{----------} \quad \text{(E.6)}$$

M_{AVE} = 361 g/mol

$\nu_C^{\,m}$ = Critical specific mass volume, mL/g

$$\nu_C^{\,m} = (7.5214 \times 10^{-3}) \cdot T_b^{\,0.2896} \cdot SG^{-0.7666} \qquad \text{----------} \quad \text{(E.7)}$$

The critical specific mass volume of liquid was calculated using a correlation by Raizi and Daubert (Ahmed, 1989)

The variables are defined as:

$\nu_C^{\,m}$ = Critical specific mass volume, ft^3/lb

T_b = Average boiling point temperature = 575 °F

$SG_{15.6}$ = Specific gravity at 15.6°C = 0.900

These values lead to the following results:

$\nu_C^{\,m}$ = 3.8 mL/g

ν_C = 826 mL/mol

ν_i = 325.11 mL/mol

$D_i = D_S = D_N = 2.3 \times 10^{-6}$ cm^2/g to -5.99×10^{-6} cm^2/g

$[D_S]_E = [D_N]_E = 1.93 \times 10^{-5}$ cm^2/g to $5.0332.3 \times 10^{-5}$ cm^2/g

The effective diffusivity values lead to isothermality ratios of:

$\beta_{HDS} = 6.95 \times 10^{-5}$ to 8.56×10^{-5}

$\beta_{HDN} = 9.7 \times 10^{-6}$ to 11.97×10^{-6}

The values of β were used to find the maximum temperature change that occurs due to exothermic HDS and HDN reactions. Since these two reactions occur simultaneously, the sum of the calculated temperature raise (for HDS and HDN) will yield the maximum possible total temperature change in catalyst pellet with respect to the catalyst surface temperature. This gives a highest possible ΔT_{MAX} value of 0.06 K, which can be considered negligible indicating isothermality in catalyst pellet

Anderson's Criterion:

$$\frac{|\triangle H_{R,i}| \cdot \{R_i\} \cdot d_P{}^2}{k_t \cdot T_S} < \frac{3 \cdot T_S \cdot R}{E_i} \qquad \text{----------} \quad \text{(E.8)}$$

The variables are defined as:

$\{R_i\}$ = Global reaction rate: HDS/HDN, mol/(s·mL)

k_t = Catalyst thermal conductivity = 0.155 W/(cm·K)

R = Universal gas constant = 8.314 J/(mol·K)

E_i = Energy of activation for HDS or HDN reaction, J/mol

The range of operating conditions tested, the values for the left and right hand side of Anderson's criterion were as follows:

Left hand side of Anderson's criterion (HDS) = 0.1672×10^{-5} to 1.634×10^{-5}

Right hand side of Anderson's criterion (HDS) = 0.009 to 0.0212

Left hand side of Anderson's criterion (HDN) = 1.889×10^{-8} to 6.124×10^{-8}

Right hand side of Anderson's criterion (HDN) = 0.017 to 0.0401

The results confirm that isothermal behaviour can be assumed when examining the internal mass transfer resistances of the hydrotreating process. Summary of the relevant parameters and results of the catalyst pellet isothermality study is given as Appendix-F.

Calculation of Φ:

A dimensionless modulus (**Φ**), analogous to the Thiele modulus found without knowledge of the intrinsic reaction rate, was found for each collected sample in the kinetic study. The dimensionless modulus was used to represent an estimation of the pore diffusion resistance (Satterfield, 1970).

$$\Phi = \frac{{d_P}^2}{4 \cdot [D]_E} \cdot \frac{\{R_i\}}{[C_i]_S} \qquad \text{----------} \quad \text{(E.9)}$$

The variables are defined as:

d_P = Average diameter of the catalyst particle = 0.17 cm

$\{R_i\}$ = Global reaction rate: HDS/HDN, mol/(s·mL)

$[D_i]_E$ = Effective diffusivity of sulphur/nitrogen compounds, cm^2/g

$[C_i]_S$ = Catalyst surface concentration of sulphur/nitrogen species, mol/mL

The change in the global reaction rate and the change in surface concentration of sulphur and nitrogen heteroatoms were used to determine the dimensionless modulus at both the inlet and outlet of the reactor. After finding the dimensionless modulus, the effectiveness factor (η) can be determined by the rough approximation of equations E.10 and E. 11 in unison (Satterfield, 1991)

$$\Phi = (\varphi)^2 \cdot \eta \qquad \text{----------} \quad \text{(E.10)}$$

$$\eta = \frac{3}{\varphi}\left[\frac{1}{\tanh(\varphi)} - \frac{1}{\varphi}\right] \qquad \text{----------} \quad \text{(E.11)}$$

Solving for the effectiveness factor using equations (E.10) and (E.11) will only provide a rough estimate of both η and φ, the true Thiele modulus. This is because equation E.10 only applies to integer-power rate equations for spherical catalyst pellets. Additionally, equation E.11 only applies to isothermal first-order reactions for spherical catalysts. Nonetheless, these equations to provide a measure of comparison between the effectiveness factors for each collected sample.

Appendix -G provides a summary of all the dimensionless modulus values for the inlet and outlet ($[\Phi_O]_S$ and $[\Phi_P]_S$), as well as all the determined effectiveness factors ($[\eta_O]_S$ and $[\eta_P]_S$), for the hydrodesulphurization kinetic study.

Appendix -H provides a summary of all the dimensionless modulus values for the inlet and outlet ($[\Phi_O]_N$ and $[\Phi_P]_N$), as well as all the determined effectiveness factors ($[\eta_O]_N$ and $[\eta_P]_N$), for the hydrodenitrogenation kinetic study.

APPENDIX - F

Summary of isothermality evaluation for NiMo/mC catalyst pellets:

Parameter	Symbol	Units	Value	Range
Pressure	P	Mpa	8.8	7.8-9.8
Temperature	T	^0C	350	330-370
Average boling point of KLGO	T_B	^0C	436	-
Liquid hourly space velosity	LHSV	hr^{-1}	2	1.0-2.5
Feed flow rate	L	g/hr	9	4.5-11.25
Catalyst particle size	d_p	cm	1.7	-
KLGO density @ 150C	ρ	kg/m3	900	-
KLGO viscosity @ operating temp	μ_L	cP	0.48	0.437-0.538
Heat of HDS reaction	ΔH_{HDS}	kJ/mol	260	-
Heat of HDN reaction	ΔH_{HDN}	kJ/mol	265	-
Effective diffusivity of sulfur	$(D_E)_S$	x 10^{-6} cm^2/s	5.24	2.3-5.99
Effective diffusivity of Nitrogen	$(D_E)_N$	x 10^{-6} cm^2/s	5.24	2.3-5.99
Porosity of catalyst pellet	ε_p	-	0.3	-
Parameter m (Probst and Wohlfahrt, 1979)	m	-	1.05	-
Porosity /tortuosity ratio	ε_p/ν_L	-	0.119	-
Diffusivity of S compounds	D_S	x 10^{-5} cm^2/s	4.41	1.93 - 5.033
Diffusivity of N compounds	D_N	x 10^{-5} cm^2/s	4.41	1.93 - 5.033
Surface concentration in KLGO -Sulphur	$C_{S,S}$	mol/l	0.0835	0.0444-0.2076
Surface concentration in KLGO- Nitrogen	$C_{N,S}$	mol/l	0.0438	0.0171-0.0618
Thermal conductivity of catalyst pellet	k_T	W/cm-K	0.155	-
Activation energy of HDS	E_{HDS}	kJ/mol	189	-
Activation energy of HDN	E_{HDS}	kJ/mol	100	-
β for HDS	β_{HDS}	$x10^{-5}$	7.74	6.95-8.56
β for HDN	β_{HDN}	$x10^{-6}$	10.79	9.7-11.9
Global HDS reaction rate	$r_{hds\ global}$	mol/s.cc $x10^{-5}$	0.7	0.208-2.17
Global HDN reaction rate	$r_{hds\ global}$	mol/s.cc $x10^{-8}$	4.5	2.35-8.12
Anderson's criteria LHS (HDS)	$(A_{HDS})_{LHS}$	$x10^{-5}$	0.5	0.1672-1.634
Anderson's criteria RHS (HDS)	$(A_{HDS})_{RHS}$	-	0.0206	0.009-0.0212
Anderson's criteria LHS (HDN)	$(A_{HDN})_{LHS}$	$x10^{-8}$	3.47	1.889-6.124
Anderson's criteria RHS (HDN)	$(A_{HDN})_{RHS}$	-	0.0389	0.017-0.0401

APPENDIX – G

Summary of the dimensionless modulus and effectiveness factors for the internal mass transfer resistance study of KLGO hydrodesulphurization:

T	P	LHSV	Gas/oil ratio	$\Phi_{Inlet,HDS}$	$\Phi_{Outlet,\ HDS}$	$\eta_{Inlet,HDS}$	$\eta_{Outlet,\ HDS}$
°C	MPa	hr^{-1}	Nm^3/m^3				
370	8.8	2	600	0.613	7.125	0.960	0.629
370	8.8	2	600	0.614	7.292	0.960	0.622
370	8.8	2	600	0.615	7.461	0.960	0.616
370	8.8	2	600	0.621	8.397	0.959	0.583
370	8.8	2	600	0.616	7.663	0.960	0.609
370	8.8	1.5	600	0.465	6.247	0.969	0.663
370	8.8	1.5	600	0.468	6.775	0.969	0.642
370	8.8	1	600	0.312	4.590	0.979	0.737
370	8.8	1	600	0.311	4.243	0.979	0.754
370	8.8	2.5	600	0.766	8.915	0.950	0.566
370	8.8	2.5	600	0.765	8.732	0.950	0.572
350	8.8	2.5	600	0.813	5.435	0.947	0.698
350	8.8	2.5	600	0.815	5.508	0.947	0.695
350	8.8	2	600	0.668	5.268	0.956	0.705
350	8.8	2	600	0.667	5.213	0.956	0.708
350	8.8	1.5	600	0.504	4.122	0.967	0.760
350	8.8	1.5	600	0.506	4.299	0.967	0.751
350	8.8	1	600	0.341	3.168	0.977	0.809
350	8.8	1	600	0.343	3.313	0.977	0.801

T	P	LHSV	Gas/oil ratio	$\Phi_{Inlet,HDS}$	$\Phi_{Outlet,\ HDS}$	$\eta_{Inlet,HDS}$	$\eta_{Outlet,\ HDS}$
°C	MPa	hr^{-1}	Nm^3/m^3				
330	8.8	1	600	0.337	1.437	0.978	0.908
330	8.8	1	600	0.337	1.446	0.978	0.908
330	8.8	1.5	600	0.500	2.070	0.967	0.870
330	8.8	1.5	600	0.498	2.026	0.967	0.873
330	8.8	2	600	0.648	2.455	0.958	0.848
330	8.8	2	600	0.646	2.426	0.958	0.850
330	8.8	2.5	600	0.749	2.353	0.951	0.854
330	8.8	2.5	600	0.768	2.543	0.950	0.843
350	8.8	2	800	0.670	5.384	0.956	0.700
350	8.8	2	800	0.670	5.395	0.956	0.700
350	8.8	2	400	0.615	3.125	0.960	0.811
350	8.8	2	400	0.617	3.177	0.960	0.808
350	8.8	2	1000	0.667	5.201	0.956	0.708
350	8.8	2	1000	0.666	5.101	0.956	0.713
350	7.8	2	600	0.650	4.331	0.957	0.749
350	7.8	2	600	0.631	3.605	0.959	0.786
350	9.8	2	600	0.658	4.691	0.957	0.732
350	9.8	2	600	0.658	4.687	0.957	0.732

APPENDIX – H

Summary of the dimensionless modulus and effectiveness factors for the internal mass transfer resistance study of KLGO hydrodenitrogenation:

T	P	LHSV	Gas/oil ratio	$\Phi_{Inlet,HDN}$	$\Phi_{Outlet,\ HDN}$	$\eta_{Inlet,HDN}$	$\eta_{Outlet,\ HDN}$
°C	MPa	hr^{-1}	Nm^3/m^3				
370	8.8	2	600	0.443	1.307	0.971	0.916
370	8.8	2	600	0.452	1.388	0.970	0.911
370	8.8	2	600	0.458	1.444	0.970	0.908
370	8.8	2	600	0.454	1.409	0.970	0.910
370	8.8	2	600	0.450	1.365	0.970	0.913
370	8.8	1.5	600	0.365	1.334	0.976	0.915
370	8.8	1.5	600	0.372	1.423	0.975	0.909
370	8.8	1	600	0.271	1.417	0.982	0.909
370	8.8	1	600	0.270	1.394	0.982	0.911
370	8.8	2.5	600	0.533	1.465	0.965	0.907
370	8.8	2.5	600	0.529	1.438	0.965	0.908
350	8.8	2.5	600	0.427	0.770	0.972	0.950
350	8.8	2.5	600	0.432	0.789	0.972	0.949
350	8.8	2	600	0.393	0.808	0.974	0.947
350	8.8	2	600	0.389	0.791	0.974	0.948
350	8.8	1.5	600	0.326	0.755	0.978	0.951
350	8.8	1.5	600	0.331	0.780	0.978	0.949
350	8.8	1	600	0.255	0.763	0.983	0.950
350	8.8	1	600	0.261	0.823	0.983	0.946

T	P	LHSV	Gas/oil ratio	$\Phi_{Inlet,HDN}$	$\Phi_{Outlet,\ HDN}$	$\eta_{Inlet,HDN}$	$\eta_{Outlet,\ HDN}$
°C	MPa	hr^{-1}	Nm^3/m^3				
330	8.8	1	600	0.182	0.311	0.988	0.979
330	8.8	1	600	0.183	0.313	0.988	0.979
330	8.8	1.5	600	0.246	0.393	0.984	0.974
330	8.8	1.5	600	0.243	0.384	0.984	0.975
330	8.8	2	600	0.303	0.463	0.980	0.970
330	8.8	2	600	0.297	0.449	0.980	0.970
330	8.8	2.5	600	0.347	0.506	0.977	0.967
330	8.8	2.5	600	0.338	0.488	0.978	0.968
350	8.8	2	800	0.399	0.834	0.974	0.946
350	8.8	2	800	0.402	0.848	0.973	0.945
350	8.8	2	400	0.375	0.737	0.975	0.952
350	8.8	2	400	0.382	0.762	0.975	0.950
350	8.8	2	1000	0.405	0.862	0.973	0.944
350	8.8	2	1000	0.402	0.845	0.974	0.945
350	7.8	2	600	0.367	0.705	0.976	0.954
350	7.8	2	600	0.364	0.695	0.976	0.955
350	9.8	2	600	0.418	0.919	0.972	0.940
350	9.8	2	600	0.414	0.903	0.973	0.941

APPENDIX – I

Effect of operating parameters on HDS and HDN reaction rates

I-1. Effect of Pressure

(Feed: KLGO; LHSV: 2.0 hr^{-1}; Gas/Oil ratio: 600 Nm^3/m^3; Temperature: 350°C)

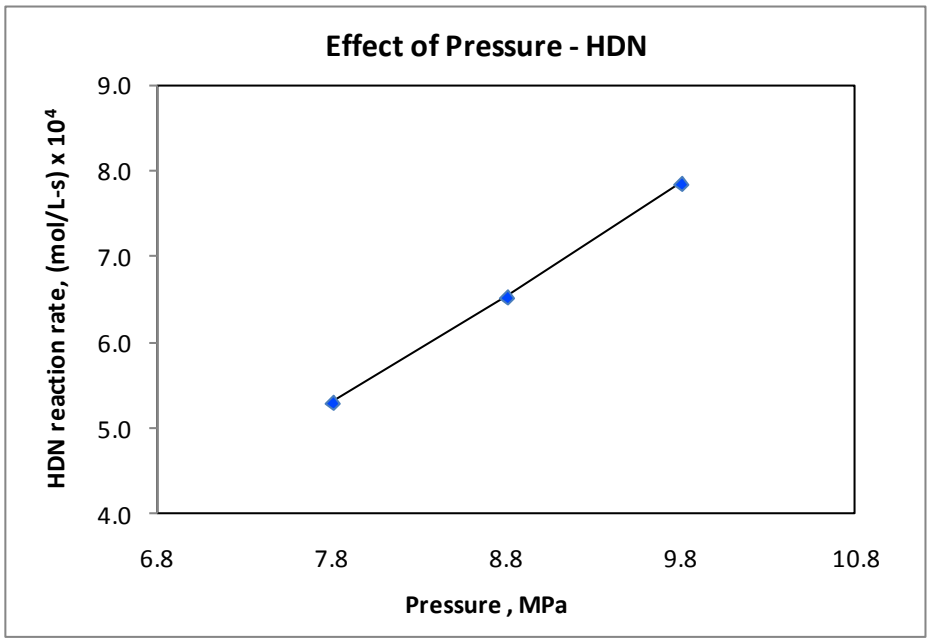

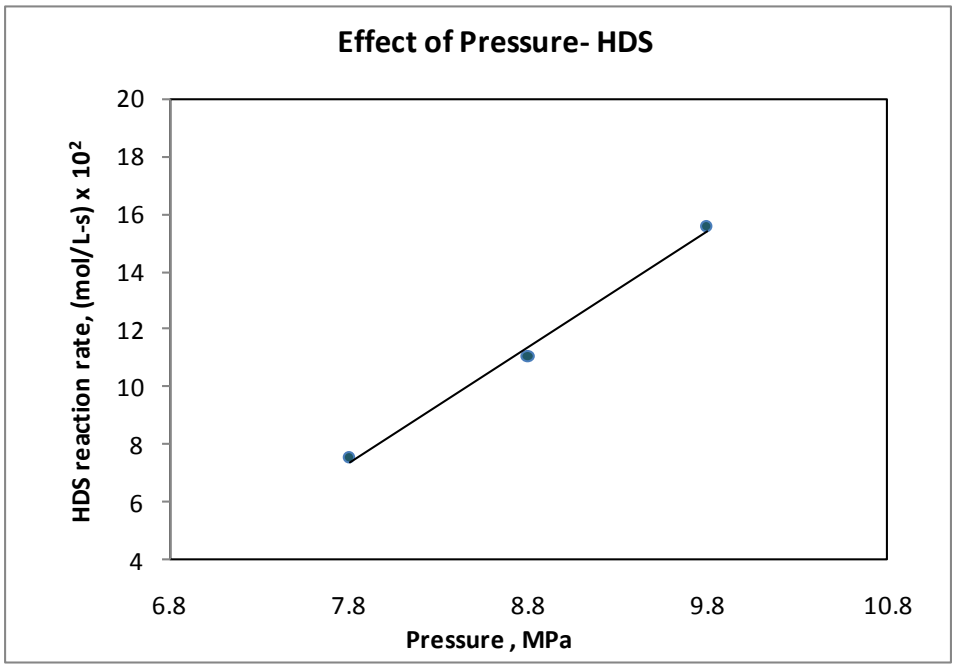

I-2. Effect of Temperature

(Feed: KLGO; LHSV: 2.0 hr^{-1}; Gas/Oil ratio: 600 Nm^3/m^3; Pressure 8.8 MPa)

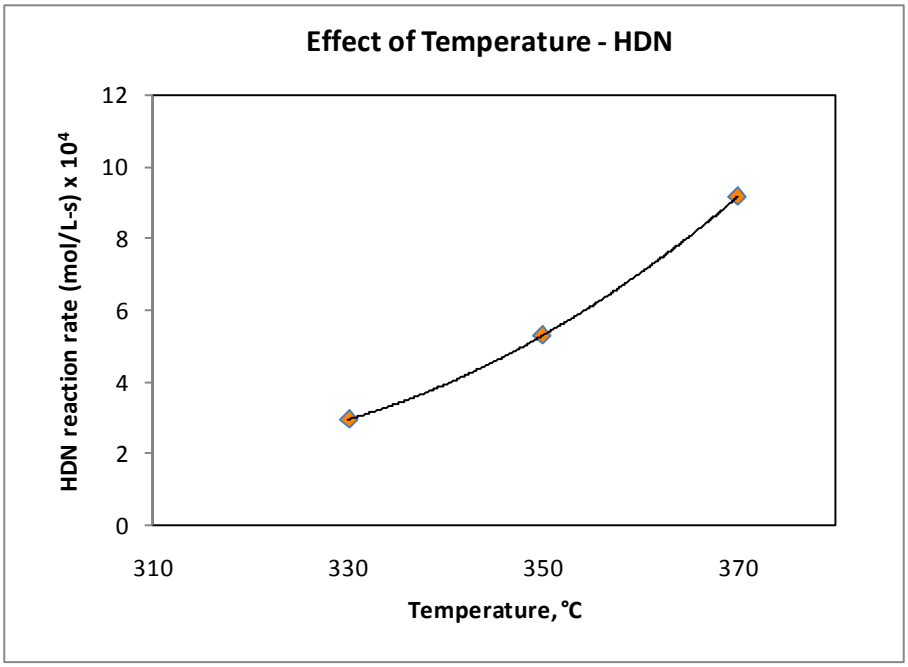

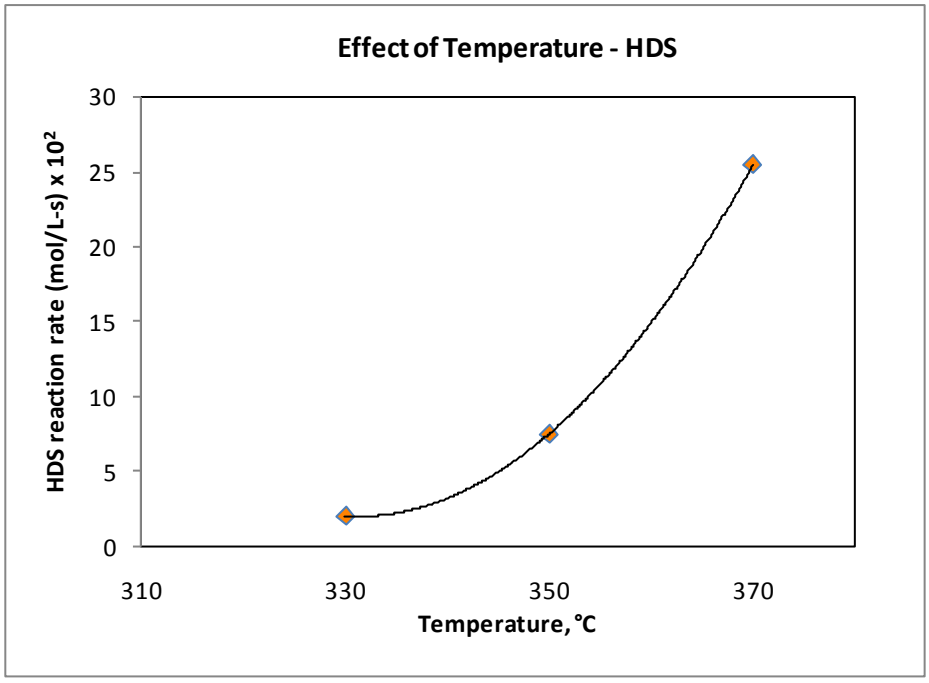

I-3. Effect of Gas/oil ratio

(Feed: KLGO; LHSV: 2.0 hr^{-1}; Pressure 8.8 MPa; Temperature: 350^{o}C)

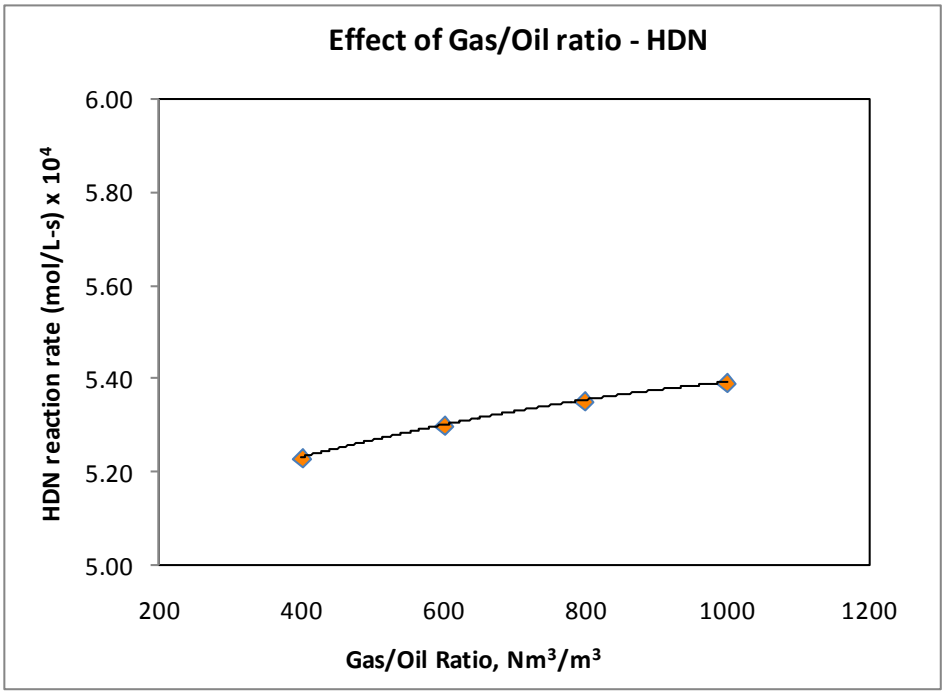

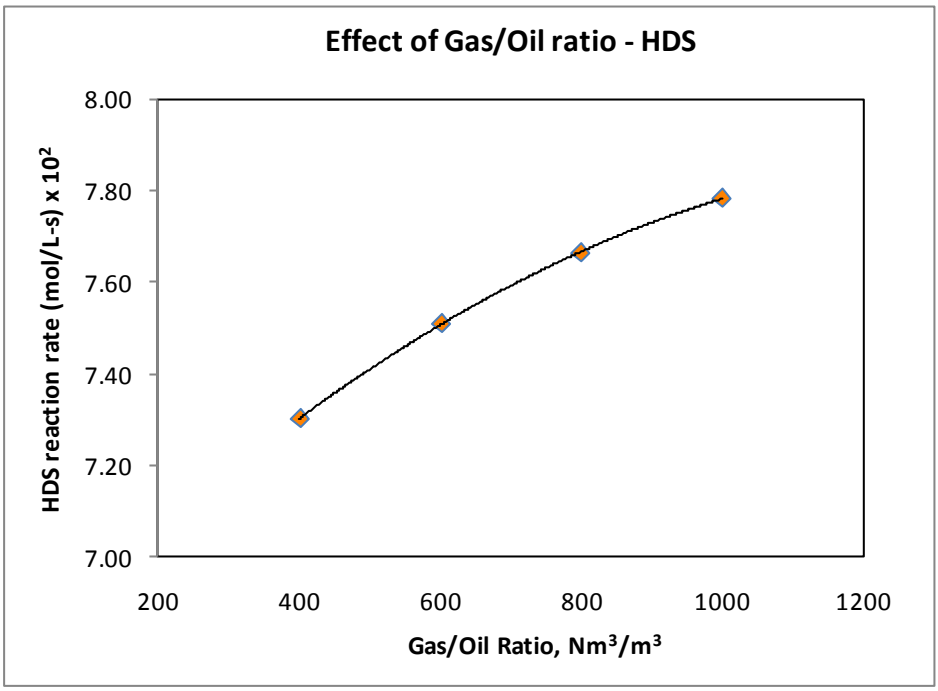

APPENDIX – J

Arrhenius plot, Van't hoff plot and Regression plots for kinetic models

J-1A. Arrhenius plot for Power law model

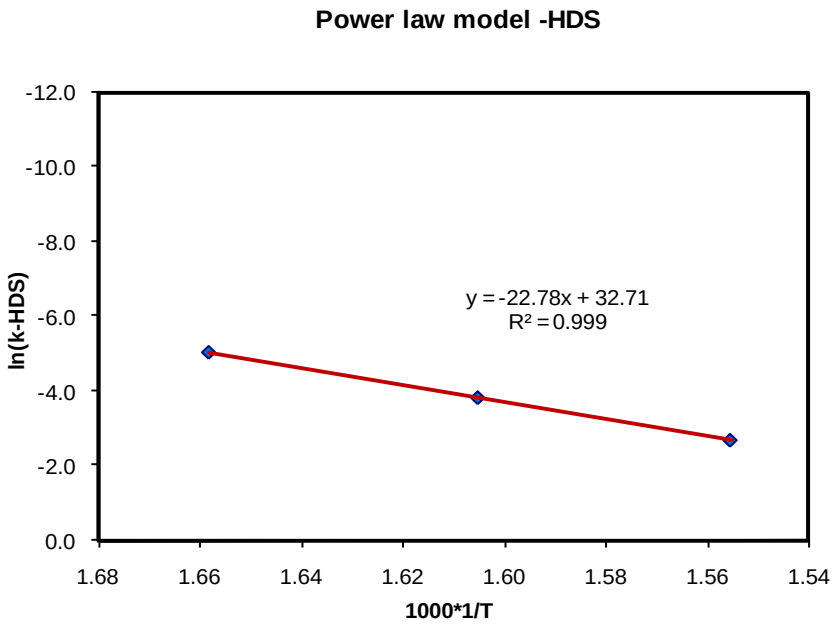

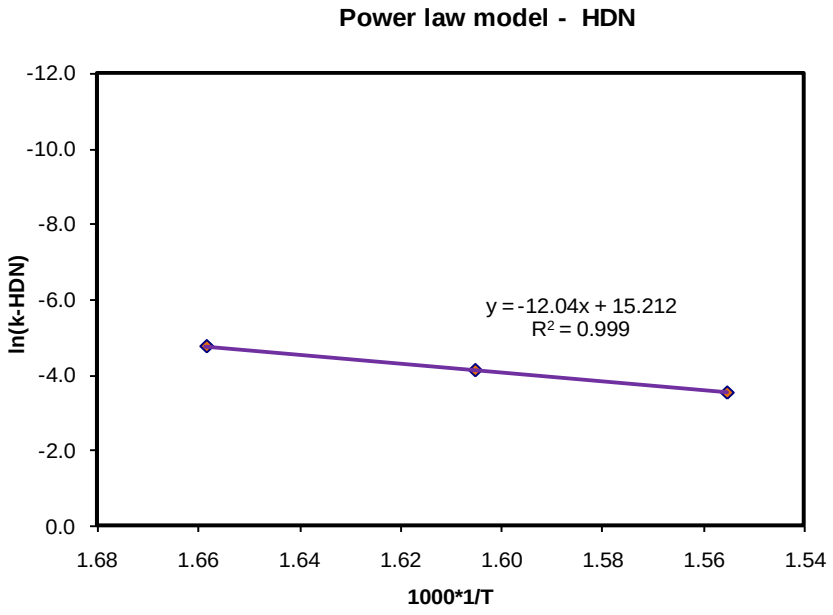

J-1B. Regression plot for Power law model

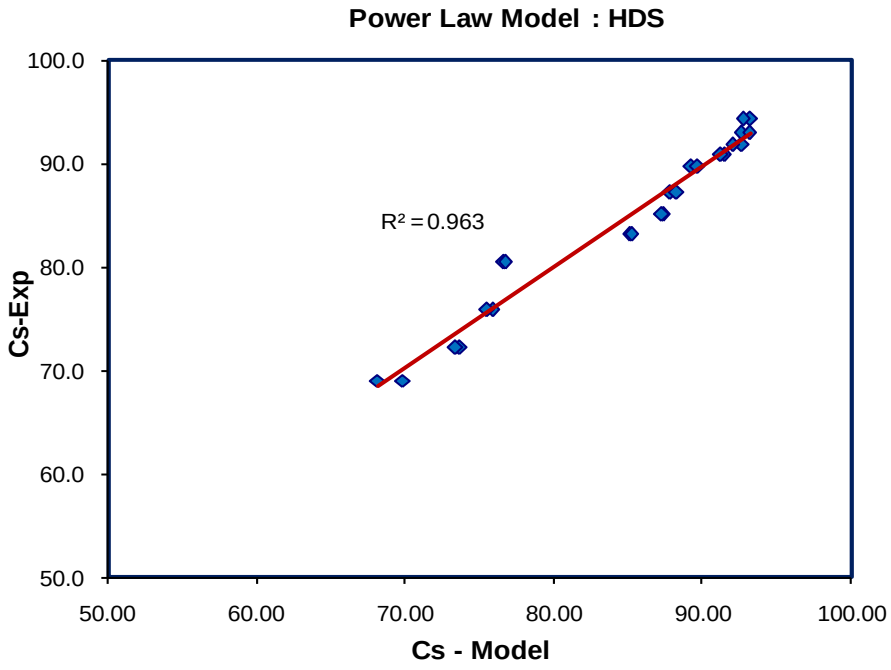

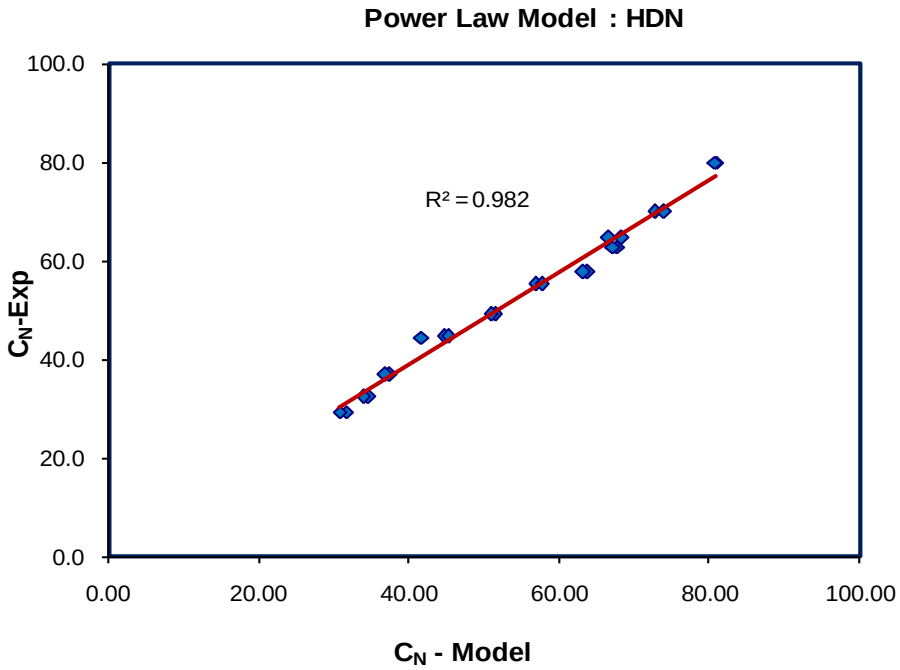

J-2A. Arrhenius plot for Multiparameter model

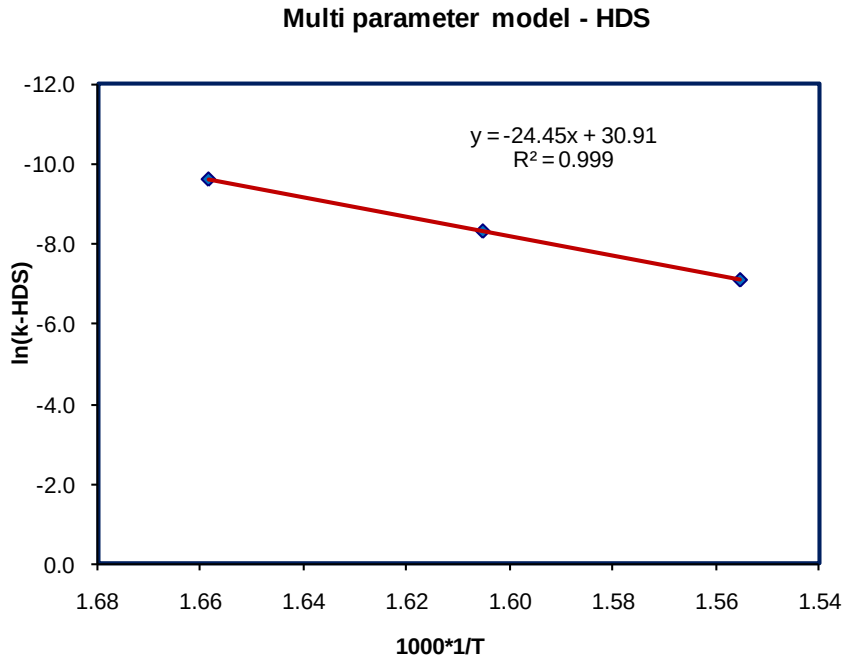

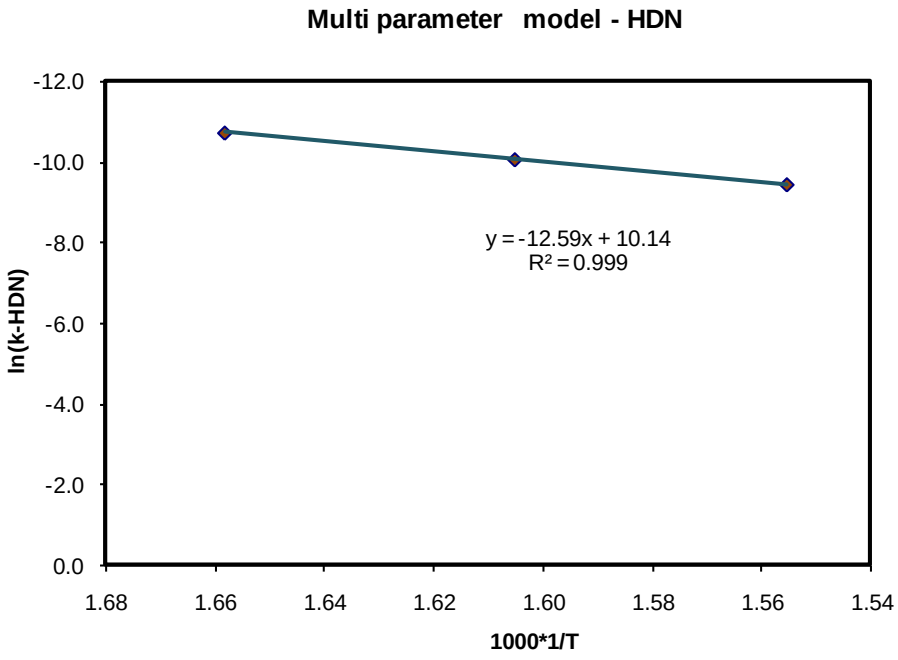

J-2B. Regression plot for Multiparameter model

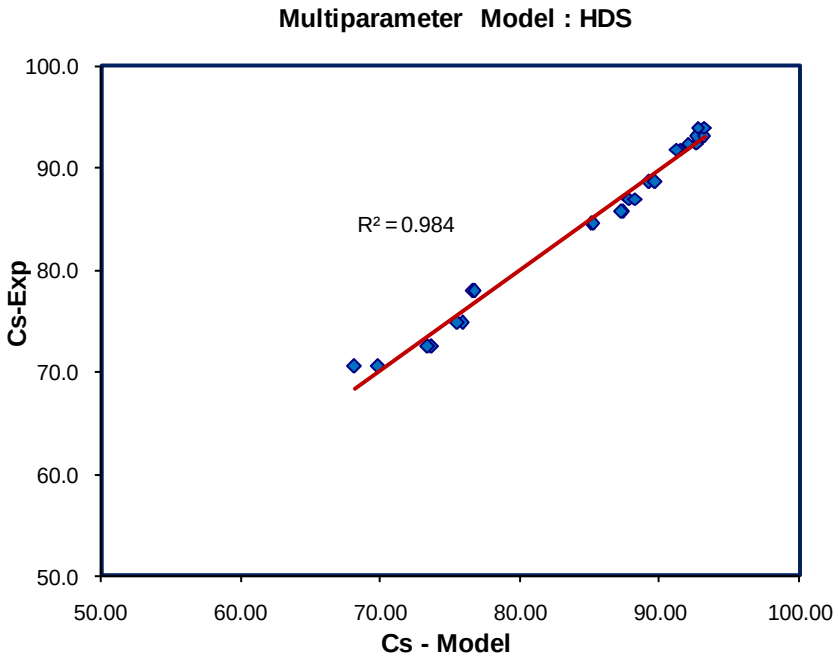

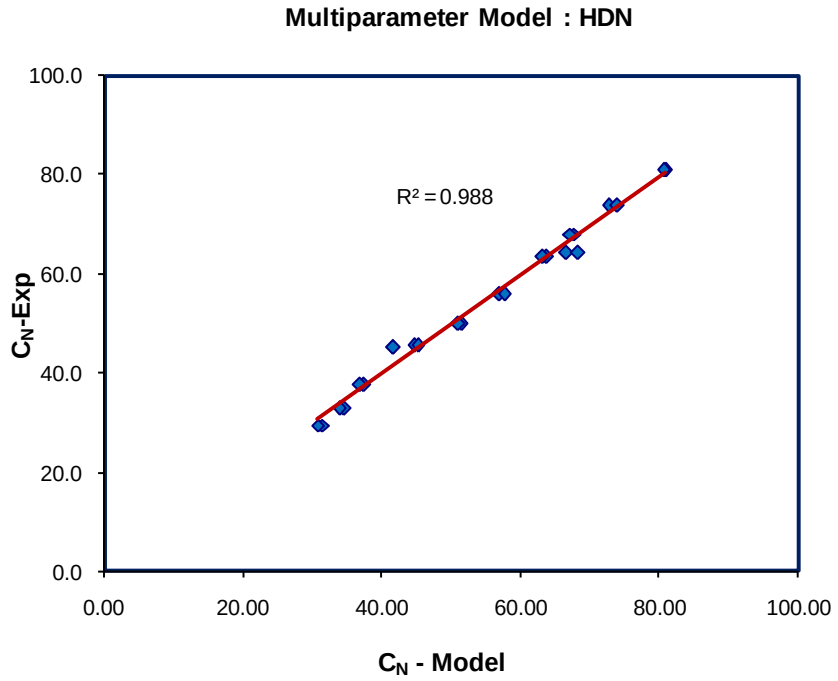

J-3A. Arrhenius plot for L-H Model –I

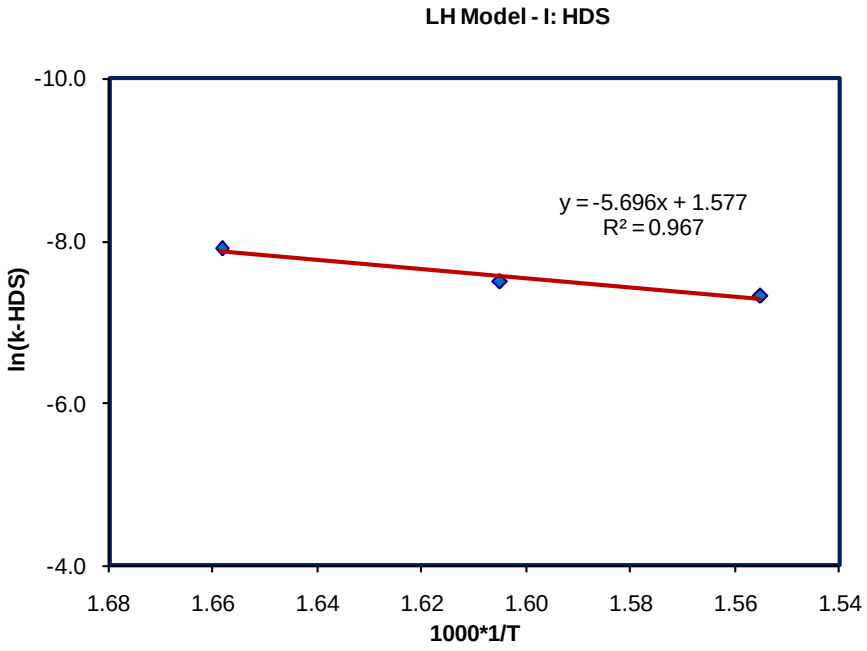

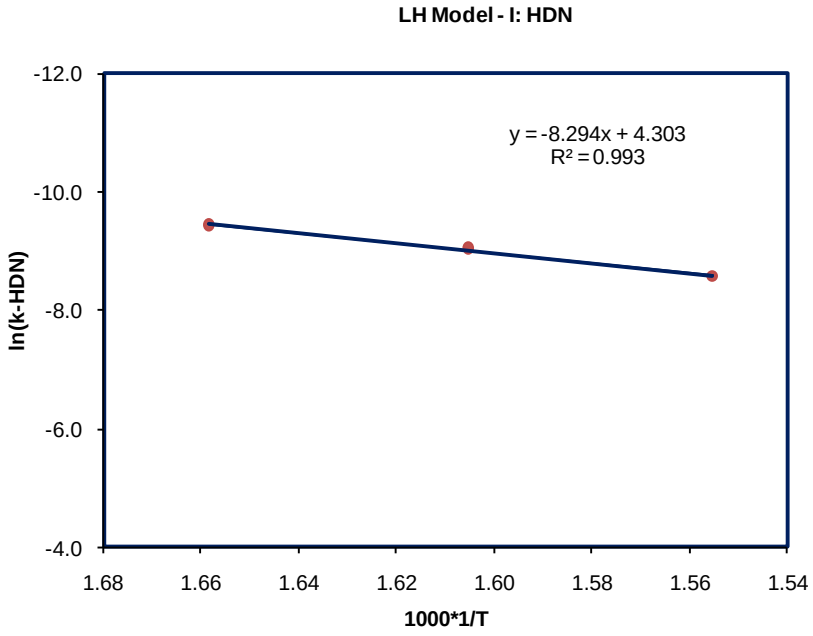

J-3B. Van't hoff plot for L-H Model -I

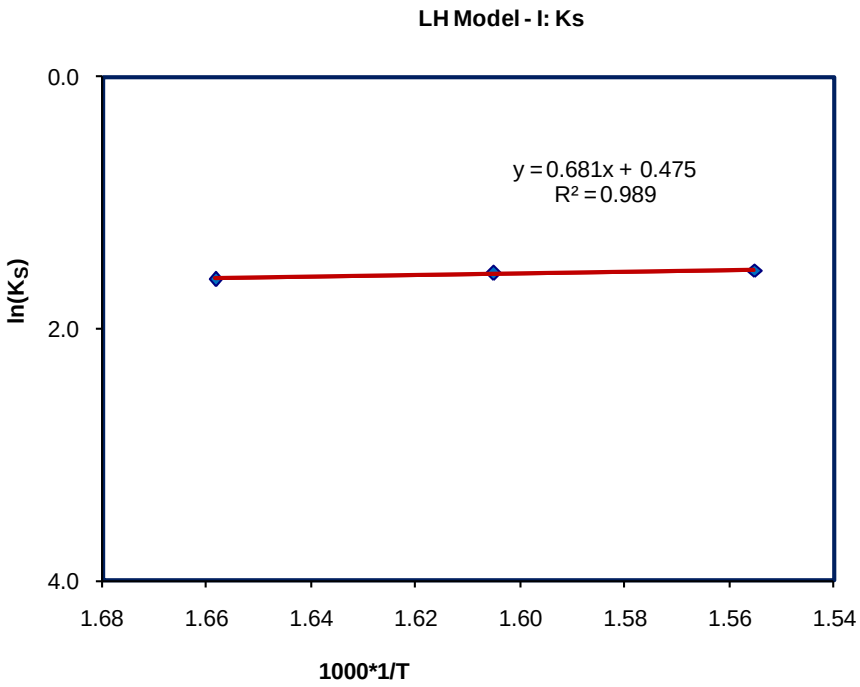

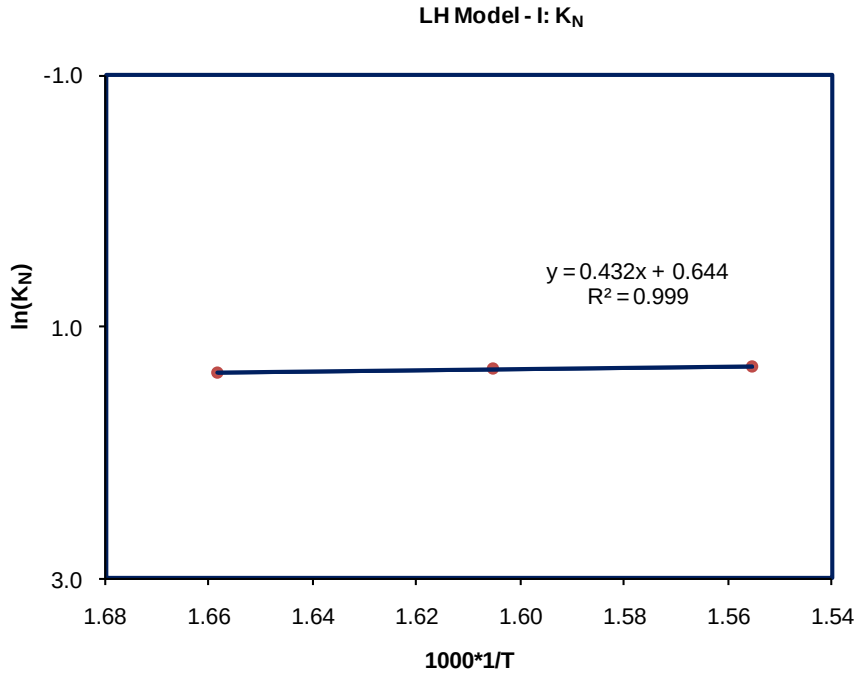

J-3C. Regression plot for LH Model-I

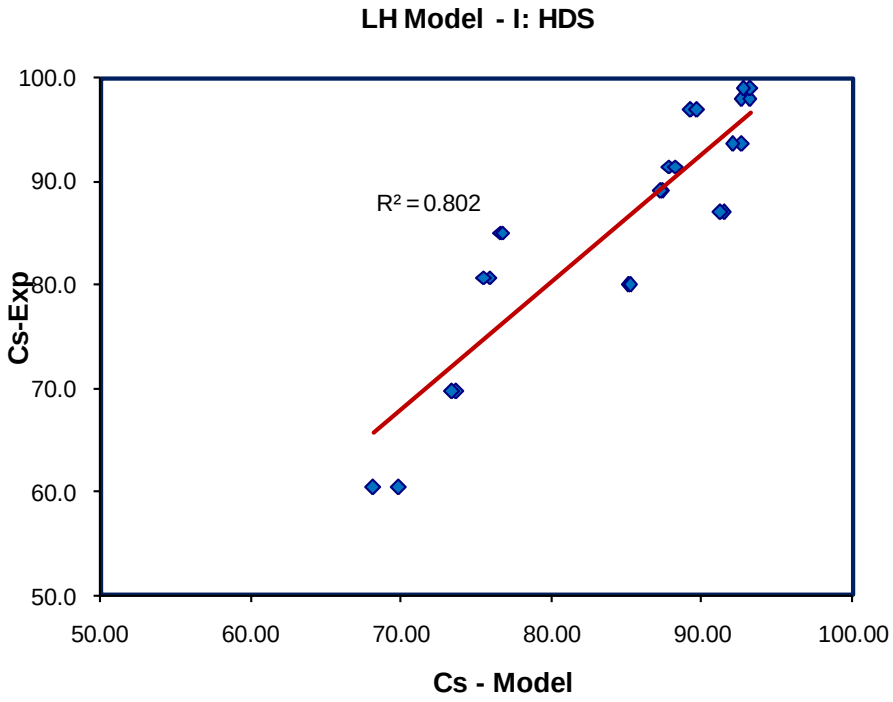

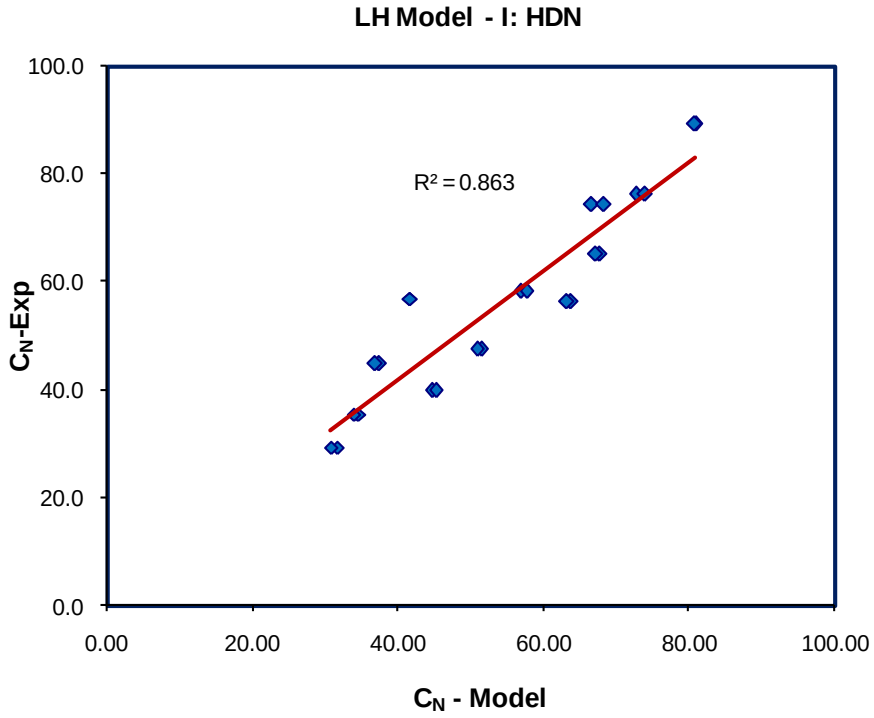

J-4A. Arrhenius plot for L-H Model –III

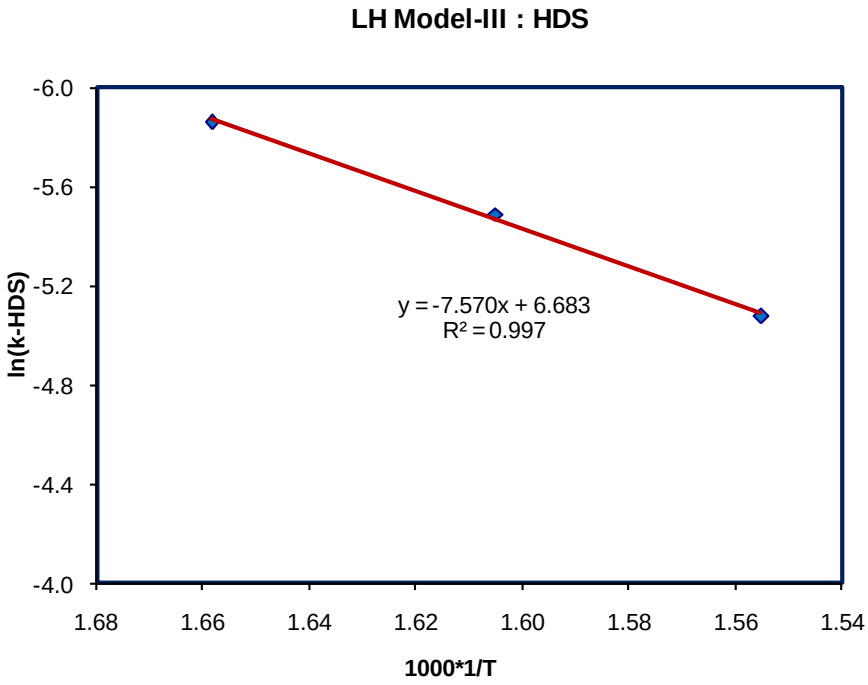

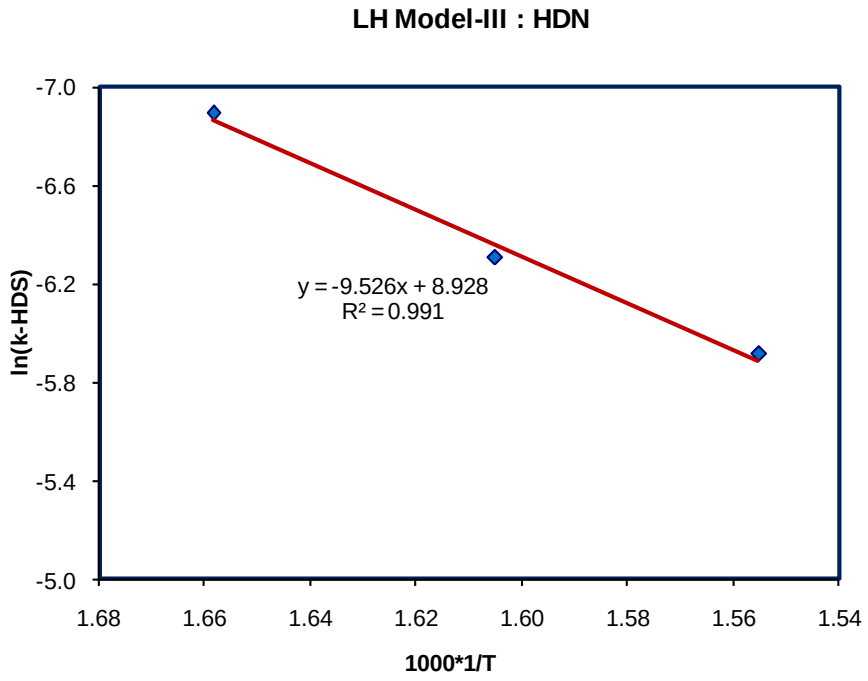

J-4B. Van't hoff plot for L-H Model -III

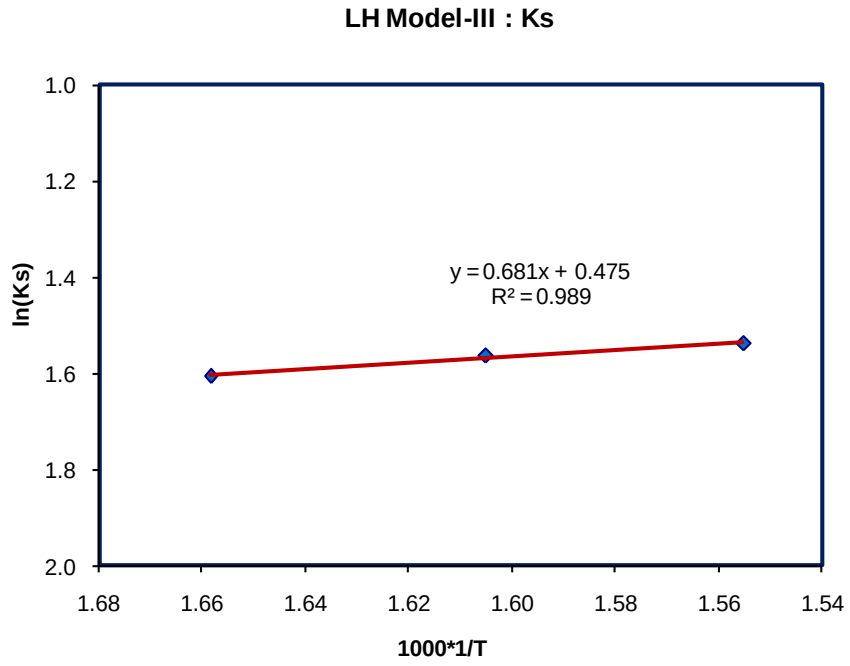

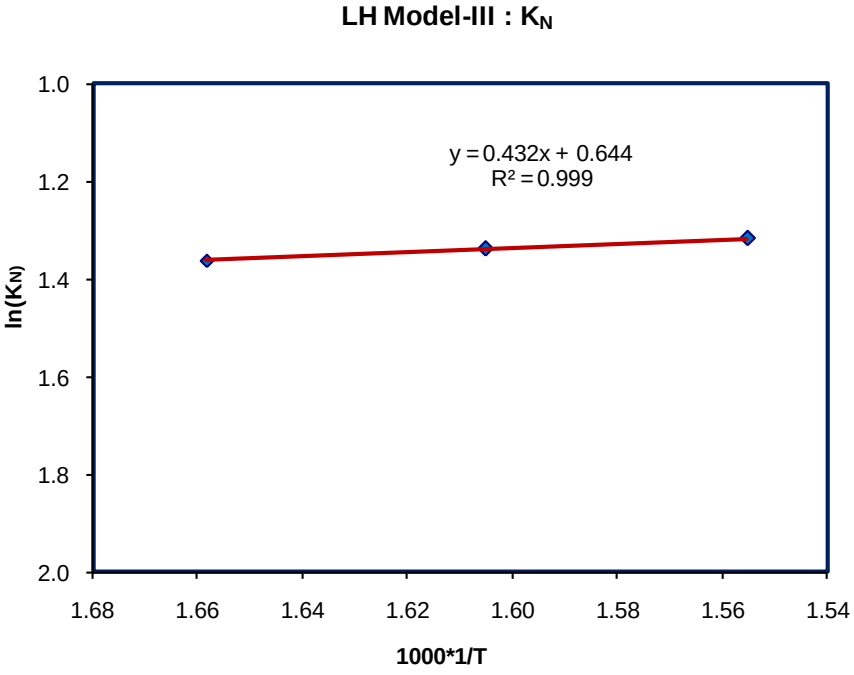

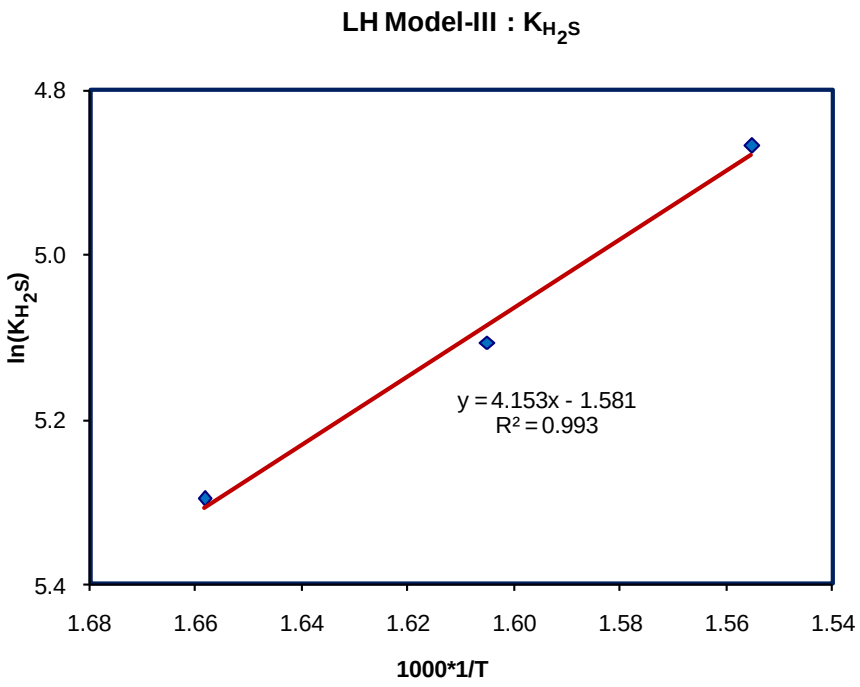
LH Model-III : K_{H_2S}
4.8
5.0
5.2
5.4
ln(K_{H_2S})
y = 4.153x - 1.581
R² = 0.993
1.68
1.66
1.64
1.62
1.60
1.58
1.56
1.54
1000*1/T

J-4C. Regression plot for LH Model-III

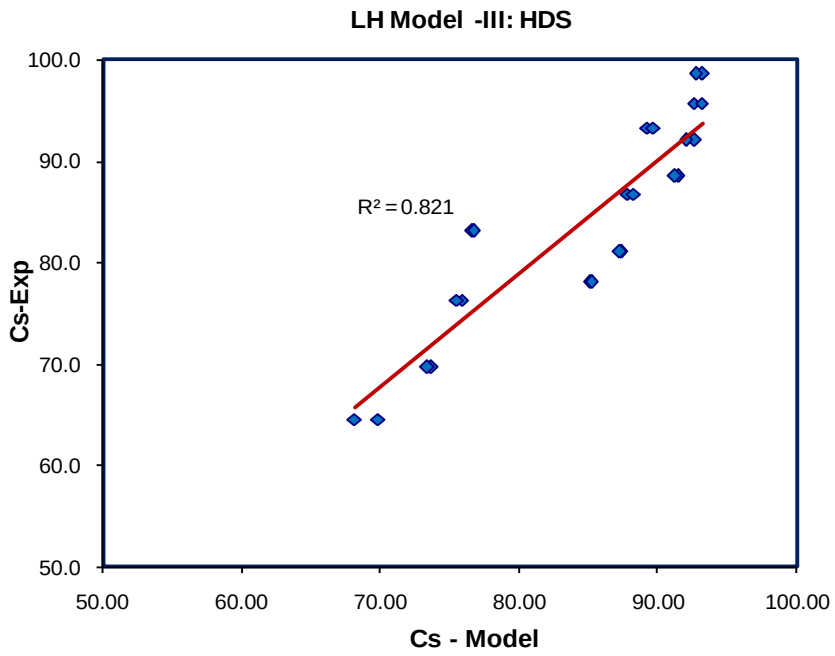

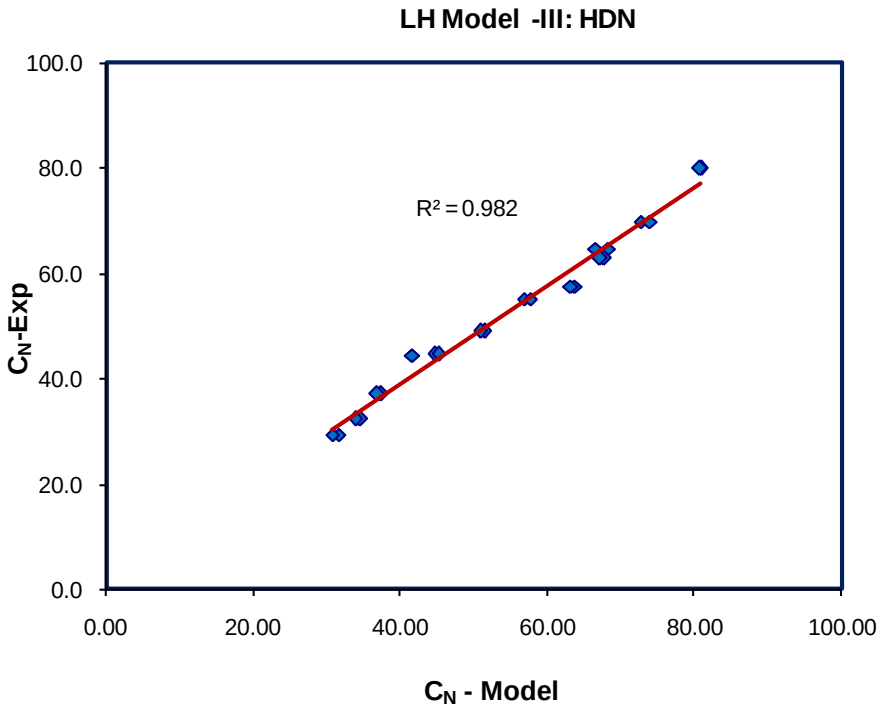

APPENDIX – K

Permission for the use of Figure 2.1

Prabhu

From: Yui, Sok [Yui.Sok@syncrude.com]
Sent: Wednesday, May 04, 2011 1:58 PM
To: Prabhu
Subject: RE: Permission for using figure from literature
Attachments: Yui OGJ 121707 - Syncrude upgrader revamp.pdf

Dear Prabhu,

Thank you for showing your interest in my paper. The figure appears in an open literature; therefore, no problems to use it as far as you properly refer to the literature.

For your information, I am sending you my earlier O&GJ paper that is ref. no. 6 in the JPI paper. You will learn some more about the Syncrude upgrading process that may or may not help you develop the background of your research project.

Thanking you again and wishing all the best for your endeavor.

Sok Yui
Syncrude Canada Ltd.
Edmonton Research and Development Centre
9421 - 17 Avenue, Edmonton, Alberta T6N 1H4

Tel: (780) 970 - 6872

This communication is intended for the use of the recipient to which it is addressed, and may contain confidential, personal and/or privileged information. Please contact the sender immediately if you are not the intended recipient of this communication. Do not copy, distribute, or take action relying on it. Any communication received in error, or subsequent reply, should be deleted or destroyed.

From: Prabhu [mailto:prn241@mail.usask.ca]
Sent: Wednesday, May 04, 2011 11:37 AM
To: Yui, Sok
Subject: Permission for using figure from literature

Respected Sir,

Greetings.

My name is Prabhu, and I am pursuing my M.Sc in Chemical engineering at University of Saskatchewan. I am working on the development of new hydrotreating catalyst support for the hydrotreating of coker gas oil. My project title is, " Mesoporous carbon supported NiMo catalyst for the hydrotreating of coker gas oil".

I am writing my thesis and I would like to use one of the figures (Figure 1 . Simplified Syncrude's upgrading process) from your article as indicated below

Yui, S., "Producing quality synthetic crude oil from Canadian oil sands bitumen," Journal of the Japan Petroleum Institute. 51, 1-13 (2008).

I kindly request you for the permission on using the above mentioned figure in my thesis.

1

Permission for the use of Figure 2.6:

Rightlink Printable License May 05, 2011

AMERICAN CHEMICAL SOCIETY LICENSE TERMS AND CONDITIONS

This is a License Agreement between Prabhu Narayanasarma ("You") and American Chemical Society ("American Chemical Society") provided by Copyright Clearance Center ("CCC"). The license consists of your order details, the terms and conditions provided by American Chemical Society, and the payment terms and conditions.

All payments must be made in full to CCC. For payment instructions, please see information listed at the bottom of this form

License Number	2662570021525
License Date	May 05, 2011
Licensed content publisher	American Chemical Society
Licensed content publication	Industrial & Engineering Chemistry Research
Licensed content title	Reactivities, reaction networks, and kinetics in high-pressure catalytic processing
Licensed content author	Michael J. Girgis et al.
Licensed content date	Sep 1, 1991
Volume number	30
Issue number	9
Type of Use	Thesis/Dissertation
Requestor type	Not specified
Format	Print and Electronic
Portion	Table/Figure/Micrograph
Number of Table/Figure//Micrographs	1
Author of this ACS article	No
Order reference number	Fig-2.6_HDS_Rxn_Pathway
Title of the thesis / dissertation	Mesoporous Carbon Supported NiMo Catalyst for the Hydrotreating Of Coker gas oil
Expected completion date	May 2011
Estimated size(pages)	230
Billing Type	Invoice
Billing address	Department of Chemical Engineering University of Saskatchewan, Saskatoon, SK S7N5A9 Canada
Customer reference info	
Total	0.00 USD

Permission for the use of Figure 2.8a

Rightlink Printable License May 05, 2011

AMERICAN CHEMICAL SOCIETY LICENSE TERMS AND CONDITIONS

This is a License Agreement between Prabhu Narayanasarma ("You") and American Chemical Society ("American Chemical Society") provided by Copyright Clearance Center ("CCC"). The license consists of your order details, the terms and conditions provided by American Chemical Society, and the payment terms and conditions.

All payments must be made in full to CCC. For payment instructions, please see information listed at the bottom of this form

License Number	2662570864634
License Date	May 05, 2011
Licensed content publisher	American Chemical Society
Licensed content publication	The Journal of Physical Chemistry
Licensed content title	Surface structure and catalytic activity of a reduced molybdenum oxide-alumina catalyst. 2. The mechanism of pyridine hydrogenation and piperidine dehydrogenation
Licensed content author	J. Sonnemans et al.
Licensed content date	Sep 1, 1976
Volume number	80
Issue number	19
Type of Use	Thesis/Dissertation
Requestor type	Not specified
Format	Print and Electronic
Portion	Table/Figure/Micrograph
Number of Table/Figure//Micrographs	1
Author of this ACS article	No
Order reference number	Fig-2.8_HDN_Path_Pyridine
Title of the thesis / dissertation	Mesoporous Carbon Supported NiMo Catalyst for the Hydrotreating Of Coker gas oil
Expected completion date	May 2011
Estimated size(pages)	230
Billing Type	Invoice
Billing address	Department of Chemical Engineering University of Saskatchewan, Saskatoon, SK S7N5A9 Canada
Customer reference info	
Total	0.00 USD

Permission for the use of Figure 2.8b

Rightlink Printable License May 05, 2011

AMERICAN CHEMICAL SOCIETY LICENSE TERMS AND CONDITIONS

This is a License Agreement between Prabhu Narayanasarma ("You") and American Chemical Society ("American Chemical Society") provided by Copyright Clearance Center ("CCC"). The license consists of your order details, the terms and conditions provided by American Chemical Society, and the payment terms and conditions.

All payments must be made in full to CCC. For payment instructions, please see information listed at the bottom of this form

License Number	2662571156488
License Date	May 05, 2011
Licensed content publisher	American Chemical Society
Licensed content publication	Industrial & Engineering Chemistry Process Design and Development
Licensed content title	Chemical equilibriums among quinoline and its reaction products in hydrodenitrogenation
Licensed content author	Joseph F. Cocchetto et al.
Licensed content date	Jan 1, 1981
Volume number	20
Issue number	1
Type of Use	Thesis/Dissertation
Requestor type	Not specified
Format	Print and Electronic
Portion	Table/Figure/Micrograph
Number of Table/Figure//Micrographs	1
Author of this ACS article	No
Order reference number	Fig-2.8_HDN_Path_Quinoline
Title of the thesis / dissertation	Mesoporous Carbon Supported NiMo Catalyst for the Hydrotreating Of Coker gas oil
Expected completion date	May 2011
Estimated size(pages)	230
Billing Type	Invoice
Billing address	Department of Chemical Engineering University of Saskatchewan, Saskatoon, SK S7N5A9 Canada
Customer reference info	
Total	0.00 USD

Permission for the use of Figure 2.12

Rightlink Printable License May 05, 2011

ELSEVIER LICENSE
TERMS AND CONDITIONS

This is a License Agreement between Prabhu Narayanasarma ("You") and Elsevier ("Elsevier") provided by Copyright Clearance Center ("CCC"). The license consists of your order details, the terms and conditions provided by Elsevier, and the payment terms and conditions.

All payments must be made in full to CCC. For payment instructions, please see information listed at the bottom of this form

Supplier	Elsevier Limited The Boulevard,Langford Lane Kidlington,Oxford,OX5 1GB,UK
Registered Company Number	1982084
Customer Name	Prabhu Narayanasarma
Customer Address	Department of Chemical Engineering, Saskatoon, SK S7N5A9
License Number	2662571493153
License Date	May 05, 2011
Licensed content publisher	Elsevier
Licensed content publication	Journal of Catalysis
Licensed content title	Structure-Function Relations in Molybdenum Sulfide Catalysts: The "Rim-Edge" Model
Licensed content author	M. Daage, R. R. Chianelli
Licensed content date	October 1994
License content Volume number	149
License content Issue number	2
Number of pages	14
Start Page	414
End Page	427
Type of Use	reuse in a thesis/dissertation
Intended publisher of new work	Other
Portion	figures/tables /illustrations
Number of figures/tables/illustrations	1
Format	Print and Electronic
Are you the author of this Elsevier article?	No
Will you be translating?	No
Order reference number	Fig-2.12_Rim-Edge
Title of the thesis / dissertation	Mesoporous Carbon Supported NiMo Catalyst for the Hydrotreating Of Coker gas oil
Expected completion date	May 2011
Estimated size (number of pages)	230
Elsevier VAT number	GB 494 6272 12
Permissions price	0.00 USD
VAT/Local Sales Tax	0.0 USD / 0.0 GBP
Total	0.00 USD

Permission for the use of Figure 2.13

Rightlink Printable License May 05, 2011

AMERICAN CHEMICAL SOCIETY LICENSE TERMS AND CONDITIONS

This is a License Agreement between Prabhu Narayanasarma ("You") and American Chemical Society ("American Chemical Society") provided by Copyright Clearance Center ("CCC"). The license consists of your order details, the terms and conditions provided by American Chemical Society, and the payment terms and conditions.

All payments must be made in full to CCC. For payment instructions, please see information listed at the bottom of this form

License Number	2662580178696
License Date	May 05, 2011
Licensed content publisher	American Chemical Society
Licensed content publication	The Journal of Physical Chemistry B
Licensed content title	Synthesis of Highly Ordered Carbon Molecular Sieves via Template- Mediated Structural Transformation
Licensed content author	Ryong Ryoo et al.
Licensed content date	Sep 1, 1999
Volume number	103
Issue number	37
Type of Use	Thesis/Dissertation
Requestor type	Not specified
Format	Print and Electronic
Portion	Table/Figure/Micrograph
Number of Table/Figure//Micrographs	1
Author of this ACS article	No
Order reference number	Fig-2.13_Vol_Templating
Title of the thesis / dissertation	Mesoporous Carbon Supported NiMo Catalyst for the Hydrotreating Of Coker gas oil
Expected completion date	May 2011
Estimated size(pages)	230
Billing Type	Invoice
Billing address	Department of Chemical Engineering University of Saskatchewan, Saskatoon, SK S7N5A9 Canada
Customer reference info	
Total	0.00 USD

Permission for the use of Figure 2.14

Prabhu

From: Rights DE [RIGHTS-and-LICENCES@wiley-vch.de]
Sent: Friday, May 06, 2011 12:24 AM
To: 'prn241@mail.usask.ca'
Subject: AW: Permissions for using a illustration

Dear Prabhu Narayanasarma,

Thank you for your email.

We hereby grant permission for the requested use expected that due credit is given to the original source.

If material appears within our work with credit to another source, authorisation from that source must be obtained.

Credit must include the following components:

- Books: Author(s)/ Editor(s) Name(s): Title of the Book. Page(s). Publication year. Copyright Wiley-VCH Verlag GmbH & Co. KGaA. Reproduced with permission.
- Journals: Author(s) Name(s): Title of the Article. Name of the Journal. Publication year. Volume. Page(s). Copyright Wiley-VCH Verlag GmbH & Co. KGaA. Reproduced with permission.

With kind regards

Bettina Loycke

Bettina Loycke
Senior Rights Manager
Wiley-VCH Verlag GmbH & Co. KGaA
Boschstr. 12
69469 Weinheim
Germany

Phone: +49 (0) 62 01- 606 - 280
Fax: +49 (0) 62 01 - 606 - 332
Email: rights@wiley-vch.de

Wiley-VCH Verlag GmbH & Co. KGaA
Location of the Company: Weinheim
Chairman of the Supervisory Board: Stephen Michael Smith
Trade Register: Mannheim, HRB 432833
General Partner: John Wiley & Sons GmbH, Location: Weinheim
Trade Register Mannheim, HRB 432295

1

Permission for the use of Figure 2.14 (contd.)

Managing Directors : Christopher J. Dicks, Bijan Ghawami, William Pesce

Von: Goldweber, Paulette - Hoboken **Im Auftrag von** Permissions - US
Gesendet: Donnerstag, 5. Mai 2011 5:48
An: Rights DE
Betreff: FW: Permissions for using a illustration

Paulette Goldweber
Associate Manager, Permissions
Global Rights
John Wiley & Sons, Inc.
ph: 201-748-8765
f: 201-748-6008
pgoldweb@wiley.com

From: Prabhu [mailto:prn241@mail.usask.ca]
Sent: Wednesday, May 04, 2011 2:46 PM
To: Permissions - US
Subject: Permissions for using a illustration

Respected Sir / Madam

Greetings.

My name is Prabhu, and I am pursuing my M.Sc. in Chemical engineering at University of Saskatchewan, Canada. My thesis title is, " Mesoporous carbon supported NiMo catalyst for the hydrotreating of coker gas oil". I am writing my thesis and I would like to use one of the illustrations (Scheme 1 illustration) from the article as indicated below.

Ryoo, R., S.H. Joo, M. Kruk and M. Jaroniec, "Ordered mesoporous carbons," Adv Mater. 13, 677-681 (2001).

I kindly request you for the permission on using the above mentioned figure in my thesis. I will use it after redrawing it and not by copying it directly.

Looking forward to hearing from you.

Thanking you

Regards

Prabhu Narayanasarma

2

Permission for the use of Figure 2.16

Prabhu

From: CONTRACTS-COPYRIGHT (shared) [Contracts-Copyright@rsc.org]
Sent: Thursday, May 05, 2011 4:21 AM
To: 'Prabhu Narayanasarma'
Subject: RE: Website Email: Permission for using figure in thesis

Dear Prabhu

The Royal Society of Chemistry hereby grants permission for the use of the material specified below in the work described and in all subsequent editions of the work for distribution throughout the world, in all media including electronic and microfilm. You may use the material in conjunction with computer-based electronic and information retrieval systems, grant permissions for photocopying, reproductions and reprints, translate the material and to publish the translation, and authorize document delivery and abstracting and indexing services. The Royal Society of Chemistry is a signatory to the STM Guidelines on Permissions (available on request).

Please note that if the material specified below or any part of it appears with credit or acknowledgement to a third party then you must also secure permission from that third party before reproducing that material.

Please ensure that the published article carries a credit to The Royal Society of Chemistry in the following format:

[Original citation] – Reproduced by permission of The Royal Society of Chemistry

and that any electronic version of the work includes a hyperlink to the article on the Royal Society of Chemistry website. The recommended form for the hyperlink is http://dx.doi.org/10.1039/*DOI suffix*, for example in the link http://dx.doi.org/10.1039/b110420a the DOI suffix is 'b110420a'. To find the relevant DOI suffix for the RSC paper in question, go to the Journals section of the website and locate your paper in the list of papers for the volume and issue of your specific journal. You will find the DOI suffix quoted there.

Best wishes

Gill

Gill Cockhead (Mrs), Contracts & Copyright Executive
Royal Society of Chemistry, Thomas Graham House
Science Park, Milton Road, Cambridge CB4 0WF, UK
Tel +44 (0) 1223 432134, Fax +44 (0) 1223 423623
http://www.rsc.org

-----Original Message-----
From: Prabhu Narayanasarma [mailto:prn241@mail.usask.ca]
Sent: 04 May 2011 20:25
To: CONTRACTS-COPYRIGHT (shared)
Subject: Website Email: Permission for using figure in thesis

To: Contracts
This Email was sent from the following RSC.ORG page:

My name is Prabhu, and I am pursuing my M.Sc. in Chemical engineering at University of Saskatchewan, Canada. My thesis title is, " Mesoporous carbon supported NiMo catalyst for the hydrotreating of coker gas oil". I am writing my thesis and I would like to use one of the figures (Scheme 1) from the article as indicated below.

Sangjin Han and Taeghwan Hyeon, "Simple silica-particle template synthesis of mesoporous carbons" Chemical Communications., 1955-1996 (1999).

I kindly request you for the permission on using the above mentioned figure in my thesis. I will use it after redrawing it and not by copying it directly.

Looking forward to hearing from you.

1

Permission for the use of Figure 2.17a

Rightlink Printable License May 05, 2011

ELSEVIER LICENSE
TERMS AND CONDITIONS

This is a License Agreement between Prabhu Narayanasarma ("You") and Elsevier ("Elsevier") provided by Copyright Clearance Center ("CCC"). The license consists of your order details, the terms and conditions provided by Elsevier, and the payment terms and conditions.

All payments must be made in full to CCC. For payment instructions, please see information listed at the bottom of this form

Supplier	Elsevier Limited, The Boulevard,Langford Lane Kidlington,Oxford,OX5 1GB,UK
Registered Company Number	1982084
Customer Name	Prabhu Narayanasarma
Customer Address	Dept of Chemical Engineering, Saskatoon, SK S7N5A9
License Number	2662581173349
License Date	May 05, 2011
Licensed content publisher	Elsevier
Licensed content publication	Journal of Colloid and Interface Science
Licensed content title	Interactions between Molybdenum and Activated Carbons on the Preparation of Activated Carbon-Supported Molybdenum Catalysts
Licensed content author	G. de la Puente, A. Centeno, A. Gil, P. Grange
Licensed content date	1 June 1998
License content Volume number	202
License content Issue number	1
Number of pages	12
Start Page	155
End Page	166
Type of Use	reuse in a thesis/dissertation
Intended publisher of new work	Other
Portion	figures/tables /illustrations
Number of figures/tables/illustrations	1
Format	Print and Electronic
Are you the author of this Elsevier article?	No
Will you be translating?	No
Order reference number	Fig-2.17a_Mo_Interaction
Title of the thesis / dissertation	Mesoporous Carbon Supported NiMo Catalyst for the Hydrotreating Of Coker gas oil
Expected completion date	May 2011
Estimated size (number of pages)	230
Elsevier VAT number	GB 494 6272 12
Permissions price	0.00 USD
VAT/Local Sales Tax	0.0 USD / 0.0 GBP
Total	0.00 USD

Permission for the use of Figure 2.17b

Rightlink Printable License May 04, 2011

ELSEVIER LICENSE
TERMS AND CONDITIONS

This is a License Agreement between Prabhu Narayanasarma ("You") and Elsevier ("Elsevier") provided by Copyright Clearance Center ("CCC"). The license consists of your order details, the terms and conditions provided by Elsevier, and the payment terms and conditions.

All payments must be made in full to CCC. For payment instructions, please see information listed at the bottom of this form

Supplier	Elsevier Limited, The Boulevard,Langford Lane Kidlington,Oxford,OX5 1GB,UK
Registered Company Number	1982084
Customer Name	Prabhu Narayanasarma
Customer Address	Dept of Chemical Engineering, Saskatoon, SK S7N5A9
License Number	2662140101951
License Date	May 04, 2011
Licensed content publisher	Elsevier
Licensed content publication	Carbon
Licensed content title	Carbon black-supported molybdenum sulfide catalysts
Licensed content author	J.P.R. Vissers, S.M.A.M. Bouwens, V.H.J. de Beer, R. Prins
Licensed content date	1987
License content Volume number	25
License content Issue number	4
Number of pages	9
Start Page	485
End Page	493
Type of Use	reuse in a thesis/dissertation
Intended publisher of new work	Other
Portion	figures/tables /illustrations
Number of figures/tables/illustrations	1
Format	Print and Electronic
Are you the author of this Elsevier article?	No
Will you be translating?	No
Order reference number	Fig 2.17b_Mo_Interaction
Title of the thesis / dissertation	Mesoporous Carbon Supported NiMo Catalyst for the Hydrotreating Of Coker gas oil
Expected completion date	May 2011
Estimated size (number of pages)	230
Elsevier VAT number	GB 494 6272 12
Permissions price	0.00 USD
VAT/Local Sales Tax	0.0 USD / 0.0 GBP
Total	0.00 USD